This work is protected by copyright and other intellectual property rights and duplication or sale of all or part is not permitted, except that material may be duplicated by you for research, private study, criticism/review or educational purposes. Electronic or print copies are for your own personal, non-commercial use and shall not be passed to any other individual. No quotation may be published without proper acknowledgement. For any other use, or to quote extensively from the work, permission must be obtained from the copyright holder/s.

ELECTRON SPECTROSCOPIC STUDIES OF SLOWLY OXIDISED BERYLLIUM AND MAGNESIUM SURFACES

A thesis presented for the degree of Doctor of Philosophy at the University of Keele

by

MEHRI FADAVI, B.Sc.

Physics Department,
University of Keele,
Staffordshire.

January, 1981

BRITISH LIBRARY

IMAGING SERVICES NORTH

Boston Spa, Wetherby
West Yorkshire, LS23 7BQ
www.bl.uk

The following has been redacted from this digital copy of the original thesis at the request of the awarding university:

Fig.2.3 between pages 14 and 15

Fig.2.4 and 2.5 between pages 15 and 16

Fig.2.6 between pages 15 and 16

Fig.2.7 between pages 16 and 17

Fig.2.15 between pages 33 and 34

Fig.3.11 between pages 69 and 70

Fig.5.15 between pages 98 and 99

Fig.5.17 between pages 100 and 101

Fig.6.19 between pages 115 and 116

CONTENTS

		Page
ACKNOWLEDGEMENTS		
ABSTRACT		
CHAPTER 1	INTRODUCTION	1
1.1	Surface Science	3
CHAPTER 2	SECONDARY ELECTRON EMISSION	
2.1	Introduction	10
2.2	The secondary Electron Yield	11
2.2.1	The Yield Curve	12
2.2.2	Universal Yield Curve	13
2.2.3	Dependence of Yield (δ) on The Angle of Incidence of the Primaries	14
2.2.4	Angular Distribution of Secondaries	14
2.3	Energy Distribution of Secondaries	16
2.4	Review of Some of the More Relevant Previous Theoretical and Experimental Works on Secondary Electron Emission	17
2.5	A Formulation of Secondary Yield	24
2.5.1	Penetration Range of Primary Electrons in Solid Materials	24
2.5.2	Absorption Coefficient α and Escape Depth $x_\alpha = (\frac{1}{\alpha})$	27
a	α and $\frac{1}{\alpha}$ for Metals & Semiconductors	27
b	α and x_α for Insulators	29
2.5.3	Secondary Yield Due to Primary Electrons	30
2.5.4	Secondary Yield Due to Back-Scattered Electrons	31
2.5.5	Universal Secondary Yield Curve	32
2.6	Quantitative Characteristics of Secondary Electron Emission	33
2.7	Conclusion	36
CHAPTER 3	AUGER ELECTRON SPECTROSCOPY AND CHARACTERISTIC ENERGY LOSSES	
3.1	Introduction	37
3.2	Auger Electron Spectroscopy (AES)	38
3.2.1	Auger Process	40
3.2.2	Auger Electron Energies	42
3.2.3	Surface Sensitivity of Auger Electrons	45
3.2.4	The Sources of Excitation	46
3.2.5	Quantitative Analysis of AES	48
3.2.6	Chemical Effects in AES	50
3.2.7	The Concept of Cross Transition	52

3.3 Characteristic Energy Losses in Solids (CEL) 54

3.3.1 Characteristic Excitation in Solids 56
3.3.1.1 Collective Excitation of Valence Electrons (plasmon losses) 56
a.volume plasmons 56
b.surface plasmons 61
3.3.1.2 One Electron Excitation of Valence Electrons (Inter-/Intra-Band transition) 62
3.3.1.3 Excitation of Core Electrons (Ionization Losses) 63
3.3.1.4 Excitation of Surface Vibrations (Quasi-elastic Electrons) 65
3.3.2 Changes of Energy-Loss Spectra by Adsorbed Layers 65

3.4 Electron Spectrometers and Instrumentation 66

3.4.1 Retarding Field Analyser (Auger-LEED Device) 67
3.4.2 Cylindrical Mirror Analyser (CMA) 68

3.5 Conclusion 71

CHAPTER 4 APPARATUS AND EXPERIMENTAL TECHNIQUES

4.1 Introduction 72
4.2 General Features 73

4.2.1 The UHV System 73
4.2.2 Preparation of UHV 73
4.2.3 The Retarding Field Analyzer 74
4.2.4 Pressure Measurement 75
4.2.5 Electron Gun 75
4.2.6 Target Manipulation and Transfer System 76
4.2.7 Gas Admittance System 77

4.3 Surface Cleaning Facilities 78

4.3.1 Specimen Heating by Electron Bombardment 78
4.3.2 The Saddle Field Ion Source 80
4.3.3 Thin Film Evaporation 81

4.4 Detection System for AES and CELS $(\frac{dN}{dE})$ and SEE Yield 81

4.4.1 Detection Method for AES and CELS $(\frac{dN}{dE})$ 81
4.4.2 Detection Circuit for $\frac{dN}{dE}$ (AES and CELS detection) 84
4.4.3 Experimental Apparatus for the SEE Yield Measurement 85
4.4.4 Experimental Measurement Method 87

CHAPTER 5 RESULTS AND DISCUSSIONS OF Be → BeO

5.1 Introduction 89
5.2 Preparation of Be 91
5.3 Results of Be → BeO 91

5.3.1 Auger Spectra 91
5.3.2 Characteristic Energy Loss Spectra 92
5.3.3 Secondary Electron Emission Yield (SEE) 94

5.4 Discussion of Results of Be → BeO 96

5.4.1 Auger Spectra 96
5.4.2 Energy Loss Spectra 100
5.4.3 Secondary Electron Emission Yield 102

5.5 Conclusion 107

CHAPTER 6 RESULTS AND DISCUSSION OF Mg → MgO

6.1 Introduction 108
6.2 Preparation of Clean Mg 109
6.3 Results of Mg → MgO 110

6.3.1 Auger Spectra 110
6.3.2 Characteristic Energy Loss Spectra (CELS) 111
6.3.3 Secondary Electron Emission Yield (SEE) 112

6.4 Discussion of Results of Mg → MgO 115

6.4.1 Auger Spectra 115
6.4.2 Characteristic Energy Loss Spectra 118
6.4.3 Secondary Electron Emission Yield 120

6.5 Conclusion 125

CHAPTER 7 CONCLUSIONS AND SUGGESTIONS FOR FUTURE WORK 126

APPENDICES

REFERENCES

ACKNOWLEDGEMENTS

The author wishes to express her gratitude to:

Professor W. Fuller for the use of the laboratory facilities of the Physics Department.

Dr. E. B. Pattinson for his supervision, encouragement and guidance throughout the course of this work.

Dr. K. Kandasamy, Mr. G. Kavei and Mr. R. Moran and other colleagues in the Physics Department for useful suggestions and discussions.

The technical staff of the department and in particular Mr. G. Dudley and his staff in the workshop, and members of the electronics workshop for their helpful assistance throughout this work.

Mr. M. Daniels for his photographic work.

Mrs. S. Cooper for her efficient typing of this thesis.

ABSTRACT

The topic of electron stimulated secondary electron emission is introduced in relation to studies in surface physics together with some of the experimental techniques used in their investigation. In particular the techniques of Secondary Electron Emission (SEE) Yield, Auger Electron Spectroscopy (AES) and Characteristic Energy Loss Spectroscopy (CELS) are outlined in detail with an appraisal of recent developments in these subjects.

The apparatus suitable for performing electron stimulated surface investigations is described, along with its associated circuitry. The apparatus incorporates a hemispherical retarding field energy analyser, suitable for AES and CELS. Additional features of the apparatus are in situ target cleaning facilities. A suitable pumping arrangement to evacuate the system to ultra high vacuum pressures ($\sim 10^{-10}$ torr) is outlined as well as the electronic detection circuitry which was developed to obtain an output proportional to SEE yield (in normal mode, $\delta(E)$) and AES and CELS (in differential mode, $\frac{dN(E)}{dE}$).

Changes in the electron spectra (SEE yield, AES and CELS) of beryllium (Be) and magnesium (Mg) due to slow oxidation from residual oxygen were extensively studied. For these metals fine structure in the Auger spectra involving the valence band has been interpreted in terms of the density of states of the valence band. Additional fine structures in the Auger spectra of clean Be and Mg have been attributed to plasmon loss and the ionisation loss mechanisms. In addition explanations of various other changes in the electron spectra of these metals as a result of oxidation have been included.

Perhaps the most significant new results relate to changes in the SEE yield (δ) of Be and Mg during the oxidation. As the oxidation

proceeds the δ_{max} of Be and Mg increases from 0.65 to 4.73 and from 0.89 to 2.74 respectively. The increase of δ_{max} (during the oxidation) is discussed and interpreted as a reduction of potential barriers caused by band bending . In particular results of quantitative characteristics of SEE have been discussed in relation to the recent theoretical work of Kanaya et al. (1978) and Ono and Kanaya (1979). By using their theoretical work the changes of escape depth of secondaries and the range of primaries has been calculated for Be and Mg during their oxidation. The escape depth (which is proportional to the range) of secondaries in Be and Mg has changed from 33A^{o} to 53A^{o} and from 55A^{o} to 71A^{o}, respectively, as the oxidation proceeds. In general good agreement has been found in some aspects particularly in the case of Be, whilst in other parts (namely, escape depth of secondaries in Mg) the necessity for further work is indicated.

CHAPTER 1

Introduction

Since near the beginning of the century, it has been known that when a solid is bombarded with a beam of charged particles of sufficient kinetic energy, many interactions and excitations take place in or near the surface which may result in the emission of electrons. In particular these emitted secondary electrons can produce useful information about the surface such as, for example, aspects of the electronic structure, the species of atoms present and the chemical environment of these atoms. One of the most effective means of exciting such electrons is electron stimulation using a primary electron beam. This is due to the fact that;

1) An electron interacts quite strongly in matter.
2) Electrons have an inelastic mean free path of a few A^{o} depending on the energy. The energy and momentum of an emitted electron may therefore be characteristic of elementary excitations near the surface.
3) Electrons are easily focused into beams and the energy may be varied by applying appropriate potentials.
4) Electrons are efficiently detected and counted.
5) Electrons may be analyzed with respect to angular and energy distribution using electrostatic lenses and deflection systems.
6) Another major advantage of electrons, is that electrons unlike atoms or molecules or ions disappear from the vacuum system after being used for the surface analysis.

The main topics of this thesis will be concerned with various aspects of the secondary electron emission of surfaces bombarded with electrons of incident energy up to 1.8 KeV. In addition to its intrinsic scientific interest, the subject of surface physics has proved to have considerable

technological applications in fields such as friction, corrosion, fracture, adhesion etc. Furthermore, materials with a high yield of secondary electrons are very important in the design of such instruments as electron multipliers, image intensifiers etc., and substances of low secondary yield find application in, for example, reducing the 'multipactor' effect in high power electron beam tubes. The energy distribution of secondary electrons can also provide an extremely sensitive method of surface analysis; i.e. Auger electron spectroscopy (AES) and characteristic energy loss spectroscopy (CELS). It is the technique of AES which has enabled the reasonably confident determination of the 'atomically' clean surface. (It must be remembered, however, that AES will not detect hydrogen.)

The subject matter of this thesis is intended as a contribution to the surface study of selected materials. We aim particularly at obtaining detailed secondary electron emission yield (SEE yield), Auger, and energy loss spectra from pure elements and then proceeding to observe the quite considerable changes produced upon the first stages of oxidation.

In the following section of this chapter some information about surface science and the different techniques used in surface analysis are briefly discussed. In chapter two the subject of SEE yield is reviewed with chapter three devoted to AES and CELS, particular emphasis being placed on the more recent developments in these techniques. Chapter four describes the construction and operation of a suitable apparatus for SEE yield, AES and CELS. The remaining chapters are devoted to presenting the results from the solid surfaces; beryllium (Be) and magnesium (Mg) both in the atomically clean form and as they are subsequently oxided slowly. The final chapter is concerned with general conclusions and suggestions for future work.

1.1 Surface Science

The subject of surface science is the study of the chemical compositions and atomic arrangements at the surfaces of solids and the theory and observation of their mechanical, electronic and chemical properties. The measurement and understanding of phenomena at a surface (a surface is normally thought of as the top few atomic layers of a solid) is one of great scientific interest and enormous technological significance. However, still the knowledge about fundamental processes at surfaces and interfaces is rather limited. The great difficulties in the understanding of heterogeneous catalysis, corrosion protection, semiconductor and thin film technology have spurred many scientists to develop new tools for the study of surfaces and to learn more about the chemical and physical nature of the solid in its outermost atomic layers. Concurrently, the commercial availability of surface analysis instruments and the mature stage of ultra high vacuum equipment in general is already beginning to have a major impact on further progress of the applied sciences.

The use of ultra high vacuum is in general considered as an advantage since it permits the investigation of surfaces under near static and stable conditions. However, for many questions of technical importance especially those in the field of catalysis and corrosion, the high vacuum required by the surface analytical technique itself may actually be a drawback. The availability of surface analytical tools that operate while the surface is in contact with a liquid or high gas pressure remains a major need in this section of surface science. While such a technique would allow analysis of the surface under the conditions to which they are exposed in reality, the present tools are limited to investigations under static very low gas pressure conditions. Possible major differences in composition and structure of surfaces

under these two conditions are the reason for a "credibility gap" between pure surface science and some applied technology.

Surface analytical tools mostly make use of particles such as photons, electrons, atoms, molecules or ions. As in material science in general, the most valuable information is obtained by various kinds of spectroscopies. Surface spectroscopies, however, encounter the difficult problem of being selective to a rather small number of surface atoms compared to bulk atoms sampled at the same time. The natural way to circumvent this problem is to reduce as far as possible the number of contributing bulk atoms by using particles of an appropriate energy that probe only a few A^{o} into the solid. Nevertheless separation between surface and bulk properties may still remain difficult.

Each particular method of investigation usually provides different information about the surface and the usefulness of any specific technique will depend on the particular property of interest and the material to be investigated, generally it is best to use several techniques in conjunction.

A brief description of a few of the important techniques used in surface science may be given as follows:-

1) LEED. (Low Energy Electron Diffraction), (Estrup and McRae 1971, Prutton 1971). LEED has found widespread use for the investigation of surface structures. However, there are two limitations to the LEED technique. First, for optimum use, the atoms under study must have a periodic array (single crystal) and, second, because of multiple scattering effects, detailed calculations of LEED intensities are often required to determine the structure. Present interest is mostly focussed on the use of LEED for the investigation of surface imperfections such as steps, kinks and adatoms. In the LEED technique, a low energy (10 - 1000 eV) electron beam is made to strike a crystal surface at normal incidence.

Elastically scattered electrons are post deflection accelerated on to a fluorescent screen and usually produce a geometrical pattern of bright spots on the screen. Diffraction occurs when the primary electron wavelength is a simple fraction of the surface atomic spacing.

2) RHEED. (Reflection High Energy Electron Diffraction). Electrons of higher energy (about 30 Kev) have also been used for surface studies when introduced at glancing incidence ($\sim 3^{o}$) to the surface plane. Because of the glancing angle, the diffracted beams are extremely sensitive to surface topography. This sensitivity is advantageous in studying such phenomena as the nucleation of oxides, faceting of surfaces, and, in fact, it is possible to obtain information on the morphology of surface nuclei at very small total coverages.

3) AES and CELS. In the few years since the utility of AES for surface study was demonstrated (Harris, 1968), AES has rapidly become an essential instrument in surface physics laboratories. With AES and a mass spectrometer to monitor partial pressures in a vacuum system the experimenter can make a fairly complete chemical analysis of an adsorption system - both gases impinging on a surface and the chemical composition of the surface itself. The characteristics of AES which make it so useful are that all elements except hydrogen can be detected with roughly comparable sensitivities, and the height of an AES peak for a surface species is approximately proportional to its density for monolayer or submonolayer densities. The latter assumes that peak shape changes due to chemical shifts can be accounted for and that the adsorbate is confined to the surface layer. Both of these characteristics are predicted theoretically and have been verified experimentally in all systems so far examined. With characteristic energy loss spectroscopy, electronic transition and surface vibrations of clean and gas-covered surfaces have been investigated. CELS provides information about the spectrum of unfilled electron states near the surface in combination with valence and core level spectroscopies.

The recent application of electron energy loss spectroscopy in the very low energy region of a few millielectron volts to studies of surface vibrations modes may be even more important. Indeed, the localized vibrations of adsorbates contain collective and structural information about the degree of dissociation, binding energies, binding sites and lateral interactions. These studies may therefore contribute significantly to catalytic research. This latter type of experimentation requires however very special instrumentation much more elaborate and refined that the usual CELS. The electron stimulated AES and CELS techniques are easy to use and commercial apparatus of good sensitivity and resolution are available. These two techniques are more fully discussed in chapter three.

4) XPS and UHV. (X-ray and Ultra Violet Photo Electron Spectroscopy). Photon excited electron spectroscopies have attracted much attention in the past, and the basic principle of the photoelectric effect, has been known and reasonably well understood for about seventy years. The development of XPS or equivalently ESCA (electron spectroscopy for chemical analysis) (Siegbahn et al., 1967, 1969) techniques to their current state of refinement have required advances in UHV technology, the development of intense x-ray sources, improvement in electron detection equipment, and the continual refinement of spectrometer design to achieve instrumental energy resolution comparable to natural energy level widths. In ordinary laboratory conditions, the photon energy for UPS and XPS are up to 40.8 eV (He II line) and $\sim$ 1-1.5 Kev (typically Al-K_α and Mg-K_α with 1486.6 eV and 1253.6 eV), respectively, although the recent use of syncrotron radiation has extended the field considerably. Both spectroscopies probe the electronic spectrum with an information depth determined by the kinetic energy of the excited electron. Surface sensitivity ranges from 10^{-1} to 1 monolayer for UPS and XPS,

respectively. Because of the higher energy of the x-ray photons XPS will probe electrons in the core levels of the atoms whereas UPS will only excite the valence band electrons of solids. By analysing the ejected particles the binding energy of the electrons within the specimen can be deduced so that elemental identification, at least with XPS is possible. Additionally, the influence of the chemical environment of an atom and the chemical bond is reflected in the "chemical shift" of the core level and in changes in the overall shape of the spectra in the valence band region. Photons cause less radiation damage than electrons and little or no surface charging of the specimen but the cross-section for photo-electron emission is small and intense sources (other than the previously mentioned syncrotron radiation sources) cannot be obtained so that long counting times are needed for photoelectron spectroscopy, nevertheless XPS and UPS are powerful techniques for probing the electronic structure of solids, and they have a distinct advantage over AES in that they allow one to determine the valence state of the analyzed species. They are also more applicable to the chemical analysis of polymeric materials than AES.

5) APS. (Appearance Potential Spectroscopy), (Park et al., 1970, Park, 1975). In APS, a solid surface is bombarded with electrons and the total soft x-ray yield (SXAPS) is detected as a function of the incident electron energy (0-1500 eV, variable during the experiment). When the energy of the incident electron is in excess of the binding energy of the core electron, there is the possibility of exciting this electron to an empty state above the Fermi level. It is normally assumed that the de-excitation process leads to a contribution to the observed x-ray intensity. The technique can be used to probe the empty states above the Fermi level.

6) EXAFS. (Extended X-Ray Absorption Fine Structure), (Lytle et al., 1975; Stern et al., 1975 and Knapp and Fradin, 1979). This technique

is only beginning to be applied as a tool to determine structural properties in materials science. The usefulness of this technique is its unique capability to yield information on identities, numbers, and radial distances of near neighbours around the x-ray absorbing atom. An EXAFS experiment requires a very accurate determination of the x-ray absorption coefficient. Large numbers of photons must be utilized in order to achieve this determination. The pioneering experiments of Lytle et al. (1975) were carried out using fluxes of only 10^3 to 10^4 photons per sec., by using a conventional 1 KeV x-ray generator and a flat crystal monochromator. However, today most EXAFS experiments are carried out at the Stanford Synchrotron Radiation Laboratory (SSRL), which has an x-ray intensity of 10^8 to 10^{10} photons/eV/sec. The EXAFS technique, especially utilizing detection schemes that emphasize the surface such as Auger (Lee, 1976) or electron energy loss (Stohr et al., 1978), has advantages for many surface structure problems. EXAFS is sensitive to the local environment of the x-ray absorbing atom. Thus it is suitable for both ordered and disordered layers.

7) The Atom Probe and Field Ion Microscopy (Müller, 1970). These methods are powerful surface characterization techniques. The atom probe field ion microprobe identify single atoms. There is considerable restriction on the specimens however, which must be in the form of fine spherical tips (radius of a few hundred Angstrums). In addition, the surfaces must be studied under very large applied electric fields, and the methods are usually only applicable to refractory metals.

8) Secondary Ion Mass Spectroscopy (SIMS) and Ion Scattering Spectroscopy (ISS). In SIMS (Park et al., 1970) ions of a rare gas (Ar^+, Ne^+, He^+) are formed into a beam and focussed on to the surface of a solid. If the incident ions are sufficiently energetic ($\sim$ 500 eV) they interact in a nearly classical manner with the atoms knocking them into the

vacuum with billiard ball-like collisions. Some of the ejected particles are ionized and can be detected by a mass spectrometer. The high sensitivities of quadrupole mass spectrometers and electron multipliers means that 10^{-6} of a monolayer can be detected by this method. However the technique is surface destructive although the rate of removal of atoms can be controlled and in fact made quite small. ISS methods measure the change in energy of light ions, usually H^+ or He^+ scattered inelastically from a surface (Smith, 1971). The energy loss may be related to the scattering particle and ion masses, hence the scattering particle can be identified. The method requires an accelerator and incident energies from KeV to MeV have been used. This technique is also destructive and is without quantitative interpretation.

In the foregoing introduction, we have briefly described why surfaces are studied and some of the techniques which may be used in their investigation. The next section will consider the important features of SEE yield, Auger Electron Spectroscopy and Characteristic Energy Loss Spectroscopy in more detail as these techniques are particularly relevant to the work presented in this thesis.

CHAPTER 2

SECONDARY ELECTRON EMISSION

2.1 Introduction

An electron may be emitted from a solid surface if it reaches the surface with sufficient energy to overcome the surface potential barrier. Secondary electrons may originate in a variety of ways; some will have energies that are characteristic of the surface atoms and others not so. Those electrons with characteristic energies can give much information about the physical and chemical make-up of the surface, whilst the 'random' energy electrons have largely only a nuisance value at present, by a giving noise problem.

In this chapter some properties of those secondary electrons with characteristic energy will be defined, and in addition a brief review of previous works on secondary electron emission is given followed by some of its theoretical aspects and their quantitative calculations.

2.2 The Secondary Electron Yield

When a surface is bombarded with electrons, it may be possible for the surface to emit more, or less electrons than those in the incident primary beam. Hence, conventional current can either flow to or from the target. The secondary electron yield δ, is a ratio which quantifies this property. If i_s and i_p are the total secondary and primary currents respectively, then δ is defined as

$$\delta = \frac{i_s}{i_p} \qquad (2.1)$$

According to this definition, the yield includes these three categories of emitted electrons which are;

a) Elastically reflected primaries

b) Inelastically reflected primaries

c) 'True' secondaries

(These are illustrated by the secondary electron distribution in section 2.3). The two former categories are the so-called backscattered electrons and the latter one is defined as 'true' secondary electrons with energies less than 50 eV, this latter figure being somewhat arbitrary.

For the great majority of specimens, the escape depth (section 2.5.2) of secondary electrons is one or two orders of magnitude smaller than the penetration depth of primaries (section 2.5.1), and it is therefore legitimate to subdivide the secondaries into two categories, Fig (2.1) (Wells, 1974). First there are the secondaries that are excited by the primaries as they enter the specimen. The secondary emission yield for these is δp. Also, there is the probability that a backscattered electron will generate a secondary as it leaves the specimen. Then the total secondary electron yield is defined as (section, 2.5.5)

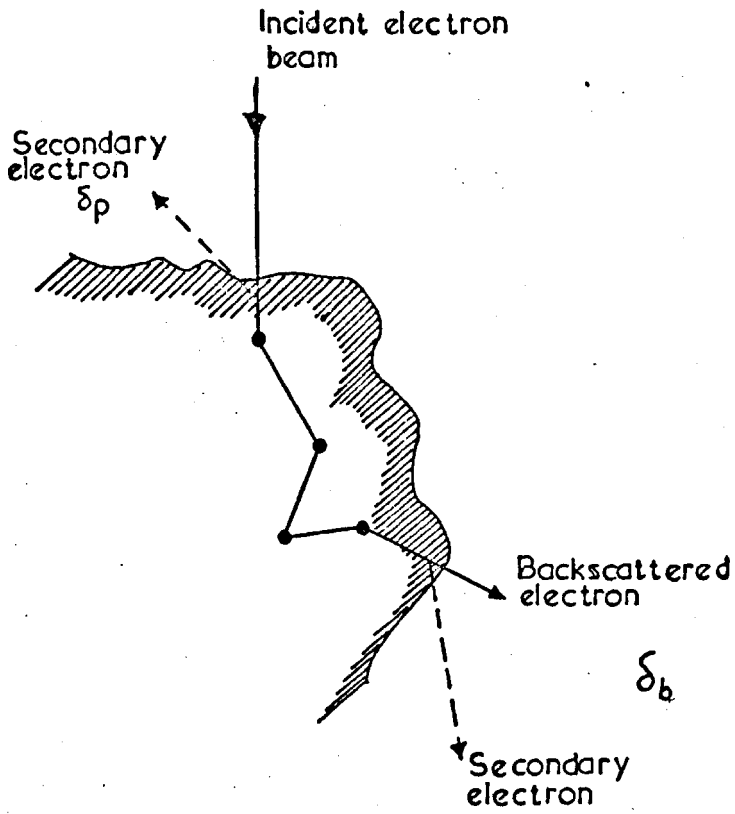
Incident electron beam
Secondary electron
δ_p
Backscattered electron
δ_b
Secondary electron

FIG.2.1

$$\delta = \delta p + \delta_B$$

For high-resolution scanning microscopy the first of these is beneficial, while the second adds noise to the signal.

2.2.1 The Yield Curve

One of the most important phenomena in secondary electron emission is the variation of δ with the energy Ep of the incident primaries known as the "yield curve". In general this curve has the same overall shape for all materials which is shown in Fig. (2.2).

The yield increases from low primary energies, then goes through a maximum value δ_{max} at E_{Pmax} and finally decreases for high primary energies. Insulators, oxide of metals like BeO and MgO (Chapters 5 & 6) and alkali halides have a maximum yield much greater than unity ($\delta_{max} > 1$). Low yield surfaces such as metal blacks may have yield values as low as 0.5.

The yield curves have the following qualitative interpretation. When the energy of primaries is low, the penetration depth of the primaries is relatively small, therefore, most of the secondaries are created near the surface region, where their escape probability is high. When the primary energy is increased the number of internal secondaries increases as well, but, since the penetration depth of the primaries is increased some of the secondaries lose so much energy through repeated collisions on the way to the surface, or some of them are backscattered. Therefore, the number of escaping secondaries is proportional to the increasing of the primary energy. As the primary energy increases, the penetration depth increases further, and the yield continues to increase until it gets to its maximum value at some value of the primary energy E_{Pmax}. After E_{Pmax}, when primary energy increases, the penetration depth increases further, so that the secondary electrons

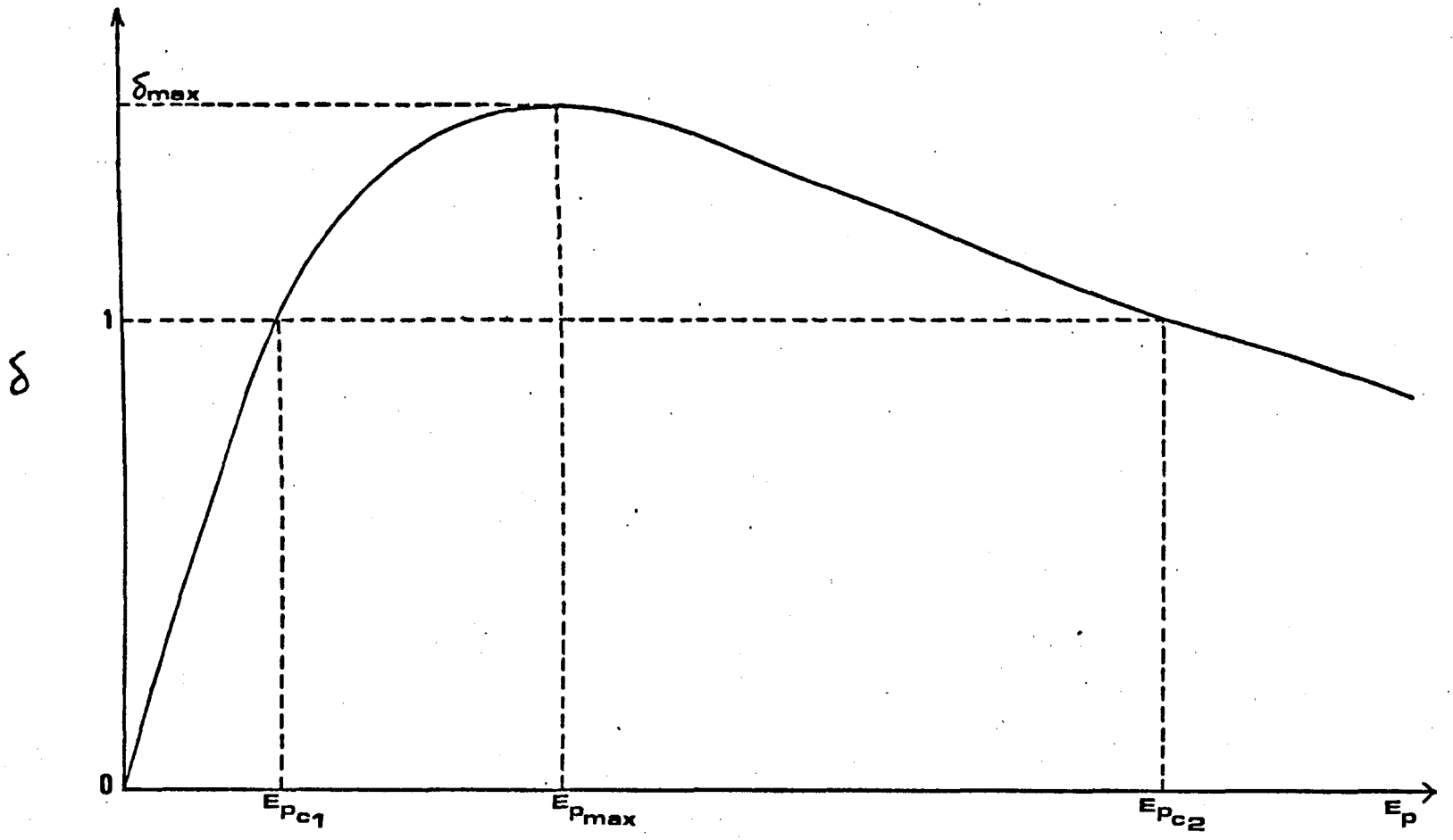

FIG-2.2 The Yield Curve

are created at distances greater than their escape depth and as a result the yield will decrease.

There are two other parameters in the yield curve, apart from δ_{max} and E_{max} which are termed the first and second primary energy crossovers (E_{Pc_1} and E_{Pc_2}); these are the points on yield curve where $\delta = 1$, as shown in Fig. (2.2). It is obvious that we can define these points on the yield curve only for those materials where their $\delta_{max} > 1$. Dionne (1975) suggested that δ_{max}, E_{Pmax}, E_{Pc_1} and E_{Pc_2} depend on the surface and bulk properties of the emitting material through simple relations, and in particular the first crossover energy can be very dependent on surface properties, whereas the energy at maximum yield is almost entirely controlled by bulk properties.

2.2.2 Universal Yield Curve

Although no entirely satisfactory quantitative theory of secondary electron emission has been developed to date (for review see Bruining, 1954; Hachenberg and Brauer, 1959), several attempts have been made to formulate a unified theory, which predicts a "Universal Yield Curve" for all materials, in view of the fact that, apart from quantitative differences, the secondary yield curves exhibit the same general shape.

For the first time Baroody (1950) pointed out that if one plots $\frac{\delta}{\delta_{max}}$ as a function of $\frac{E}{E_{Pmax}}$, a universal yield curve is obtained which should be valid for all materials. A somewhat different universal curve was obtained by Jonker (1952). Recently Kanaya et al. (1978) and Ono et al. (1979) have formulated the universal yield curve for insulators, metals and semiconductors, which are in reasonably good agreement with the experimental results. These universal curves have the same shape, but quantitatively they have some differences in their high energy parts, which depend on the properties of solids. More detail of their calculation is shown in section (2.5.5).

2.2.3 Dependence of Yield (δ) on the Angle of Incidence of the Primaries

Numerous investigators have determined the secondary emission yield with primary electrons under an oblique angle of incidence and have observed a larger yield than under normal incidence (Tate, 1921; Bruining, 1954; Oatly et al., 1965).

Two cases can be distinguished depending on whether the specimen is a single crystal or amorphous. With an amorphous specimen, the yield is a minimum with normal electron incidence, increasing smoothly as the incident angle becomes more nearly glancing (Müller, 1937) (Fig. 2.3a). With a single crystal, a fine structure is superimposed on the curve as determined by the Bragg planes in the crystal lattince (Laponsky and Whetton, 1960) (Fig. 2.3b), and in addition very recently surface resonances have been found (non stationary surface states) (McRae et al., 1979).

In the emission microscopes, an oblique angle of incidence is chosen to improve the image contrast (Möllenstedt and Lenz, 1963). Also, in scanning electron microscopes, as shown by Oatley et al. (1965), an oblique illumination is very effective in the satisfactory collection of the secondary electron emission, since too small a number of secondary electrons is subject to statistical quantum noise.

2.2.4 Angular Distribution of Secondaries

The energy angular distribution of the secondaries is a function which is of great significance in the formulation of any theory of SEE. The classical work in this field was done by Jonker (1951, 1957) who studied the angular distribution of secondaries from a nickel target. Alekseev and Borsov (1962) studied the same using MgO layers as a target.

FIG.2.3 Secondary electron emission versus incident angle. (*a*) For amorphous metals (*Müller 1937*) (*b*) for single-crystal MgO. (*Laponsky and Whetten 1960*)

One of Jonker's most outstanding results is that the low energy secondaries have an approximate cosine distribution. Ganachaud and Cailler (1979) also by using the Monte-Carlo calculation indicated that the true secondary electrons of Al have a nearly cosine distribution. This is shown in Fig. (2.4) for two primary energies E_p = 100 eV and 600 eV. These theoretical results are in good agreement with the experimentally observed behaviour quoted by Jahrreiss and Oppel (1972) which is quite general for metals. Owing to the cosine distribution of true secondaries outside the target, theoreticians infer that the true secondary electrons reach the surface after a complicated cascade process leading to a quasi isotropic inner angular distribution which in turn leads to the cosine outer distribution. This result is approximately independent of E_p.

As is reported by Ganachaud et al. for the backscattered electrons, the angular distribution depends strongly on the primary energy. At high values of E_p, the penetration of the primary beam is large. An important fraction of the electrons backscattered in the bulk of the solid thus has to suffer many collisions before emission. This favours an isotropic internal behaviour. At low E_p values, on the contrary the penetration is reduced and the number of collisions is also greatly reduced. Thus the external distribution can depart strongly from a cosine one. The overall shape of these distributions, drawn in a polar plot, which they have characterized by an eccentricity parameter $\chi = \frac{a}{b}$ as shown in Fig. (2.5). Their theoretical estimations for χ have been reported in this figure for several primary energies and Fig. (2.6) presents the calculated angular distribution for E_p= 150 eV. It may be noticed that χ varies quite strongly with E_p.

For oblique incidence of the primary electrons, Jahrreiss and Oppell (1972) and others found considerable deviations from the cosine

FIG.24 Angular distribution of the true secondaries in Al for E_p = 100 and 600 eV, compared with a cosine law (straight line).

FIG.2.5 Primary energy dependence of the excentricity parameter χ for the angular distribution of the backscattered electrons ($E_s > 50$ eV) in Al.
Ganachaud et al(1979).

FIG.2.6 Polar plot of the angular distribution of the back-scattered current in Al for E_p =150eV Ganachaud et al (1979)

distribution and show a correlation to the direction of primary electrons incidence. In re-emission they have found a maxima of intensity near the primary electron direction as well as near the direction of regular reflection (Fig. 2.7).

2.3 Energy Distribution of Secondaries

When investigating the secondary electrons, one of the more obvious features which may be studied, is the energy distribution. It is of prime importance both in applications of secondary emission and in the theoretical interpretation of the process.

If the number of secondary electrons emitted by the target, in the energy interval E and E + dE is plotted against E, a typical energy spectrum results. The general shape of the energy distribution of secondary electrons under primary electron excitation is shown in Fig. (2.8). The secondary electron distribution curve is usually known as the $N(E, E_p)$ curve where E is the energy of the electrons leaving the surface of the solid and E_p is the kinetic energy of the impinging electrons.

This energy distribution curve may be sub-divided into three characteristic parts:

a) Part I: At the high energy end of the spectrum dominates a narrow peak of elastically and quasi-elastically ($E = E_p$) scattered electrons. The small peaks (loss peaks) close to this elastic peak with energy $E = E_p - E'$ are presumably due to the electrons which have suffered inelastic collisions. E' is an energy characteristic mechanism producing the peak which may be for example, plasmons or interband transitions. These loss peaks are characteristic of the material and are usually known as characteristic energy losses (CEL). The CEL peaks move on changing primary energy along the energy scale by the same amount as E_p is altered, i.e. they are measured relative to the primary

FIGURE 2.7 Angular distributions of η electrons from Ag and Ni in re-emission, normalized to 0° direction. The deviations from the cosine distribution are given separately on the right half of the figure. T = target. Jahrreiss and Opell(1972)

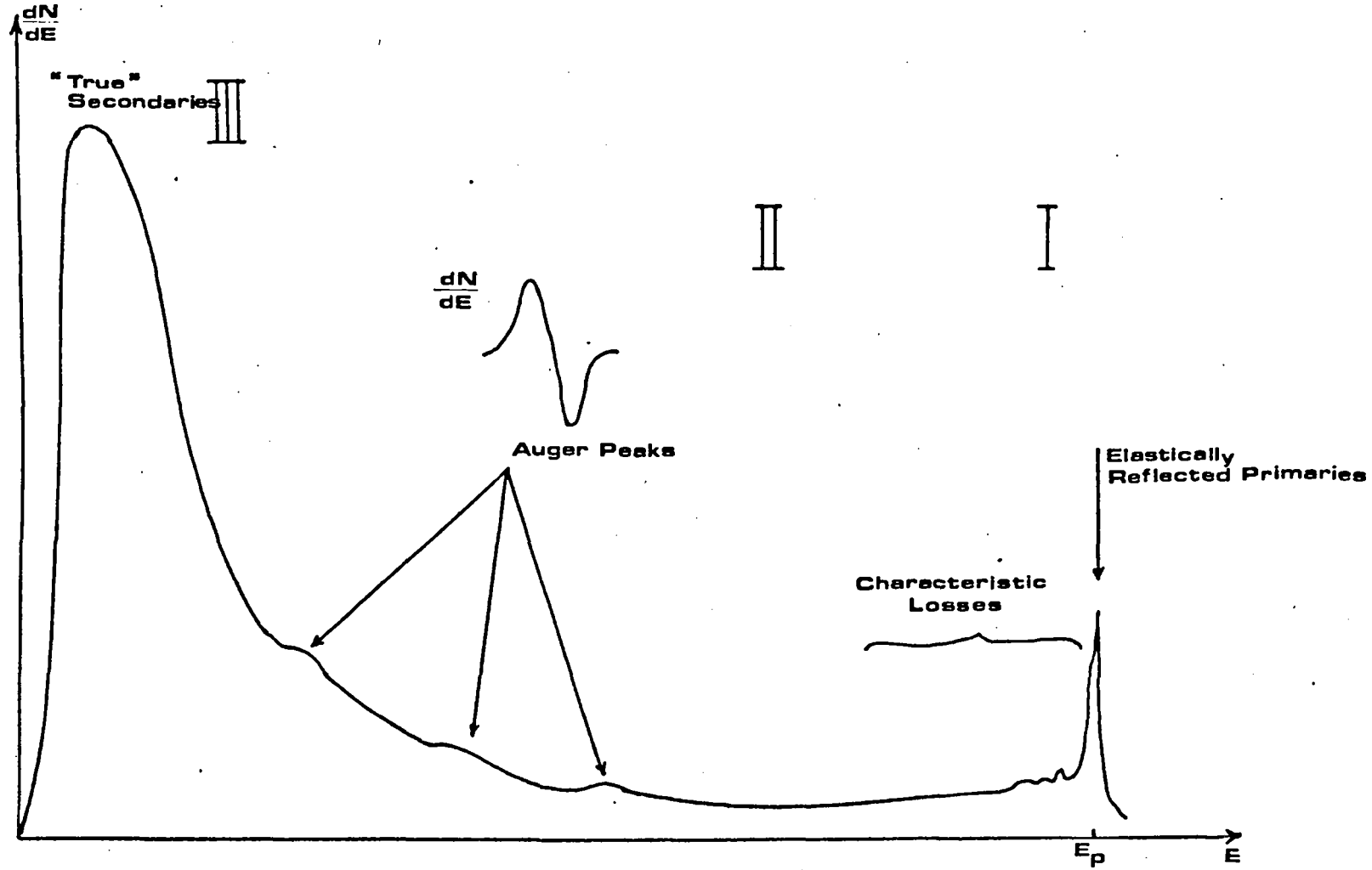

FIG. 28 The Secondary Electron Emission (SEE) Spectrum Exited By Primary Electrons of Energy E_p.

energy (for more detail, see part two in Chapter 3).

b) Part III: The low energy side consists of the so-called "true secondaries" which has a broad maximum (at 2-5 eV) compared to the elastic peak. The energy position of this low energy peak is essentially independent of primary energy E_p, and electrons emitted in this region are essentially the result of secondary processes, i.e. the emitted electrons have no "knowledge" of the initial excitation energy.

c) Part II: Both parts I and III join through a more or less flat background to a continuous distribution. In order to observe them more easily, it is clear that a convenient means must be found for suppressing the large background current. Harris (1968) first pointed out that this could readily be done by electronically differentiating the energy distribution, thereby obtaining $\frac{dN(E, E_p)}{dE}$ and suppressing the background. (The details of the method are discussed in chapter 4). The energy positions of these peaks are also independent of primary energy E_p. Hence, the Auger peak is easily detected by the fact that its energy does not change as E_p is varied. However, the magnitude of particular structure will invariably change with E_p variations, resulting from changes in the excitation strength. There are in addition to these classes of structure a number of other features. These include a broad high energy background of secondaries, which while featureless, is important with respect to measurement problems.

2.4 Review of some of the more Relevant Previous Theoretical and Experimental works on Secondary Electron Emission

Austin and Starke (1902) discovered the phenomena of secondary electron emission, for the first time, while they were studying the reflection of cathode rays from metal surfaces, they observed more electrons were emitted from the surface than electrons hitting it. This obviously could not be explained merely as reflection but rather

as the additional liberation of electrons from the metal under the influence of the bombarding electrons.

Since the work of Austin and Starke, many attempts have been made to explain secondary electron emission induced by electron bombardment qualitatively and quantitatively. The theories range from relatively simple empirical treatments to highly complex quantum mechanical investigations. Considerable experimental evidence has been gathered from metals, insulators and semiconductors under different conditions. Despite the long history of the phenomenon and the vast amount of study on it, many questions have yet to be answered regarding the actual production and escape mechanism of secondary electrons.

Early investigations on secondary electron emission had a very straightforward approach. Primary electrons bombard the surface of the material, where, by certain mechanisms, electrons are caused to leave the material. In recent years much interest has arisen in the use of secondary electron emission from bombardment of various solid targets with a finely focussed and highly accelerated beam of electrons for scanning electron microscopes. Accordingly, the quantitative analysis of secondary electron microscope images requires the exact values of yield, the escape depth of secondary electrons, and the contribution of backscattered electrons within a solid target.

Based on the assumption of two mechanisms in the secondary electron emission process (the production and escape mechanisms of secondary electrons), there have been several theories of secondary emission, such as:

a) The free electron Theory of Baroody (1950). Baroody in employing a Fermi model for the conduction electrons in metals, improved the situation considerably for this group of materials. His theory shows, among other things that the secondary yield for metals with high work

function is larger than for those of low work function. This had been found experimentally but could not be explained by the elementary theory. In fact, one would expect metals of high work function to have a low yield because it is difficult for secondaries to escape in that case.

b) The quantum Theory of the production of secondaries by Fröhlich (1932). Fröhlich pointed out that a completely free electron gas cannot produce secondary emission, since conservation of energy and momentum for the system consisting of the incident electron plus the free electron gas will make it impossible for secondaries to be emitted in a direction opposite to the direction of incidence of primary, whereas Baroody in his theory assumed that the incident primary electrons interact only nearly with the/"free" conduction electrons. This theory has been developed by Wooldrige (1939), Dekker and Van der Ziel (1952). There have been a number of modifications to the Theory by many investigators (Marshall, 1952; Van der Ziel, 1953; Baroody, 1953, 1956). The approach by these people gives an account of the production of internal secondaries in the metal. But to account for the secondary electrons emitted from the metal surface, it is necessary to study the escape mechanism of the internally produced secondaries. This could be done in a simplified manner on the basis of the assumptions made by Baroody.

c) The cascade Theory by Wolff (1954). He is of the opinion that the escape mechanism is more important than the production of these internal secondaries and he gave a theory of electron cascade process in which these secondaries diffuse through the solid, multiplying and losing energy, until they either are emitted as true secondaries or return to the sea of conduction electrons. In order to describe the electron cascade process, he used the Boltzman equation which was introduced by Marshak (1947) for neutron diffusion. Recently Bindi et al. (1978) have presented a new formulation and a method of resolution of the

transport Boltzman equation applied to SEE. This new approach incorporates for the first time in such models, both elastic and inelastic scattering.

d) The semi-empirical theories, the earlier theories formulated by Salow (1940), Bruining (1954) and Jonker (1952, 1954). In this theory, the process of SEE is divided into two distinct steps; the energy loss of primaries and the consequent production of internal secondaries and the escape of these internal secondaries. Without paying much attention to the actual velocity distribution of internal secondaries, Bruining assumed that the secondary electron yield, δ, may be written as

$$\delta = \int n(x, E_p)\ f(x)dx \qquad (2.2)$$

where $n(x, E_p)$ is the average number of internal secondaries produced per incident primary of energy E_p, in a thickness dx, at a depth x below the surface. The factor f(x) represents the probability for a secondary to escape from the surface. It is generally assumed that $n(x, E_p)$ is proportional to the average energy loss per unit path length and may be related by

$$n(x, E_p) = -\frac{1}{\xi}\frac{dE}{dx} \qquad (2.3)$$

where ξ is the energy required to excite one secondary electron inside the solid. The escape probability is determined by an exponential absorption,

$$f(x) = B\ e^{-\alpha x} \qquad (2.4)$$

where α is the absorption coefficient and B is a constant. The equation (2.2) may now be written as

$$\delta = -\frac{B}{\xi}\int \frac{dE}{dx}\, e^{-\alpha x}\, dx \qquad (2.5)$$

All the semi-empirical theories involve some form of this relation.

e) Power Law (Lye and Dekker, 1957; Dekker, 1958). In this law it is assumed that every incident primary penetrates to a depth R and gives up its energy according to the power law defined by equation (2.6)

$$\frac{dE}{dx} = -\frac{A}{E^{n-1}} \tag{2.6}$$

where A is a constant, characteristic of the material and (n-1) an arbitrary power, i.e. the energy loss is inversely proportional to some power of the energy and hence the name is "power law". By integrating the equation (2.6) it becomes

$$E^n(x) = E_p^n - An^x \tag{2.7}$$

If n = 2 we get

$$E^2(x) = E_p^2 - 2Ax \tag{2.8}$$

This is the celebrated Whiddington's Law (Whiddington, 1912) used by Bruining, Baroody and Jonker in their calculations.

When the energy of the primaries becomes zero, i.e. when $E^n(x) = 0$ they have attained their maximum range x = R. Then

$$R = \frac{E_p^n}{An} \tag{2.9}$$

Substituting this in equation (2.7) we get in general

$$E^n(x) = An(R - x) \tag{2.10}$$

or
$$E^{n-1}(x) = [An(R - x)]^{(n-1)/n} \tag{2.11}$$

A combination of equations (2.6) and (2.11) substituted into equation (2.5) produces an expression for the yield, δ as:-

$$\delta = \frac{B}{\xi} (An)^{1/n} \int_0^R \frac{e^{-\alpha x}\, dx}{n(R-x)^{(n-1)/n}} \tag{2.12}$$

Considering the large disagreement between the experimental results and the theoretical predictions Jonker (1952) attempted to modify the above theory. He assumed that the internal secondaries move in straight lines from their point of origin towards the surface. The distance the electron has to travel before reaching the surface must be measured from the point of origin to the surface, along the direction of flight. Thus, an electron originating at a depth x, below the surface, but moving at an angle θ, to the normal to the surface, has to travel a distance $\frac{x}{\cos \theta}$. In considering the probability of escape of secondaries, x has to be replaced by $\frac{x}{\cos \theta}$. Further he assumed that the internal secondaries produced, at any point in the medium, are isotropically distributed.

f) Constant loss law. This method is a more realistic model than the power law, because the scattering of the primaries is also taken into account. For the first time Young (1956), based on the results of his experiments, proposed a modification to the above model (Power law) to take into account the scattering of primaries. Although the power law would still govern the energy loss gradient, it was suggested that all primaries did not reach a depth R but scattered in a manner which caused a constant loss of energy throughout the range. In other words, the energy loss per unit path length is approximately constant throughout the primary electron range. Young (1956), from his experiments obtained that the practical range R of electrons in Al_2O_3, follows the relationship

$$R = \frac{1.15 \times 10^{-6}}{\rho} E_p^{1.35} \text{ cm} \qquad (2.13)$$

where ρ is the density in gm/cm^3, E_p is the primary energy in kilovolts. Assuming the validity of Young's results one can modify the elementary theory of SEE so as to take into account the scattering of the primaries.

One needs only replace $-\frac{dE}{dx}$ in equation (2.5) by its effective value $\frac{E_p}{R}$, and integrate between 0 and R, thus, the yield equation is

$$\delta = \frac{B}{\xi} \frac{E_p}{R} \int_0^R e^{-\alpha x} dx \qquad (2.14)$$

In recent works, Kanaya and Kawakatus (1972) and Dionne (1973, 1975) have developed the theory of secondaries by the generalized power law concerning the energy loss of electrons penetrating into a solid target making use of range measurements by Glendenin (1948), Katz and Penfold (1952), Lane and Zaffarano (1954), Young (1956), Holiday and Sternglass (1959) and by Cosslett and Thomas (1964). As a result of the development of computer simulation techniques, Monte-Carlo-Calculations are very useful to evaluate the secondary electron emission mechanisms from metals by electron beam bombardment and these have been developed recently by Shimuzu and Murata (1971), Shimuzu (1974), Pillon and Ganachaud (1977) and Ganachaud and Cailler (1979). However, even more recently Ono and Kanaya (1979) have presented a satisfactory solution of the secondary electron yield of metals and semiconductor compounds by applying free electron scattering theory to the absorption of secondary electrons generated within a solid target, also Kanaya et al. (1978) have presented a promising solution to the high yield and an explanation of the different yields appearing in terms of integral multiples of plasmon losses and in effect combined the free-electron scattering theory with the plasmon theory. Since in most of the calculations for Be and Mg in the present work the results of these two later papers have been used extensively, their calculations are explained in more detail in the next section.

2.5 A Formulation of Secondary Yield

For the formulation of secondary yield, there are two important factors which are needed for calculations;

i) The penetration range of primaries,

ii) The escape depth of secondaries $x_\alpha = \frac{1}{\alpha}$, where α is the absorption coefficient of secondary electrons generated within the solid target, and it is the most significant factor in the quantitative evaluation of the maximum yield δ_{max}, which in practice, is measured with its corresponding incident energy E_{pmax}.

These factors described quantitatively using the recent works of Ono and Kanaya (1979), Kanaya et al. (1978) and Kanaya and Ono (1978).

2.5.1 Penetration Range of Primary Electrons in Solid Materials

When a stream of electrons penetrates into a solid target, electrons may be scattered either elastically or inelastically. The energy of electrons are progressively reduced due to inelastic collisions with atomic electrons in which the incident electron excites or ejects atomic electrons or by excites valence electrons belongs to solid as a whole (i.e. plasmons) with loss of energy. The corresponding momentum transfer is small because electrons are light particles, but the energy loss is very large. Thus electrons are often supposed to travel straight into the target, suffering energy loss both due to ionization and plasma oscillation.

The energy loss may be defined as (Kanaya and Ono, 1978)

$$-\frac{dE}{dx} = N \int_0^{T_m} (d\sigma_i/dT)\, T dT \qquad (2.15)$$

where N is the number of atoms per unit volume, $N = (\rho/A)N_a$, (N_a is the Avogadro's number, ρ the density and A the atomic number), $d\sigma_i$ is

inelastic scattering cross-section, and T and T_m are the energy transfer in the collision and its maximum.

The basic range concept is then obtained simply by integration of dE/dx:

$$R = \int_0^E dE/(dE/dx) \qquad (2.16)$$

Both equations (2.15 and 2.16) give a simple connection between range, energy loss and differential cross-section.

The inelastic cross-section for energy loss due to the electronic collision have been obtained (Kanaya and Ono, 1978) by considering the potential energy of the incident electron in the atomic field of the target and assuming the diffusion model of electron beam penetration in the target [Fig. (2.9)]. [A diffusion model represents the electron scattering by a sphere whose centre is located at the maximum energy dissipation depth, which in turn is related to the diffusion depth and the range]. Then the differential of inelastic cross-section has been obtained as:

$$\frac{d\sigma_i}{d(T/T_m)} = \frac{\lambda^2 n\, \Gamma^2(1/n)\, 4Z\pi\, (a/a_H)^2 \sin^2\left[\left(\frac{1}{n}\right)(\pi/2 - \phi)\right]}{K^2\, \theta^2 \left[1 + (\theta/\theta_0)^2\right]^{1/n}} \qquad (2.17)$$

where θ and ϕ are scattering and deflection angle in the centre of gravity system, $K = 2n/\lambda$ (λ is the wave length of the electron) and $\theta_0 = \frac{\lambda}{2\pi a}$ (a is the screened atomic radius).

Now by substituting (2.17) in equation (2.15), the average energy loss $\frac{dE}{dx}$ is calculated:

$$\frac{dE}{dx} = \left[NZ\pi 4\Gamma^2 \left(\frac{1}{n}\right) \lambda_n^2\, a^{2-2/n}\, a_H^{2/n}\, E_R^{1+1/n}\, E^{-1/n} \left(\frac{n}{n-1}\right) \frac{(1+2\varepsilon E^2)}{(1+\varepsilon E)^{1+1/n}}\right.$$

$$\left. \times \left[1 - \frac{E_I\,(1 + 2\varepsilon E)}{4E(1 + \varepsilon E)}\right]^{1-1/n}\right] \qquad (2.18)$$

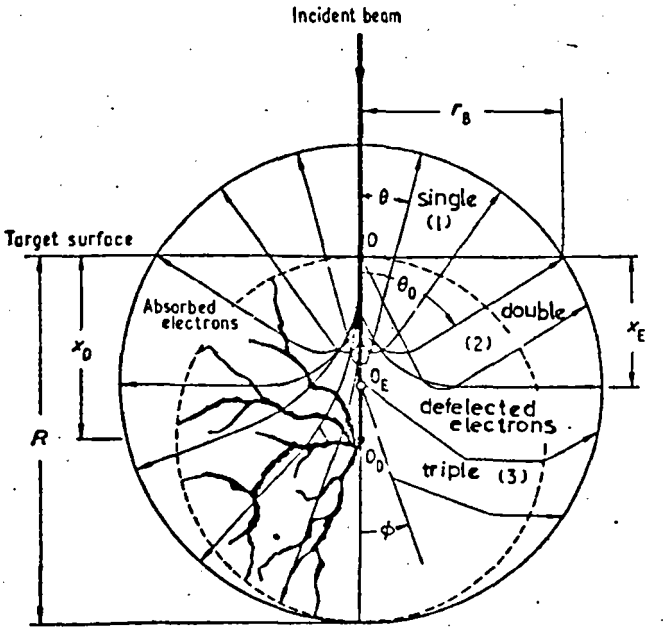

FIG·2·9 Modified diffusion model of electron-beam penetration in a target: R is the maximum range; x_D the diffusion depth; x_E the maximum energy dissipation depth; r_B the backscattering range; $\tan\theta_0 = r_B/x_E$. (1), (2) and (3) refer to the number of times the electrons are deflected.

where E_I is the suitably averaged ionization loss energy (E_I = 100 - 200 eV, Rauth and Simpson, 1964) depending on the excitation or ionization energy I, E_R is the Rydeberg energy, ε the relativistic correction factor giving the well-known relationship $\varepsilon = e/(2m_0c^2) = 0.978 \times 10^{-6}$ (eV^{-1}), $a = 0.77\, a_H Z^{-1/6}$ (A^o) the screened atomic radius, a_H the Bohr radius of hydrogen, Z the atomic number and λ_n is the scaling correction factor; $\lambda_n^2 = \frac{1}{2}$ for $n \lesssim 4$, $\lambda_n^2 = 0.1$ for $n \gtrsim 10 \sim \infty$, $\Gamma(\frac{1}{n})$ is the Gamma function.

On an empirical basis, the value of $\underline{n}$ as a function of the incident energy E_p and the value of $\underline{a}$ are both determined from the quantitative comparison between the theoretical and experimental results of interest in connection with the fundamental theory of electron scattering, such as mass range (Kanaya and Kawakatsu, 1972), energy loss and scattering amplitude (Zeithler, 1965). Fig. (2.10) shows the value of n versus the incident energy E, where the numerical parameter n is empirically formulated as:-

$$n = 1 + 2\exp(-\zeta + 2 \times 10^{-\zeta}) \qquad (2.19)$$

with $\zeta = \log(\frac{\varepsilon_i}{2})$ and $\varepsilon_i = {}^{a}/_{b}$, where ε_i is defined as the reduced energy (dimensionless) (Kanaya et al., 1973) and b is the so-called 'Collision diameter', given by

$$b = {}^{2e^2}/_{E_p} = 4a_H \left(\frac{E_R}{E_p}\right) (1 + 2\varepsilon E_p)/(1 + \varepsilon E_p) \qquad (2.20)$$

Now, by integrating (2.16) after substituting (2.18) in it, the range relation will obtain;

$$R = \frac{E_{p/E_R}}{C}^{1+{}^{1}/_{n}} \qquad (2.21)$$

with

$$C = 2\pi\,(n+1)\,NZ\Gamma^2\left(\frac{1}{n}\right) a^2 \left(\frac{a_H}{a}\right)^{2/n} (1 + 2\varepsilon E_p)^2 \times$$

$$\times \sin^2\left\{\frac{1}{n}\left[\frac{\pi}{2} - \tan^{-1}\left(\frac{aE_I\,(1 + 2\varepsilon E_p)}{4a_H\left[E_pE_R(1+\varepsilon E_p)\right]^{\frac{1}{2}}}\right)\right]\right\}\left[(n-1)\,(1+\varepsilon E_p)^{1+{}^{1}/_{n}}\right]^{-1} \qquad (2.21a)$$

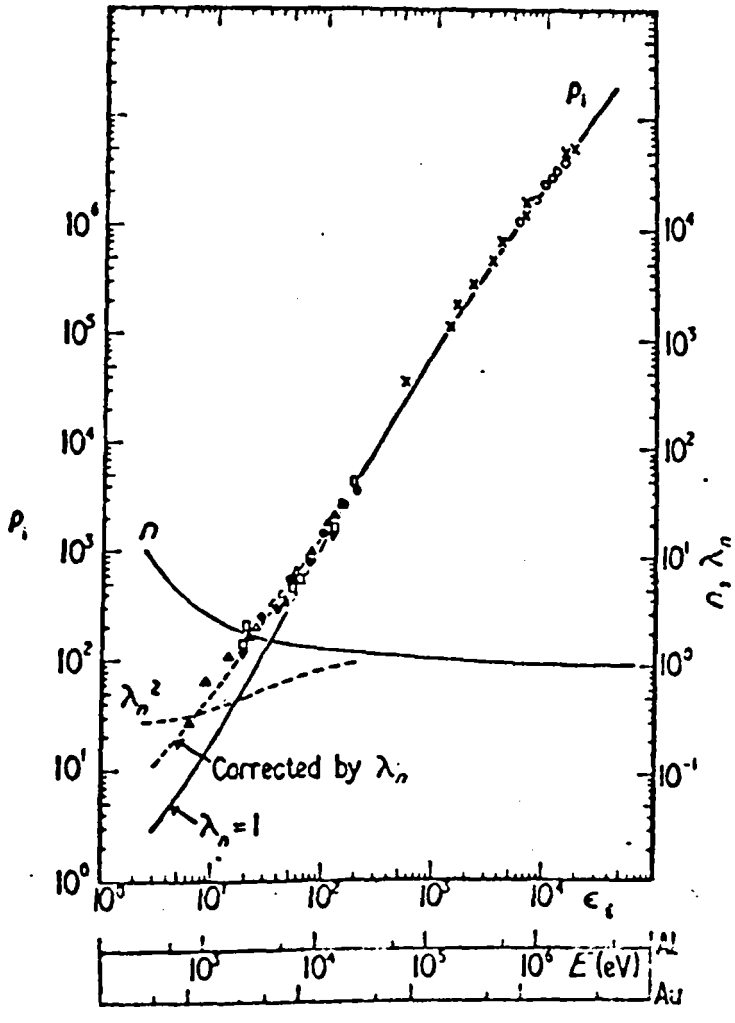

FIG.2.10 Reduced range ρ_l ($=RNZ\pi a^2$) and numerical parameter n as functions of the reduced energy ϵ_l ($=a'_l b=aE/4a_H\epsilon_R$) and the incident energy E for Al and Au, with $n=1+2\exp(-\xi+2\times10^{-\xi})$ and $\xi=\lg(\epsilon_l/2)$. Experimental points: ×, Al, Glendenin (1948); ○, Al, Katz and Penfold (1952); △, Al, Young (1956); □, Al, Holliday and Sternglass (1959); ●, Al, Cosslett and Thomas (1964); ■, Cu, Cosslett and Thomas (1964); ▲, Ag, Cosslett and Thomas (1964); ▼, Au Cosslett and Thomas (1964). Theoretical work:—Kanya et al (1976)

This satisfies quantitatively the experimental results of Young (1956), Holliday and Sternglass (1959), Glendenin (1948), Katz and Penfold (1952), Cosslett and Thomas (1964) and the calculations of Berger and Seltzer (1964), as shown in Fig. (2.11), where $\lambda^2 n = \frac{1}{2}$.

From equations (2.18) and (2.21) the energy E of electrons at depth x is expressed in terms of the reduced depth $y = \frac{x}{R}$.

$$E/E_p = (1 - y)^{n/(1+n)} \tag{2.22}$$

The back-scattering energy E_B of electrons at depth y is also given by

$$E_B/E_p = (1 - y)^{n/(n+1)} \left(1 - \frac{y}{\cos\theta}\right)^{n/(n+1)} \simeq (1 - y)^{2n/(1+n)} \tag{2.23}$$

where θ is the scattering angle of electrons relative to the normal.

The most probable energy dissipation depth $y_c = \frac{x_c}{R}$ in the diffusion model (Kanaya and Ono, 1978) is related with the mean energy of back-scattered electrons $\bar{E}_B$ as follows

$$\bar{E}_B/E_p = (1 - y_c)^{2n/(1+n)} \tag{2.24}$$

which is in close agreement with the empirical formula of Sternglass (1954), $\bar{E}_B/E_p = 0.45 + 2 \times 10^{-3} Z$

The equations (2.22) and (2.23) are called the energy retardation relationships of the primary and backscattering beam.

2.5.2 Absorption Coefficient α and Escape Depth $x_\alpha = \left(\frac{1}{\alpha}\right)$

a: α and x_α for Metals and Semiconductors

By assuming that the secondary electrons are distributed according to the Lenard (1918) law after their dislodgement, and that these secondaries relate with the suitably averaged ionization loss, since their energy produced by the first collision of the primary electrons

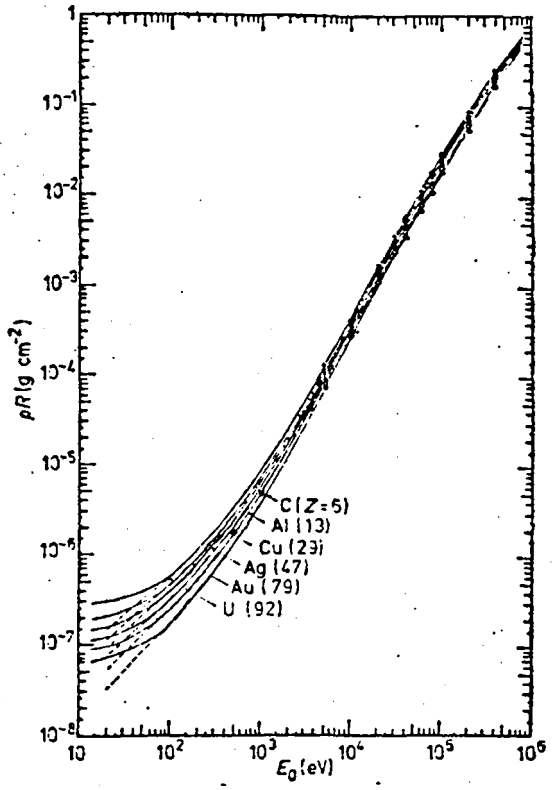

FIG·2·11 Energy dependence of mass-range ρR for several targets. Experimental points: Berger and Seltzer (1964); Cosslett and Thomas (1964a); Glendenin (1948); Katz and Penfold (1952); Young (1956); Holliday and Sternglass (1959) for U (+), Au (○), Ag (×), Cu (△), Al (○) and C (●).

with the target is very small, i.e. E_s = 100 - 200 eV (Rauth and Simpson, 1964), Ono and Kanaya (1979) have obtained the escape depth, x_α of secondaries as a function of first ionization energy I, atomic number Z, atomic weight A_0 and density ρ.

On this assumption, they have assumed that the fractional distribution of secondary electrons obeys an exponential relation

$$\frac{i_s}{i_p} = \exp(-N\sigma_i x) = \exp(-\alpha x) \qquad (2.25)$$

where i_s is the secondary emission current, i_p the primary beam current, N the number of atoms per unit volume, and σ_i is the total scattering cross-section due to the loss of secondaries. The total cross-section σ_i (Kanaya and Ono, 1976) is given by

$$\sigma_i = \lambda^2_\infty \, 4\pi \, Za^2 \left(\frac{E_R}{E_s}\right) \ln\left(\frac{4E_s}{I}\right) \qquad (2.26)$$

where λ^2_∞ = 0.1, which is determined empirically and n = ∞ is assumed because the energy of secondary electrons is very low. The ionization energy E_s is ranged between 92 and 235 eV for Al, Cu, Si and Ai (Rauth and Simpson, 1964), and it can be approximated as:-

$$E_s = n_s I \qquad (2.27)$$

where n_s, the constant is taken to be n_s = 20.

Accordingly, the most probable escape depth of secondary electrons x_α, in a similar manner to the diffusion model by Archard (1961), from $\frac{i_s}{i_p} = \frac{1}{e}$, is given by

$$x_\alpha = \frac{1}{\alpha} = 2.67 \, A_0 I/\rho Z^{2/3} \, A^o \qquad (2.28)$$

This relation for escape depth of secondaries is in good agreement with Seiler's (1967) data for most of the materials (metals and semiconductors). Figure (2.12) shows the escape depth of secondary electrons x_α as a

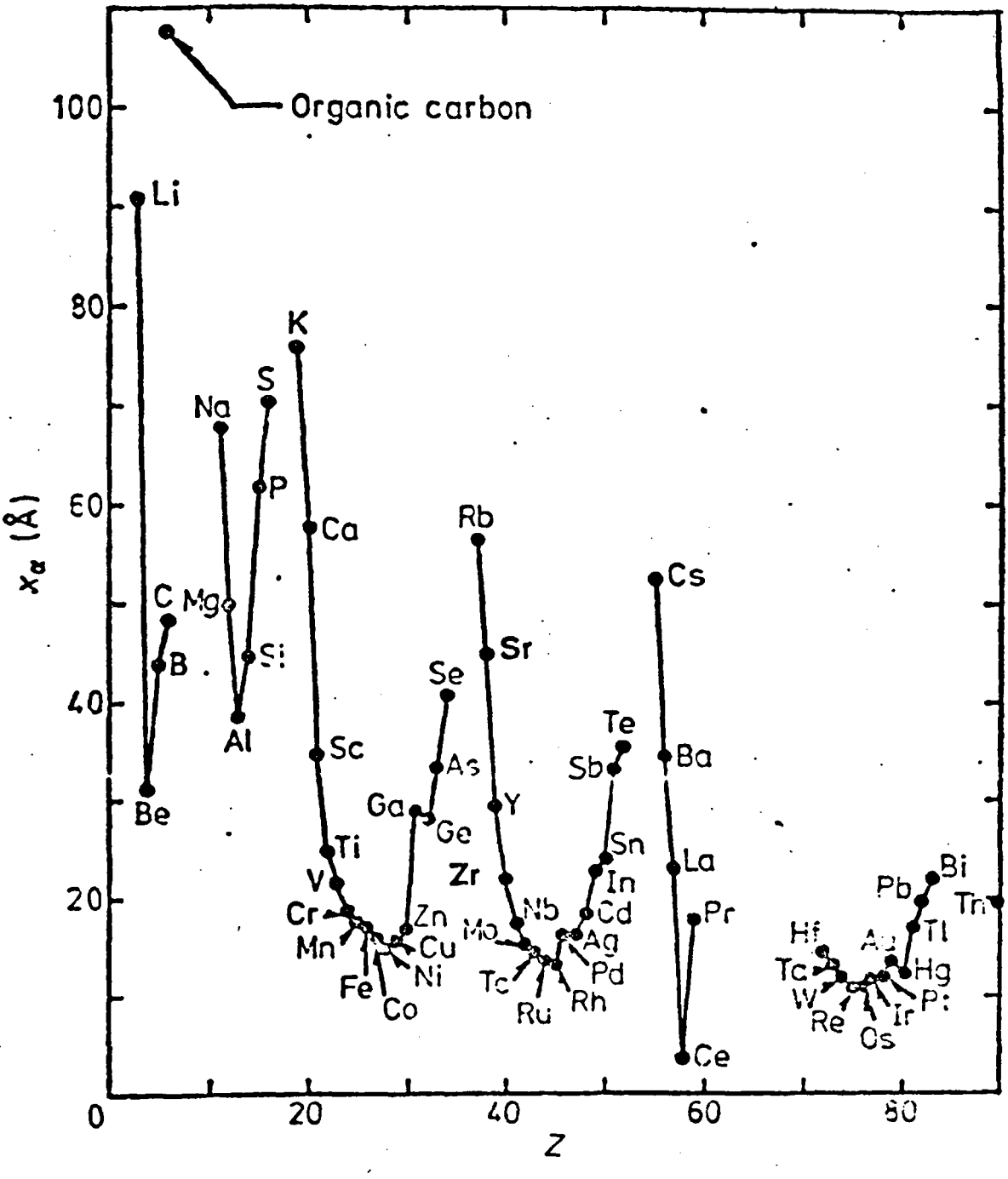

FIG 2.12 The escape depth of secondary electrons X_α as a function of atomic number Z. $X_\alpha = 2.67\, A_0 I / \rho Z^{2/3}(A^\circ)$.
Ono and Kanaya (1979)

function of the atomic number Z.

b: α and x_α For Insulators

As mentioned by Kanaya et al. (1978) the high yield δ = 1.5 - 20 of secondary electron emission from insulators due to electron bombardment may be caused by the very large escape depth x_α = 500 - 1000 A^o; namely the small absorption coefficient. Then the most dominant energy losses are considered to the suitably averaged ionisation loss in the first collision and to the plasmon loss due to the interaction with the valence electrons of the higher energy escaping secondaries because of the large energy gap about 5 - 15 eV.

By the same assumptions as the previous subsection, the transmission fraction of secondaries is given by

$$\frac{i_s}{i_p} = \exp(- N_p \sigma_p x) = \exp(- \alpha x) \qquad (2.29)$$

where $N_p = N_a \rho \nu / A$ is the electron density contributing the plasmon loss, ν the number of the valence electrons and σ_p the scattering cross-section due to plasmon loss. If the amount of energy transfer can only occur in integral multiples of elementary energy loss of $\hbar w_p$ (Marton et al., 1954), where w_p is the frequency of plasma oscillations ($\hbar = \frac{h}{2\pi}$), and the total cross-section $N_p \sigma_p$ (Ferrell, 1956) becomes;

$$N_p \sigma_p = \lambda^2_p \left(\frac{\theta_E}{a_H}\right) \ln \frac{4E}{\Delta E} \qquad (2.30)$$

in which $\theta_E = \frac{\Delta E}{2E}$, $\Delta E = 28.8 \, (\rho\nu/A)^{\frac{1}{2}}$ (eV) and $N_p = \Delta E^2/(16\pi \, a^3_H E_R^2)$ where $\lambda^2_p = 0.054$ is the correction factor necessary at low energy, $E \lesssim 1$ KeV.

Accordingly, the most probable escape depth of secondaries x_α is, from $\frac{i}{i_p} = \frac{1}{e}$ and $E = E_s$, given by

$$x_\alpha = \frac{1}{\alpha} = \frac{2 a_H E_s}{\lambda^2_p \, P \, \Delta E \, \ln(4E_s/\Delta E)} \qquad (2.31)$$

where Kanaya et al. (1978) define p as the normalised ratio of the plasmon loss ΔE_p under consideration to the most probable plasmon loss ΔE; i.e. $p = \frac{\Delta E_p}{\Delta E}$, however, by way of explanation this sentence leaves something to be obscured; alternatively p may be thought of as the probability of a given electron exciting a plasmon.

Owing to the ionization E_s is ranged between 153 and 232 eV for Al_2O_3 (Rauth and Simpson, 1964), by using equation (2.27) Kanaya et al. (1978) have approximated $n_s = 20$ from the assumption of $E_s = 190$ eV and $I = 9.46$ eV for Al_2O_3.

Accordingly, based on the foregoing empirical basis, the most probable escape depth of secondary electron emission x_α can be obtained as:-

$$x_\alpha = \frac{393}{p} \left(\frac{I}{\Delta E}\right) \left(\ln \frac{80I}{\Delta E}\right)^{-1} \qquad (2.32)$$

Figure (2.13) shows the calculated values of x_α versus $\frac{I}{\Delta E}$ for insulators of metallic oxides.

2.5.3 Secondary Yield due to Primary Electrons

As mentioned before, according to elementary theory (Salow, 1940; Baroody, 1950; Dekker and Van der Ziel, 1952; Dekker, 1958; Hachenberg and Brauer, 1959), the number of secondaries released in the material is proportional to the energy loss, and these secondaries are isotropically distributed in a solid target, following the absorption law after their dislodgement.

Suppose a primary beam current i_p falls perpendicularly on the solid target, as shown in Fig. (2.14). If any part of the secondary emission current i_s originates at a point x and reaches the surface by travelling a distance $l = x/\cos\theta$ through the material; then i_s is given by Jonker (1952) as:-

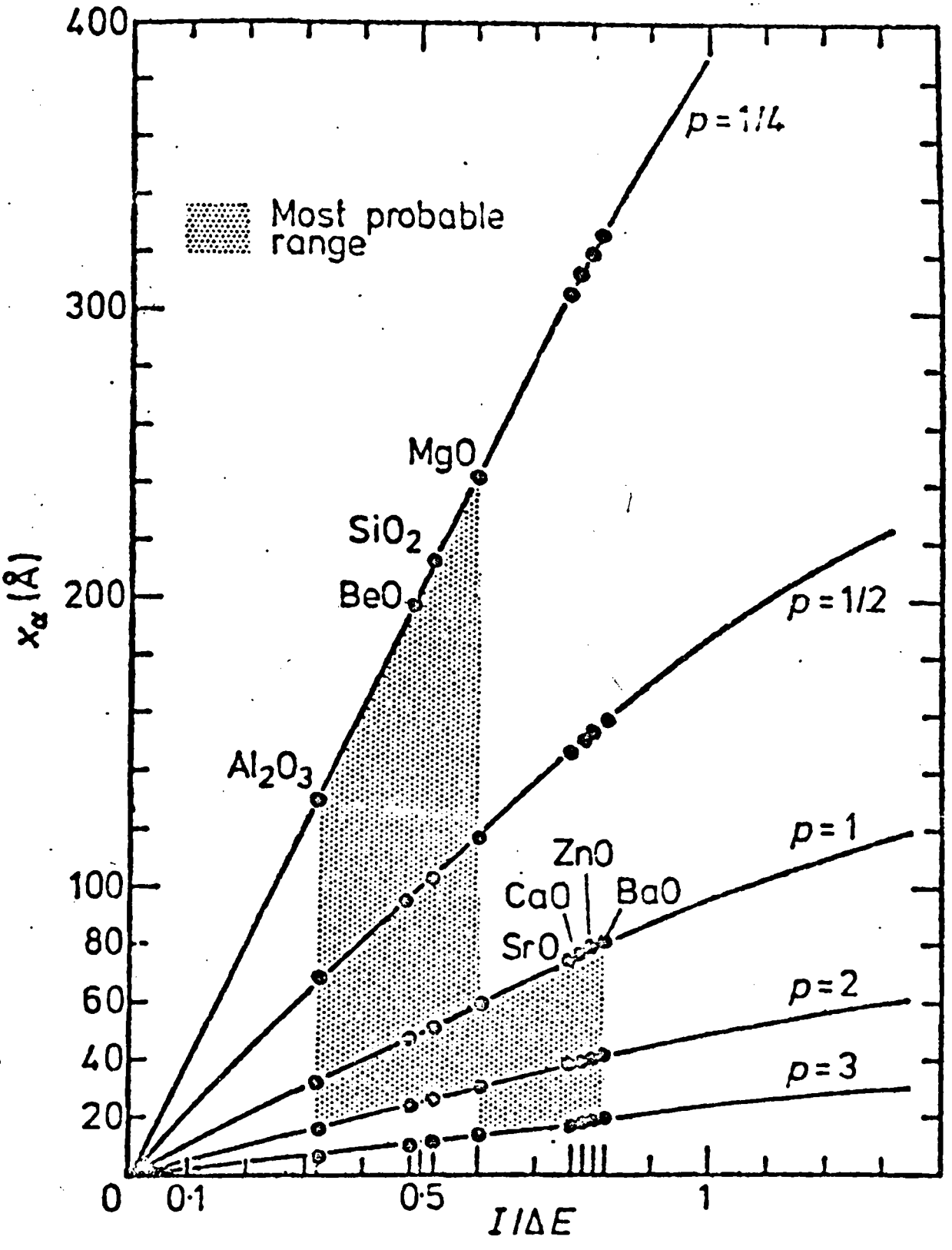

FIG.2-13 Escape depth of secondary electron emission for insulators of metalic oxides with $X_\alpha = (393/p)(I/\Delta E)[\ln(80I/\Delta E)]^{-1}$. (Dotted area shows the range between maxima and minia of the experimental results.) Kanaya et al (1978)

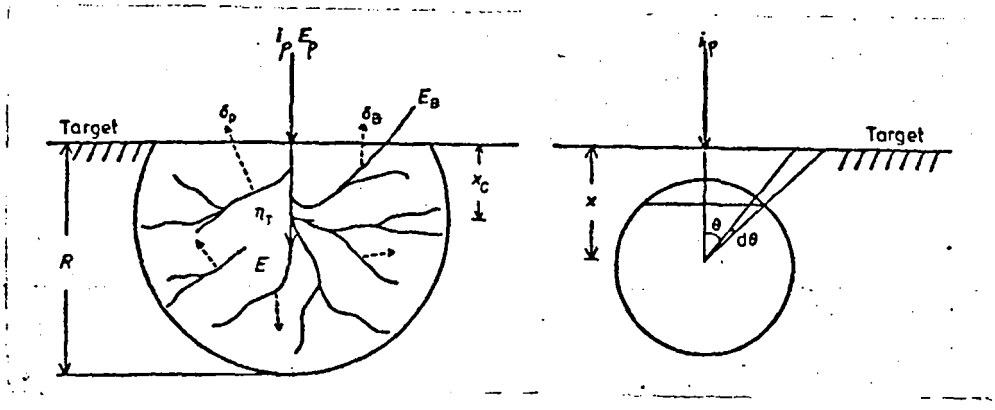

FIG.2.14 Production of secodary electron emission.

$$i_s = \frac{K}{2} i_p \int_0^R \frac{dE}{dx} \int_0^{\pi/2} \exp\left(\frac{-\alpha x}{\cos\theta}\right) \sin\theta d\theta \, dx \qquad (2.33)$$

where K is the constant depending on the penetration of electrons.

By using the range relationship, equation (2.21), and the resulting energy retardation, equation (2.22), the rate of energy loss is then given by:-

$$\frac{dE}{dy} = -\frac{n}{1+n} (RC)^{n/(1+n)} (1 - y)^{-1/(1+n)} / E_R \qquad (2.34)$$

by substituting (2.34) with (2.22) into (2.33), the secondary yield due to primary electrons, $\delta_p = \frac{i_s}{i_p}$, can be calculated as (Ono and Kanaya, 1979):-

$$\delta_p = \frac{K}{2} \left(\frac{C}{\alpha}\right)^{n/(n+1)} \int_0^1 \frac{n}{1+n} A^{n/(1+n)} (1 - y)^{-1/(1+n)} \left[\exp(- Ay + AyE_i (- Ay) \, dy \right] \qquad (2.35)$$

where $A = \alpha R = (\alpha/C) (E_p/E_R)^{1+\frac{1}{n}}$ and $E_i(- x) = - \int_x^\infty \exp(- t)/t dt$ is the function of the exponential integral.

2.5.4 Secondary Yield Due to Back-Scattered Electrons

Most incident electrons are scattered through small angles as they interact with atoms and the penetration increases as the primary beam spreads in a gaussian manner. In addition to the small angle scattering, however, some electrons approach close enough to an atomic nucleus to be scattered through large angles ranging up to 180^o. In such cases, many electrons will then be reflected back by large angle scattering. Consideration of these back-scattered electrons becomes especially important. According to Kanter (1961) the back-scattered electrons that diffuse back from the interior of the material follow a cosine distribution. Therefore the rate of energy loss and the path lengths

of backscattered electrons in the secondary escape region are large compared with those of the incoming primaries. Thus the proportion of the secondary electron yield due to backscattered electrons cannot be disregarded even when the back-scattering coefficient η_B is relatively small, and also it should be remembered that, they have a component of momentum outward towards the surface and are thus in a better situation to escape or to give an outward component of momentum to other electrons.

From the energy retardation formula for back-scattered electrons (equation 2.23), and the range relationship (equation 2.21), the rate of energy loss due to back-scattered electrons is given by:-

$$\frac{dE}{dy} = - \left(\frac{2n}{1+n}\right) (RC)^{n/(n+1)} (1 - y)^{(n-1)/(1+n)} / E_R \qquad (2.36)$$

Thus by considering the production of secondary electrons by back-scattered electrons, from the generalized case of primary electrons and, by substituting (2.36) with (2.23) into (2.33), the secondary yield due to back-scattered electrons can be calculated as (Kanaya et al., 1978):-

$$\delta_B = \eta_B \left(\frac{K}{2}\right) \left(\frac{C}{\alpha}\right)^{n/(1+n)} \left(\frac{C}{\alpha}\right)^{n/(1+n)} \int_0^{\frac{1}{2}} \frac{2n}{n+1} (1 - y)^{(n-1)/(n+1)} A^{n/(1+n)}$$

$$x \left[\exp(- Ay) + Ay\, E_i(- Ay)\right] dy \qquad (2.37)$$

2.5.5 Universal Secondary Yield Curve

For plotting δ/δ_m vs E/E_m to get a universal secondary yield curve, the total secondary yield $\delta = \delta_p + \delta_B$ was obtained by (Kanaya et al., 1978, and Kanaya and Ono, 1979). The total yield has been expressed as a function of $f_p(A)$ and $f_B(A)$, [$f_p(A)$ and $f_B(A)$ are the integrations in equations (2.37) and (2.35), respectively] together with the back-scattered coefficient η_B as:-

$$\delta / \left[\left(\frac{K}{2}\right) \left(\frac{c}{\alpha}\right)^{n/(n+1)} \right] = f_p(A) + \eta_B f_B(A) \qquad (2.38)$$

Both $f_B(A)$ and $f_p(A)$ have maxima as shown in figure (2.15), and the second term changes by η_B as well.

Accordingly, the value of the total yield normalized by the maximum yield δ/δ_m can be obtained as a function of E/E_m:-

$$\frac{\delta}{\delta_m} = \left[f_p(A) + \eta_B f_B(A) \right] / \left[f_p(A) + \eta_B f_B(A) \right]_{max} \qquad (2.39)$$

for $E/E_m = (A/A_m)^{n/(1+n)}$. For the sake of simplicity for the calculation, it can be numerically approximated (Kanaya et al., 1978) as:-

$$\left[f_p(A) + \eta_B f_B(A) \right]_{max} = 0.365 \ (1 + 1.26r) \qquad (2.40)$$

and

$$A_m = (1 + 5r^2) \qquad (2.41)$$

where the back-scattering coefficient $r = [\eta_B]_{y=\frac{1}{2}}$, where η_B is the back-scattering fraction with depth $y = \frac{x}{R}$, is used from the diffusion model (Kanaya and Ono, 1978).

Figures (2.16) and (2.17) represent the comparison between the theoretical calculations and the experimental results of the universal yield curve for metals and insulators respectively, which are in good agreement.

2.6 Quantitative Characteristics of Secondary Electron Emission

In this section the values of the incident energy E_m for which the maximum yield occurs, and the value of the maximum yield, for metals (Ono and Kanaya, 1979) and insulators (Kanaya et al., 1978) have been obtained.

The value of the incident energy E_m for which the maximum yield occurs is related to α and C. From the range relationship (equation

FIG 2.15 The variation of secondary yield curves $f_P(A)$ and $f_B(A)$ as a functions of A and n, Kanaya et al (1978)

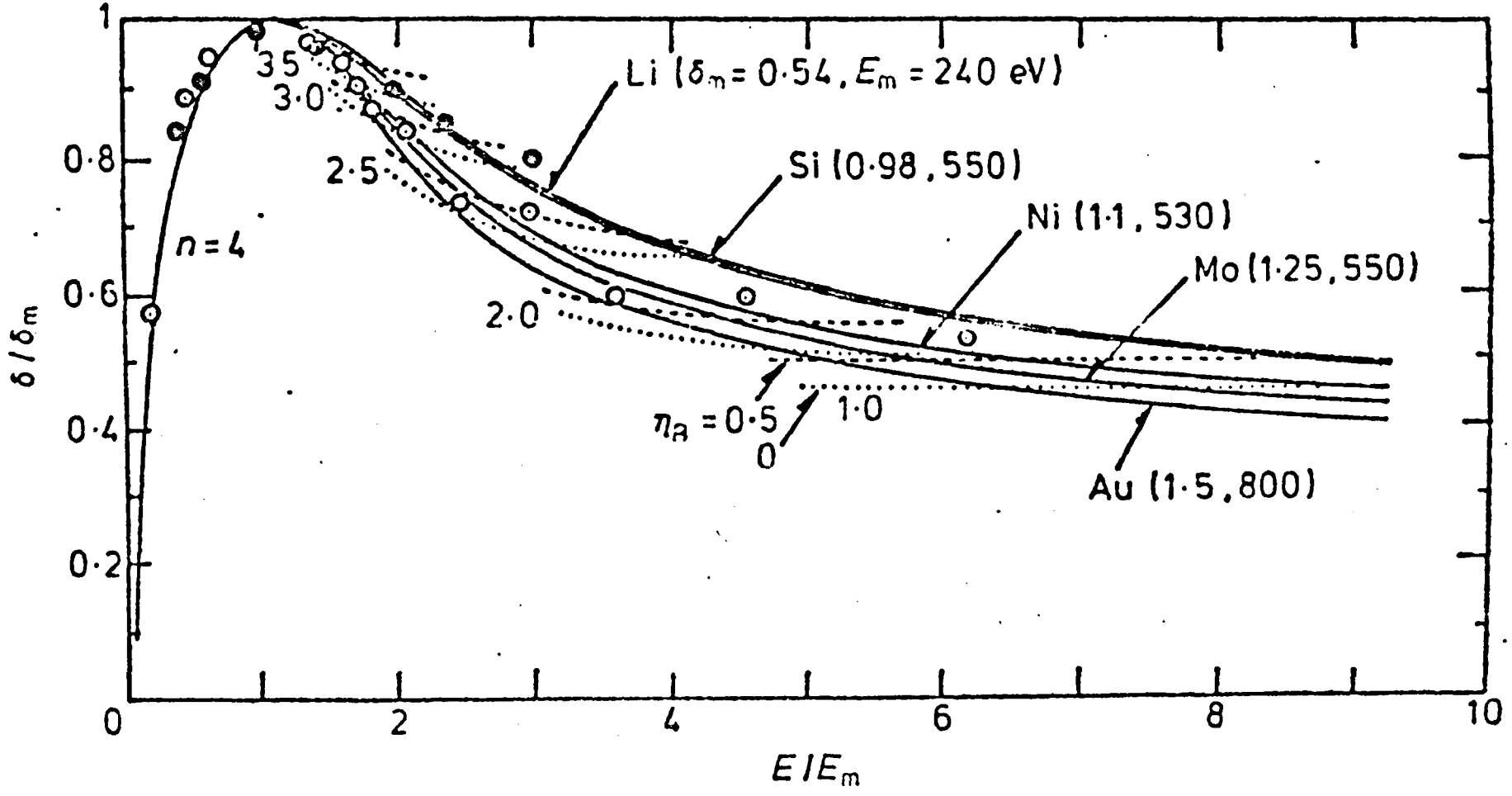

FIG·2.16 The theoretical and experimental comparison of the universal yield–energy curve for the energy-dependent parameter *n*. ◉ Si (Dionne 1975), ⊙ Ni (Knoll 1935), ○ Mo (Bruining 1942).—(Ono and Kanaya 1979)

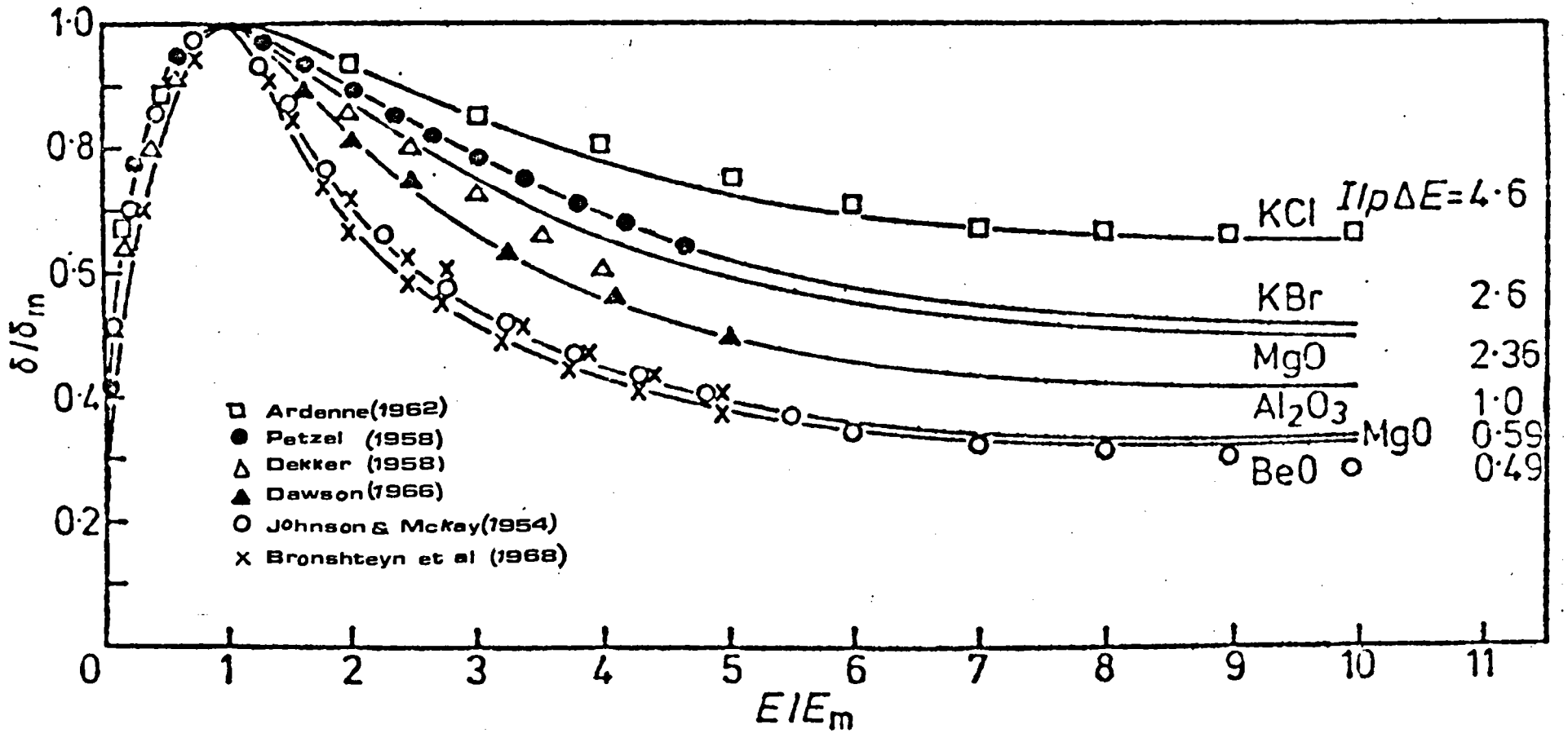

FIG 2·17 Theoretical and experimental comparison of the normalized yield curve of insulators. (Kanaya et al, 1978)

2.21), when $E_p = E_m$, the E_m could be obtained as follows:-

$$\left(\frac{E_m}{E_R}\right)^{1+1/n} = \left(\frac{C}{\alpha}\right) A_m = \left(\frac{C}{\alpha}\right) (1 + 5r^2) \qquad (2.43)$$

where A_m is approximately given by equation (2.41) related with the back-scattering coefficient r.

By substituting C (equation 2.21a) and α (equation 2.28) into (2.43), and with the assumption that n = 4 (the special case of the power law) in the first collision, which corresponds to the energy E_m = 0.5 - 2 KeV, and the empirical data for Au : E_m = 800 eV, r = 0.45, I = 9.2 eV, Ono and Kanaya (1979) approximated the characteristic energy E_m for metals as:-

$$E_m = 57.9 Z^{1/15} I^{4/5} (1 + 5r^2)^{4/5} \text{ eV} \qquad (2.44)$$

On the other hand, the maximum yield δ_m is given by

$$\delta_m = \frac{K}{2} \left(\frac{C}{\alpha}\right)^{n/(1+n)} 0.365 (1 + 1.26r) \qquad (2.45)$$

According to the empirical relationship $\frac{\delta_m}{E_m}$ leads to

$$\frac{\delta_m}{E_m} = \left(\frac{K}{2}\right) \frac{0.365 (1 + 1.26r)}{E_R (1 + 5r^2)^{4/5}} \simeq K_0 \frac{(1 + 1.26r)}{E_R (1 + 5r^2)^{4/5}} \qquad (2.46)$$

where $K_0 = 2.1 \times 10^{-3}$ (eV^{-1}) is closely fitted to $\delta_m = 1.5$ for Au.

Then, the maximum yield δ_m is empirically given by

$$\delta_m = 0.12 Z^{1/15} I^{4/5} (1 + 1.26r) \qquad (2.47)$$

The above calculated results, compared with experimental results (Dekker, 1958; Seiler, 1967; Kollath, 1956; von Ardenne, 1956; Gobrecht and Speer, 1953) for different metals are in agreement within the differences of 10%.

For insulators, by substituting the equations (2.21a) and (2.31) into (2.43), and with the assumption that n = 4 in the first collision

and the empirical data for NaCl; E_m = 690 eV, I = 10 eV, ΔE = 7.85 eV, ν = 2, Kanaya et al. (1978) approximated the characteristic energy E_m for insulators as:-

$$E_m = 58.3 \left[\frac{I(1 + 5r^2)}{p} \right]^{0.8} \left[\frac{\rho}{A\nu} \right]^{0.4} Z^{0.6} \text{ eV} \qquad (2.48)$$

where E_s = 200 eV, n_s = 20, and λ_p^2 = 0.054 are determined empirically.

On the other hand, the maximum yield δ_m is given by equation (2.46). According to the empirical relationship $\frac{\delta_m}{E_m}$ leads to

$$\frac{\delta_m}{E_m} = \left(\frac{K}{2}\right) \frac{0.365\ (1 + 1.26r)}{E_R\ (1 + 5r^2)^{4/5}} \simeq C_0\ (1 + 1.26r) \qquad (2.49)$$

where $C_0 = 7.4 \times 10^{-3}$ eV^{-1} is best fitted to δ_m = 6.5 for NaCl. Then, the maximum yield δ_m for insulators is empirically given by

$$\delta_m = 0.43\ (1 + 1.26r) \left[\frac{I(1 + 5r^2)}{p} \right]^{0.8} \left(\frac{\rho}{A\nu} \right)^{0.4} Z^{0.6} \qquad (2.50)$$

Figure (2.18) shows the maximum yield values for insulators of metallic oxides corresponding to their characteristic energies which are shown in Fig. (2.19).

The experimental results are from Bruining and De Boer (1939a, b), Hachenberg and Brauer (1959) and Ardenne (1962), which are shown in figures by ⊙. The solid lines are the theoretical calculations of δ_m and E_m by using the equations (2.48) and (2.50).

The highest yield values of insulators which are experimentally observed and explained as being due to the lower plasmon losses occurring. From these results Kanaya et al. (1978) arrived at the conclusion that the high yield of insulators, the large escape distance, and especially different values of the yield in the same compound can be explained by the different plasmon losses which may occur in any multiple of the lower plasmon loss for the given material.

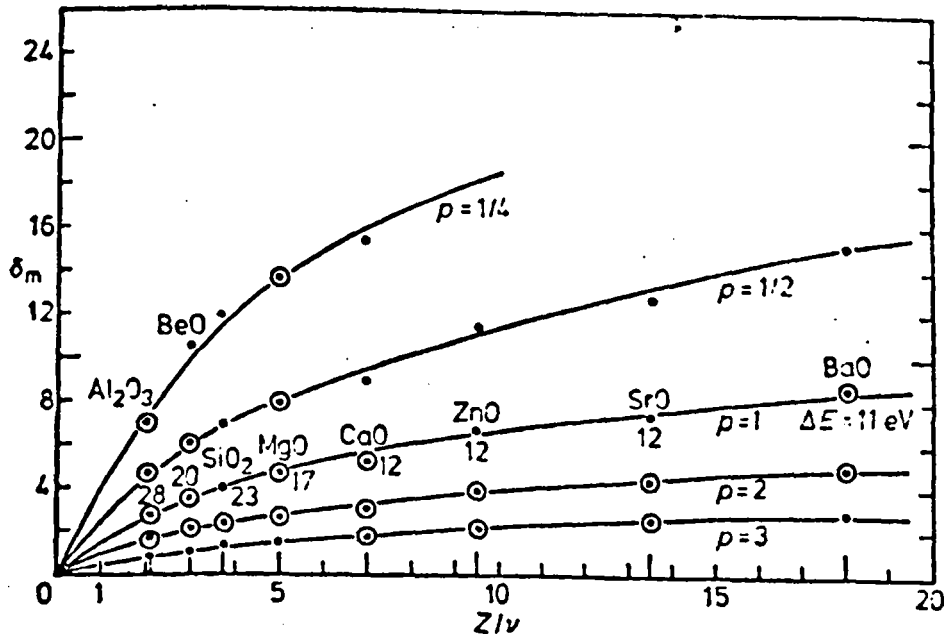

FIG.2.18 Maximum secondary electron emission yield for insulato rs of metallic oxides. $\delta_m = 0{\cdot}43 \quad (1+1{\cdot}26r)[I(1+5r^2)/p]^{0{\cdot}8}(\rho/Av)^{0{\cdot}4}Z^{0{\cdot}6}$ eV. Experim ental points (⊙): Bruining and De Boer (1939a, b); Hachenberg and Brauer (1959); Ardenne (1962).

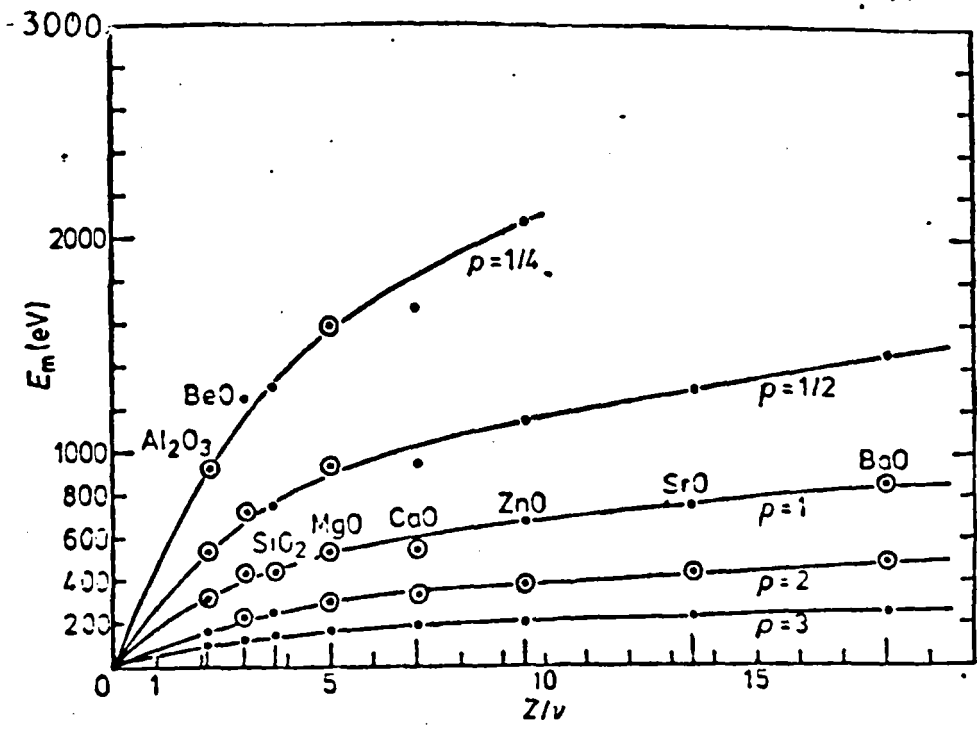

FIG 2.19 Characteristic energy of secondary electron emission giving maximum yield for insulators of metallic oxides. $E_m = 58{\cdot}3\,[I(1+5r^2)/p]^{0{\cdot}8}(\rho/Av)^{0{\cdot}4}Z^{0{\cdot}6}$ eV; references for experimental points as in figure 2.18

2.7 Conclusion

There are three aspects of secondary electron emission which are highly significant. These are

1) The total secondary yield,

2) Auger electron emission,

3) The characteristic energy losses.

In this chapter the basic processes involved in the first of these viz secondary electron yield have been discussed, together with various mechanisms which can contribute to the generalized secondary electron yield. In addition some of the literature in the field of secondary electron yield has been reviewed. Finally the formulation and quantitative calculations of various parameters in secondary electron emission has been presented in this chapter and is largely due to the works of Kanaya et al. (1978), Ono and Kanaya (1979) and Kanaya and Ono (1978). Their work has been reproduced in considerable detail due to the importance of their results in interpreting the present experimental work.

The chapter which follows, contains some brief theoretical aspects of Auger electron emission and characteristic energy loss.

CHAPTER 3

AUGER ELECTRON SPECTROSCOPY AND CHARACTERISTIC ENERGY LOSSES

3.1 Introduction

Although Auger spectroscopy is not an old technique for surface studies, a very considerable amount of work has been done on it. The technique is now quite highly developed in compatible with a variety of energy analysers in addition to the LEED system with which it was originally so often employed. It is now almost always available as a matter of routine in any surface analysis system.

In this chapter some theoretical aspects of AES and CELS have been reviewed and discussed, followed by a brief discussion of the electron spectrometers and appropriate instrumentation for detection of Auger electrons.

3.2 Auger Electron Spectroscopy (AES)

One of the most important surface characterization techniques is that of Auger electron spectroscopy. By using this technique which is based on the energy analysis of secondary electrons, the atomic species in the first few atomic layers of a solid can be identified with sensitivities down to $\sim 10^{-3}$ of a monolayer. Apart from the use of AES to determine surface atomic species there are current developments to make Auger electrons quantitative. [It has already been pointed out in section (2.3), Fig. (2.8), that the small peaks in the region II of the energy distribution curve may be due to Auger electron emission.]

The Auger effect takes its name from Pierre Auger who in 1925 observed traces of electrons on photoplates which had been exposed to x-ray radiation. He interpreted the formation of these electrons as a radiationless transition in atoms excited by the primary x-ray photons, whereby the emission of an electron from an outer level with an energy equal to that released by the filling of the core hole competes with the emission of characteristic x-ray radiation. These "Auger" electrons have since been the subject of extensive theoretical (Burhop, 1952; Asaad, 1966; Chattarji, 1976) and experimental (Bergstrom and Nordling, 1965) investigations.

It was, however, Lander (1953) who first pointed out the applicability of using Auger electrons for surface analysis and suggested that the technique provided a complement to soft x-ray emission for the determination of energy band density of states. However, it seems that Lander's work went virtually unnoticed (perhaps due to the lack of ultra-high vacuum technology) and it was not until 1967 that the idea was followed up.

Tharp and Sheibner (1967) demonstrated that the ordinary electron

optics of LEED experiments could be used as a retarding field energy analyser for the detection of Auger electrons by differentiation of the integral energy distribution [to give the energy distribution, i.e. N(E)]. The disadvantage however was the fact that only very small peaks appeared on the large slowly varying background of secondary electrons which are emitted from a surface bombarded by low energy primary electrons. Under these conditions it is rather difficult to identify the transitions at all accurately.

In 1968, an important step was made by Harris. He reported studies of the Auger spectra of metals obtained by detecting the differential of the energy distribution ($\frac{dN(E)}{dE}$) as suggested by Leder and Simpson in 1958. Almost simultaneously Weber and Peria (1967) and Palmberg and Rhodin (1968) used electronic differentiation techniques in combination with conventional 3-grid LEED electron optics and obtained spectra comparable in quality to those of Harris. Further progress was made by Palmberg (1968), who showed that the addition of a fourth grid to a commercial 3-grid LEED optics improved the resolution of the spectrometer considerably. Another important step in the experimental development of this method was also made by Palmberg *et al*. (1969) by using a cylindrical mirror analyser to detect the Auger electrons. With this technique the sensitivity, resolution and signal to noise ratio could be improved to the extent that even a fast oscillograph scan of the Auger spectra and the detection of surface impurities with concentrations as low as 10^{-3} of a monolayer became possible. There has been rapid growth in the AES field up to the present time and although as indicated Auger electron spectroscopy was introduced only twelve years ago, it has reached a high level of sophistication and has perhaps found the most widespread use of the various surface analysis methods. Up to now more than several hundreds of papers have

been published dealing with Auger spectroscopy (see the bibliography compiled by Hawkins, 1977).

In view of the relatively brief introduction to the topic of AES, the reader is referred to the following introductory papers, Tracy (1972), Chang (1974), Ertl and Küppers (1974), Sickafus (1974), Stein (1975) and Barrie et al. (1979).

3.2.1 Auger process

The Auger process can be explained by considering a neutral atom which is then excited above its ground state resulting in the creation of a "hole" or vacancy within one of its inner shells. This can be most efficiently done by electron impact although ions and x-rays are also suitable. An atom which has been ionized in one of the inner (core) states may then return to its electronic ground state via one of the following processes:

a) An electron of an energetically higher level "falls" into the core hole, the energy thereby released being emitted as a quantum of characteristic x-radiation (Fig. (3.1a)).

b) The core hole is filled by an outer electron, but the available energy is transmitted in a radiationless process to a second electron which may then leave the atom with a characteristic kinetic energy (Fig. (3.1b)).

This second process is called the Auger effect. In the Auger effect the atom is left in a doubly ionized state and may continue to de-excite by x-ray or Auger processes, in the absence of externally supplied electrons.

If the probability for x-ray emission is 'w' (often called the fluorescence yield 'w') and that for Auger electron emission is 'a', then clearly 'a + w' must equal unity. However, for binding energies

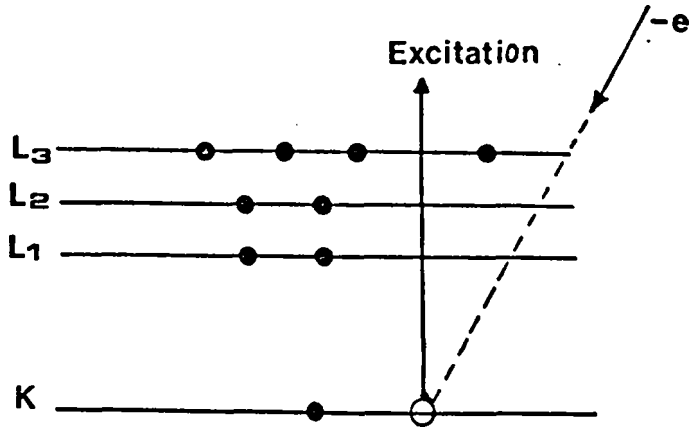

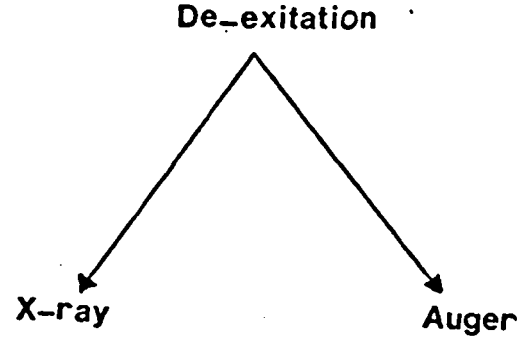

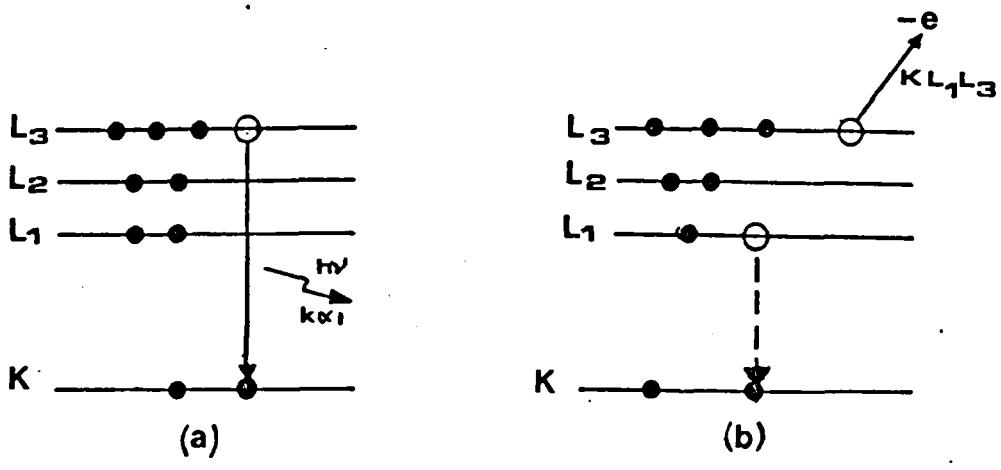

FIG. 3.1 Processes for de exitation of atomic core holes

a) Emission of x-ray radiation

b) Emission of an Auger electron

< 2 KeV, the fluorescence yield is less than 10% and the Auger mechanism dominates.

Auger electrons are often classified by referring to the energy levels involved in their production. The starting point is a core hole created by ionization of the atom. This hole for example in the K-shell may be filled by transition from a higher shell, say L_2. If the emitted electron, excited by energy transfer, originates from the L_3 shell, then in this example the Auger electron would be called a KL_2L_3 electron in the standard notation. Similarly for a KL_2M_1 - Auger electron, the emitted electron would originate from the M_1 shell. Thus the Auger transitions are usually designated according to the three levels participating in the process. The above is the so-called x-ray notation. Atomic notation may also be used e.g. K - 1s; L_1 - 2s; $L_{2,3}$ - $2p\frac{1}{2}$ or $2p\frac{3}{2}$; M_1 - 3s; $M_{2,3}$ - $3p\frac{1}{2}$ or $3p\frac{3}{2}$; $M_{4,5}$ - $3d\frac{3}{2}$ or $3d\frac{5}{2}$ etc.

To quote a specific example, in the present work on Be there is a major transition occurs at 104 eV. The initial hole for this transition is the K level and the two participating electrons originate in the valence band. The designation is thus KVV.

Inner shell ionization for primary energies of 3 KeV occurs in times less than 10^{-6} sec. The lifetime of a core hole is usually a little greater than 10^{-15} sec., therefore it is easy to see why the Auger electron energy distribution is independent of the primary energy. Hence, Auger electrons are characteristic of the excited atoms from which they are emitted.

In order to maximize the number of inner shell vacancies, the primary electron beam energy is normally set to between three and six times the core level binding energy (Bishop and Riviere, 1969). In other words, this primary energy gives an approximate maximum for the

ionization cross-section of the inner shell level. Complications to this "rule of thumb" statement can arise since many ionizations are produced by backscattered electrons (Neave et al., 1972). However in practice, this general rule is satisfactory.

Finally, among the Auger electrons one type deserves special mention, i.e. when a vacancy in an inner shell of an atom is filled by another electron of the same shell but different subshell with the ejection of an electron from an outer shell with lower energy, the resulting radiationless transition is termed a Coster-Kronig transition (e.g. L_1L_2M, $L_1L_2L_3$, $M_1M_2M_3$ etc.). These transitions are very strong when energetically allowed, and cause a rapid redistribution of core holes which strongly influences the relative intensities of the observed lines in the L and M group. Tracy (1973) was able to measure the intensity of the $L_{2,3}VV$ phosphorus Auger peak versus primary beam energy and recorded a kink at the ionization energy of the L_1 level due to enhancement of the intensity by Coster-Kronig transitions.

An account of the theory of the Auger process is given by Carlson (1975) with references to its applications in compositional and chemical analysis,

3.2.2 Auger Electron Energies

In an Auger process an atom is initially ionized in an inner level A and Auger emission results in an atom with two final state holes in levels B, C and an Auger electron of energy E(ABC). Three approaches are possible in the calculation of E(ABC) of an Auger electron in the atom, which are briefly discussed below and which is followed by a brief discussion of Auger energies in the solid state.

1) First principles calculations;

The Auger energy may be written as:-

$$E(ABC;\ X) = E(A) - E[B,\ C;\ X] \qquad (3.1)$$

where E(A) is the energy of the atom ionized in level A and E[B, C; X] is the energy of the doubly ionized atom with appropriate final multiple state, both energies relative to the neutral atom energy. Calculation of E(A) and E[B, C; X] requires "self consistent field" values for one hole and two hole defect states with proper inclusion of relativistic effects for inner levels (Larkins, 1975). In view of the difficulties of such calculations this approach has not been widely used but it is capable of predicting Auger energies correct to within a few eV.

2) Semi-empirical methods;

This approach uses the fact that accurate one electron binding energies may be obtained from XPS or x-ray emission measurements and has been the most widely used approach to date. The Auger energy is written as:-

$$E(A,\ B,\ C;\ X) = E_A - E_B - E_C - W[B,\ C;\ X] \qquad (3.2)$$

where E_A E_B and E_C are experimental one electron atomic binding energies and W[B, C; X] is the recombination energy of the two final state holes in configuration X, also termed the hole-hole interaction energy. W[B, C; X] consists of two terms, i) F(B, C; X) which is a final state interaction term depending on the Auger transition and the final state of the atom and R_s(B, C) which is the static relaxation energy corresponding to a reduction in the binding energy of the emitted Auger electron due to relaxation of the remaining electrons towards the vacancy created in the process (Shirley, 1973). By using the relation (3.2), Shirley was able to calculate theoretical values for KLL Auger energies for the elements $10 < Z < 100$ and obtained good agreement with experimental values.

3) Empirical methods;

If outer electrons are involved in the Auger transition the Auger energy may be calculated entirely from experimental data using tabulated binding energies for inner core levels (Sevier, 1972; Bearden and Burr, 1967). The Auger energy (as mentioned before) is

$$E(A, B, C; X) = E(A) - E(B, C; X)$$

The energy $E(B, C; X)$ is obtained from optical data by summing the energies required to produce the final two hole state

$$E[B, C; X] = IP(I) + IP(II) + \epsilon(X) \qquad (3.3)$$

where IP(I) and IP(II) are the first and second ionization potentials and $\epsilon(X)$ is the energy of the required two hole state above the ground state of the doubly ionized species. This method gives very good agreement with experiments for those cases where it is possible to obtain optical data.

It should also be mentioned about the $Z/(Z + 1)$ formula (Bergstrom and Hill, 1954), which has been used for calculating the Auger energies for many years by experimental surface physicists. This formula attempts to allow for the hole-hole interaction by using data from the element with the next highest atomic number

$$E^Z(A, B, C) = E(A)^Z - E(B)^Z - E(C)^Z - DZ(E(_C)^Z - E(_C)^{Z+1}) \qquad (3.4)$$

with ΔZ taken as 1, this reduces to

$$E^Z(A, B, C) = E(A)^Z - E(B)^Z - E(C)^{Z+1} \qquad (3.5)$$

This gives relatively poor agreement with experiments for free atoms even in the symmetrized form (Chung and Jenkins, 1970), and cannot, of course, predict multiplet structure.

Thus it is concluded that semi-empirical methods and methods

involving optical data, when available, provide a good basis for calculating free atom Auger energies.

4) Auger energies in the solid state;

The foregoing discussions were about free atom Auger energies. A similar formula as the semi-empirical relation for free atoms but more generally applicable to the solid state has been proposed by Matthews (1973). The kinetic energy of a ABC Auger transition is then given by;-

$$E_s(A, B, C; X) = E(A) - E(B) - E(C) - H + P \qquad (3.6a)$$

again E(A), E(B), E(C) are the binding energies of the electrons as say determined from X.P.S., H is the extra energy needed to remove the second electron from the ion core due to interaction with the other core electrons and P is the extra conduction of valence electron polarization energy associated with a double core hole relative to the sum of the polarization energies of two individual holes. The sum of hole-hole and polarization energies may be combined to give an effective potential U_{eff} so that equation (3.6a) may be written as:-

$$E_s(A, B, C; X) = E(A) - E(B) - E(C) - U_{eff} \qquad (3.6b)$$

Further developments by Shirley and co-workers (Shirley, 1972; Kowalczyk et al., 1973 and 1974) to include the effects of a solid state environment has been extensively used in calculations on metals.

3.2.3 Surface Sensitivity of Auger Electrons

The surface sensitivity of Auger electron spectroscopy is determined by the mean inelastic free path length (escape depth) of the escaping Auger electron. But it should be mentioned that the word "escape depth" has different shades of meaning for Auger and secondary electrons. For secondary electrons (section 2.5.2) we are concerned

with the total depth from which secondaries can escape and a typical estimate is 20 to 200A° for metals and 50 to 500A° for insulators. In Auger electron emission, we are more concerned with whether an electron loses enough energy to move the electron away from the Auger peak value, i.e. not to be detected as an Auger electron of given energy, and a much smaller distance is involved.

In Fig. (3.2) a plot of the mean-free path lengths (escape depth) of electrons versus the energy range normally of interest in Auger electron spectroscopy is shown. This diagram is reproduced from the review of the mean free path of electrons in metallic solids published by Ertl and Küppers (1974), and is a summary of the results obtained by a large number of workers on different materials. Note that the mean free paths are on the order of 4 - 20A°, or a few atomic layers. Auger electrons are created deeper in the specimen, but before they are emitted into the vacuum where they could be measured, they lose sufficient energy such that they are lost in the background. Maximum sensitivity is typically 0.1% atomic concentration (Linford, 1980).

3.2.4 The Sources of Excitation

The initial vacancy in an inner atomic level can be created by several methods. Electron induced ionization is mainly discussed here, although other methods are also briefly mentioned.

Electron beam stimulation is still perhaps the most common means of exciting Auger spectra, because a primary electron beam of high intensity $\sim$ 100 μA in a spot size of 5 μm and with energies up to 5 KeV can easily be obtained, using commercial guns and further such a beam can be readily focussed electrostatically and positioned by simple deflection plates onto various points of the target. Since the atomic ionization cross-sections for electron impact are in the range of 10^{-22} cm^2 and are fairly

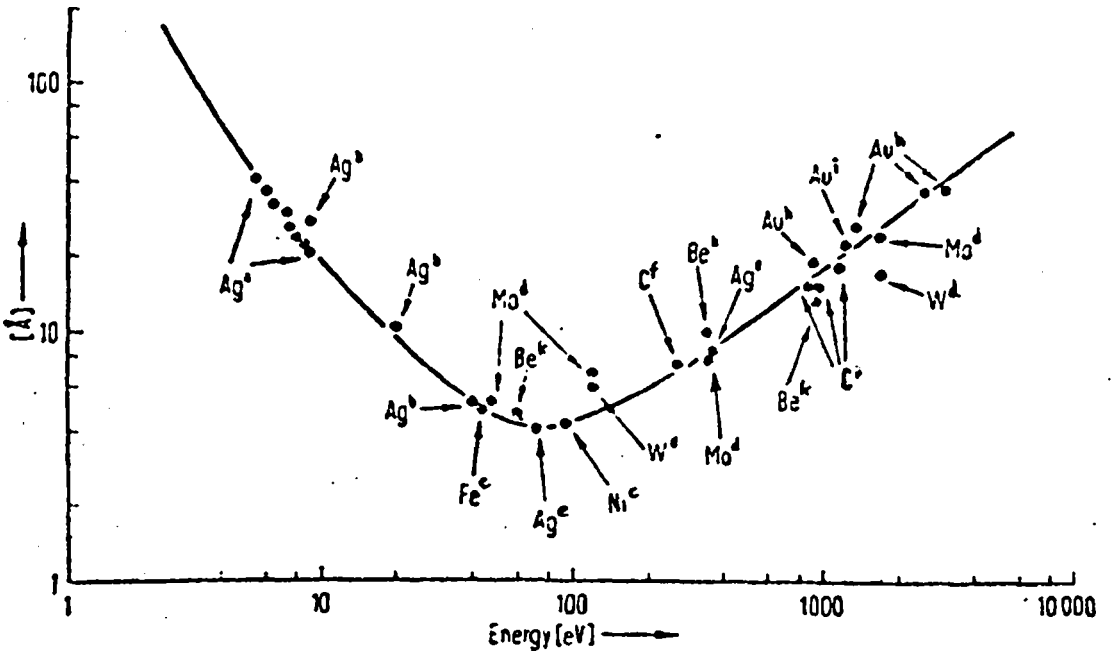

Fig.3.2. Mean free path of electrons in metallic solids as a function of their energy.
a: H. Kanter, Phys. Rev. *B1*, 522 (1970) (Electron transmission). b: D.E. Eastman, 32nd Physical Electronics Conference, Albuquerque, N. Mex. 1972 (UPS). c: J.W.T. Ridgeway and D. Haneman, Surface Sci. *24*, 451 (1971); *26*, 683 (1971) (AES). d: M.L. Tarng and G.K. Wehner, J. appl. Phys. *43*, 2268 (1972) (AES). e: P.W. Palmberg and T.N. Rhodin, J. appl. Phys. *39*, 2425 (1968) (AES). f: K. Jacobi and J. Hölzl, Surface Sci. *26*, 54 (1971). g: R.G. Steinhardt, J. Hudis and M.L. Perlman, in: Electron Spectroscopy (D.A. Shirley, ed.) North Holland, Amsterdam (1972), p. 557 (XPS). h: M. Klasson, J. Hedman, A. Berndtson, R. Nilsson and C. Nordling, Physica Scripta *5*, 93 (1972) (XPS). i: Y. Baer, P.F. Heden, J. Hedman, M. Klasson and C. Nordling, Solid State Comm. *8*, 1479 (1970) (XPS). k: M.P. Seah, Surface Sci. *32*, 703 (1972) (AES).

independent of the primary energy, this type of excitation lends high sensitivity to AES. One disadvantage of electron induced ionization is that the high current densities can induce absorption and desorption effects (ESD) (Madey and Yates, 1971, 1977) as well as the cracking of molecules onto the specimen surface. Also electron induced ionization gives rise to a large secondary electron background upon which the much smaller Auger peaks are superimposed, so that differentiation of the spectrum is usually necessary to readily observe these features. An additional complication is that a large number of rediffused secondary electrons constitute a back-scattered current which is capable of producing additional ionization so that the measured Auger current will not be simply related to the primary current and ionization cross-section.

Auger electrons may also be excited by x-ray radiation. Maintaining an x-ray source in ultra-high vacuum is more complicated than an electron gun, and the time needed for recording a spectrum is much longer (the scan time is usually in the order of tens of minutes, whilst electron beam stimulation gives scan times of only a few seconds). This is mainly due to the fact that with normal x-ray tubes maximum photon fluxes at the sample of about 10^6 photons/s are obtained (Parratt, 1959) whereas a primary electron current of 1 μA corresponds to an electron flux of $\sim 6 \times 10^{12}$ electrons/s. The cross-section for x-ray induced ionization decreases with reduced energy whereas it increases for electron induced ionization, Barrie (1975). Moreover the background is much lower with excitation by means of x-rays since the large contribution from the "rediffused" primary electron background is absent. Spectra are therefore usually recorded as N(E) instead of $\frac{dN(E)}{dE}$. Furthermore the damage caused by the primary radiation on sensitive surface layers is much less than with an electron beam. Examples of x-ray induced Auger spectra are given by Siegbahn *et al.* (1967, 1969)

and by Smith and Huchital (1972).

Finally, it should be mentioned that excitation may also be achieved by high energetic particles like protons (60 - 220 KeV) (Powell et al., 1977) or ions (60 KeV) (Viel et al., 1976) which produce core holes in the surface region within the escape depth of low energy Auger electrons. The straight line trajectories of the incident particles largely eliminate any back-scattering correction as used in the electron impact excitation. However, a high energy ion accelerator is needed and only low beam currents ($\sim$ 1 μA) are obtainable. Additionally some sputtering of the surface layers cannot be avoided. Though this technique has some advantages (in particular for quantitative analysis) it will certainly be restricted to only few applications.

3.2.5 Quantitative Analysis of AES

The relative amount of a species on the surface is obtainable since the emission current of the Auger electrons is proportional to the number of excited atoms (n_i). As Needham (1972) suggested, the peak to peak height of the differential Auger line (in the $\frac{dN(E)}{dE}$ curve) is proportional to n_i, and this quantity is frequently used as a measure of relative surface concentrations, and it has been of great value in many investigations. However, more recently, it has been reported that the excursion of the negative peak as a measure of intensity is perhaps a better tool for quantitative analysis of AES than the usual peak to peak value (Seah, 1979).

The determination of absolute surface concentrations (i.e. number of particles per cm^2) from the Auger peak heights should in principle be possible on the basis of a knowledge of all factors which contribute to the emitted current (such as the variation of the escape depth of Auger electrons with energy, the Auger peak widths, transition probabilities

and the influence of fine structure, etc.). This problem is very complex and is not yet completely solved. Consequently the use of reference data from independent calibrations is necessary for determining absolute surface concentrations. Such independent calibration points may for example be obtained from the following techniques

a) LEED. If from the LEED pattern the unit cell of the absorbate structure and the positions of the adsorbed particles relative to each other can be unequivocally determined (which is not always the case) then also the surface density is known and may be compared with Auger signal height. It is further possible to correlate this quantity with the intensity of the LEED 'extra' spots at varying coverages. An outstanding example of this kind of work is the adsorption of Xe on Pd (100) as studied by Palmberg (1971).

b) Radioactive tracer. This method was used by Perdereau (1972) for the $\frac{S}{Ni}$ system to determine the surface concentration of adsorbed sulphur.

c) Evaporated films. The thickness of evaporated metal films may be determined from mass measure by micro balance (Bauer and Poppa, 1972).

d) Ellipsometry. Vrakking and Meyer (1972) have calibrated the absolute surface quantities of several gases (C, N, O, P, S and Cl) on the substrates of Si and Ge using the quantitative technique of ellipsometry (King, 1972).

As with all relative measurements the calibrations are only valid for one set of experimental parameters and are not readily transferable from one experiment to another.

For metallic alloys of known compositions, it has been shown that by breaking them in an ultra high vacuum environment and immediately recording the Auger spectra that the ratio of the peak heights is proportional to the concentration (Bouwman et al., 1972; Mathieu and

Landolt, 1975).

Finally, in adsorption studies, the heights of the Auger peaks are monitored as a function of the exposure to a particular gas and a number of authors have assigned structure in the Auger peak height versus exposure graph to one monolayer coverage of the substrate by the adsorbing gas: Florio and Robertson (1969) identified saturation of the chlorine Auger peak signal in the adsorption of Cl on Si as one mono layer coverage. Musket and Ferrante (1970) identified the saturation coverage of O_2 on W(110) as detected by the Auger signal peak height with one mono layer and Kirby and Lichman (1974) also identified the saturation of the Auger peak of oxygen with exposure as one monolayer coverage of the silicon surface.

3.2.6 Chemical Effects in AES

It is well known in the AES field that the chemical environment of an atom can strongly influence the Auger peak energies of that atom and can also affect 'the line shape' of its spectrum. There are two types of chemical effects which need to be distinguished in the AES of compounds. On the one hand are the changes produced in Auger peaks involving the valence band, these will be strongly affected by the alteration in the valence band density of states produced as a result of the chemical combination. Such peaks will undergo a shift in energy as well as a possible change in shape. The chemical effects on the Auger transitions involving the core levels of an element on the other hand are expected to undergo a shift in energy only. Chemical shifts may concern all three atomic levels which are involved in the Auger process. The occurrence of such chemical shifts of up to several eV in the energies of the atomic levels when an atom undergoes chemical bonding has been frequently measured by x-ray measurements. Hence we

may expect the Auger electron energy to shift upon atomic bonding by an amount ΔE_{ABC} given by:

$$\Delta E_{ABC} = \Delta E_A - \Delta E_B - \Delta E_C \qquad (3.7)$$

where ΔE_A, ΔE_B and ΔE_C are the shifts of the individual levels involved. Equation (3.7) can be useful in a situation where one wishes to detect the presence of impurities in the surface region. For example, the adsorption of an electronegative gas-like oxygen onto a clean metal surface leads to a charge transfer from the metal atoms to the adsorbed atoms. As the electron density around a metal atom decreases, the remaining electrons in this atom "see" a greater nuclear charge and their binding energies are increased. If in equation (3.7) one takes, as a first approximation, the shift of the individual levels to be nearly equal, i.e. $\Delta A \simeq \Delta B \simeq \Delta C$, then $\Delta E_{ABC} = - \Delta E_B$. These considerations were employed by Haas et al. (1972) in their Auger studies on the chemisorption of oxygen on refractory metal surfaces such as MO(110), Nb(110) and Ta(110).

Chemical effects are often much more complicated than a simple shift of energy levels. In an element characterized by groups of Auger lines in different energy ranges, the lower energy lines may quite often involve ejection of an electron from the valence band, while the higher energy lines correspond to the emission of a core electron. Changes in the chemical environment have a greater influence on the former. This may lead to a change in the relative intensity of one group of Auger lines to another, in addition to the energy shift described above.

The chemical environment also leaves a distinctive imprint on Auger spectra involving valence band transitions. Valence electron wave functions are obviously the most susceptible to changes in bonding.

Assuming, therefore, that the escape probability is a smoothly varying function of energy, the external Auger distribution should reflect these changes. It was shown by Haas and Grant (1970) and Haas et al. (1972) that the resulting changes in the carbon KLL spectrum could be used as a fingerprint for carbon occurring in the diverse chemical forms of graphite, diamond, silicon carbide and MO_2C. In particular, this can be useful in defining the state of surface atoms. For example, following bakeout in vacuum, most materials show the presence of carbon in their Auger spectra. In almost every case, the peak shape is identical to that of graphite. This indicates that the carbon comes from a decomposition of such residual gases as CO, CO_2, hydrocarbons, etc.

Most of the reported work on chemical effects are of an empirical nature since the Auger processes involved are not well understood. However, even in this limited capacity, chemical effects are extremely useful for surface compositional studies.

3.2.7 The Concept of Cross Transition

Auger spectra from compounds sometimes contain peaks which appear to have shifted about (or more than) 10 eV with respect to the transition of one of the constituents. Some examples of an increasing list are the oxides of Al (Quinto and Robertson, 1971), Mg (Suleman and Pattinson, 1973), Li (Clausing and Easton, 1973) and Si (Meyer and Vrakking, 1973). In other cases prominent peaks in the spectrum cannot be attributed to either one of the components at all. Provided the peaks in question do not indicate a contaminant, they are transitions characteristic of the compound. Of course there is generally a possible explanation in terms of the preceding section if one invokes unusually big changes in the density of states (Bauer, 1972) or enormous

chemical shifts. While this is not generally accepted a slightly different interpretation in terms of cross transitions is conceivable.

To explain the concept of cross transitions the presence of two distinct elements A and B at the surface is supposed. There are two different schemes of energy levels and hence a spectrum will be observed that may contain all possible transitions of each of the components. Suppose further these components form a compound, then in first approximation, the combined energy level scheme consists of the total of all levels of A and B, with their energies modified by normal chemical shifts. As shown on the left hand side of the Figure (3.3), there are two sets of energy levels A and B with an initial vacancy in the atomic core level E_1. A regular Auger transition (1, 1') in atom A is drawn. Assuming interactions between electrons populating levels of A and B the second stage of transition 1 may also be 1" thus leading to a cross transition (1, 1"). The expelled electron would then appear to have "shifted" in energy by Δ with respect to the transition (1, 1'). A second cross transition (2, 2') indicated by the same core level excitation emits an electron of similar energy. It was Gallon and Matthews (1970) who first interpreted structure in the Auger spectra of LiF as being due to the cross transitions.

The concept of cross transitions is conceivable also if band states of a solid are involved. Provided the local density of states varies from the environment of site A to that of B, a transition is proposed on the right hand side of Figure (3.3). In such a case distinct peaks of the total density of states are supposed to consist of electrons whose wave functions are of different symmetry. One peak may be populated by, say, s-electrons of A while in another peak d-electrons of B prevail (Müller, 1975).

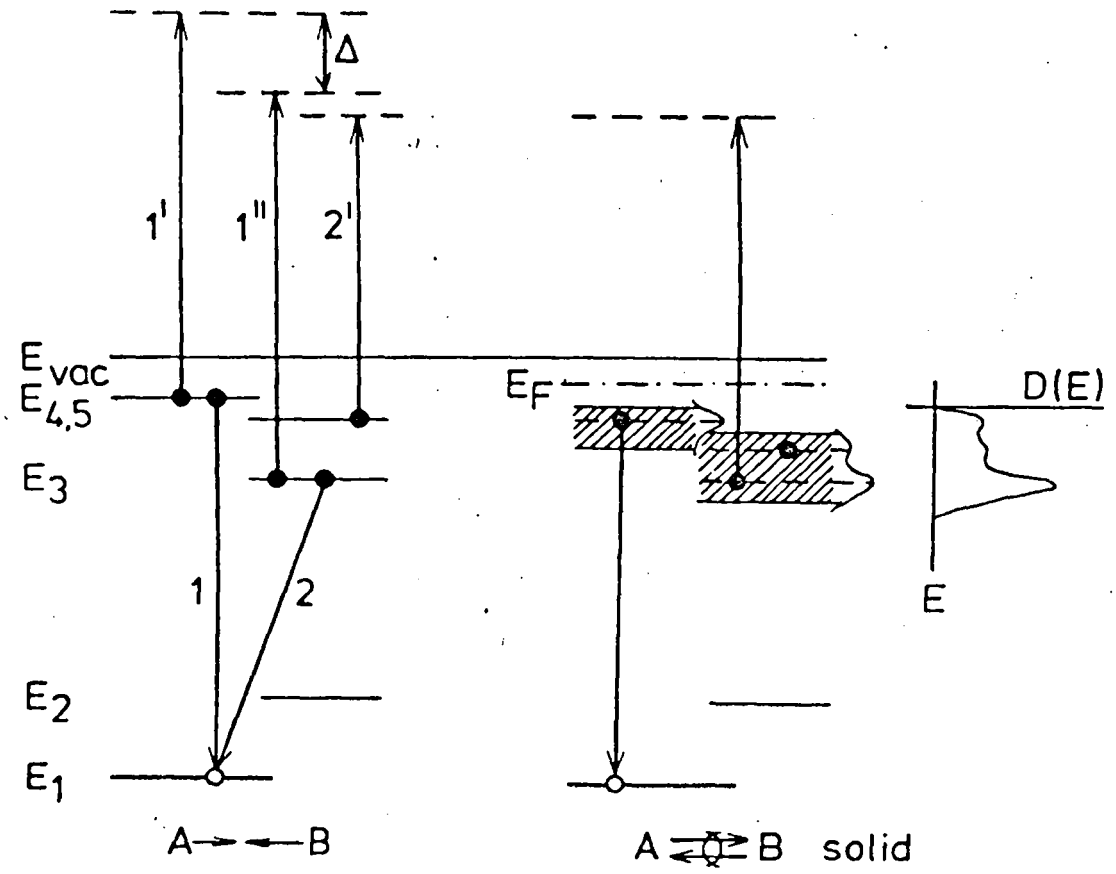

FIG.3.3

The concept of cross transitions. Left: A and B are energy level schemes for different atoms. (1,1') regular Auger process. (1,1'') and (2,2') cross transitions. Right: Cross transition involving band states in a solid.

3.3 Characteristic Energy Losses in Solids (CEL)

The electrons which have undergone characteristic energy losses (inelastic scattering of primary electrons) in the surface region may also be used for surface characterization.

CEL in solids have been studied since the 1930's, but most of the earlier measurements were made on freshly evaporated films, in moderate vacuum ($\sim 10^{-6}$ torr). The information is obtained by measuring the energy losses, ΔE of the electrons, fast or slow, which are transmitted through a thin film of solid or have been reflected at its boundary. Transmission is mainly used in experiments with high energy monoenergetic electrons and in such a case the energy of the beam transmitted through a thin specimen ($\simeq 2000A^{o}$) is analyzed to determine C.E.L. of the primary electrons. Alternatively the reflection method is usually well adapted for low energy electrons (energy less than 1000eV) and in this case the energy of the secondary electrons is analyzed where the characteristic losses are then detected on the low energy side of the elastic peak as shown in Fig. (2.8). Electrons which have suffered energy losses by inelastic collisions may be distinguished from the other features in the energy distribution curve by using the energy of the primary electrons, Ep, as a reference. Peaks due to energy losses have a constant energy difference with respect to Ep, so that a variation ΔE of Ep also shifts the loss peaks by ΔE. On the other hand Auger electrons and true secondaries have fixed energies relative to zero, and only the shapes of their peaks may change on the variation of Ep. It is evident that characteristic energy losses may not only be undergone by primary electrons (Robins and Swan, 1960) but also by any secondary electron. In particular it is true for Auger electrons (Bishop and Riviere, 1970), the result being to

give rise to small satellites in the vicinity of the low energy side of Auger peaks.

The characteristic losses of primaries may be subdivided into the four categories:

1) Collective excitations of valence electrons (plasmon losses).

2) One electron excitation of valence electrons.

3) Excitation of core electrons (Ionization).

4) Excitation of surface vibrations (Quasielastic Electrons).

A more detailed discussion of these categories is given in sections (3.3.1 - 3.3.4).

The theoretical analysis of the electron plasma excitation modes of (Bohm and Pines, 1953; Ferrell, 1957; Ritchie, 1957; Watanabe, 1962; Pines, 1963) provides a basis for the interpretation of some of the experimental results. These papers are mainly concerned with bulk properties and the experiments at this time were primarily understood in terms of the classical "Dielectric theory" which is still valid under certain conditions. Beside some excitations in the bulk several surface effects could be observed in these experiments, but the interest in these effects did not arise before the interest in surface physics was developed. Consequently the development of ELS of solid state surfaces was strongly connected with the reproducible preparation of well-defined solid surfaces which is possible with today's U.H.V. techniques.

Because of the scattering mechanism, and not because of the penetration depth of electrons as is often believed, primary energies of less than 1 KeV are particularly advantageous when studying surface effects. This means that one has to work in the reflection mode, therefore, only reflection kinematics is discussed in this survey.

In the CEL field several reviews by Raether (1965, 1980), Servier

(1972), Ertl (1974), Froitzheim (1977) are available. Raether (1980) has discussed the physics of electron loss spectroscopy (ELS) with electrons of different energies. His emphasis is on the collective excitations or 'plasmons' in the bulk as well as on the surface and the interband transitions.

3.3.1 Characteristic Excitations in Solids

As mentioned in the previous section, we now outline some of the characteristic losses which can be excited in a solid.

The main concern of this subsection consists in describing electronic excitation which results in energy ΔE and momentum $\hbar K$ being transferred to the electrons of the solid. The process can be roughly described as follows.

3.3.1.1 Collective Excitation of Valence Electrons (plasmon losses)

These are collective oscillations of conduction electrons whose energy of excitation lies between 5 and 60 eV. The oscillations run as longitudinal charge density fluctuations through the volume of the crystal (volume plasmons) and along its surface (surface plasmons) and the quanta of these oscillations are known as volume and surface plasmons respectively. The volume plasmon energy $\hbar w_p$, w_p frequency of the oscillation, is in general of the order of 10 eV and depends on the density of the loosely bound electrons, i.e. the valency of the solid. The loosely bound electrons are those for which $\hbar w_p$, w_p plasma frequency, is large compared with their binding energy. The frequency of the volume waves is higher than the frequency of the surface waves, the dispersion relations of both are rather different as also is their excitation probability, Raether (1980).

a) volume plasmons

A plasmon (or a plasma oscillation) may be described as a collective

oscillation of the conduction electrons with respect to the positive ion cores of the solid with frequency w_p. If the conduction electrons are displaced collectively by a distance Δx against the ion cores a restoring force proportional to Δx results due to coulomb interaction. In analogy to the mechanical system of a spring, the solution of the equation of motion represents a harmonic oscillation. According to the pioneering work of Bohm and Pines (1952, 1953), the quantum frequency (Langmuir resonant frequency) of the volume plasmon in a free electron gas with equilibrium electron density n_0 is given by

$$w_p = \left(\frac{n_0 e^2}{m}\right)^{\frac{1}{2}} \tag{3.8}$$

where m is the rest mass of the electron and e is the electron charge. Equation (3.8) for w_p is strictly valid only for a free electron gas, however in a real solid the electrons are not truly free, and the frequency of these oscillations may be written approximately as

$$w_{vp} = \left(\frac{n_v e^2}{m^*}\right) \tag{3.9}$$

where n_v is the valence band density of electrons and m* is the plasma effective mass. This equation holds well for free-electron like metals such as the alkalis, Al, Mg, Be, etc. In the case of a doped semiconductor or an insulator (Raether, 1980) whose conduction band is provided by N-electrons per cm^3, then these electrons can perform oscillations (volume oscillations as well as surface oscillations) with a smaller frequency than that of metal electrons due to the low N. In this case the volume plasma excitation is

$$w_p = \left(\frac{Ne^2}{m^* \varepsilon_0}\right)^{\frac{1}{2}} \tag{3.10}$$

where N is carrier density (conduction band density), ε_0 is high frequency dielectric constant of the solid = $(4\pi 9 \times 10^9)^{-1}$ coul (volt.

$m)^{-1}$, m* is effective mass = m $(1 + \chi_b)$, χ_b is the contribution of bound electrons to the dielectric constant and can be written as

$$\chi_b = \frac{N_b e^2}{m\varepsilon_0} \frac{1}{w^2_n - w^2 + iw/\tau}$$

where w_n is the frequency of the exterior field acting on the bound electrons, N_b is the number of electrons of the eigen frequency w_n, τ is relaxation time. It is evident that such oscillations may be excited by creating an electromagnetic a.c. field by illumination of the solid with light of an appropriate wavelength. If the frequency of the light equals the frequency of the plasma oscillation, then the energy is absorbed by the solid, so that the dielectric constant $\varepsilon(w)$ of the medium exhibits characteristic variations in this range of frequency. It is therefore possible to determine plasmon frequencies from measurements of complex dielectric constant, Raether (1965). From measurements of the reflectivity of the light, or by the transmission through thin films the complex dielectric constant $\varepsilon = \varepsilon_1 + i\varepsilon_2$ can be deduced. Measurements at different wavelength will allow ε_1 and ε_2 to be determined as a function of the photon energy.

For the ideal solid, the calculated dielectric constant, with the assumption of a free electron gas, depends on the frequency of the light (radiation). This can be given by equation (3.11) Raether (1965, 1980)

$$\varepsilon(w) = 1 - \frac{w^2_p}{w^2} \left(\frac{1}{1 - \frac{1}{iw\tau}}\right) \qquad (3.11)$$

Here the interaction with the solid is phenomenologically introduced by the relaxation time τ, Mermin (1970).

The dielectric constant consists of a real term,

$$\varepsilon_1(w) = 1 - \frac{w^2_p}{w^2} \left(\frac{1}{1 + (\frac{1}{w\tau})^2}\right) \qquad (3.12)$$

and an imaginary term

$$\varepsilon_2(w) = \frac{1}{w\tau} \frac{w^2_p}{w^2} \frac{1}{1 + (\frac{1}{w\tau})^2} \qquad (3.13)$$

It is also possible to write $\text{Re} \frac{1}{\varepsilon(w)} = \frac{\varepsilon_1}{\varepsilon_1^2 + \varepsilon_2^2}$ and $\text{Im} \frac{1}{\varepsilon(w)} = \frac{-\varepsilon_2}{\varepsilon_1^2 + \varepsilon_2^2}$

Pines (1963) has shown that the probability of a fast charge, moving through an electron gas, losing energy is proportional to $- \text{Im}(\frac{1}{\varepsilon(w,K)})$. To a good approximation it may be assumed that the momentum transfer during the interaction of an electron with electron gas is negligible, so that $K \to 0$, then the probability of a fast moving charge losing energy is proportional to $- \text{Im}(\frac{1}{\varepsilon(0,w)})$, this quantity can be obtained from the optical measurements and is known as volume loss function, which is able to describe the fundamental structure of the loss spectra, because they contain the whole information relating to the dielectric behaviour of the medium.

The dielectric function, $\varepsilon(w)$ and loss function $\text{Im}(-\frac{1}{\varepsilon})$ of a free electron gas for $\hbar w = 15$ eV and $\frac{\hbar}{\tau} = 4$ eV are shown in Figs. (3.4 and 3.5).

From the equation (3.11), it can be seen that the dielectric constant of the free electron gas is strongly dependent on the plasmon frequency, w_p. Also Pines (1963) has shown that the loss function, $- \text{Im}(\frac{1}{\varepsilon})$ of a system has a broad maxima at the plasmon frequency of its electrons as is shown in Fig. (3.5), (although maxima in $- \text{Im}(\frac{1}{\varepsilon})$ can occur due to an interband transition Rudberg et al. (1964), and this is discussed in the section (3.3.1.2)). Thus optical measurements may be used to predict the plasmon oscillation energy of solids. The ideal volume plasmon frequency, $w = w_p$ for a longitudinal mode can be obtained when dielectric constant $\varepsilon(w)$ takes zero value, then its loss function can be written as

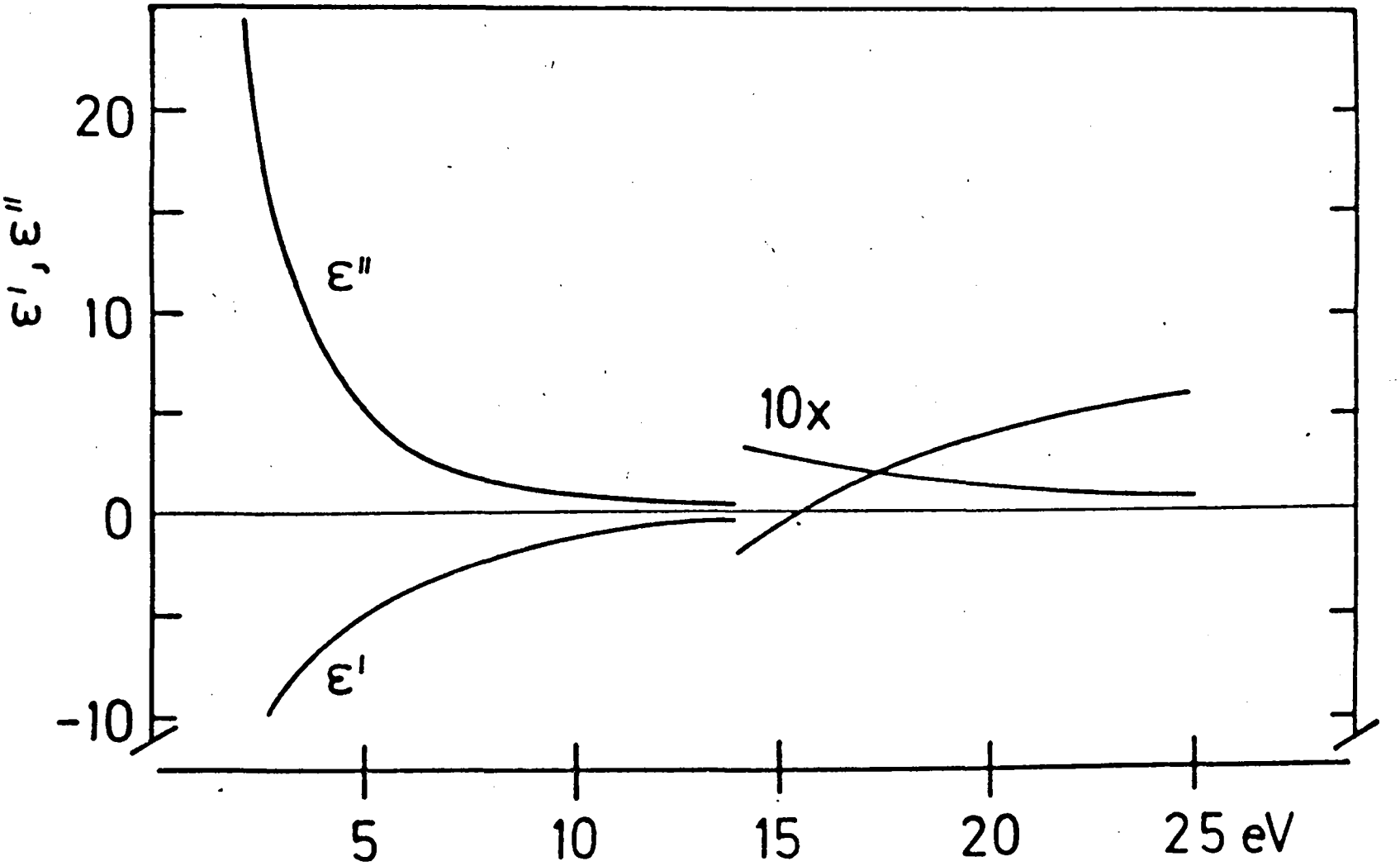

FIG. 3.4, THE DIELECTRIC FUNCTION

RAETHER (1980)

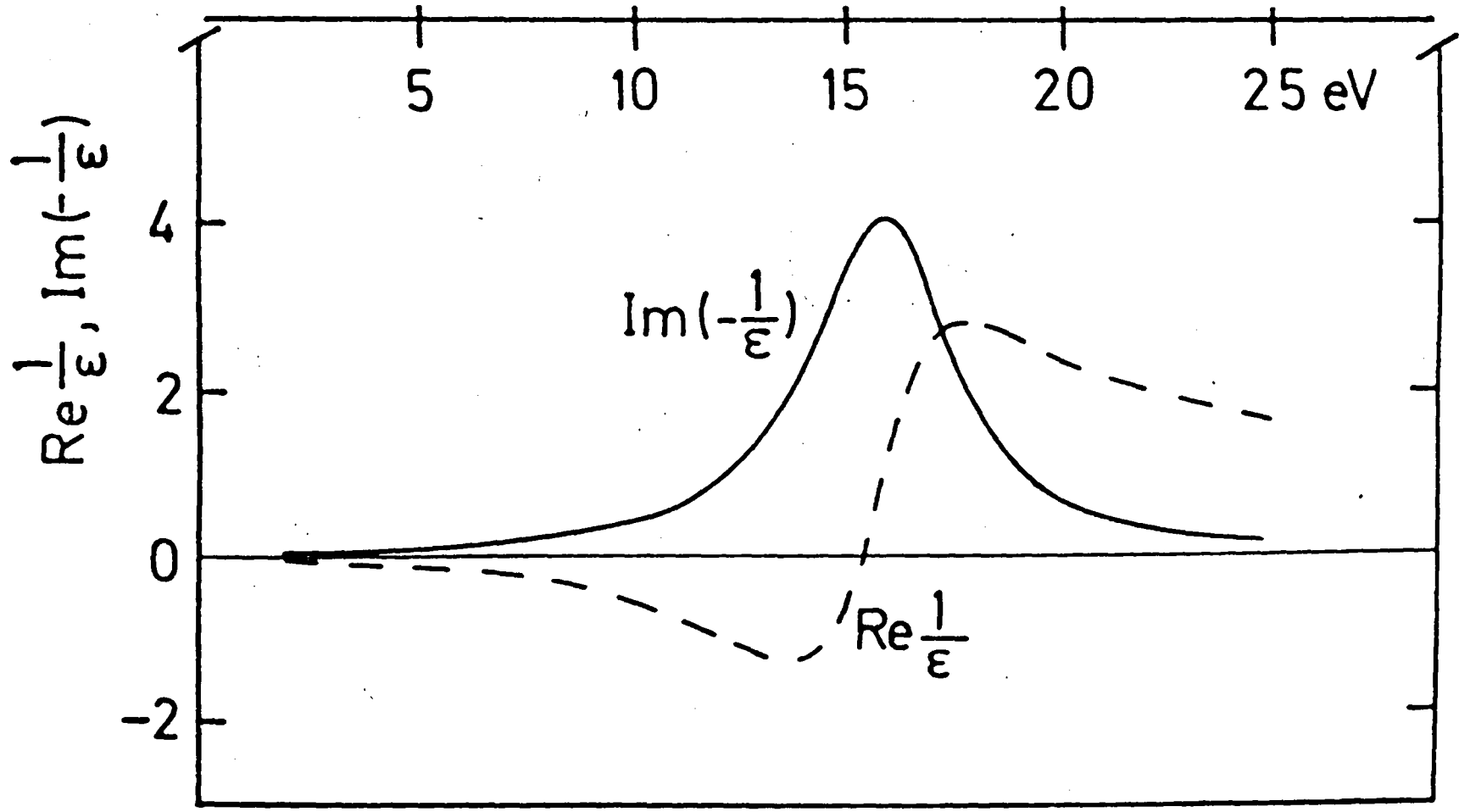

FIG.35, VOLUME LOSS FUNCTION, RAETHER(1980)

$$\text{Im}\left(-\frac{1}{\varepsilon}\right) = \frac{\pi}{2} \cdot w_p \cdot \delta(w - w_p)$$

where $\delta(w - w_p) = 1$ at $w = w_p$

therefore, $\int_0^\infty \text{Im}\left(-\frac{1}{w}\right) wdw = \frac{\pi}{2} w^2_p$ where $\int_0^\infty \delta(w - w_p)\, wdw = w_p$

Plasmons can also be created by electron interaction with the solid in addition to the previously mentioned photon interaction. The electrons penetrate into the solid and create a local coulombic fields. This is described by dielectric theory in which the polarization caused by the electrons is given by dielectric function $\varepsilon(\vec{K}, w)$ where $\vec{K}$ is the wave vector of the excitation and $\hbar w$ its energy. Before this theory had been formed Rudberg (1936) had observed characteristic energy losses for reflected electrons from solid surfaces. However Ferrel (1958) demonstrated why electrons passing through thin films may excite plasmons and his arguments are also true for electrons reflect from the surface.

An incident electron may be able to excite multiple plasmons, corresponding to the excitation of more than one plasmon during the time the electron interact with the solid. Hence, metals such as Mg and Al may show multiple loss behaviour with loss peaks occurring at E_{vp}, $2E_{vp}$, $3E_{vp}$, $4E_{vp}$, etc (the energies relative to E_p), with decreased amplitude. The number of transitions varies with the element. Experimental results have been reviewed by Pines (1955), Raether (1965, 1980). For correct identification, the surface of the solid should be clean and pure and the experiment should be conducted in a U.H.V. environment.

The dielectric theory may also be used to determine the optical constants of solids from energy losses of fast electrons, Daniels et al. (1970). Valence electron excitations with interesting features for surface physics are best studied with low primary energies (< 100 eV) In this case diffraction effects have to be taken into consideration which introduces further complexity.

b) surface plasmons

Collective excitation of electrons not only exist in the volume of a plasma but also exist in its boundary, the theory of surface plasmons was established by Ritchie (1957). Ritchie predicted the angular frequency of the surface plasmons as

$$w_s = \frac{w_p}{\sqrt{2}} \tag{3.14}$$

where w_p is the volume plasmons frequency. This result is applicable only for a clean surface. However, later Stern and Ferrell (1960) derived a relationship for a semi-infinite electron gas bounded by a semi-infinite dielectric medium and their equation is given below

$$w_s = \frac{w_p}{(1 + \varepsilon)^{\frac{1}{2}}} \tag{3.15}$$

where ε is dielectric constant. From this equation Ritchie's relationship $w_s = \frac{w_p}{\sqrt{2}}$ can deduce for clean surface since $\varepsilon = 1$. But equation (3.15) is strictly accurate for a dielectric media which is infinitely thick, however, in practice the oxide layer on a surface exists with finite thickness. Stern and Ferrell have also derived a relationship for a dielectric overlayer with varying thicknesses. This relationship is given and discussed in section (3.3.2) equation (3.17). That equation is applicable in the case of contaminated surfaces, ($\varepsilon \neq 1$), the result is that the surface plasmon loss is severely attenuated and shifted in energy. The physics of surface plasmons has been reviewed by Ritchie (1973) and for further literature see Kliever et al. (1974), Economu (1974) and Raether (1977).

Surface plasmons are important because the changes in their energy and intensity produced by sorbed layers can be used to extract information about the solid surfaces. For an example Wright (1974) was able to use the shift in the surface plasmon energy of Mg with oxygen coverage

to deduce the thickness of the oxide layer formed.

In the case of surface plasmons comparison with optical measurements is also possible as in the case of bulk plasmons. However, in the case of surface plasmons, it has been shown that the probability of a fast electron losing energy to a surface excitation is proportional to Im $(-\frac{1}{\varepsilon + 1})$ (Raether (1967), Froitzheim (1977)), (Im $(-\frac{1}{\varepsilon + 1})$, is the surface loss function). Fig. (3.6) shows the surface loss function for an electron gas, Raether (1980).

3.3.1.2 One Electron Excitation of Valence Electrons (Inter-/Intra band Transition)

These transitions are single particle excitations in contrast to volume and surface plasmons which are a many particle phenomenon. An electron in the valence band of a solid may be excited to a higher (unfilled) level of the same band (intraband transition) or into another energy band (interband transition).

The energy losses of a primary electron associated with such processes are typically of the order of 3 - 20 eV. The excited electrons have a certain probability of leaving the solid, to appear in the true secondary electron peak at the low energy side of the back-scattered energy distribution curve. In large gap insulators the conditions are not favourable for the excitation of plasmons. Here we observe interband transitions in the energy region of the valence band ($\sim$ 10 eV), and of deeper levels, e.g. K.L., ... (some 10^2 eV). This will have the effect of producing an 'edge' in the N(E) curve at the energy loss value. The position of these edges can be used to identify the chemical nature of the bombarded atom of the solid. The height of the excitation signal will be a measure of the irradiated quantity so that a chemical microanalysis is possible (Raether, 1980).

Strong interband transitions contribute to structure in the ε_1

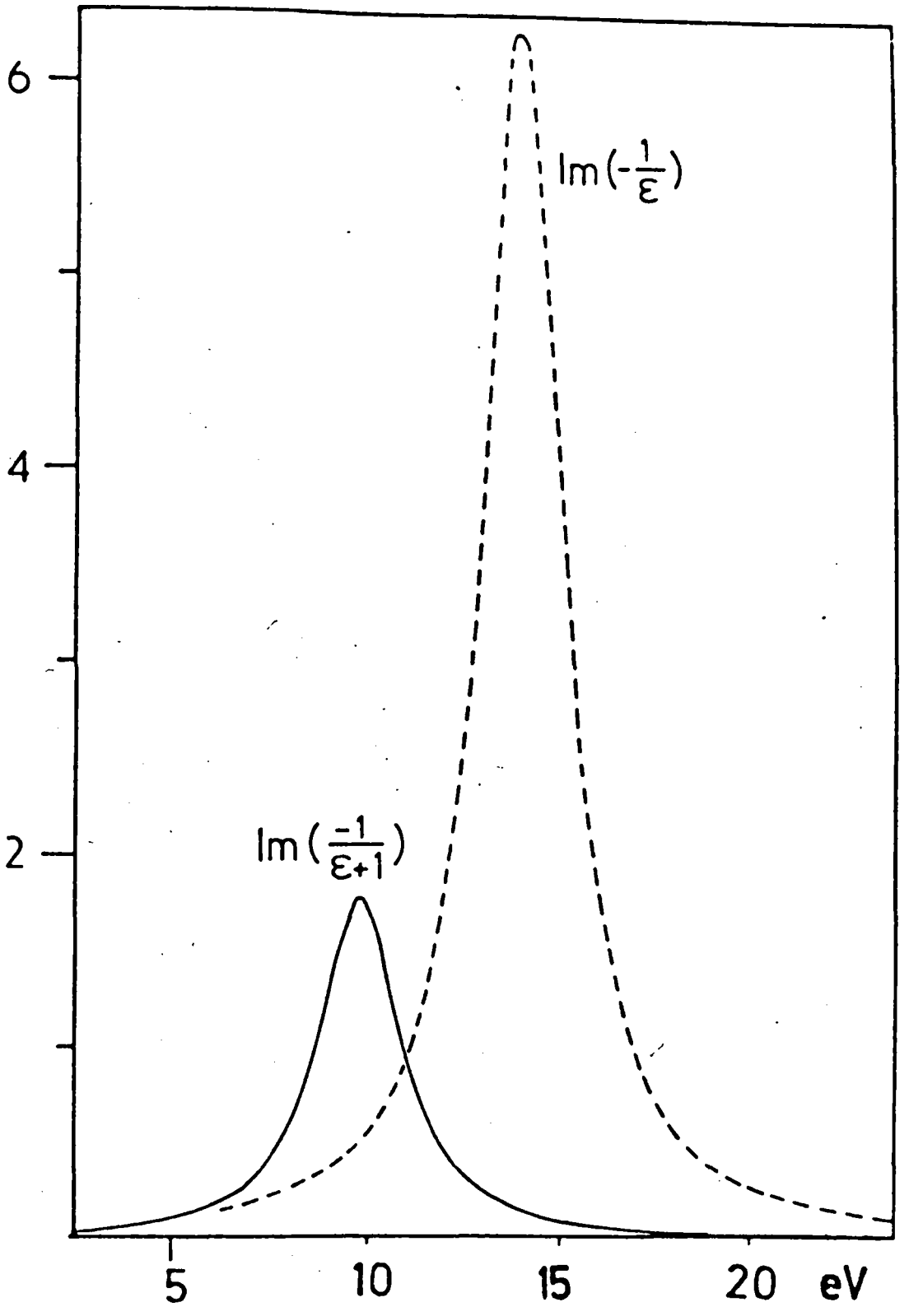

FIG. 3.6 THE SURFACE LOSS FUNCTION AND THE VOLUME LOSS FUNCTION OF FREE ELECTRON GAS RAETHER (1980)

and ε_2 components of the dielectric constant (Pines, 1963; Rowe et al., 1975) and can strongly influence the energy at which the plasmon oscillation of the valence electrons is observed. Raether (1965) has shown that the presence of a strong interband transition, whose energy is less than the calculated free electron like plasmon energy, shifts the observed value to higher energies, whereas a strong interband transition of energy greater than the calculated plasmon energy has the opposite effect. This is a simplified picture as normally several interband transitions can be excited in solid and the situation is particularly confusing for the noble elements and the transition metals in which strong interband transitions are excited with an energy close to the plasmon energy. Fig. (3.7) shows an example of the loss function of gold, in addition to the real and imaginary part of $\varepsilon(w)$, Fig. (3.8a, b). One recognizes roughly the shape of the free electron gas function on which interband transitions are superimposed.

3.3.1.3 Excitation of Core Electrons (Ionization Losses)

As shown in Fig. (3.9), if an incident electron with energy E_1 transfers energy to a bound electron in a level $-E_i$, thereby exciting it to a state E_f above the Fermi level the other electron may be ejected from the solid with an energy corresponding to the primary energy minus the binding energy of the level involved $(E_1 - E_2)$, therefore, the energy loss is given by

$$E_L = E_1 - E_2 = E_i + E_f \qquad (3.16)$$

so, the mechanism of ionization losses is determined by two electronic transitions, where in AES three electronic states are involved. The ejected core electron may be excited to any available state above the Fermi level; the minimum loss energy for excitation of a certain core state E_i is attained for excitation just to the Fermi level. A "tail"

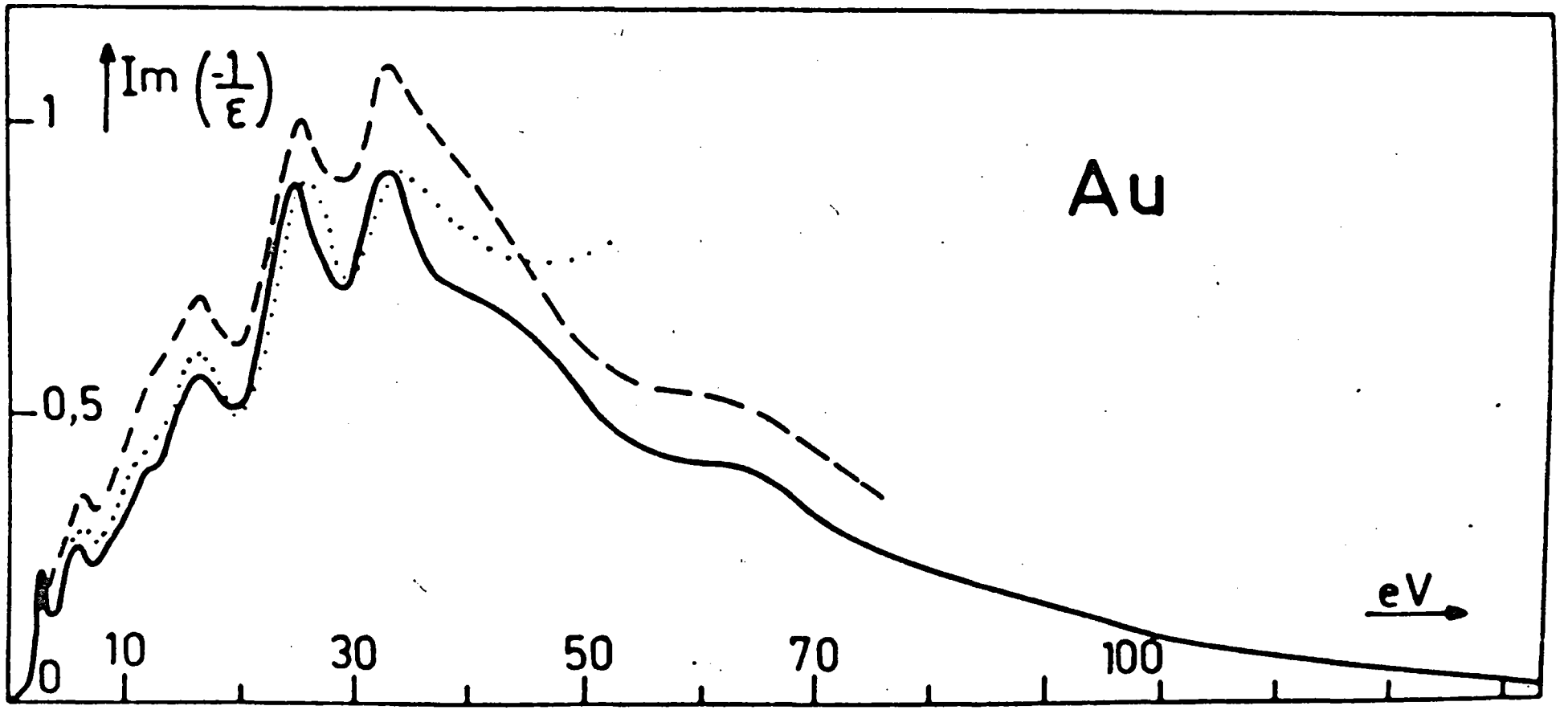

FIG. 3.7 VOLUME LOSS FUNCTION OF Au, FULL LINE WEHENKEL (1975), DASHED LINE DANIELS (1969), DOTTED LINE CANFIELD ET AL (1964).

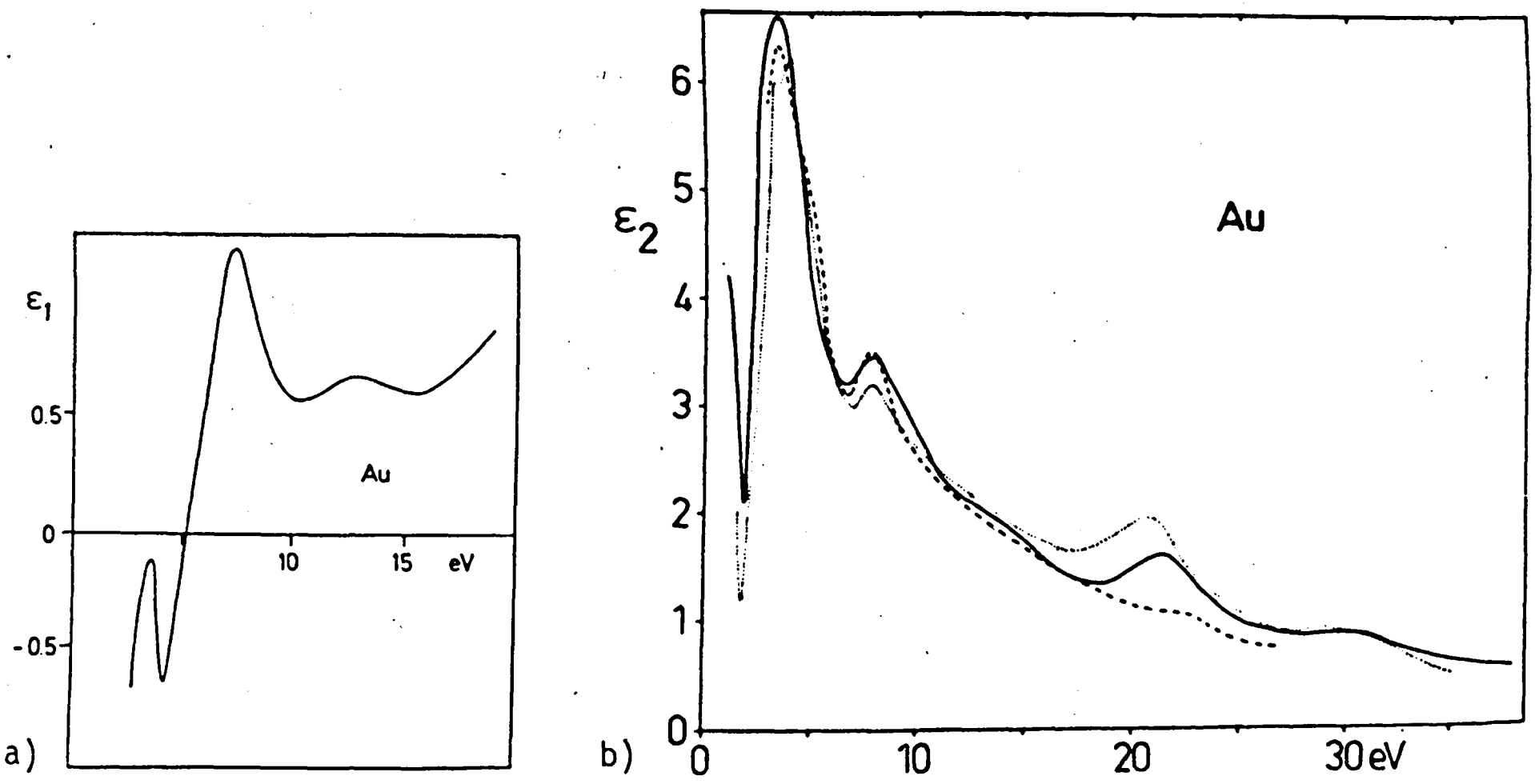

FIG. 3.8 DIELECTRIC FUNCTION OF Au . a) REAL PART, b) IMAGINARY PART, FULL LINE DANIELS (1969), DASHED LINE BEAGLEHOLE (1965), DOTTED LINE CANFIELD ET AL (1964).

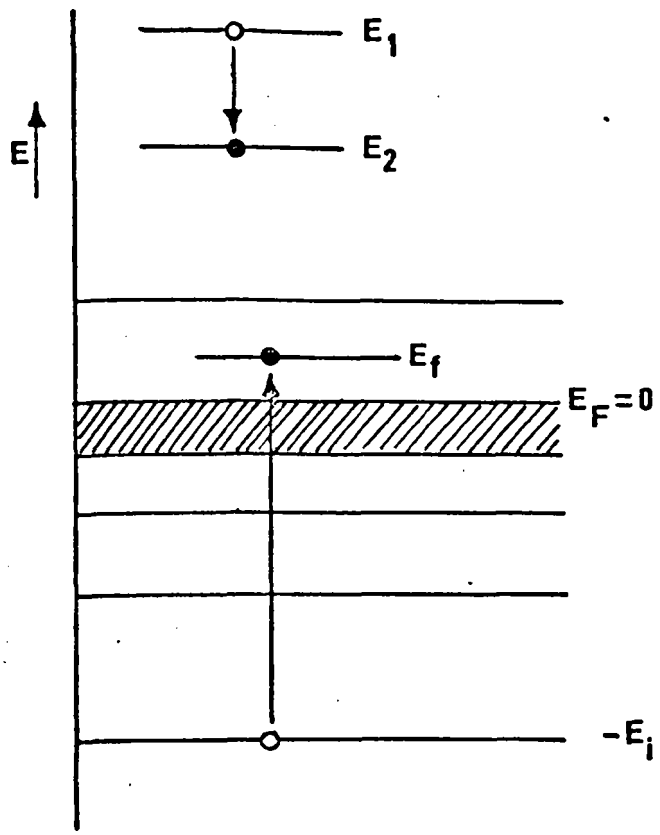

FIG. 3.9

or fine structure will be observed at higher loss energies. These features are associated with the density of unfilled state above the Fermi level E_F whereas AES probes the filled state below E_F. Such fine structure may help to characterize the chemical states of the elements on the surface.

Bishop and Riviere (1970) reported the observation of ionization losses and warned that they can be confused with Auger electron peaks if spectra with different primary energies are not taken. Gerlach et al. (1970) used special cross modulation techniques in the identification of ionization losses, and pointed out that the possible use of the technique as a direct measure of electron binding energies (core level energies of atoms), which of course is potentially useful in AES. However, Fiermans and Vennik (1973) have pointed out that the use of ionization losses to determine exact energy level positions is at present limited to a few cases where transitions into well defined energy levels occur. This is so, since many metals show maximas in the density of states above the Fermi level. This point is of special importance in the measurement of 'chemical shifts' occurring in the core levels after the atom has chemically combined with another atomic species.

The observed spectra of ionization losses are less complex than Auger spectra since fewer electronic states are involved, but the signals are much weaker than those obtained with AES and the method has found little application in surface analysis. Ionization loss spectra may be used for chemical identification in cases where Auger peaks overlap on the energy scale or where the observed Auger peaks reveal no unique evidence for the existence of an element.

The ionization losses are mainly of interest to physicists for determination of differential ionization cross sections of surface atoms

by measuring the ionization peak current which is scattered into a narrow angle, $d\Omega$, Gerlach et al. (1972).

3.3.1.4 Excitation of Surface Vibrations (Quasielastic Electrons)

The phonon assisted inelastic scattering of electrons leads to very small energy losses in the range of less than a few tenths of an eV, so that these electrons are not separated from the elastic peak in normal resolution spectrometers. Much more refined experimental techniques involving several 127^{o} analysers are necessary in order to determine the energies of these excitations (Ibach, 1977).

3.3.2 Changes of Energy-loss Spectra by Adsorbed Layers

The variation of energy loss spectra, and in particular the plasma loss features, with the chemical state of the surface have been recognized for several years, but only recently has the high sensitivity for the study of adsorbate-covered surfaces been realized.

Powell and Swan (1959, 1960) have investigated the characteristic energy losses of Mg, Al and the oxidation effects on the two metals. They observed strong plasma losses in the metals and a shift in the surface plasmon loss energy upon oxidation of the metal films. However Stern and Ferrell (1960) predicted a progressive shift in the surface plasmon energy as oxidation proceeded, and according to their theoretical work the dispersion relation of the surface plasmon frequency w_s (section 3.3.1.1.b) in the case of a semi infinite metal coated with a film with thickness d should be given by:

$$w_s = w_p \left[(\varepsilon + \tanh Kd)/(2\varepsilon + (1 + \varepsilon^2) \tanh Kd) \right]^{\frac{1}{2}} \qquad (3.17)$$

where w_s and w_p are the frequencies of the surface and the bulk plasmons, respectively, d is the thickness of the oxide film having a dielectric constant, ε and K is the surface wave vector excited by the incident

electron corresponding to the surface plasma oscillation.

By observing the energy shifts of the surface plasmons, Murata and Ohtani (1972) have studied the growth of the thin oxide layer on Al and by using equation (3.17), they suggested that the energy loss value may be used to determine the dielectric overlayer thickness. Then Wright (1974) extended this work to normal incidence electron beam, where only backscattered electrons may produce surface electron oscillation, and actually he estimated the depth of the MgO overlayer. Besides the variation of the intensities and energies of the plasmon losses caused by surface overlayers, new peaks in the loss spectrum may also appear after chemisorption. This effect was observed, for the first time by Steinrisser and Sikafus (1971).

3.4 Electron Spectrometers and Instrumentation

In order to analyse the energy of electrons with energies in the range of a few electron volts to about 1500 eV, electrostatic analysers are to be preferred over the more bulky and usually more costly, analysers of the magnetic type. The latter can become more convenient at high energies.

The electron energy analysers presently used in Auger electron spectroscopy are basically of two types, a) the retarding field analyser (REA), b) the dispersive focussing analysers namely the cylindrical 127^{o} sector (Harris, 1968), the spherical velocity analyser (Purcell, 1938; Meyer et al., 1965; Hafner et al., 1968) and the cylindrical mirror analysers (CMA). In the literature by Roy and Carette (1977) characteristics and design of different electron energy analysers are explained.

We shall confine our discussion to the basic principles underlying the two most common analysers used in Auger electron spectroscopy,

namely the retarding field analyser and the cylindrical mirror analyser. The importance of these instruments can be ascribed to the following:

1. They have high sensitivity.
2. They are relatively simple in construction and easy to operate.
3. They can be combined with other complementary experimental techniques such as LEED, RHEED, the electron microprobe, the scanning electron microscope, etc.

3.4.1 Retarding Field Analyser (Auger-LEED device)

This type of analyser is still one of the most commonly used energy analyser, since with slight modifications it can be adapted from the system used for LEED studies, work function and secondary electron yield measurements. The basic apparatus for this technique is a spherical section (often 180^{o}or 120^{o}) retarding potential analyser such as that shown in Fig. (3.10). A negative voltage (V_R) is applied to the second grid which retards those impinging electrons with a kinetic energy less than eV_R, to the first grid or target. The third grid minimises field penetration of the collector (in this case the fluorescent screen) potential into the retarding region. The sample is placed at the centre of the curvature of the grid-system. Ideally, the innermost grid should be midway between the sample and the next set of grids. It is grounded, as are the sample and all neighbouring components, to provide a field-free region between the grid and the sample. This ensures that the secondary electrons produced by the sample will travel radially towards the grid.

The sample is excited by bombardment with electrons of energy $E_p = eV_p$ from the electron gun, $-V_p$ being the cathode potential of this gun. The number of electrons $N_c(E_R = eV_R)$ reaching the collector or is recorded as a function of the retarding field voltage V_R which is

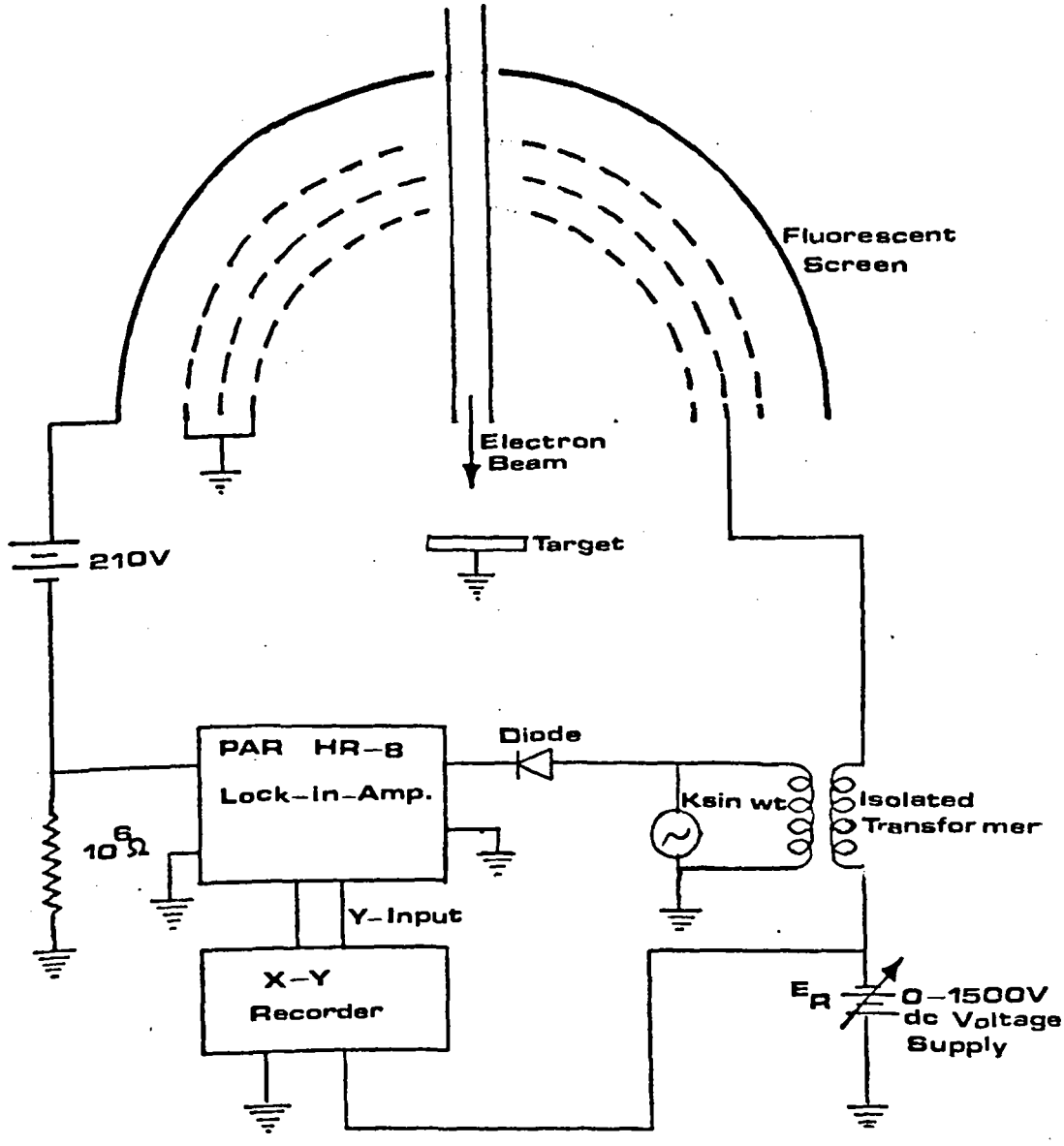

FIG. 3.10 RETARDING POTENTIAL ANALYSER USED BY PALMBERG AND RHODIN (1968)

varied from ground potential to $-V_p$ and it is related to the energy distribution of secondaries by

$$N_c(E_R) = \int_{E_R}^{E_p} N(E)dE$$

A further analysis of the detection technique is given in section (4.4.1).

Palmberg (1967) and Scheibner and Tharp (1967) independently recognized that the energy distribution N(E) could be obtained from the collector current by electronic differentiation, i.e. a small modulating voltage (K sin wt) is applied to the second grid, as well as the retarding voltage, and the component of the collector current at the modulation frequency (w) is proportional to N(E). In extracting Auger peaks using the $\frac{dN(E)}{dE}$ mode, Weber and Peria (1967) recognized that by detecting the second harmonic 2w of the collector current $\frac{dN(E)}{dE}$ could be obtained from a retarding potential spectrometer.

A double retarding grid system was first used by Palmberg (1968) to improve the energy resolution from 2.5% to 0.5%. Taylor (1969) has considered the performance of modulated retarding potential analysers in considerable detail, however such details of performance will be found in section (4.4.1).

3.4.2 Cylindrical Mirror Analyser (CMA)

One of the most important analysers for electron energy analysis of surfaces is the cylindrical mirror analyser (CMA), which was originally developed by Blauth (1957) and optimized theoretically by Hafner *et al.* (1968) and Sar-el (1967). However, it was Palmberg *et al.* (1969) who first realized its potential as an Auger spectrometer. It has the advantage of a high transmission (up to 10%) for a dispersive type of

analyser as well as a superior signal to noise ratio than a retarding field type of analyser. The arrangement, as shown schematically in Fig. (3.11), consists basically of two coaxial cylinders. The inner cylinder is grounded and has two cylindrical gridded apertures suitably positioned along its length. The outer cylinder has a negative voltage V_a applied to it so that secondary electrons leaving a suitably located grounded sample and entering the first of the apertures tend to be reflected towards the second aperture. The sample is usually placed with its centre on the axis of the cylinders. For a particular voltage V_a applied to the outer cylinder, only electrons with energy $E = eV_{pass}$ will pass through the second gridded aperture and come to a focus (strictly speaking, produce a minimum trace) in a small annular region close to the axis. The ratio $\frac{V_{pass}}{V_a}$ is determined by the geometry of the analyser and lies usually between 1 and 2. The ratio remains constant over a very wide range of energies. The energy resolution $\frac{\Delta E}{E}$ is constant and the current collected at the exit aperture of CMA is given by

$$I_c = I_p \, K \, . \, E \, . \, N(E) \qquad (3.18)$$

where K is the geometry factor.

Again the modulation techniques as described for the retarding field analyser may be applied, and the current I_c can be electronically differential by applying a modulation voltage (K sin wt) to the outer cylinder and detecting the first harmonic of the output current. However in contrast to the RFA the first derivative of the collector current yields $\frac{d\,N(E)}{dE}$ and not the second derivative. The detailed analysis of the CMA is complicated but has been treated by several authors, one of them is Roy and Carrette (1971).

There are several important differences in the electronic details

Coaxial cylindrical analyzer

FIG 3.11 Cylindrical mirror analyser (Palmberg et al 1969)

between Figs. (3.10) and (3.11). An electron multiplier is used as the pre-amplifier for the CMA because it is the lowest noise, widest band width low current amplifier available. Since the multiplier collector is at a high positive potential, it is capacitively coupled to the synchronous detector input. This arrangement permits modulation frequencies 50 KHz to be used, thereby allowing high speed scans (> 10000 eV/sec) and oscilloscope displays. The CMA produces a remarkably flat spectrum down to as low as 25 eV but the analyser is relatively insensitive in the slow peak region since the gain of the first dynode is determined by the energy of the impinging electron. Hence, the retarding potential analyser is still a desirable electron spectrometer in this low energy region since it maintains its inherent sensitivity. However, while the gain for the retarding grid system must be changed over as much as a factor of 300 over the whole energy range, the CMA will record a complete energy spectrum using only a single gain.

3.5 Conclusion

In this chapter, some of the published work on various aspects of Auger spectroscopy and characteristic energy losses have been reviewed. Many theoretical aspects of AES are still to be fully developed but some progress along these lines is now evident. The combination of AES with electron energy loss spectroscopy was shown to be a powerful tool for determining the plasma behaviour of materials and electronic energy levels. Finally, the electron spectrometers and the instrumentation have been discussed.

The chapter which follows, contains a discussion of the experimental apparatus and techniques used to obtain the experimental results of this thesis.

CHAPTER 4

4.1 Introduction

The basic design of the experimental system used, was made by Suleman (1971). However during the course of this study the system was further improved, and additional surface cleaning facilities incorporated which were necessary due to the nature of the present study.

The present detection system consists of facilities to analyse Auger Electrons, Electron Energy Loss and Secondary Electron Yield (AES, ELS, SEE). So in this chapter the ultra high vacuum system, with its cleaning facilities and detection systems for AES, ELS and SEE are described. The experimental methods are discussed sequentially in each section.

4.2 General Features

4.2.1 The UHV System

The UHV system is made of stainless steel type EN58E. The entire system except the forevacuum part is bakeable up to 450°C for degassing purposes. The main feature of the system is shown in Fig. (4.1) and Plate (4.1 and 4.2). It consists of a cylindrical shape main chamber with inner diameter of 6 ins and height 8 ins. The main chamber has six equally spaced horizontal parts. The bottom part of the chamber is connected to a sputter ion pump type FJD 140 (Ferranti) through a connecting tube of 6 ins diameter. The large diameter of the connecting tube makes it possible to achieve rapid pumping of the main chamber. The top is covered with a flange, which has a central port incorporating an electron gun, three electrical feedthroughs and facilities to fix grids, i.e. the entire analyser section is mounted on this flange.

Four of the ports on the main chamber are 2¾ ins flanges, two of them carry windows, a third one carries a feedthrough for the projector lamp (section 4.3.1) and the fourth one is connected to the ion pump type FJ8 (Ferranti) and a bakeable valve. The bakeable valve isolates the sorption pump from the main chamber.

The other two ports are 4½ ins flanges which are diametrically opposed to each other. One of them carries a window and the other one is connected to the manipulator system (section 4.2.6), evaporation feedthroughs, target connection feedthrough, window, bakeable valve, ion gauge, cold trap, diffusion pump and rotary pump, which are shown in Fig. (4.2).

4.2.2 Preparation of UHV

In the initial stage, the system was pumped out to about 1×10^{-3}

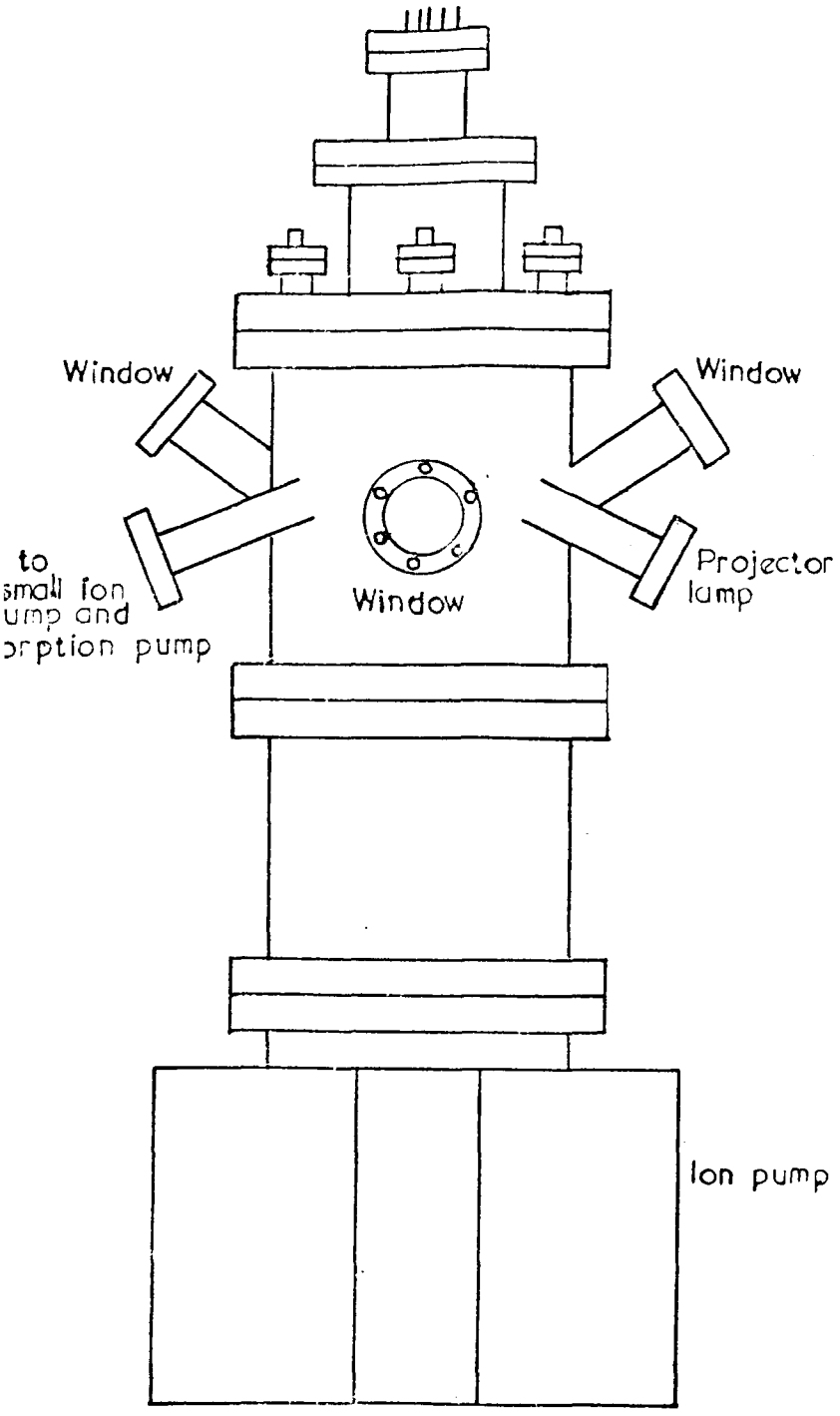

Side view of main chamber

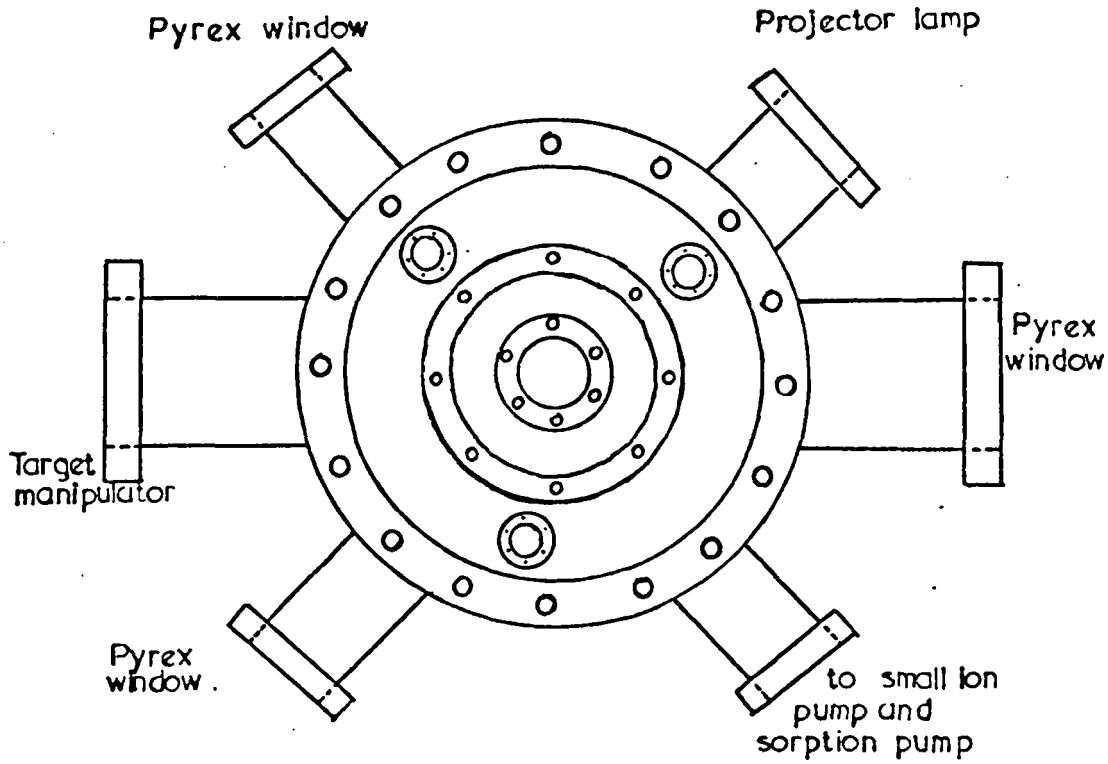

Top view: A schematic diagram of the main chamber showing the uses of various ports

FIG. 4.1

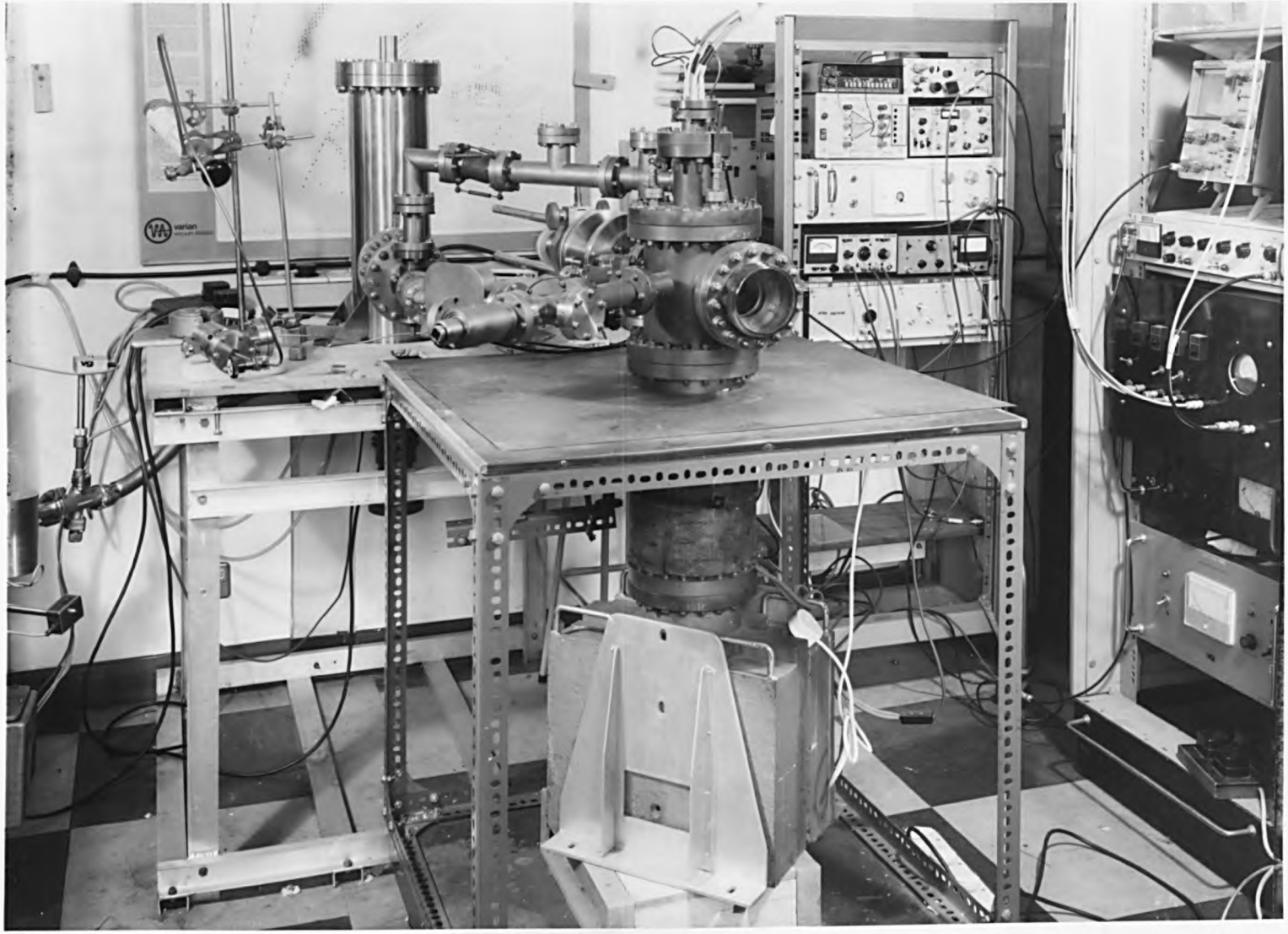

Plate 4.1

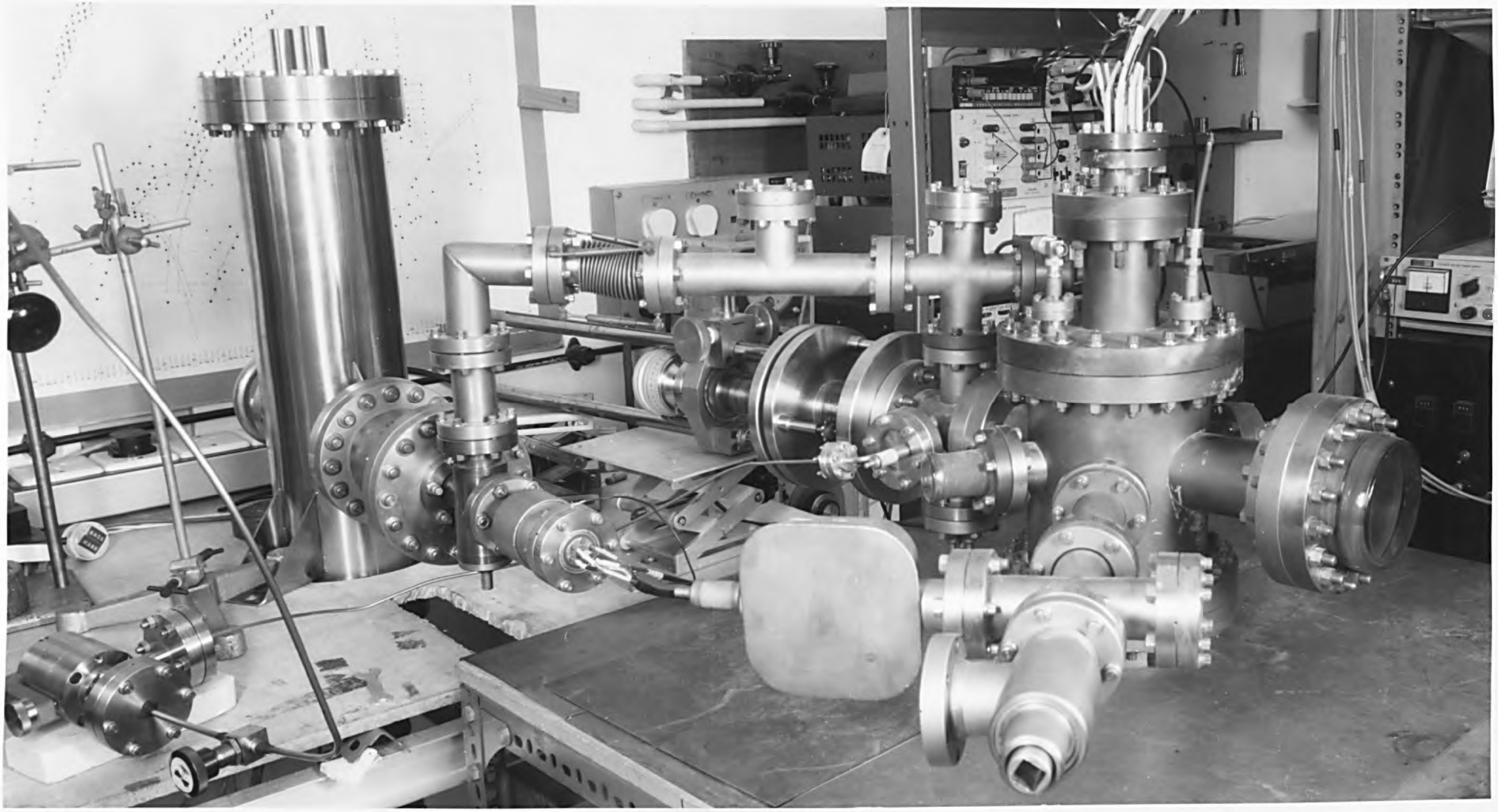

Plate 4.2

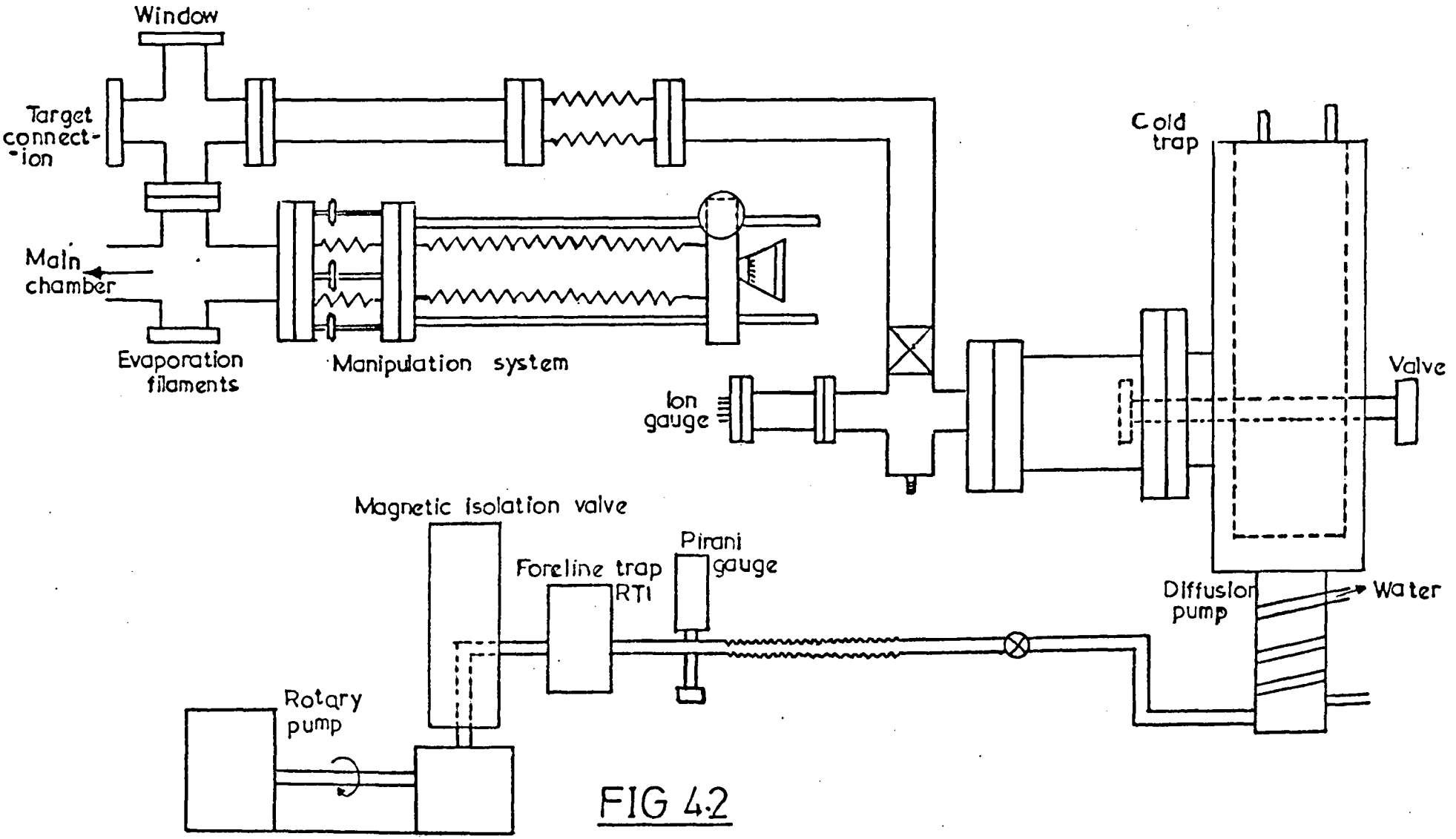
Window
Target connect-ion
Main chamber
Evaporation filaments
Manipulation system
Cold trap
Valve
Ion gauge
Magnetic isolation valve
Foreline trap RTI
Pirani gauge
Diffusion pump
Water
Rotary pump

FIG 4.2

torr with the foreline pumps (rotary pump and sorption pump type FCD23, Ferranti). The foreline valves were closed and pressure reduced to about 10^{-7} torr with the ion pumps. The complete system was baked at 250°C for 24 hours with tape heaters. The bakeout temperature was adjusted to maintain the system pressure at all times at less than 10^{-6} torr. After cooling the system and pumping for a further two days or so, the base pressure of the system was $\sim 10^{-10}$ torr.

The evaporation filaments and the projector lamp were successively outgassed over a period of about three days or more until there was no increase in the base pressure when they were raised to their normal operating temperature.

4.2.3 The retarding field Analyzer

The retarding field analyzer which was used for the measurement of both the energy distribution of secondary electron and the total yield of secondary electron, consists of a hemispherical collector and three grids concentric with it.

The collector has a hemispherical shape of radius 5 ins, and was made of type 304 stainless steel. It is connected to the top flange of the main chamber through insulated ceramic (alumina Al_2O_3) connectors. The three hemispherical tungsten grids are inside the collector. The outer and middle grids were used as retarding grids, and have diameters of 4.25 ins and 4 ins respectively. The inner grid of diameter 2.5 ins was maintained at earth potential. These grids were held together and connected to the collector via three ceramic connectors. These grids have a hole of diameter ½ ins at the centre of their hemispherical surface to allow the electron beam from electron gun to strike the sample at normal incidence. The transmission of these grids was 85% with mesh denisty 64 x 64 meshes per square ins. These grids were made by stretching and smoothing tungsten mesh over a pyrex flask of the desired

diameter. Then the mesh was fastened by a ring of nickel wire, whose diameter was fractionally bigger than the diameter of the flask. Then the mesh and the wire were welded together with the hand welder.

4.2.4 Pressure Measurement

An ionization gauge, model VG10 (Vacuum Generator) Bayard-Alpert type, with control unit IG3 was used for the pressure measurement. The pressure could be measured within the range 10^{-2} torr to 2×10^{-11} torr, the gauge having an x-ray limit of 2×10^{-11} torr. In addition to this, the pressure could also be estimated down to $\sim 5 \times 10^{-10}$ torr from the leakage current of ion pump, with the help of a calibration curve provided by the manufacturers.

4.2.5 Electron Gun

The primary electrons are obtained from an electron gun type SE-3K/5U (Superior Electronics Ltd.). This electron gun contains an indirectly heated and replaceable oxide-coated cathode type KA809F and the heater type E7291. This type of cathode is known to poison on exposure to atmosphere and its life is between five and six exposures to air. However, it does have certain advantages over the alternative tungsten filament viz higher current and operation at a much lower temperature which in particular means less carbon on any given surface.

The processing of unbalancing the cathode is known as 'activation', and may be accomplished by raising the temperature of the cathode rapidly for a few minutes (commonly known as 'flashing' technique). This so-called thermal activation is the creation of donors by partial reduction of the oxide at the metal-oxide interaface and is quite efficient. It was also found useful to maintain a small current running through filament to reduce absorption of water vapour and oxygen while the electron gun is not being used.

As an aid to focussing and positioning of the electron beam a disc of glass ceramic size 1 x 10 mm was coated with zinc orthosilicate (Willemite, $Zn_2S_iO_4$ activated with Mn). The coating process is described by Thomson and Callick (1959). By mounting this fluorescent screen beside the specimen the focussing properties and beam position were checked over the range of energies for which the spot was visible (above 200 eV).

To minimize stray magnetic fields at low energies, the ion pump magnets were shielded with a netic and co-netic screen (Perfection Mica Co. Chicago). Also an earthed shield was mounted around the electron gun to prevent electrons reaching the collector directly from the gun electrodes, this screen extended via a 6 mm diameter nozzle into the field free region within the inner grid.

The voltage to the cathode was supplied by a highly stabilized power supply type Fluke 415B, and the heater voltage (6.3 V, 0.6 A) was supplied with the stabilized power supply type Farnell L30F which was floated up at the cathode supply voltage.

The maximum working voltage of the electron gun was 3 KeV with currents up to ≃ 100 μA, but for recording Auger spectra 1.3 KeV was used.

4.2.6 Target Manipulation and Transfer System

This system consists of two parts which are viz:- "a bellows transfer manipulator (plate 4.3) and an x, y and z manipulator". The transfer manipulator was newly designed by one of my colleagues (R. Moran) and was made in the department workshop. This consists of an edgewelded bellows, an independent rotary drive (Vacuum Generators) which is located on a 2¾ ins flange on the end of this assembly and a rotating shaft which extends along the axis of the bellows from the rotary drive. The target is connected to this shaft so that it can be

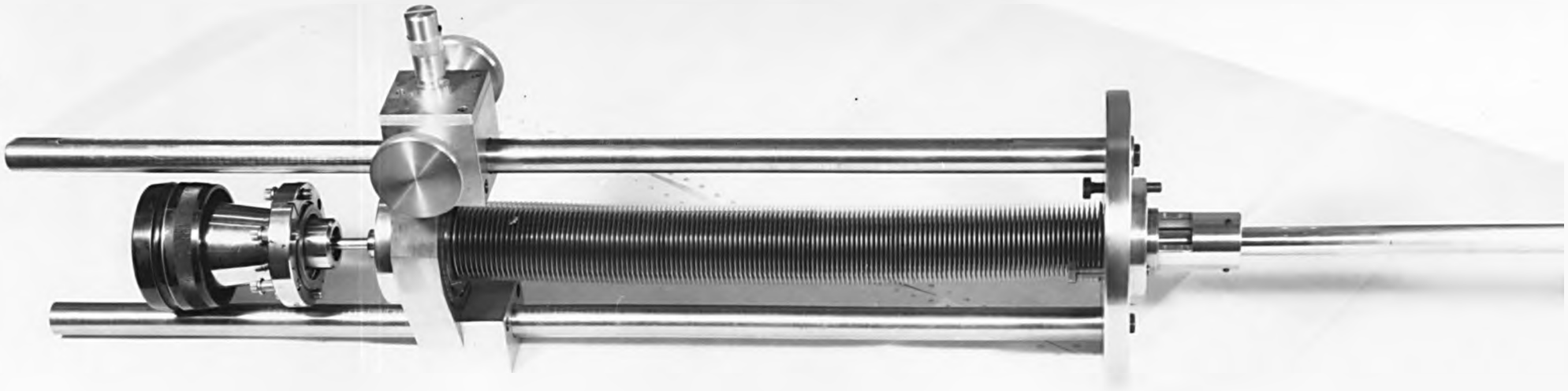

Plate 43

transferred linearly and in addition rotated through ∿ 360 degrees. The rotational motion is controlled by the rotary drive and the linear transfer movement is operated by a rack and pinion. This bellows assembly allows the target to have about 15 ins linear movement, which is relatively large in a UHV system.

This device is coupled to the x, y and z manipulator which allows three dimensional movements of the target. This movement is controlled by another bellows and three adjustable screws.

With all these movements the position of the target is reproducible. (The target is insulated from the shaft electrically).

The linear movement of the target is important for transferring the target from the main analysing chamber to an adjacent part of the system where cleaning by argon ion bombardment and evaporation from metal sources are conducted. Also with the target in the retracted position for cleaning the ceramic insulators of the analyzer do not become coated during any evaporation or other surface treatment with metal films, as they would in the main chamber.

In addition to these technical advantages the rotational movement of the target allows one to investigate surface processes sensitive to the angle of incidence or for example enables one to increase the Auger yield and intensity of any (surface) phenomena such as surface plasmon energy loss by using glancing incidence.

Furthermore, fine positional control of movement in three directions is important for optimizing the target position for best resolution, since for optimum resolution, the analysis area must be at the centre of the analyzing grids.

4.2.7 Gas Admittance System

For sputtering the surfaces by argon ion bombardment, the argon gas was supplied to the saddle-field ion source (Ion-Tech Ltd.) B22,

from the unit shown in Fig. (4.3). This unit consists of a leak valve type MD1088 (Vacuum Generator), two regulating valves (P and Q) and a cylinder (containing argon of purity 5N supplied by BDH). This unit is connected to the saddle field ion source via a stainless steel tube of diameter (1/16)" O.D.

To obtain high purity argan supply for the ion source, each time during the roughing stage of evacuation, the valves of gas admittance unit were opened and flashed by opening the cylinder valve for a few seconds. Then gas leaks from the cylinder through the tubes into the main chamber, effectively flashing out the impurity gases. All the valves were then closed and the vacuum chamber pumped to UHV pressure as normal.

In a typical experiment the argon gas could be admitted into the chamber, at a controlled rate, by slowly opening the leak valve and by regulating the gas pressure by P and Q.

4.3 Surface Cleaning Facilities

A specimen situated in an ultra high vacuum environment obviously does not necessarily have a "clean" surface, therefore, specimen surface preparation and cleaning facilities need in general to be incorporated into any UHV apparatus.

A projection lamp filament of 1 KW power for electron bombardment heating and an argon ion source for sputtering the surface of the sample were mounted inside the chamber. In some experiments thin films, with clean surfaces were prepared by evaporation.

4.3.1 Specimen Heating by Electron Bombardment

This process largely involves removing the impurities from the surface by thermal desorption. First the filament was thoroughly

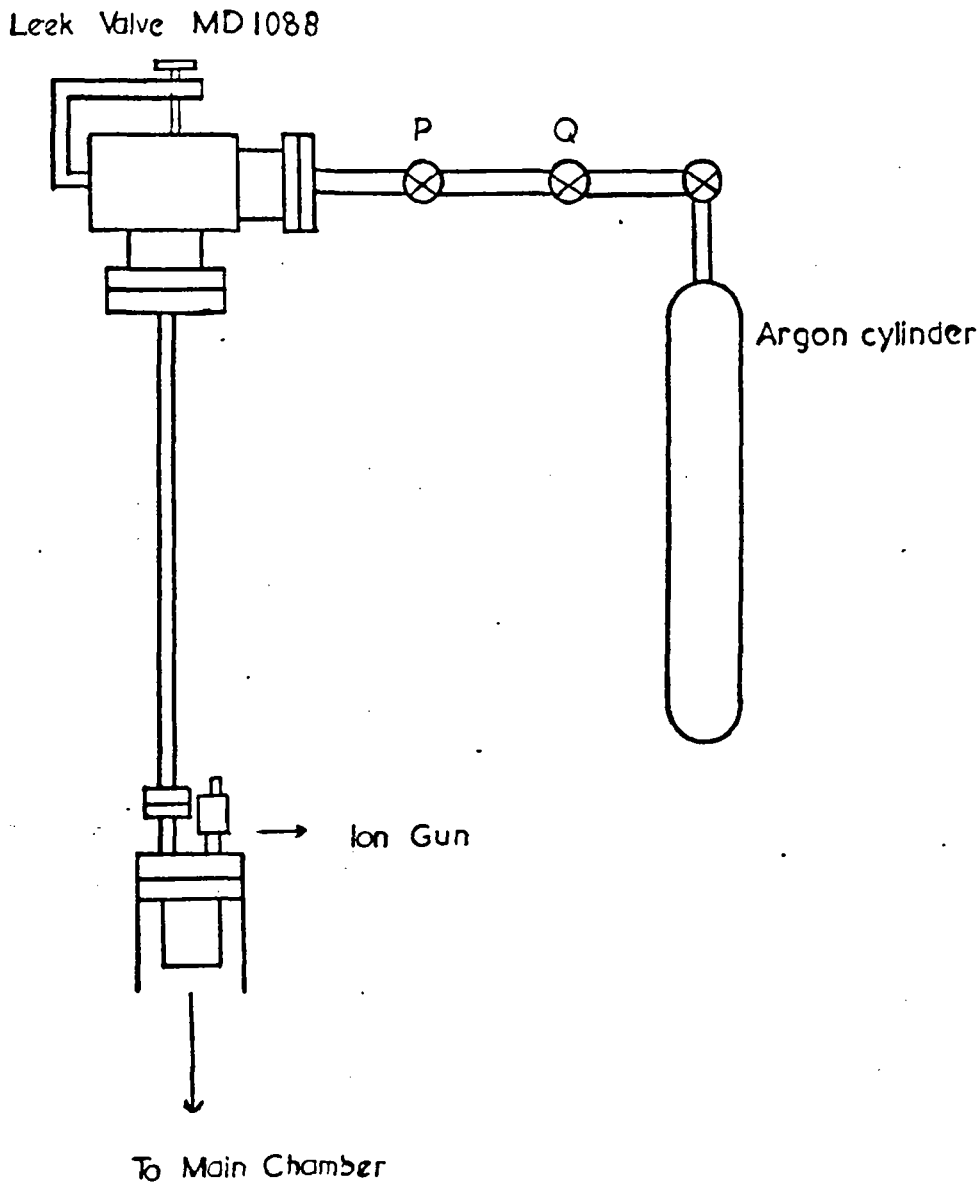

FIG.4.3 The Argon Admittance System

degassed, and then the current was gradually increased until the filament emits electron; the emission of electrons can be detectable from the fluorescent, these emitted electrons were focussed onto the target by applying +ve voltage of $\sim$ 2.2 KeV to it.

Typically a target bombarded with a 100 mA electron current and of energy 10 KeV would reach a temperature of about 2000^{o}K. However,the Be sample was cleaned by electron current of 1.2 mA with energy 2.2 KeV. In practice this was obtained by passing a current of 1.8 A through the given projection lamp filament and applying a positive voltage of 2.2 KV to the target, while keeping the pressure $< 10^{-8}$ torr.

However, the process can involve some disadvantages, which is mainly, the diffusion of bulk impurities to the surface.

A typical effect of the electron bombardment process on a Be foil is shown in Figs. (4.4 and 4.5). As may be seen in Fig. (4.4), before cleaning the target by electron bombardment, there is a large carbon peak at 275 eV, an oxygen peak at 512 eV, BeO peaks at (65, 73, 85, 95 eV), phosphorus at 119 eV and S at 148 eV are noticeable.

After the electron bombardment, Fig. (4.5), it may be seen that the carbon peak is much reduced and appears at 270 eV, P and S have disappeared completely, the BeO peaks occur at 45, 65, 77, 85 and 95 eV respectively, and these BeO peaks are larger than the peaks before the cleaning process. However, the oxygen peak has also increased on the surface, therefore, it seems that it is impractical to remove oxygen from the surface of Be foil by electron bombardment alone. This could be due to the strong bonding between Be and oxygen atoms.

To break strong bonds, large momentum transfer or in turn heavy particles bombardment is more suitable. In this regard for this surface argon ion bombardment was selected in preference of electron bombardment.

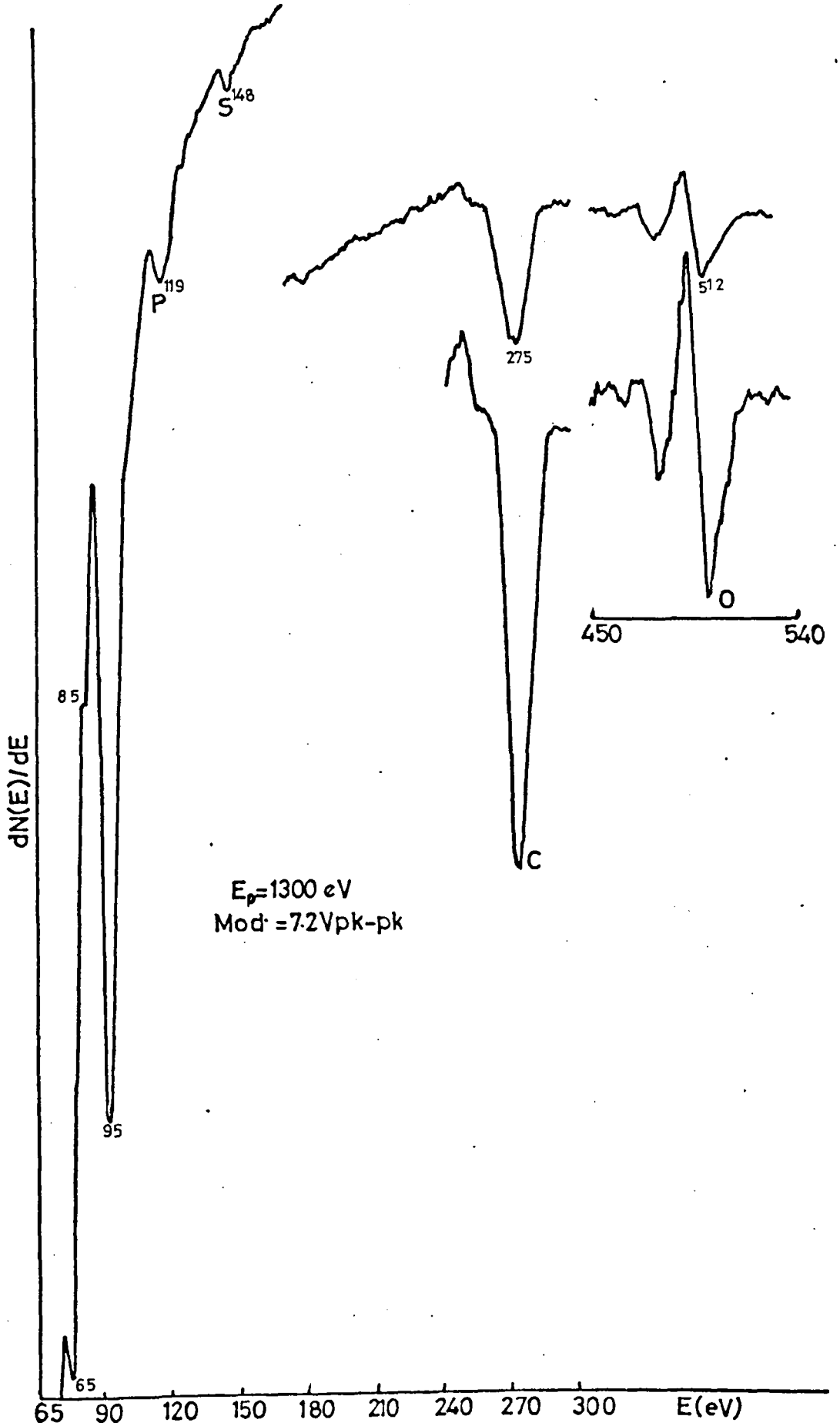

FIG.44 Auger spectrum of Be foil before cleaning

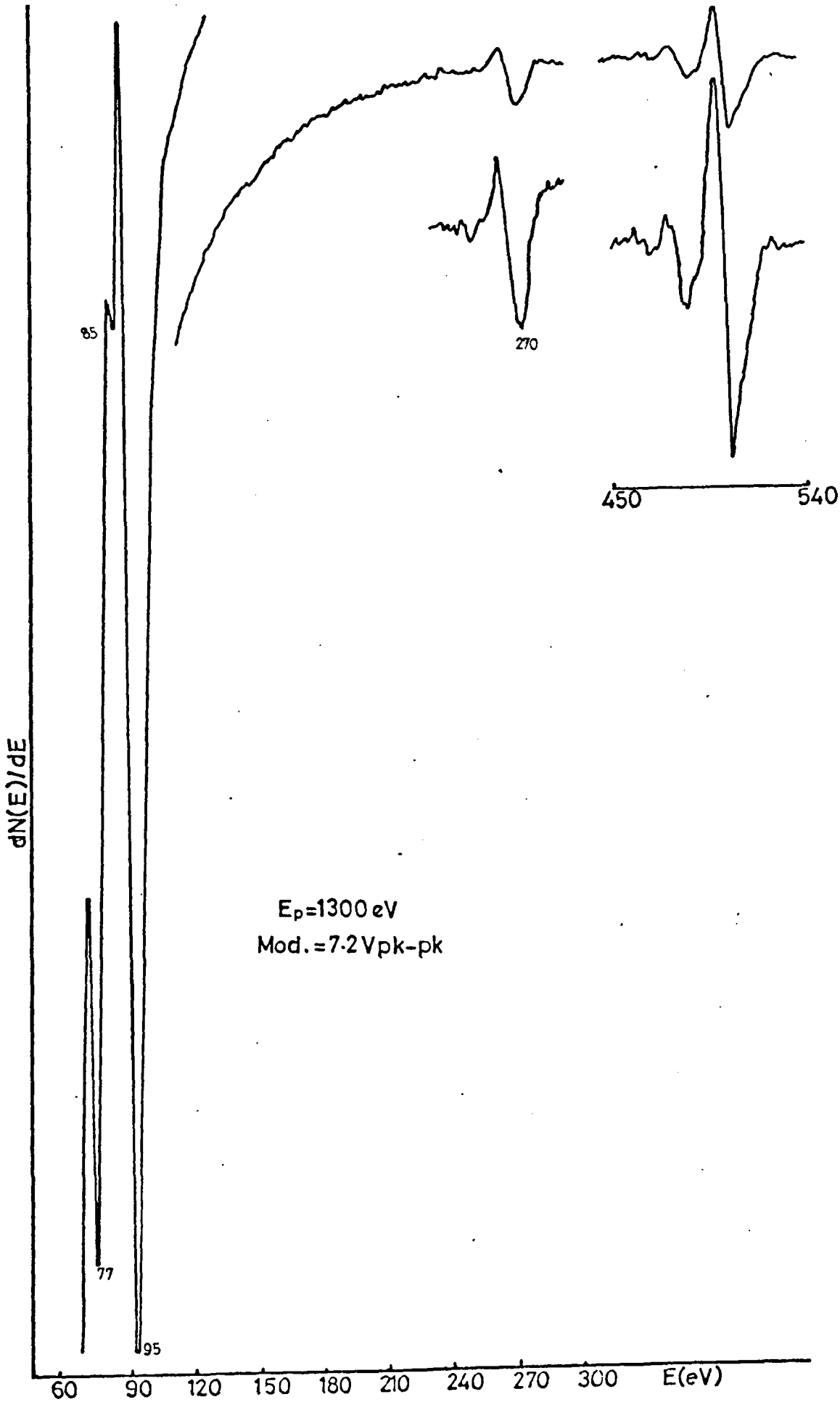

FIG. 4.5 Auger spectrum of Be foil after two hours cleaning by electron bombardment

4.3.2 The Saddle Field Ion Source

Ion sputtering is a widely used technique to remove adsorbed atoms together with one or more surface layers. As it has been mentioned by Smith (1971), the erosion time can be in the order of one monolayer per 10 minutes.

One method of ion production uses a choice of special field geometries called the saddle field ion source (Franks & Chandler, 1974). The saddle field ion source (B22) used in the present study was made by Ion Tech Ltd. and is a cold cathode device which produces an intense beam of ions (in general argon ions are used) without the aid of magnetic fields at low pressure $\sim 10^{-4}$ torr. It cleans a surface by etching away the top layers by high energy argon ion bombardment, and any changes in surface structure can be subsequently restored by annealing. This B22 device is a wide beam source which covers an area of about 1 cm^2 at 5 cm from the source, the beam density is about 150 $\mu A/cm^2$ at 5 KV; however, for the argon bombardment of the Be foil a voltage of 4 KV was used, the target current to earth was 20 μA, the operation pressure was nearly 10^{-3} torr, and the current from anode to cathode was nearly 1 mA. Some results obtained from the beryllium target, illustrating the cleaning action of the ion source are shown in Fig. (4.6). The composition of the surface under ion bombardment was monitored with AES. Argon ion sputtering is a destructive technique and this disadvantage may limit its usefulness in surface studies.

The gas admitted into the ion source needs to be pure, to prevent any possible contamination of the surface by undesirable active gas ions. This means that not only purified gas has to be used, but also the gas inlet system (section 4.2.7) has to be bakeable. If one connects the gas bottle with the inlet system, gas pollution by air cannot be prevented, only a cycle of repetitive gas introduction into

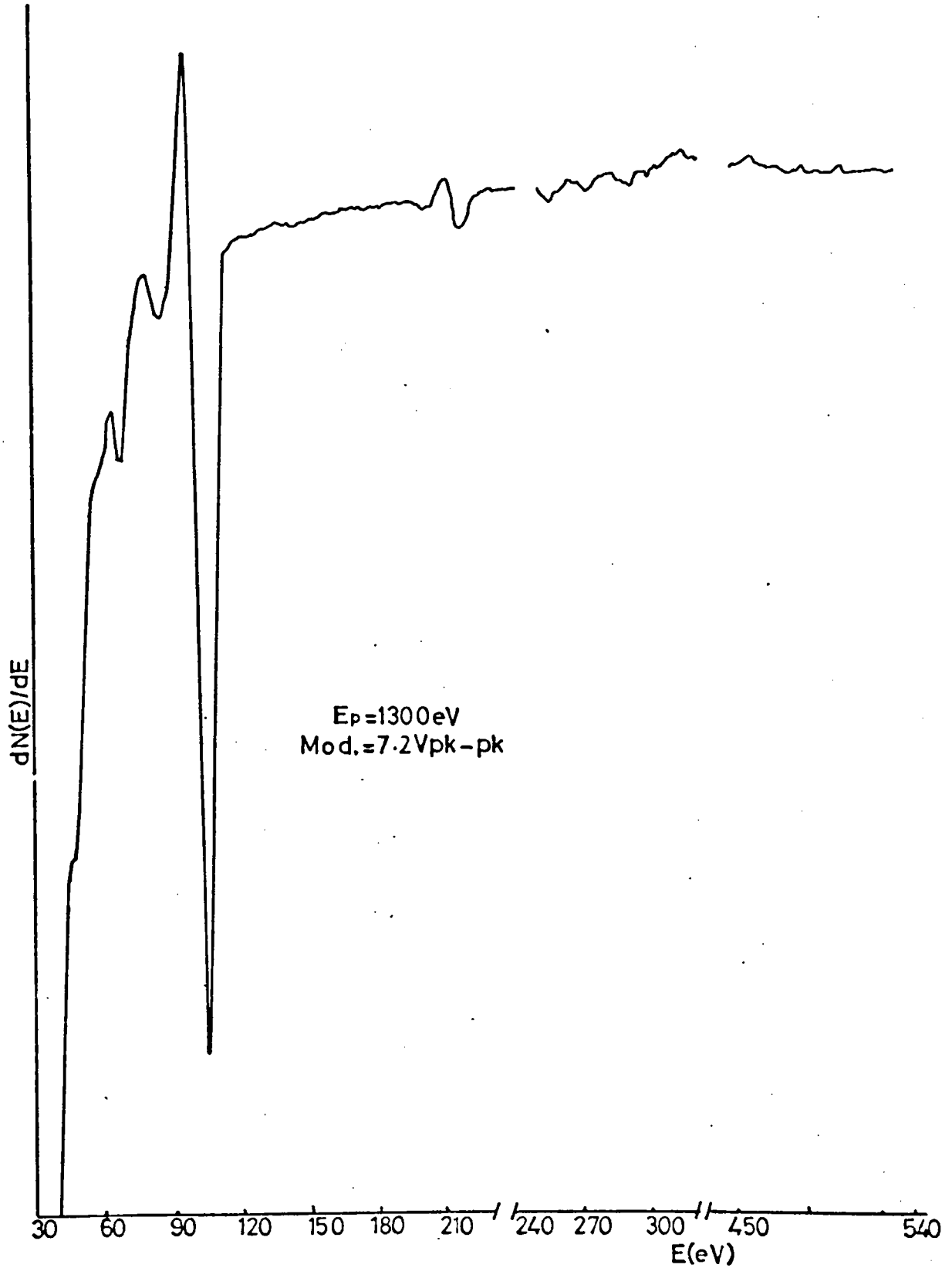

FIG.4.6 Auger spectrum of Be foil after cleaning by argon bombardment

the inlet system followed by vacuum pumping can decrease the air pollution in the gas.

During the argon bombardment, evacuating of the system with an ion pump was very difficult, because the particular ion pump used had a very low pumping speed for argon. So it was decided to evacuate the chamber with the specially trapped Edwards diffusion pump, marketed by Vacuum Generators Ltd. The specifications of this pump stated that it was capable of evacuating to UHV-pressures. The pumping scheme is shown in Fig. (4.2).

4.3.3 Thin Film Evaporation

By evaporating a material from an outgassed filament or an evaporation boat, in a UHV environment, onto a suitable substrate a clean surface characteristic of that material can be produced. Such a facility was provided in the present apparatus and was used in the investigation of the element Magnesium.

4.4 Detection System for AES and CELS ($^{dN}/_{dE}$) and SEE yield

4.4.1 Detection Method for AES and CELS ($^{dN}/_{dE}$)

There are many ways in which the kinetic energy distribution of electrons can be measured. The technique for the energy analysis of the secondary electrons which is used in the present study is based on the retarding field analyser described by Palmberg and Rhodin (1968) and Weber and Peria (1967) which was in turn based on the electronic differentiation method of Leder and Simpson (1958). Firstly a few words must be said concerning the method of retardation.

The basic requirement for this measurement is a semispherical retarding field analyser (section 4.2.3). An electron beam impinges (normal) on the surface and the secondary electrons move radially

outward in a field free region between the sample and the first grid. Retardation of these electrons is produced by applying a negative voltage, $-V_R$, to the second and third grids [previously, early types used to use one grid for retardation, which meant that a potential variation would occur between the grid wires causing a severe loss of resolution, Taylor (1969). In later types two linked grids separated by a small distance was used, Palmberg (1968).] so that those electrons travelling radially outward with energy more than $eV_R = E_R$ can pass through the grids and reach the collector. If we now measure the current I_c to the collector as a function of the retarding voltage V_R, it will be related to the energy distribution by:

$$E_c(E_R) = I_p \int_{eV_R=E_R}^{E_p} N(E)dE \qquad (4.1)$$

E_p = primary electron energy

I_p = primary electron current

where the energy is normalized so that

$$\int_0^{E_p} N(E)dE = \delta \qquad (4.2)$$

where δ is secondary yield. If E_R is more negative than E_p all secondaries will be cut off, therefore $I_c = 0$, while if E_R is positive with respect to the target then $I_c = \delta I_p$ (by assuming that all secondaries emitted from the target are collected). Now consider the current $I_c(E_R)$ at a retarding voltage V_R. The change in I_c due to the change of retarding energy can be expanded in a Taylor series. Thus:

$$I_c(E) = I_c(E_R) + \frac{dI_c(E)}{dE}\bigg|_{E=E_R}(E-E_R) + \frac{d^2I_c(E)}{dE^2}\bigg|_{E=E_R}\frac{(E-E_R)^2}{2!} + \ldots \qquad (4.3)$$

substituting from (4.1) we get

$$I_c(E) = I_c(E_R) - I_p N(E_R)(E-E_R) - I_p \frac{dN(E)}{dE}\Big|_{E=E_R} \frac{(E-E_R)^2}{2!} - \ldots\ldots \tag{4.4}$$

Now the energy distribution $N(E_R)$ can be obtained by modulating E such that $E - E_R = K \sin wt$ and measuring the component of $I_c(E)$ at the frequency w. This component will be $- KI_p N(E_R)$ for sufficiently small modulating voltages. In this way Palmberg (1967) and Scheibner and Tharp (1967) independently recognized that the energy distribution N(E) could be obtained from the measured $I_c(E)$ at w by electronic differentiation (using the LEED system).

After Harris' (1968) success in extracting Auger peaks using the $\frac{dN(E)}{dE}$ mode, Weber and Peria (1967) recognized that by detecting the second harmonic (2w) of the collector current, $\frac{dN(E)}{dE}$ could be obtained from a retarding field analyzer. Weber and Peria recognized that the third term in equation (4.4) provided a simple technique to obtain $\frac{dN(E)}{dE}$ spectra. For sinusoidal modulation of the retarding potential this term becomes,

$$I_c(2w) = - \tfrac{1}{4} K^2 I_p \frac{dN(E)}{dE}\Big|_{E=E_R} (\cos 2wt) \tag{4.5}$$

Hence by measuring the component of $I_c(E)$ at 2w the $\frac{dN(E)}{dE}$ is easily obtained.

In this experiment the Auger spectra and Energy loss spectra are detected in a differential mode, and yield measurements are detected in the normal mode.

4.4.2 Detection circuit for $\frac{dN}{dE}$ (Auger and CELS)

The electronic system, was used to measure $I_c(w, E)$ for determination of the first derivative of SEE spectrum, is shown in Fig. (4.7).

The negative voltage to the second and third grids was supplied from a programmable voltage supply (Kepco, OPS 1000) controlled by a function generator Kepco FG100/A. A small proportional voltage output from this voltage supply was supplied to the input of the x channel of the x-y recorder. This arrangement also allows one to vary the voltage supply to the grids and record at various speeds.

To obtain a strong second harmonic (2w) output signal and to collect all incident electrons, the collector was biased at +120 V which prevented the possible re-emission of electrons. The collector has a strong signal at the modulating frequency but a comparatively weak signal at the second harmonic frequency. This could overload the detection system and the extraction of the desired second harmonic would become difficult. To overcome this problem a resonant load similar to that described by Gallon et al. (1969) was used. The tuned load used in the present work was a parallel resonant circuit which is shown in Fig. (4.8). It was tuned to a frequency twice the modulation frequency (935 Hz) with a resonance impedance 100 MΩ and an w rejection $\doteq$ 100:1. If a signal developed across the tuned load at 2w, the impedance to earth would be comparable to a 10^8 ohm load resistor and the signal would be amplified. For any other frequency the tuned load would partially short circuit the signal to earth, and this signal would not be amplified. This gave a good rejection of the unwanted signals at the fundamental frequency.

This modulation signal was supplied from a low distortion oscillator (Brookdeal 5012F). The oscillator also supplied a signal with the same frequency directly to the reference unit of the phase sensitive

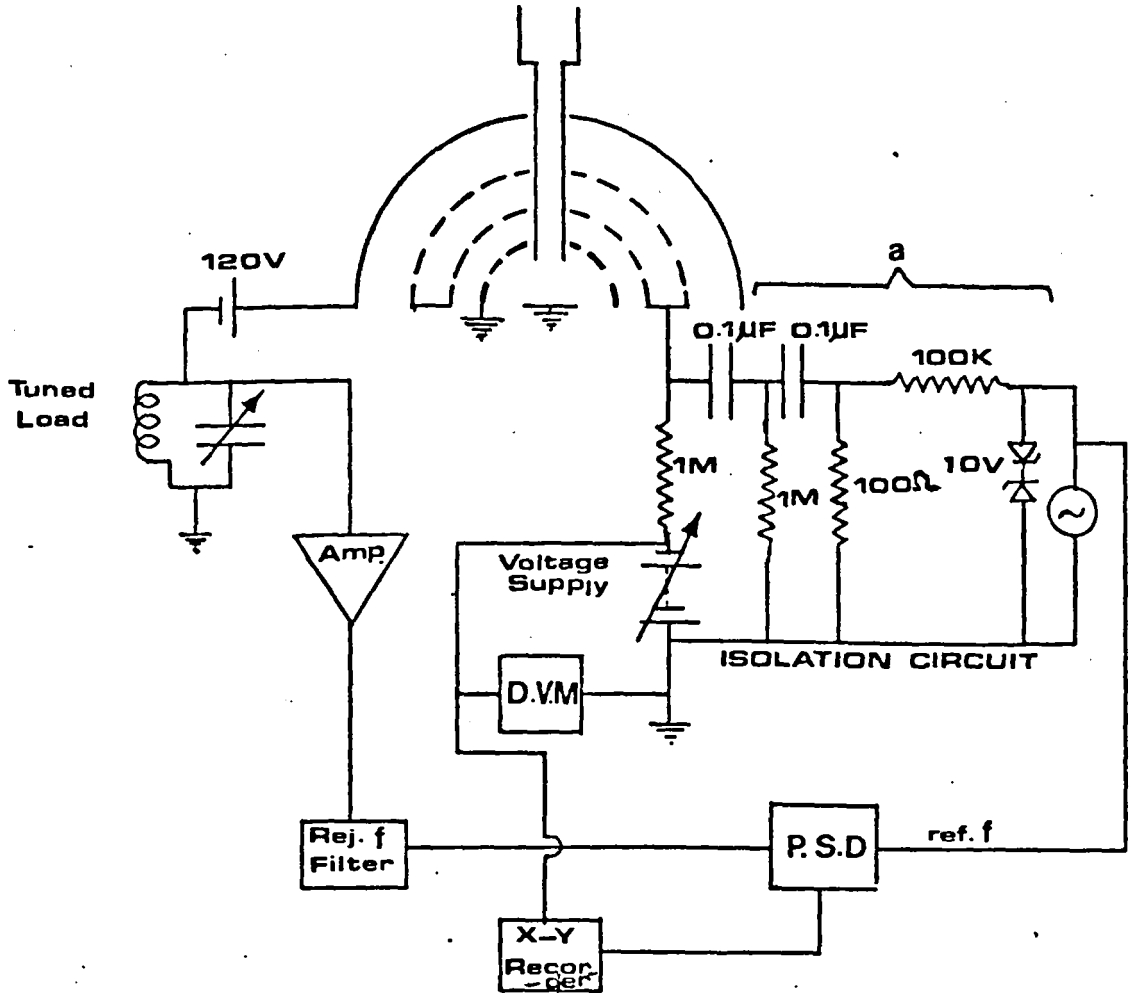
120V
a
0.1μF
0.1μF
100K
Tuned
Load
1M
1M
100Ω
10V
Amp.
Voltage
Supply
ISOLATION CIRCUIT
D.V.M
Rej. f
Filter
P.S.D
ref. f
X–Y
Recor
-der

FIG.4.7

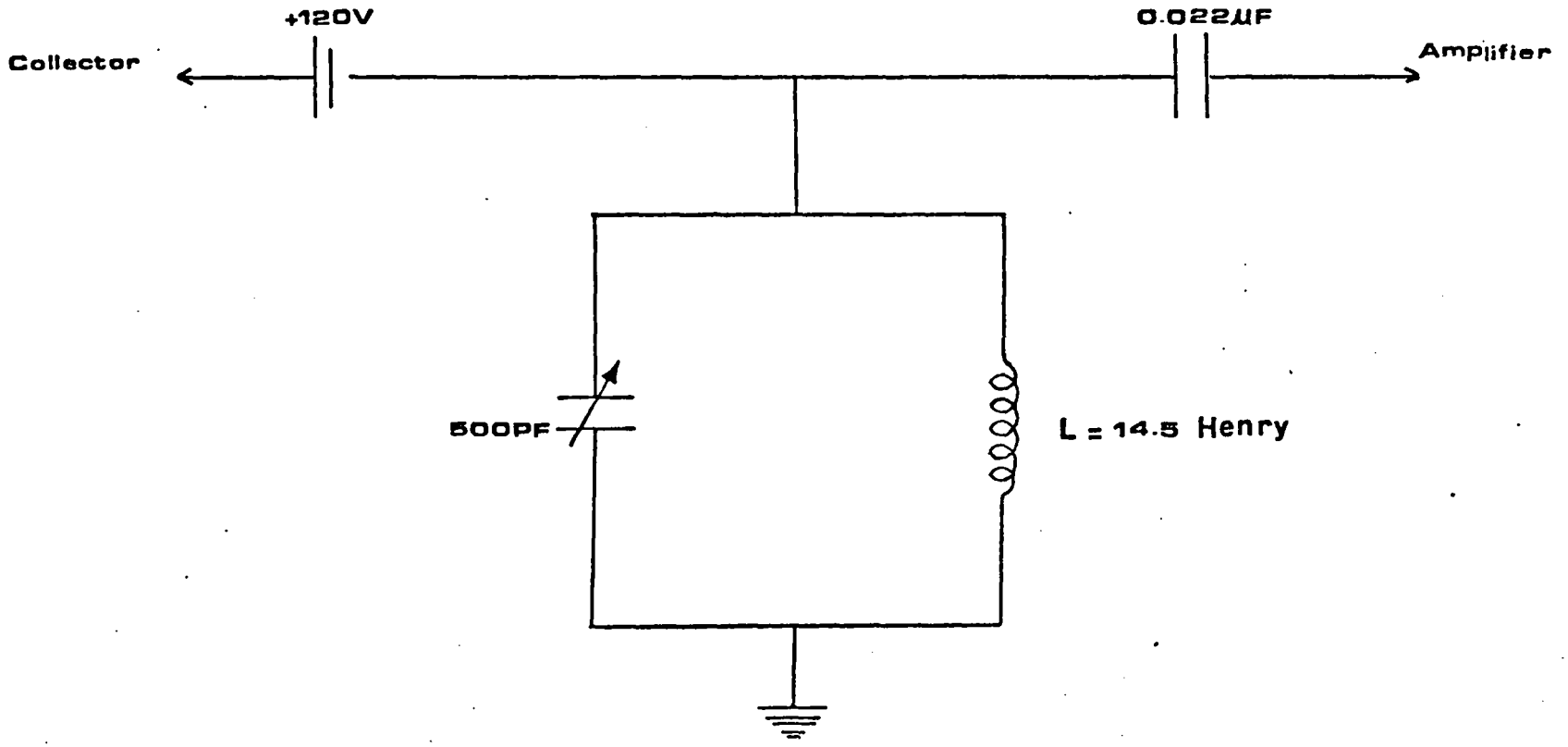

FIG.4.8 Tuned Load

detector (PSD, type Brookdeal 402). The frequency and the amplitude of the modulation signal were variable, typically in normal operation a frequency of 935 Hz and modulation voltage of 1 - 8 V pk-pk were used.

Prior to the signal entering the PSD, it was passed through a low noise amplifier (type Brookdeal 450), and then a tunable filter (Brookdeal type 5011F) to remove any w signal still present. Finally the output from the PSD was fed to the input of the y channel of the x-y recorder. So as the grid voltage is being varied, the x-y recorder records the collector signal, which is detected synchronously at 2w frequency in the PSD, as a function of grids voltage which is proportional to $\frac{dN(E)}{dE}$.

4.4.3 Experimental apparatus for the SEE yield measurement

The essential requirement of this method is electron stimulation at normal incidence in a UHV environment as in any LEED/Auger system.

When a beam of electrons strike a target the secondary emission yield of a material is defined as

$$\delta = \frac{i_s}{i_p} \tag{4.6}$$

where i_s is the secondary electron current (due to both elastic and inelastic processes) and i_p is the primary beam current. Since $i_s = i_p - i_t$, where i_t is the target current, the yield is then obtained from

$$\delta = \frac{i_s}{i_p} = \frac{i_p - i_t}{i_p} = 1 - \frac{i_t}{i_p} \tag{4.7}$$

It is clear from equation (4.7) that if (a) $i_t = i_p$ i.e. all the primary current is absorbed by the target, the yield is zero and when (b) $i_t = 0$ i.e. when no current flows through the target, $\delta = 1$. In the present method for the yield, these two conditions are required to scale the measurements.

Since the primary beam current is kept constant then the yield δ

is directly proportional to the target current i_t as a function of primary energy. This is the basis of the present method.

Previously this idea has been used by Henrich (1973) and Suleman and Pattinson (1980). Suleman made a circuit in which the detection of the target current was carried by a modulation technique, this was a much simpler and more sensitive method than Henrich's method. Suleman used two integrated circuits for the yield measurement. One of them was an operational amplifier (741) and the other one was an operational transconductance amplifier (RCA-CA3080) functioning as a modulator.

In general for any measurement from an equipment, maximum signal to noise ratio NF (noise figure) is required. So in our work we tried to measure NF by actually reducing the noise. One of the sources for the noise in Suleman's circuit was two integrated circuits. For reducing the noise, therefore, instead of using two integrated circuits (IC) only one I.C. (Gated Linear Amplifier ZN 424, Ferranti) is used which operates as an amplifier and modulator. Further we would like the shot noise of electrons to dominate the Johnson noise (thermal noise) in the circuit. To keep the shot noise dominant over thermal noise, a suitable value for the sensing resistor was used. The value of this resistor is greater than 18 KΩ. [For detail calculation see the appendix (a)]. If we take R_s = 33 KΩ which is greater than 18 KΩ then the N.F. is about 4.5 dB (Appendix (a)) which is reasonably small. The basic experimental circuit used for the yield measurements is shown in Fig. (4.9).

The electron signal, which is generated by the electron beam through the target is developed across the sensing resistor (R_s = 33 KΩ), and is amplified by the Gated Linear Amplifier ZN424.

To be able to measure the yield over the range 0 → 1000V, the gun voltage was selected as - 1000 V and the ramp voltage was varied from 0 to - 1010 V. The variation of ramp voltage gives a corresponding

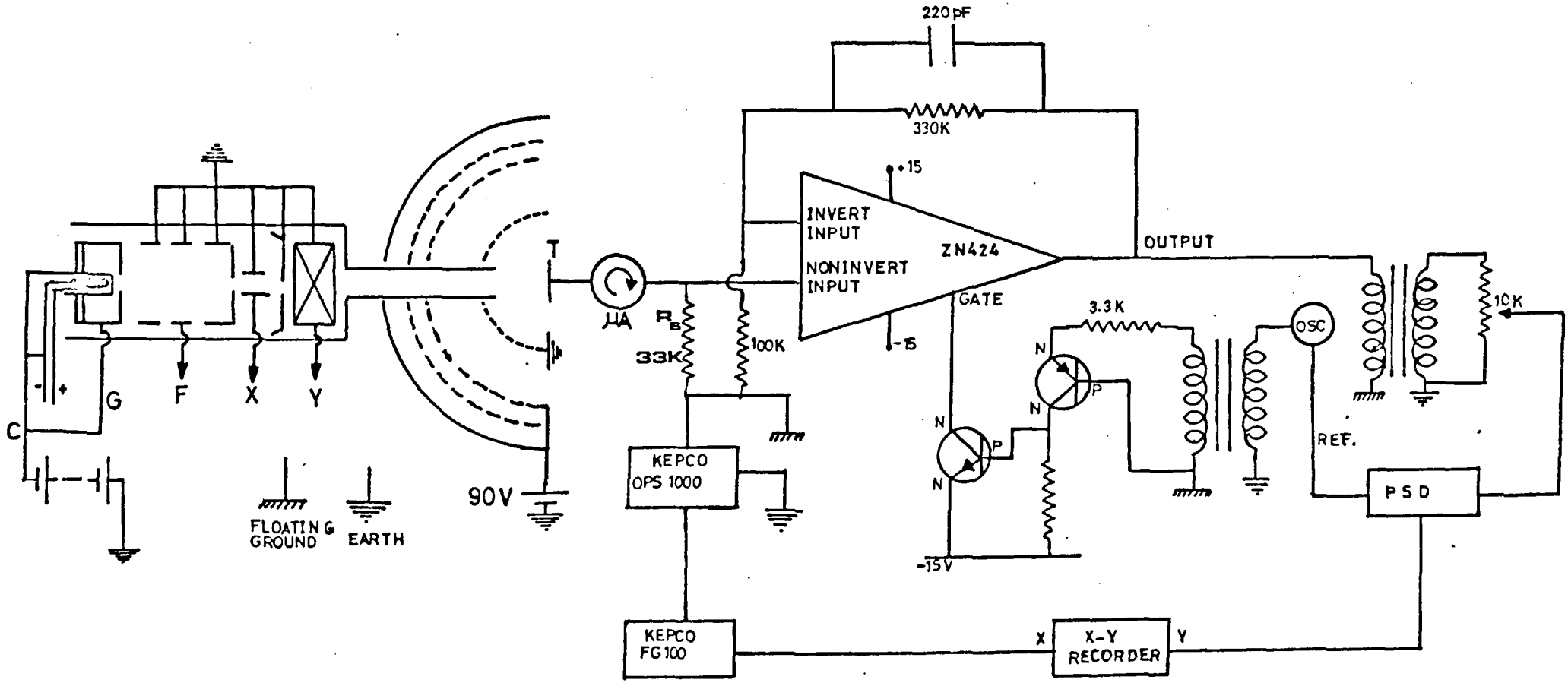

FIG.4.9 DETECTION CIRCUIT FOR YIELD CURVE

variation in DC signal which is developed across the sensing resistor. The ramp voltage in our case was supplied by a Kepco OPS 1000 operational power supply controlled by a Kepco FG100A function generator.

For the purpose of modulation an AC signal (3.4 V pk-pk), from an oscillator enters the amplifier (ZN424) via an isolation transformer and two transistors of types 2N3702 (PNP) and 2N3704 (NPN) as shown in Fig. (4.9). The modulated output from the amplifier enters the phase sensitive detector (PSD) via another isolation transformer, where this signal is detected synchronously with a reference signal from the oscillator. Then the output of PSD is recorded by an x-y recorder as a function of ramp voltage. For the purpose of recording, the output of the PSD is applied to the y-channel and a fraction of the ramp voltage is applied to the x-channel. The so-called integrated circuit is isolated from the ground.

If the circuit is functioning correctly, the PSD will give a linear output when a linear DC ramp voltage signal is applied to the input of the circuit. In order to check the linearity of this circuit, a 0-1680 mV DC ramp voltage signal was applied to the target through the sensing resistor, it developed a DC current of 0-50 μA through the sensing resistor, and the corresponding PSD output is shown in Fig. (4.10) which exhibits good linearity ($\doteq$ 1%).

4.4.4 Experimental Measurement Method

The yield measurements were taken with the same UHV system incorporating a three grid RFA Auger electron spectrometer. The three grid electron analyzer is used here only to provide a hemispherical equipotential around the sample. For yield measurements, the first grid of the RFA was kept at ground potential, the second and third grid and the collector were kept at +90 V potential.

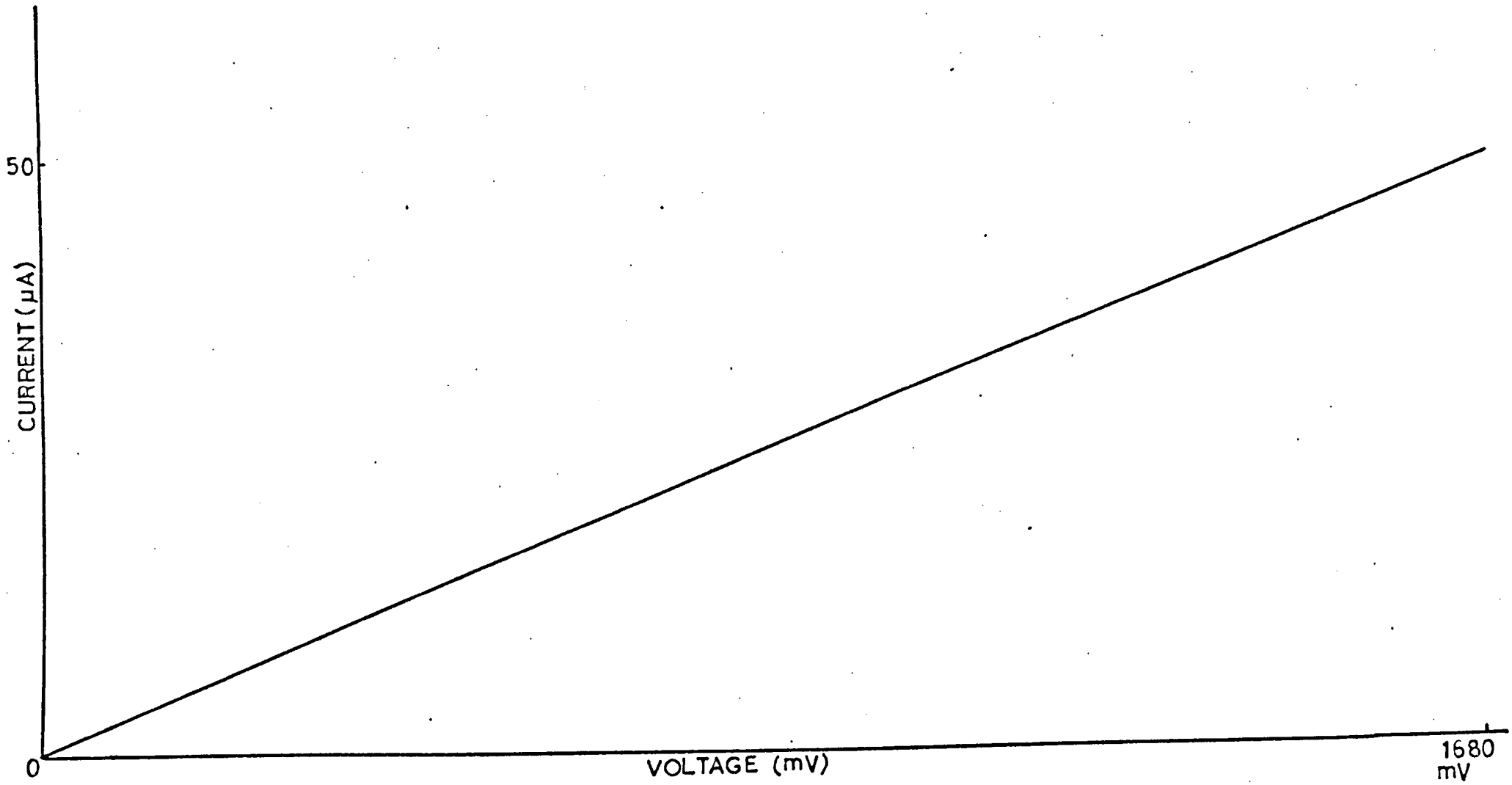

FIG 4.10

It is possible by simple external switching for the apparatus to operate in either an Auger or a yield mode. Thus the same 3 KV electron gun (section 4.2.5) was used for the yield measurements. The primary beam current for yield measurement was less than 15 μA in order to avoid any possible electron beam effects.

As mentioned in the previous section, for scaling the measurements a total collection of the primary beam striking a target is required. This is done by substituting a Faraday cup for the target. The Faraday cup is a 2.5 x 25 cm stainless steel block with an angled 3 mm hole drilled at its centre. This hole is $\sim$ 1.5 cm deep. The Faraday cup was coated with a low secondary yield surface of gold black, as described previously by Thomas and Pattinson (1970). When the Faraday cup faces the incident electron beam all the primary electrons are collected and a large signal is detected which gives a base line at zero for the yield. The other base line corresponding to a yield of unity ($\delta = 1$ when $i_t = 0$) was fixed by applying a slightly higher ramp voltage than primary electrons energy which was 1 KeV. In the present experiments, target current (yield) vs primary energy (for Faraday cup) is shown in Fig. (4.11).

In the present series of experiments the yield from slowly oxidising samples of Beryllium and Magnesium was analyzed, by varying the ramp voltage from 0 - 1010 V, while the current and the voltage of the electron gun was kept constant. Therefore when the voltage is ramped on the sample, electrons of various primary energies above the ramp voltage will land, and in effect the primary energy of the electrons hitting the target can be varied by varying the negative voltage on the target.

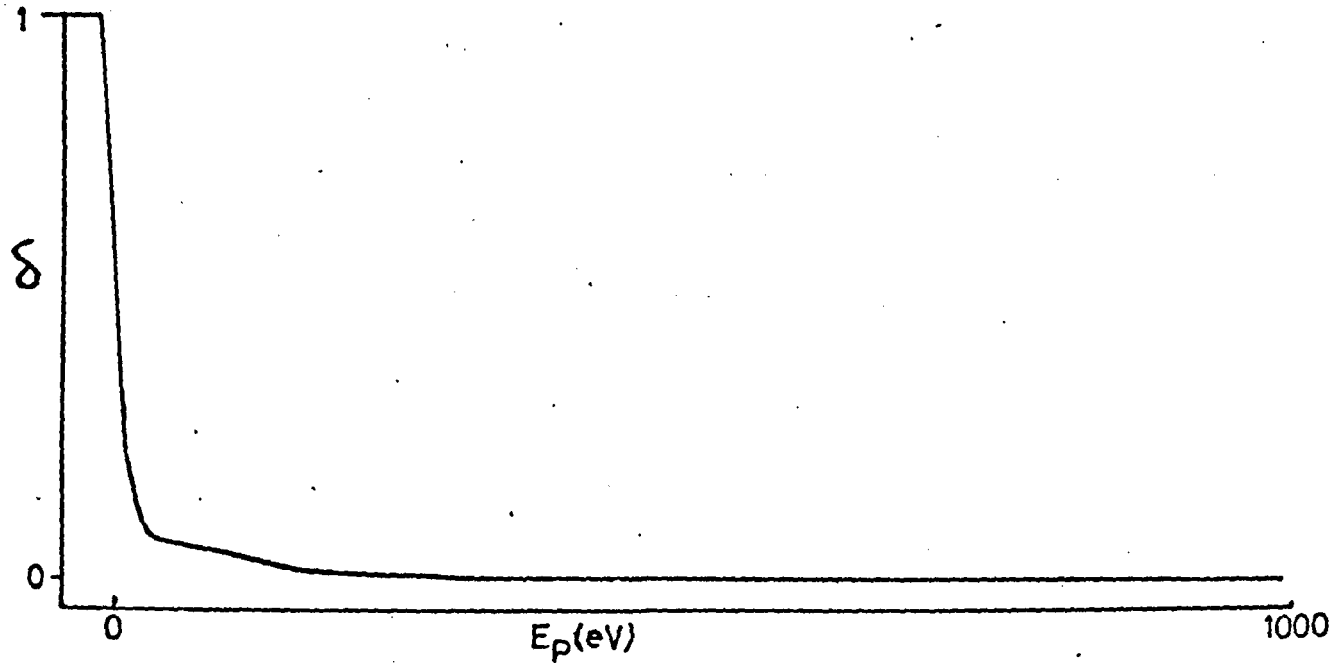

FIG-4-11

CHAPTER 5

Results and Discussion of Be → BeO

5.1 Introduction

The Auger electron spectrum of an element may reflect chemical effects such as chemical shifts in the Auger spectrum, due to different chemical environments. Small changes in the spectrum may take place due to the shifts in the inner energy levels because of redistribution of valence electrons on forming a chemical bond. Larger changes may occur if the Auger electrons originate from transitions involving the valence band. Changes of this type would reflect the changed valence band after chemical bonding. In order to observe these changes in the Auger spectrum, it is essential that the spectrum of an element in the clean form should be known with certainty. In addition the changes in the spectrum should be slow enough to permit experimental observations. Auger spectra believed to be characteristic of clean Be have been obtained. The changes in the spectra of this element due to oxidation were also observed. In addition, and as far as possible concurrently, the characteristic energy loss spectra of this element for the clean and oxidised surfaces were observed. Finally, the secondary electron emission of Be has been studied, when it was in a clean condition and whilst it was being slowly oxidised. The changes in secondary electron parameters such as, δ_{max}(maximum of yield, δ), E_{pmax}(primary energy of δ_{max}), escape depth of secondary electrons, x_α, range of primaries, R and first and second crossover energies, $E_{p_{c_1}}$ and $E_{p_{c_2}}$ (the energy of $\delta = 1$) during the oxidation have also been studied. Because of the importance of the oxide of Be as a good secondary emitter, an attempt has been made to find some reasons for the

increase of the secondary electron yield during the oxidation of Be. The details of all these observations and discussions on them are presented in this chapter.

5.2 Preparation of Be

For this experiment a Be foil (purity 99.999%) was polished by diamond and cleaned in an ultrasonic bath. After inserting it in the U.H.V. ($\sim 10^{-10}$ torr), it was cleaned by means of Argon ion bombardment from a saddle field ion source. The cleanliness of the Be surface was checked by taking Auger spectra immediately after each Argon ion bombardment then the changes in the Auger spectra due to chemisorption of the residual oxygen in the U.H.V. were noted until the relative changes in Auger spectra for a week become negligible. The oxidation rate of the sample was very low, and it was sufficiently slow for careful measurements to be taken. Occasionally checks on the other common contaminants such as C, S, Cl etc. was made by taking Auger spectrum from 0 - 550 eV, since these contaminants are known to have major Auger peaks in this energy range. In nearly six weeks a whole sequence of Auger electron spectra , characteristic energy loss spectra and secondary electron yield curves were obtained, then the surface was heated up for diffusing more oxygen in it. By plotting the Auger spectrum of this surface it was demonstrated that there was no significant contaminants on the surface other than oxygen. This heating process was repeated for several times to get maximum coverage of oxygen on the surface.

A primary beam of 15 - 25 μA with an electron gun energy 1.3 KeV was used and the commonly used modulation voltages were 3V PK-PK for the Be Auger spectras and 7.2 V pk-pk for the oxygen spectras.

5.3 Results of Be → BeO

5.3.1 Auger spectra

The AES of a clean Be surface and with different amounts of oxygen sorbed onto the Be surface are shown in Fig.(5.1). The main

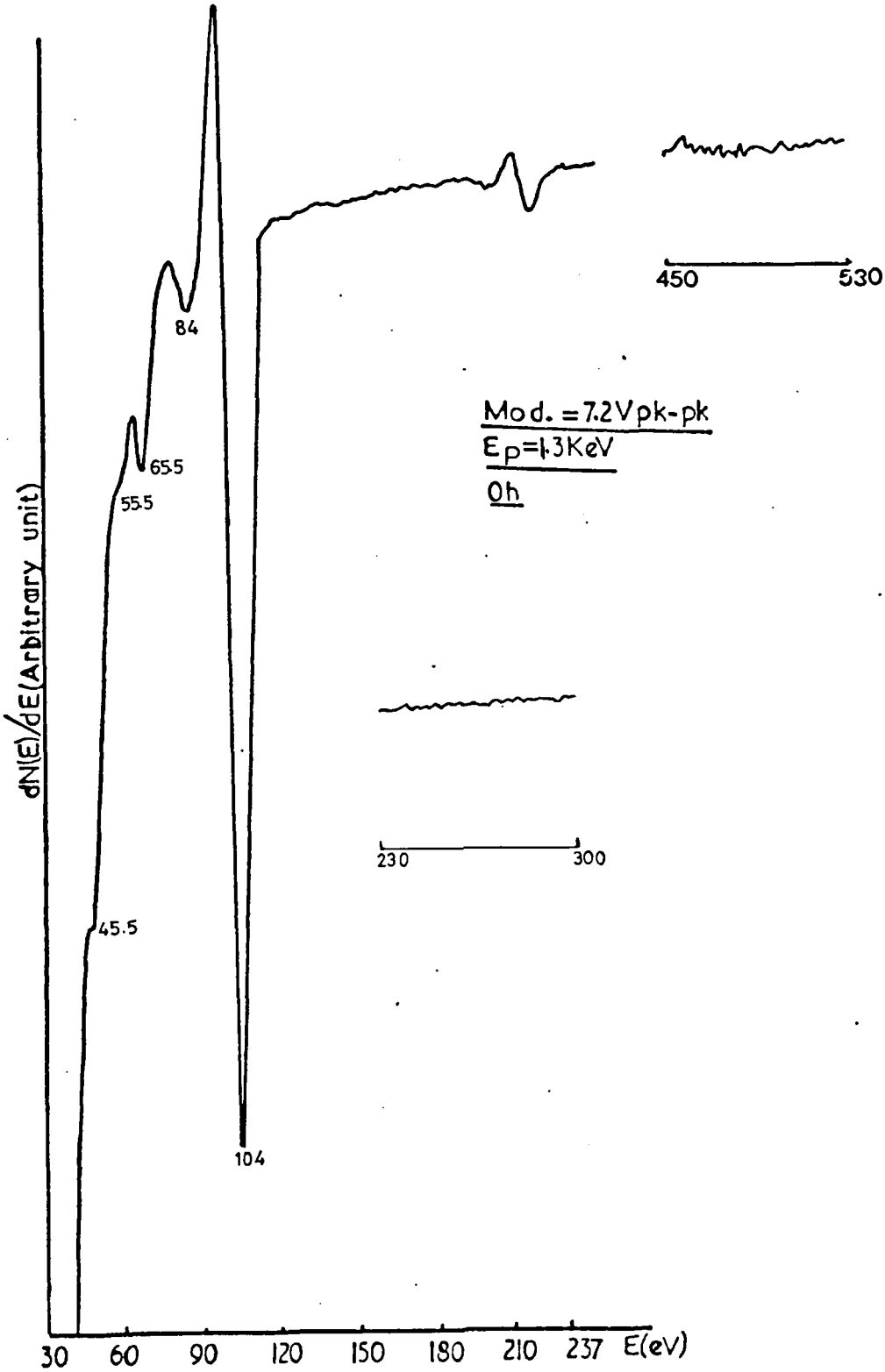

FIG. 5.1a Auger spectrum of clean Be

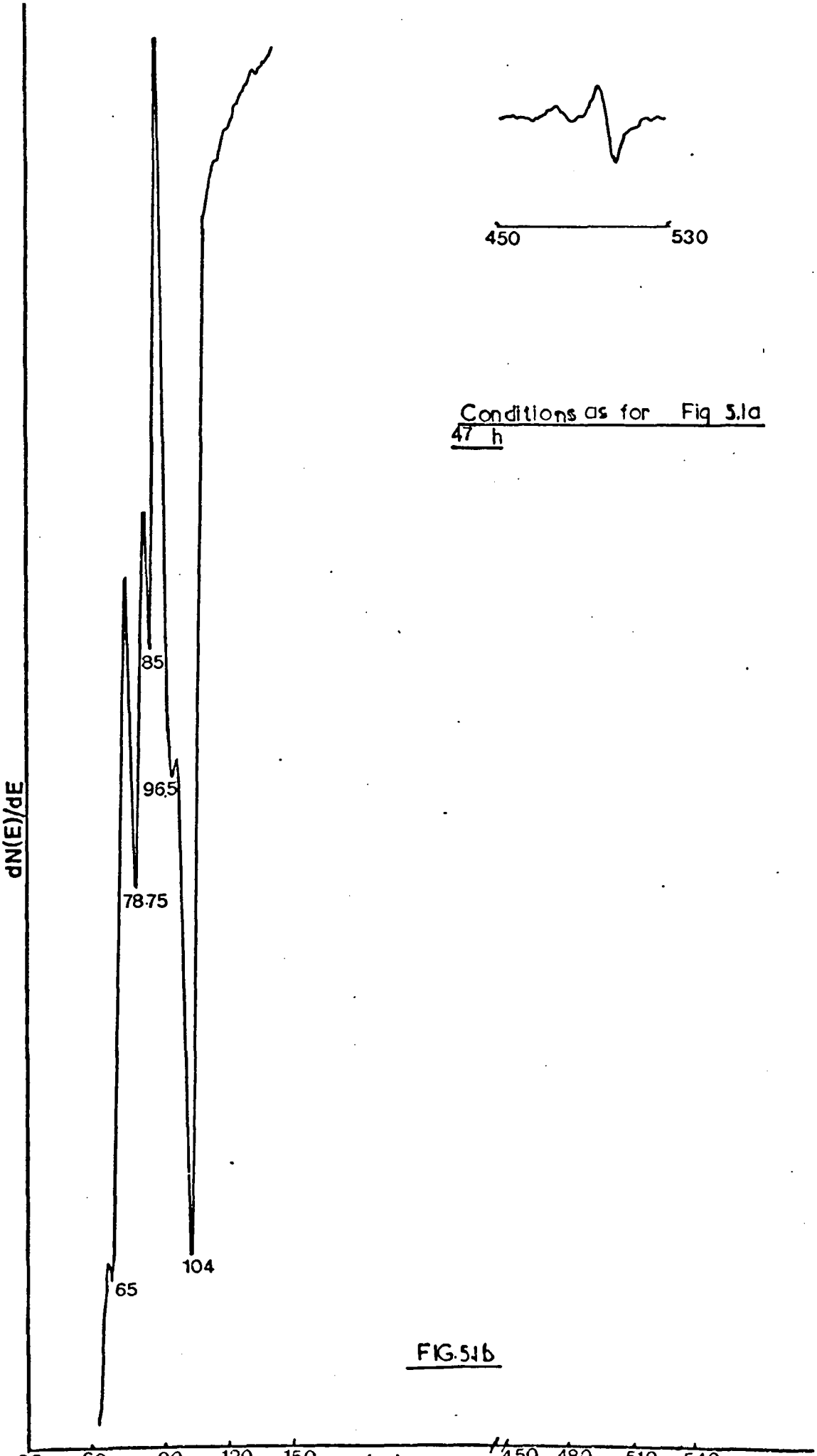
450
530
Conditions as for Fig 5.1a
47 h
dN(E)/dE
85
96.5
78.75
65
104
30
60
90
120
150
E(ev)
450
480
510
540

FIG. 5.1b

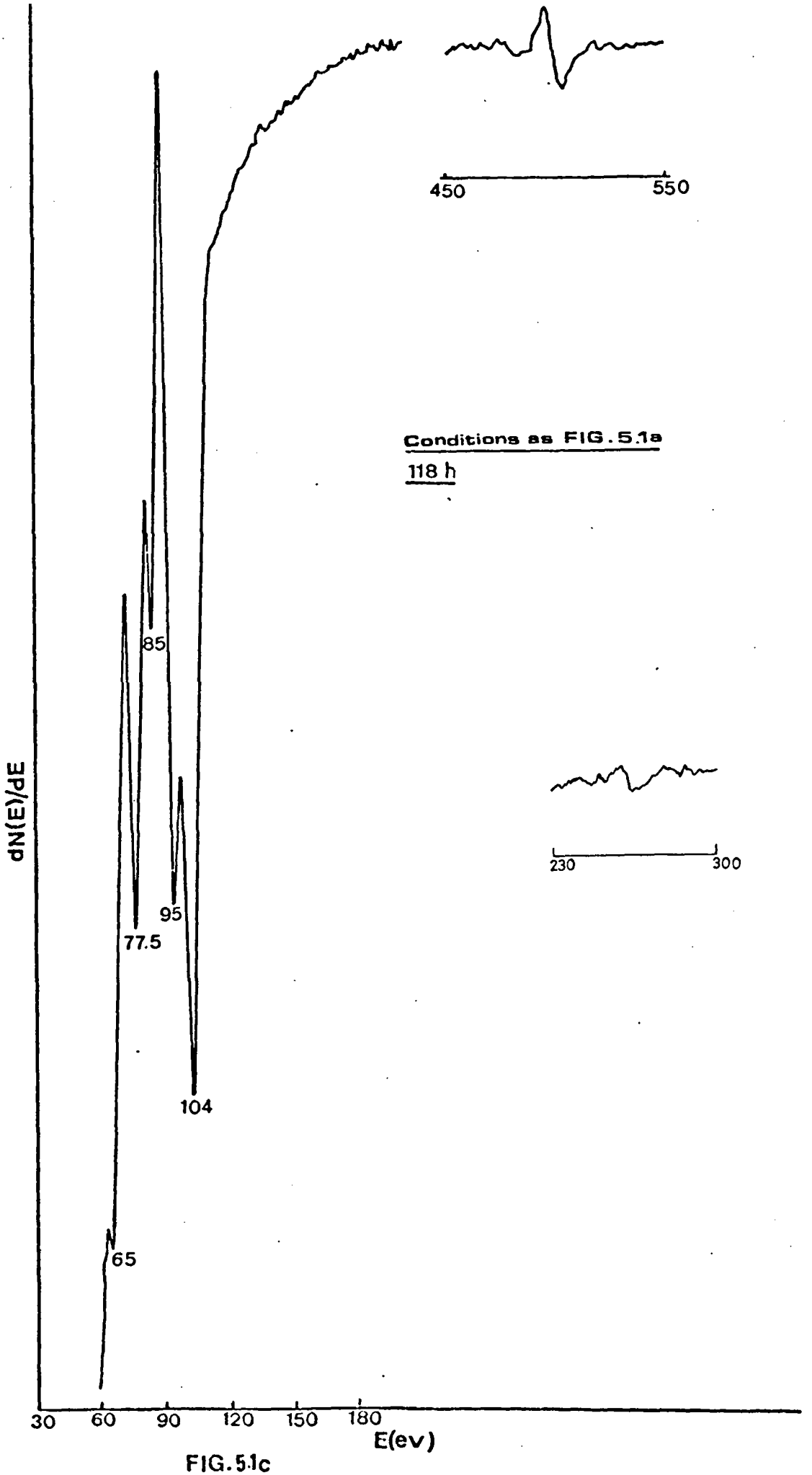
450
550
Conditions as FIG. 5.1a
118 h
230
300
dN(E)/dE
85
77.5
95
104
65
30
60
90
120
150
180
E(ev)

FIG. 5.1c

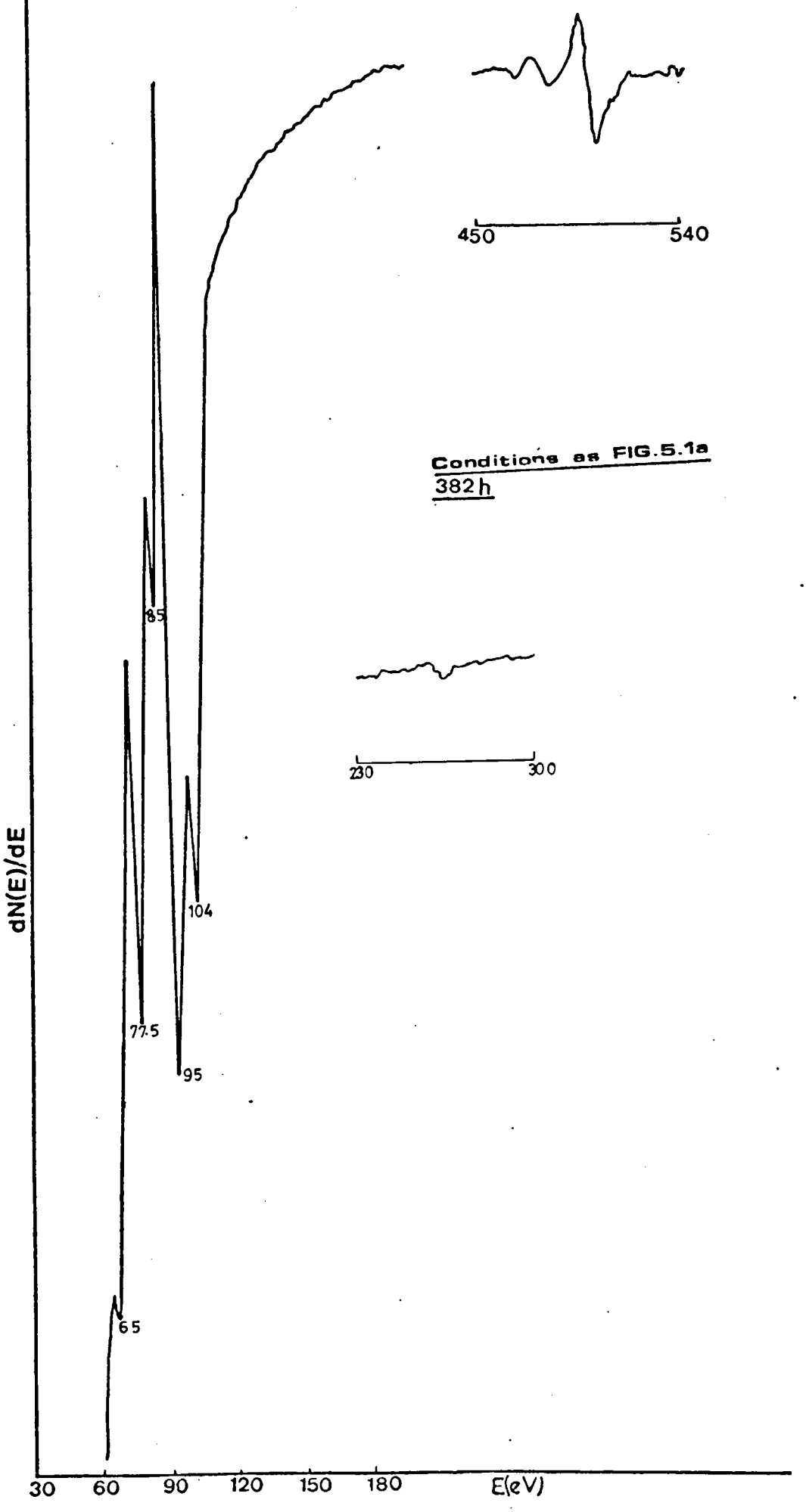
450
540
Conditions as FIG.5.1a
382 h
230
300
dN(E)/dE
85
104
77.5
95
65
30
60
90
120
150
180
E(eV)

FIG. 5.1d

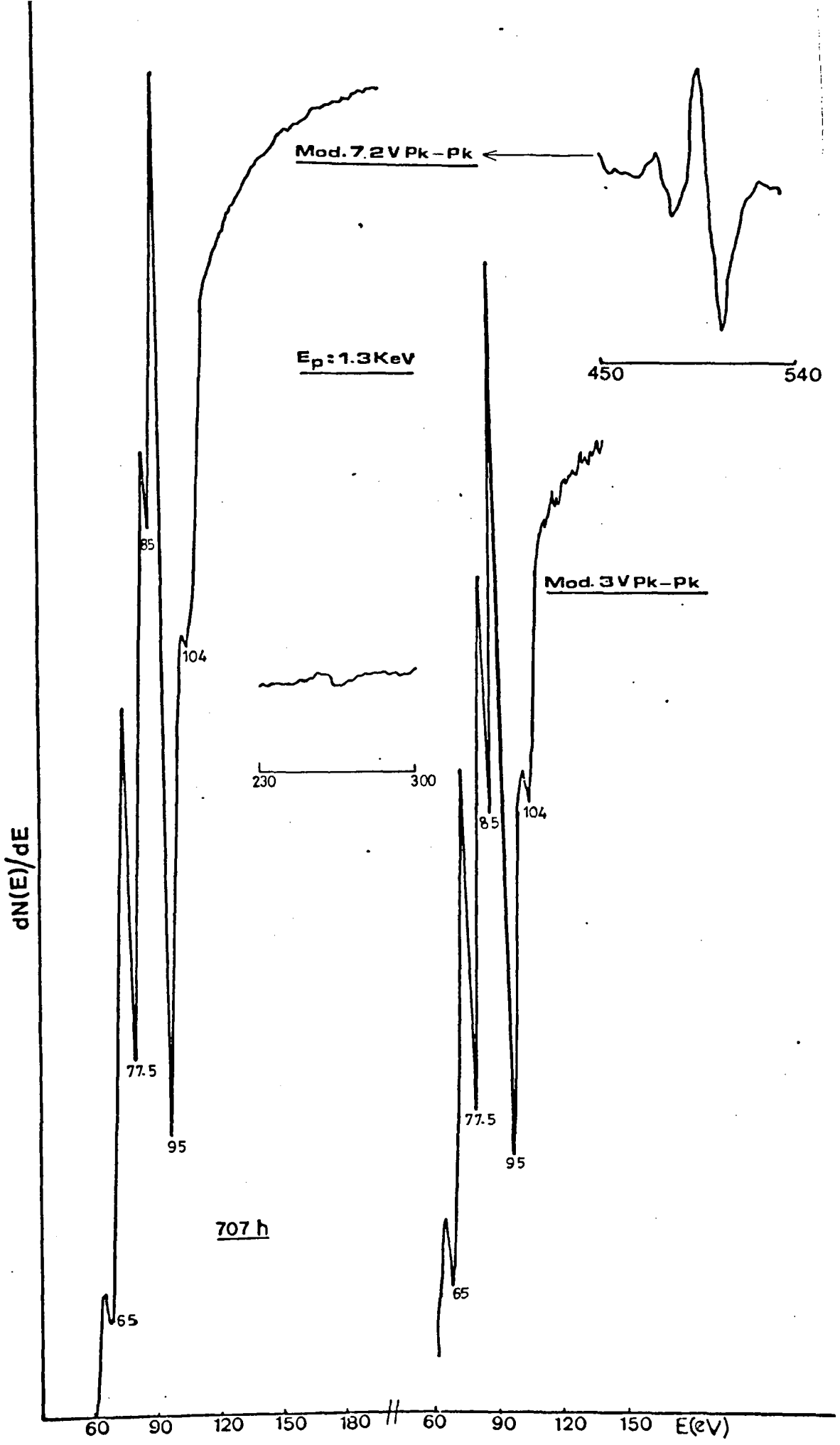
Mod. 7.2 V Pk-Pk
E_p : 1.3 KeV
450
540
Mod. 3 V Pk-Pk
230
300
85
104
77.5
95
65
707 h
dN(E)/dE
60
90
120
150
180
60
90
120
150
E(eV)

FIG.5.1e

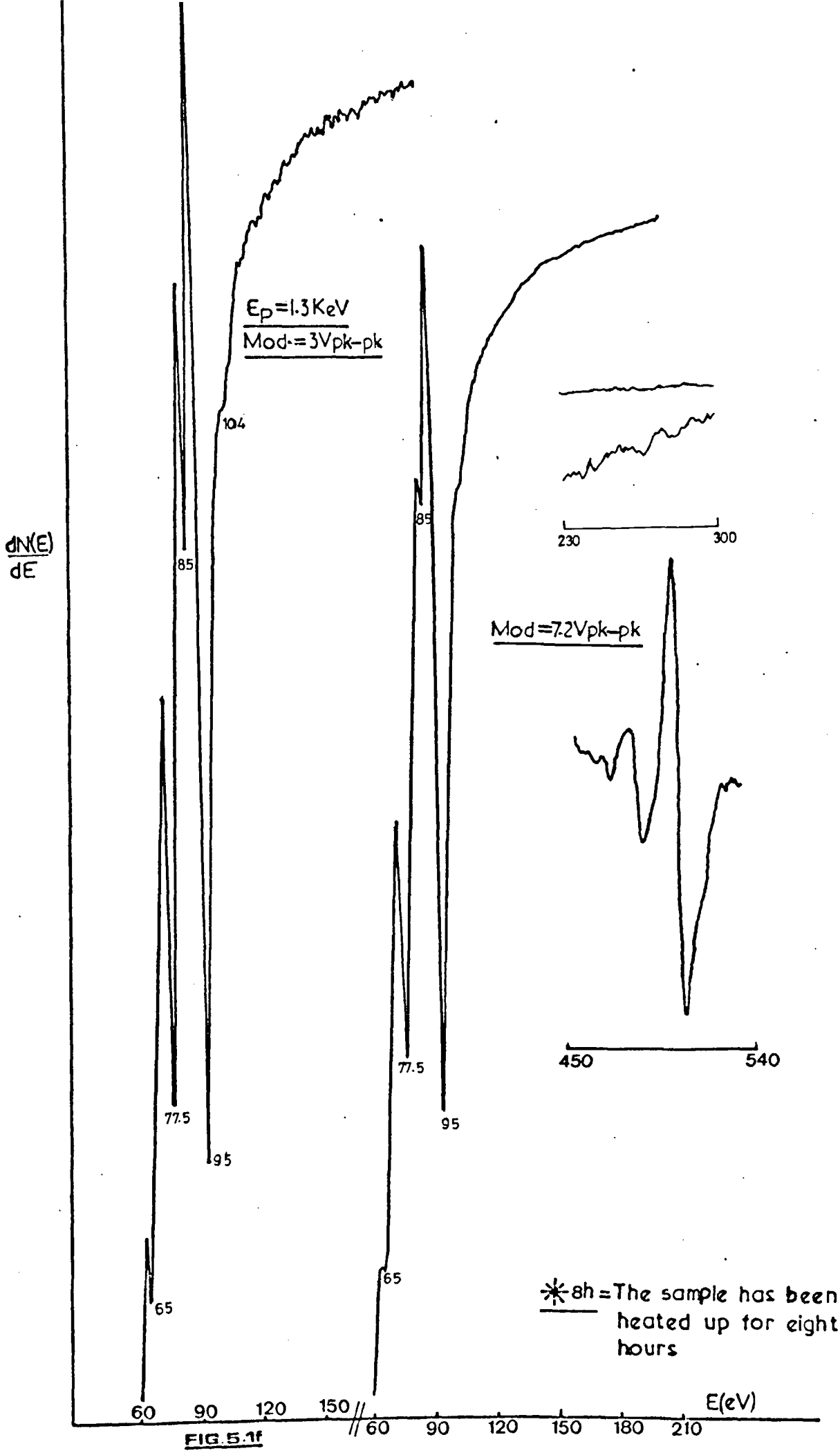
dN(E)/dE
Ep=1.3KeV
Mod-=3Vpk-pk
104
85
77.5
95
65
85
77.5
95
65
230
300
Mod=7.2Vpk-pk
450
540
60
90
120
150
60
90
120
150
180
210
E(eV)
8h=The sample has been heated up for eight hours

FIG.5.1f

features of the clean Be spectrum (Fig. 5.1a) are; a large peak at 104 eV, two small peaks at 84 eV and 65.5 eV and two small shoulder type peaks at 55.5 and 45.5 eV. However the latter peaks are not well resolved. During the oxidation of the Be surface by residual oxygen gas over many days, many changes were observed in the AES, Figs. (5.1a, b, c, d, e, f). The presence of oxygen is evident from the peak at 505 eV. In addition to this peak two new peaks (due to oxide) appeared at 485 eV and 470 eV. However, after one day's oxidation the peaks at 45.5 and 55.5 eV have disappeared and new peaks have appeared at 78.7 eV and 96.2 eV. During the initial stage of oxidation the peaks at 96.25, 78.75 and 65.5 eV slowly shifted to the lower energy side, but the peak at 84 eV shifted to higher energy side. After three days these peaks became stationary at energies 95 eV, 77.5 eV, 65 eV and 85 eV respectively. Later the amplitude of these peaks increased slowly and became constant after sixty days, in the meantime the amplitude of the peak at 104 eV gradually decreased and disappeared while the oxygen peak was increasing.

The AES of clean Be surface has a small Argon peak in addition to the peaks mentioned previously. This peak can be removed by heating the sample. However, heating produces oxygen peaks in the spectrum, therefore, in this work it was preferred to have a small amount of inert Argon rather than oxygen in the 'clean' stage of Be surface. However the amplitude of the Argon peak gradually decreased and disappeared when the surface became fully oxidised.

In the experience of some experimentalists, the admission of oxygen to a UHV system can cause problems since it can rapidly combine with carbon especially in the presence of a tungsten filament either in an electron gun or associated with an ion gauge. This problem was not encountered in the present set of experiments. At least at no stage was the carbon Auger signal after the initial cleaning and during the oxidation

sequence significantly above the noise level. Had carbon monoxide, for example, been adsorbed on the surface one would have expected the carbon and oxygen Auger signals to be comparable. Reference to the Fig.(5.1f) shows a typical state where the oxygen signal is 8.8 cm and the carbon signal can be seen to be in the noise level. The conclusion is, therefore, that even if CO is adsorbed on the surface in any quantity, there is some mechanism possibly due to electron beam effects whereby this is dissociated leaving only the oxygen.

5.3.2 Characteristic Energy Loss Spectra

The corresponding energy loss spectra of clean and oxidized Be surfaces for a primary electron energy of 700 eV, are shown in Figs. (5.2) and (5.3), respectively. For the clean Be surface the energy loss peaks appeared at 6, 13, 19, 36, 56, 74, 77, 95, 115, 135, 152, 164 and 174 eV, but for an oxide covered Be surface the peaks

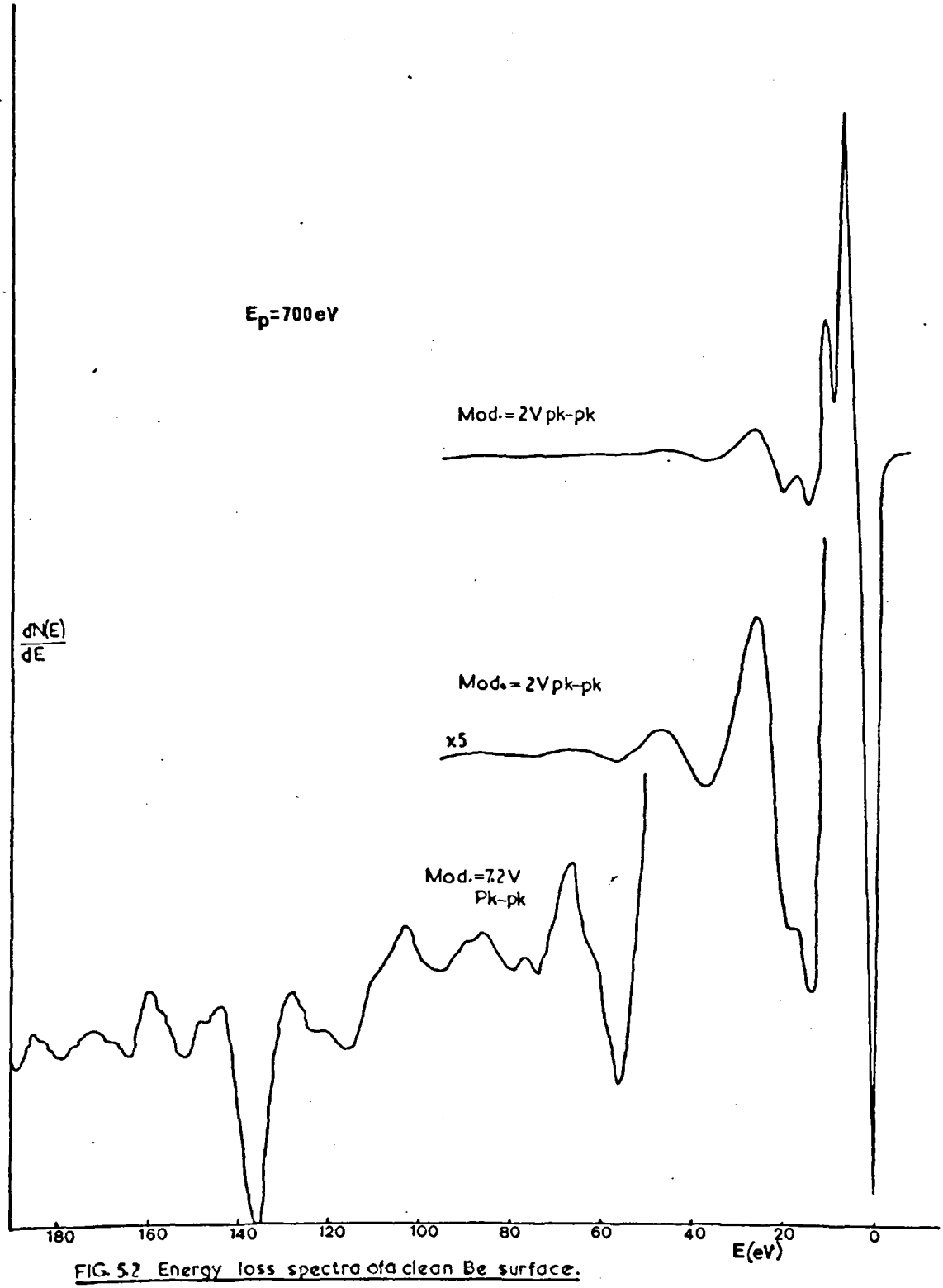

FIG. 5.2 Energy loss spectra of a clean Be surface.

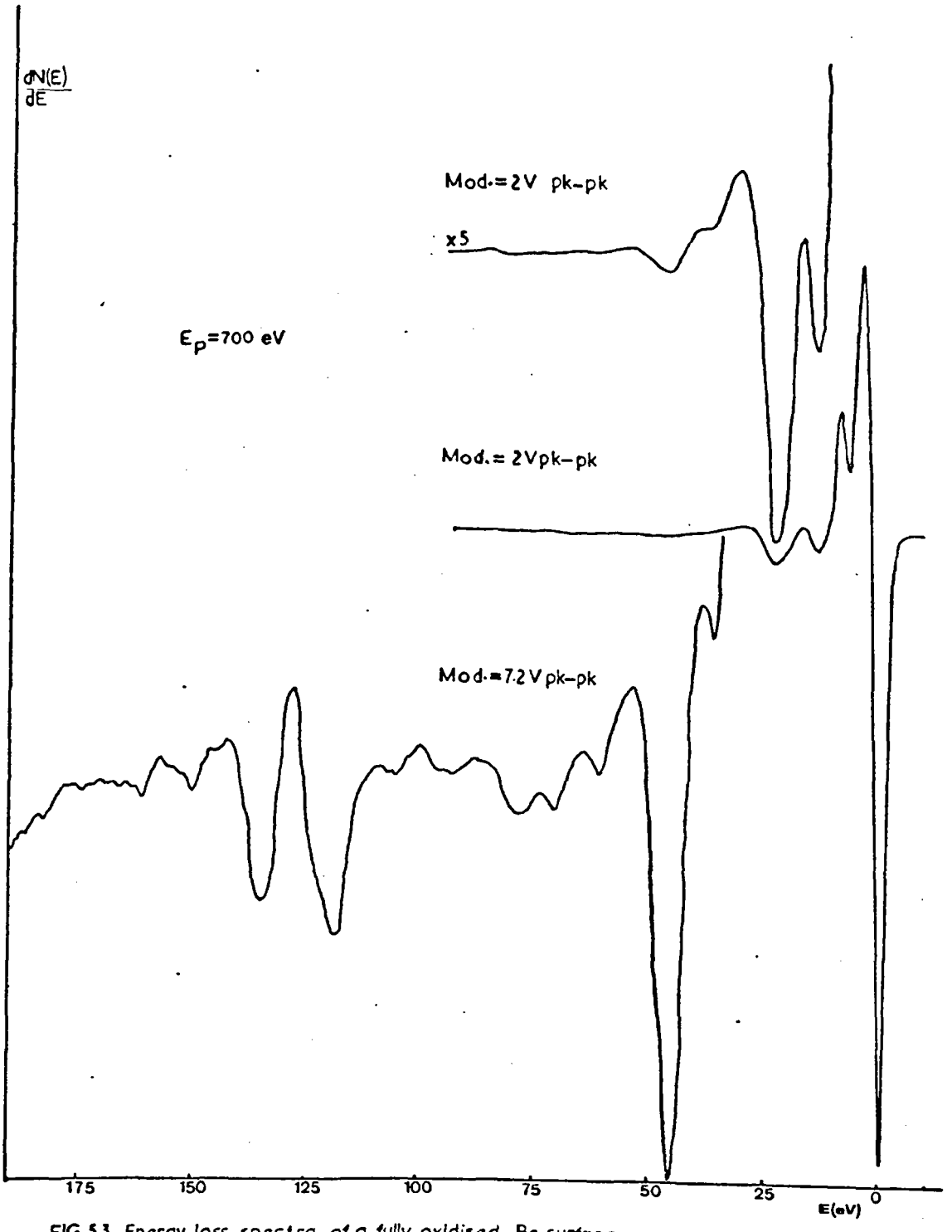

FIG. 53 Energy loss spectra of a fully oxidised Be surface.

appeared at 7, 14, 23, 36, 46.5, 62, 71, 78, 119, 135, 150 and 165 eV. The same type of loss spectra also obtained for different primary electron energies. Because of their similarities (except for the peak at 135 eV) the corresponding spectra are not given here.

The peak at 135 eV which is common for both clean and oxidized Be, shifts to higher energy (with respect to elastic peak considering as zero energy) by 7 eV, for the increase of primary energy by 50 eV. To demonstrate this effect a typical situation for the energy of primary electrons as 900 eV, shown in Fig. (5.4) in which this peak has shifted to 165 eV. This figure also shows that there is no shift in position and change in amplitude of this peak (165 eV) when the oxidization proceeded. Only at the end of this work we were able to realize that this peak is most probably due to the emission of secondary electrons from the tungsten grids. Unfortunately the author was unable to investigate further on this effect, due to the time limit of this work.

The changes in the features of the loss peaks during the oxidation over 60 days are given in Figs. (5.5, 5.6 and 5.7). The energy range of 0 - 95 eV and 30 - 195 eV in the loss spectra for primary energy 700 eV are given in Fig. (5.5) and Fig. (5.7) respectively, and Fig. (5.6) is the amplified version (by increasing modulation voltage) of Fig. (5.5). The peak at 6 eV in clean Be spectrum shifted to 7 eV when the surface became oxidised (Fig. 5.5). The intensity of the 13 eV loss peak of clean Be reduced when the oxidation started and then shifted to 14 eV (Fig. 5.6), but the 56 eV loss peak of clean Be reduced and gradually shifted to 62 eV when the oxidation proceeded (Fig. 5.7), also the peak at 19 eV (clean Be) gradually shifted to 23 eV. In contrast the peak at 115 eV (clean Be) shifted to 119 eV with an increase of intensity during the oxidation. Finally the intensity of the peak at 36 eV (clean Be) reduced, and in the meantime the peaks at

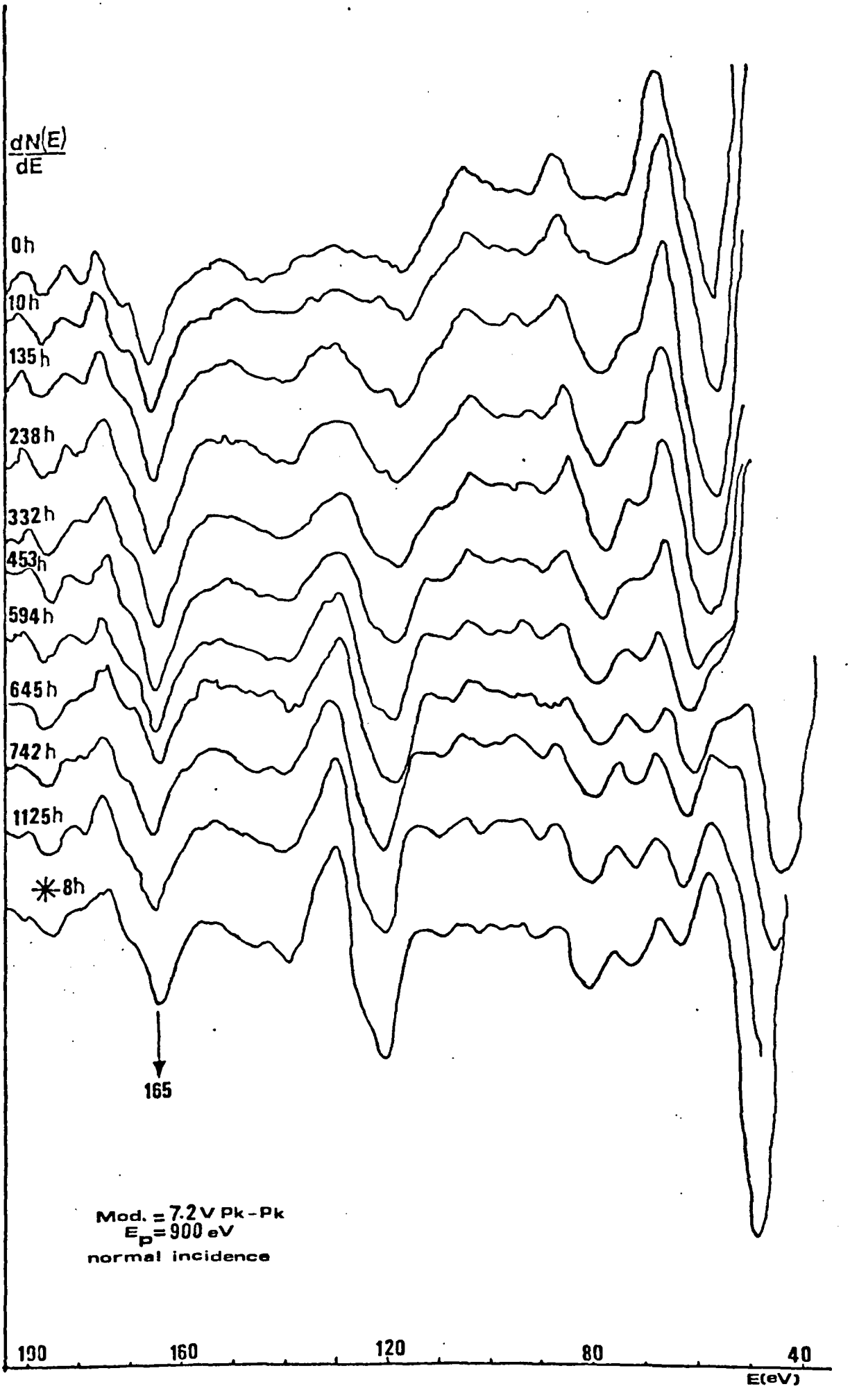

FIG. 5.4 Successive oxidation effects on the energy losses of Be

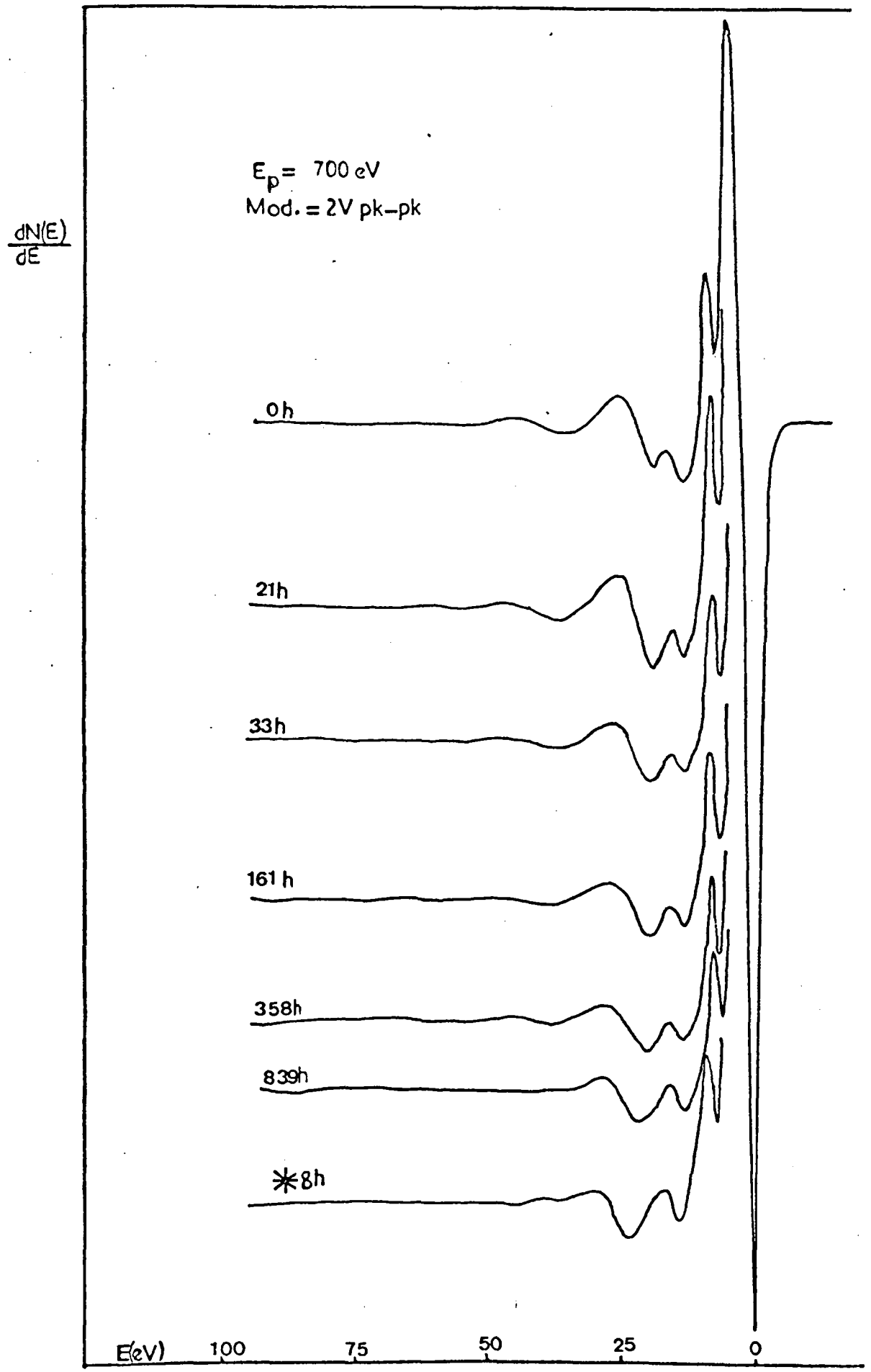

FIG. 5.5 Successive oxidation effects on the energy losses of Be.

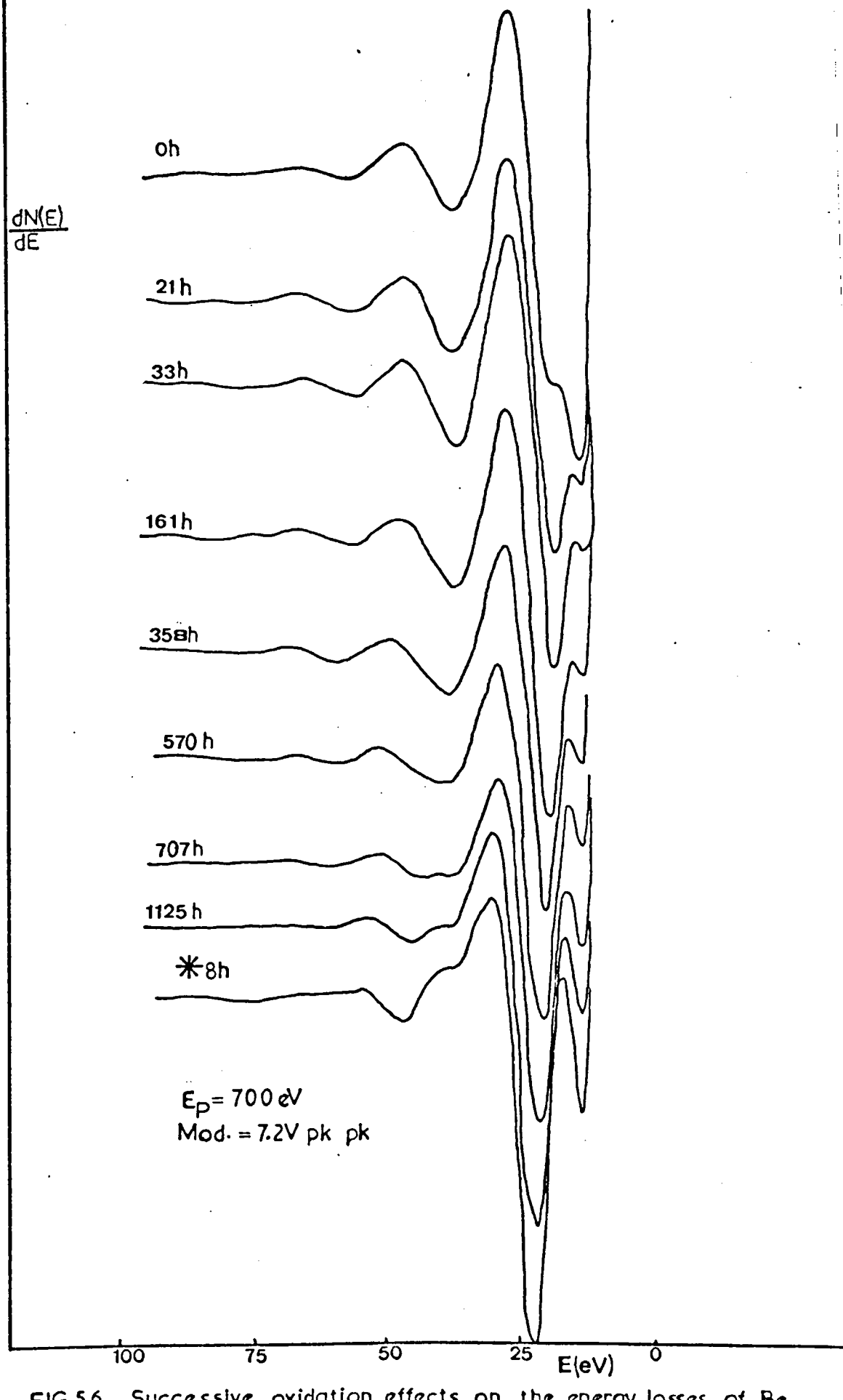

FIG.5.6 Successive oxidation effects on the energy losses of Be

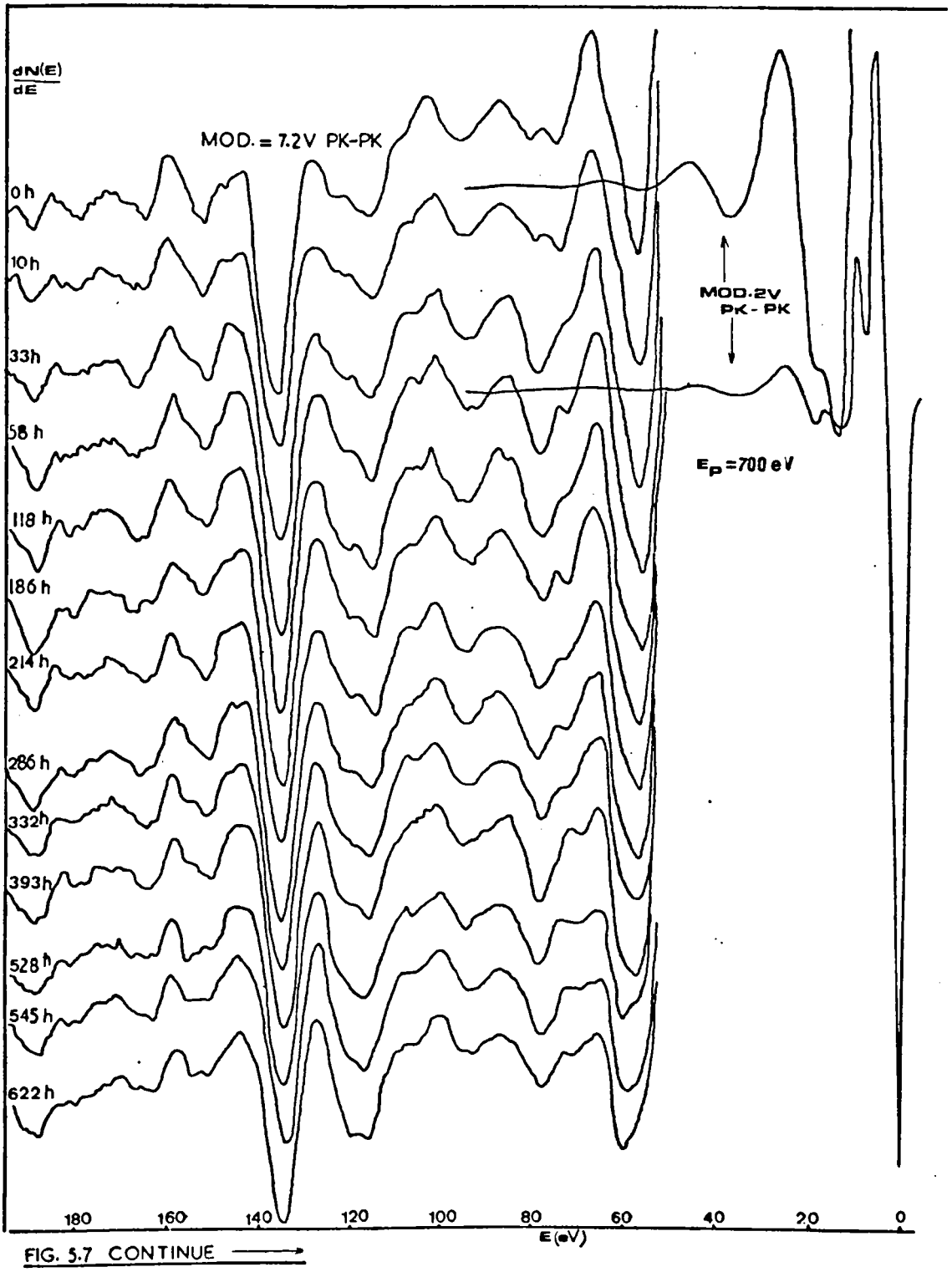

FIG. 5.7 CONTINUE ⟶

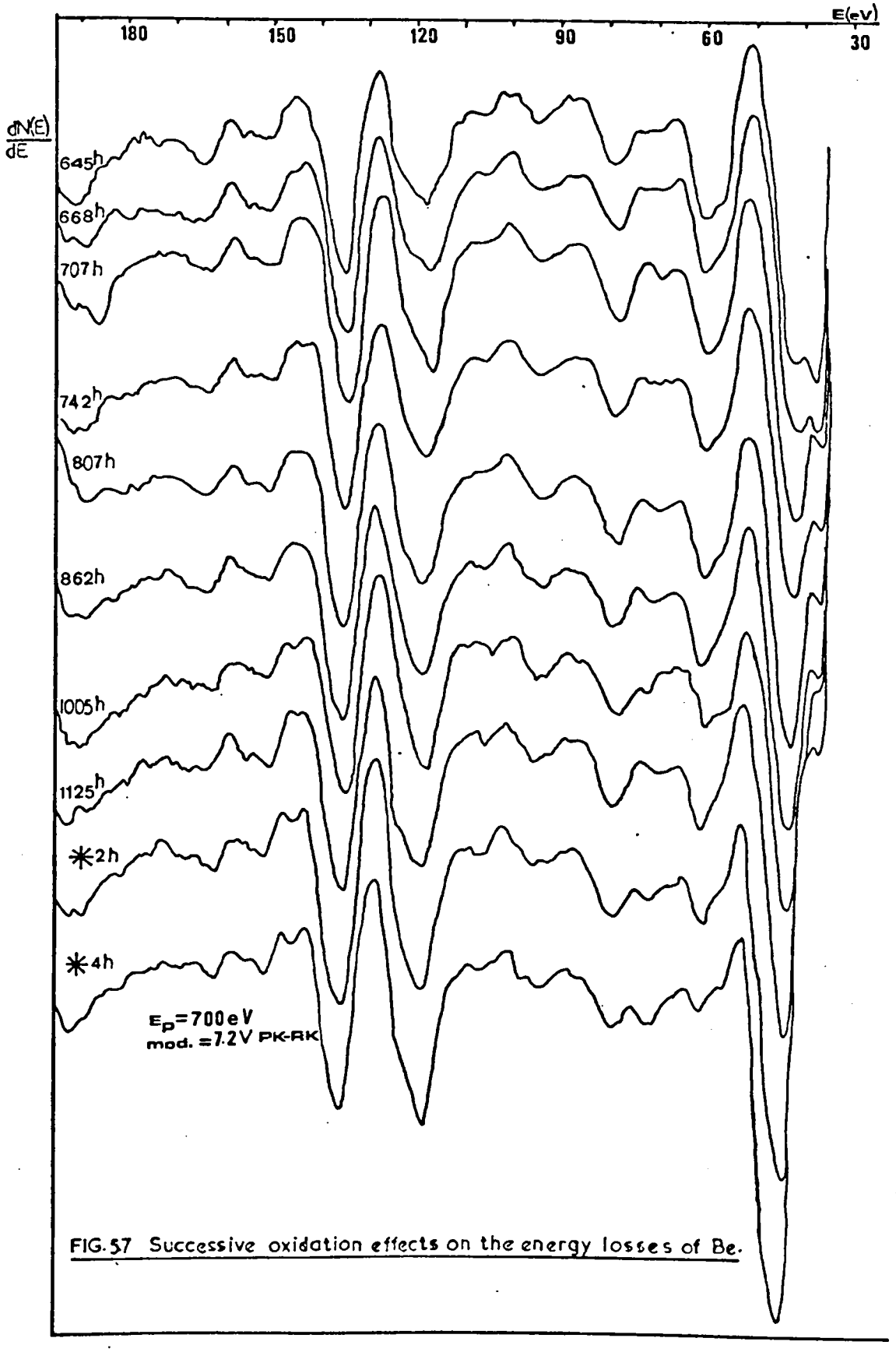

FIG. 57 Successive oxidation effects on the energy losses of Be.

74, 77, 95, 152, 164 and 178 eV of the clean Be disappeared, but new peaks at 46.5, 61, 71, 78, 156 and 168 eV appeared when the surface oxided, however, these new peaks are very small. No further change in the loss spectrum was noticed.

5.3.3 Secondary electron emission yield (SEE yield)

The system was operated in a SEE yield mode by an instant external switching. Typically a yield curve plot was obtained in the time of about one minute, which is of course small over the time scale of the oxidation changes as revealed by AES etc.

For SEE yield measurements a primary energy of 1 KeV and primary currents up to 10 μA were used (it may be added here that the primary current was kept constant for each particular yield curve although it could be changed for different curves). The secondary electron yield curve of a clean Be surface (this is known to be the characteristic of a clean Be surface because of its Auger spectrum Fig. (5.1a) which has taken immediately after the yield plot) is shown in Fig. (5.8). The main features are:

(a) A relatively flat maximum centered at a primary energy $E_{p_{max}}$ of 200 eV (δ_{max}, the maximum yield, is 0.65 at this $E_{p_{max}}$ of 200 eV).

(b) As the yield approaches zero with $E_p \rightarrow 0$, some structure is discernible at that low energy part. Whilst the nature of this structure will not be discussed in this article, it may be pointed out that it is of considerable current interest especially in connection with the study of single crystals, where some of the phenomena may be correlated with surface resonances (surface band structure) (McRae et al., 1977).

(c) The yield decreases to 0.2 at $E_p = 1$ KeV.

A sequence of yield curves is shown in Figs. (5.9) and (5.10) [the corresponding AES of this sequence are shown in appendix b]. These

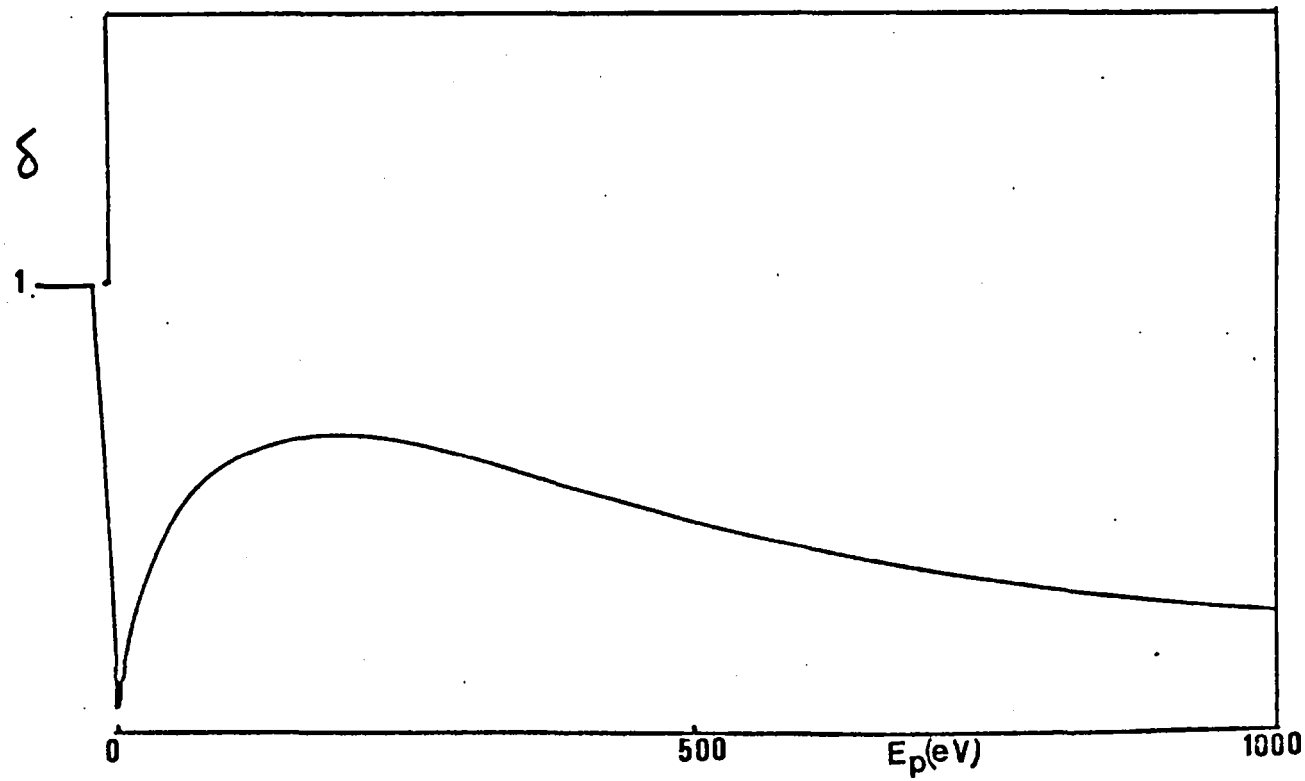

FIG. 58 Yield curve of a clean Be

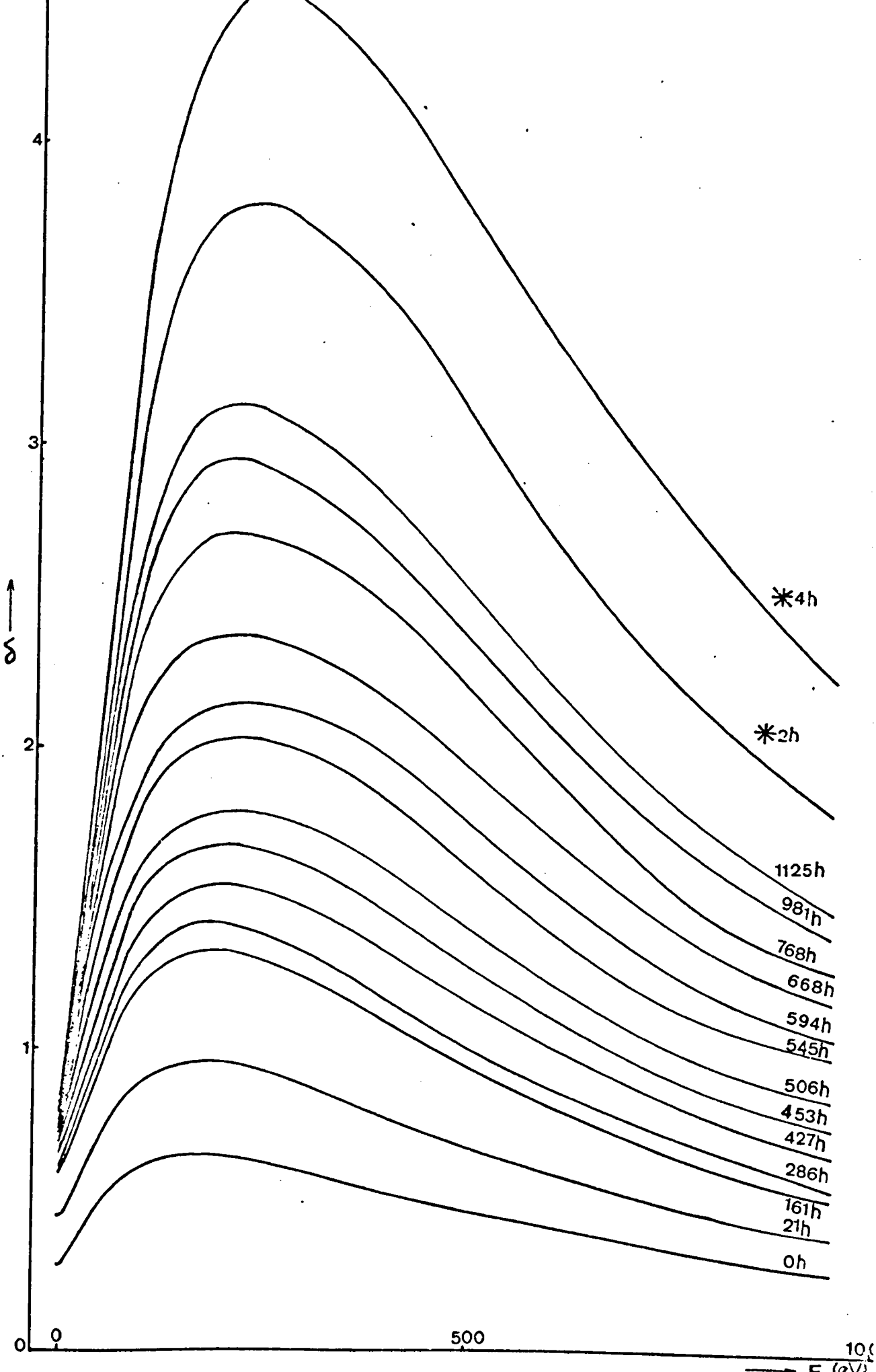

FIG. 5.9 Successive oxidation effects on the SEE yield of Be.

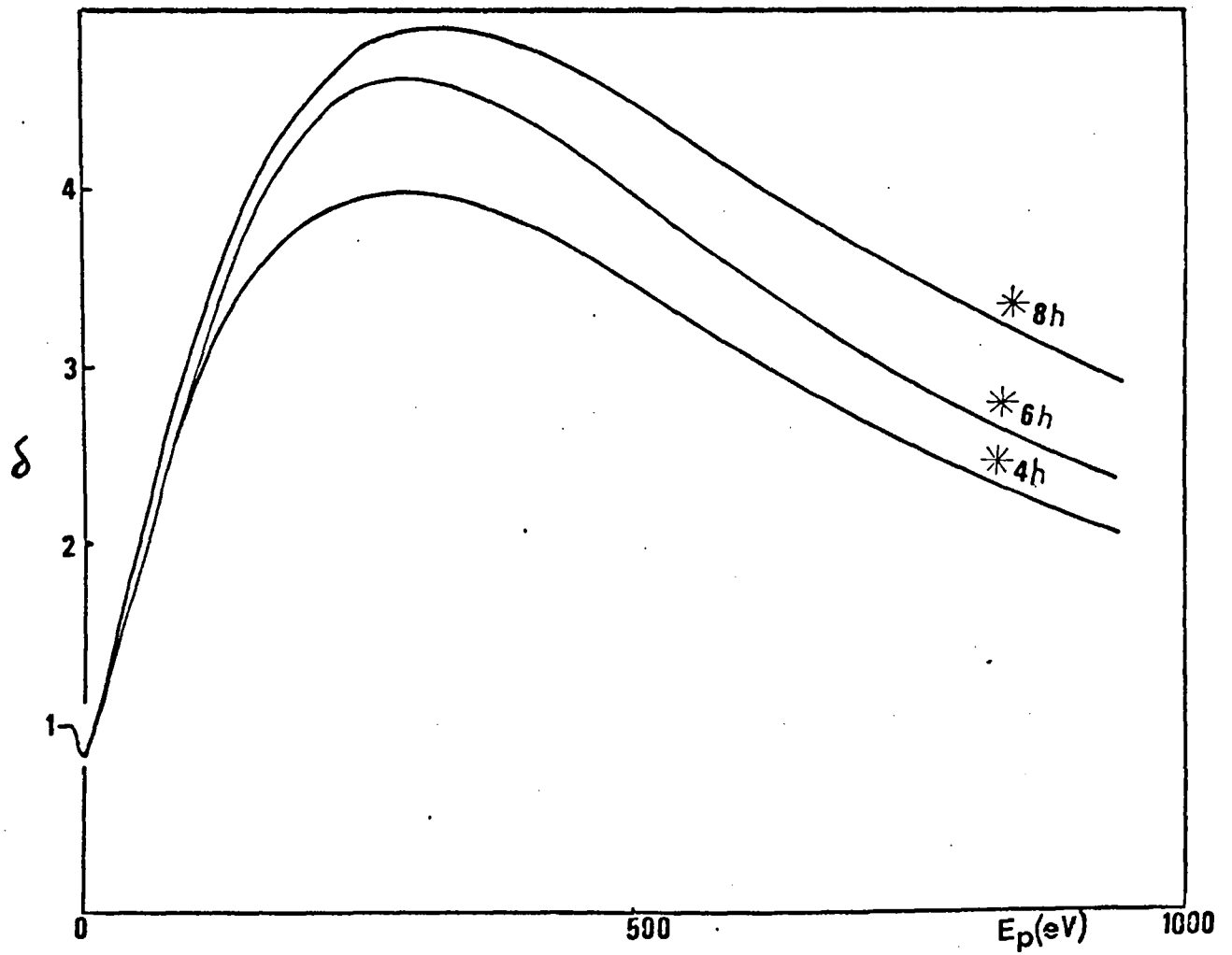

FIG. 5.10 SEE Yield of oxidised Be

curves represent the maximum change due to slow oxidisation from residual oxygen in the UHV system over a considerable period of time (60 days). From this sequence it may be seen that the δ_{max} has increased from 0.65 to 4.74 as the $E_{p_{max}}$ shifts from 200 eV to 331 eV. The full rate of change in δ_{max} as a function of oxygen coverage given by the ratio of the peak to peak height of the oxygen 505 eV peak to the peak to peak height of the Be 104 eV in the Auger spectrum is shown in Fig. (5.11a). As may be seen, after the initial rapid rise, the yield increases comparatively slowly to about 2.7 and from this point starts to rise very rapidly with increasing oxygen coverage until it reaches the value 4.74. Fig. (5.11b) also shows the full rate of change in δ_{max} as a function of the ratio of peak to peak height of oxygen (505eV)to the peak to peak height of total Be (in the form of pure Be (104 eV) and in the form of beryllium oxide (95 eV)). This figure shows the change of this ratio $(O/_{(Be+BeO)})$ from 0 to $\sim$ 6.5 whilst the δ_{max} increases from 0.65 to 1.2, and then during the increase of δ_{max} from 1.2 to 4.74, the ratio stays nearly constant (between 6.5 to 8.5). Other yield parameters like $E_{p_{max}}$ (primary energy of δ_{max}), $E_{p_{c1}}$ and $E_{p_{c2}}$ (the first and second crossover energy where $\delta = 1$) are given in table (5.1). The first crossover energy is plotted vs δ_{max} as shown in Fig. (5.12), it has a rapid decrease till δ_{max} reaches to its value 2.5, then it decreases comparatively very slowly and then becomes constant.

The data in table (5.1) may be used with simple secondary electron emission theory, relating range of primary electrons as a function of n and $E_{p_{max}}$ (section 2.5.1), the so-called range energy relation is;

$R = \dfrac{(\frac{E_p}{E_R})^{1+1/n}}{c}$, by giving E_p different values of $E_{p_{max}}$ (which has increased from 200 eV to 331 eV, by absorbing oxygen on the surface),

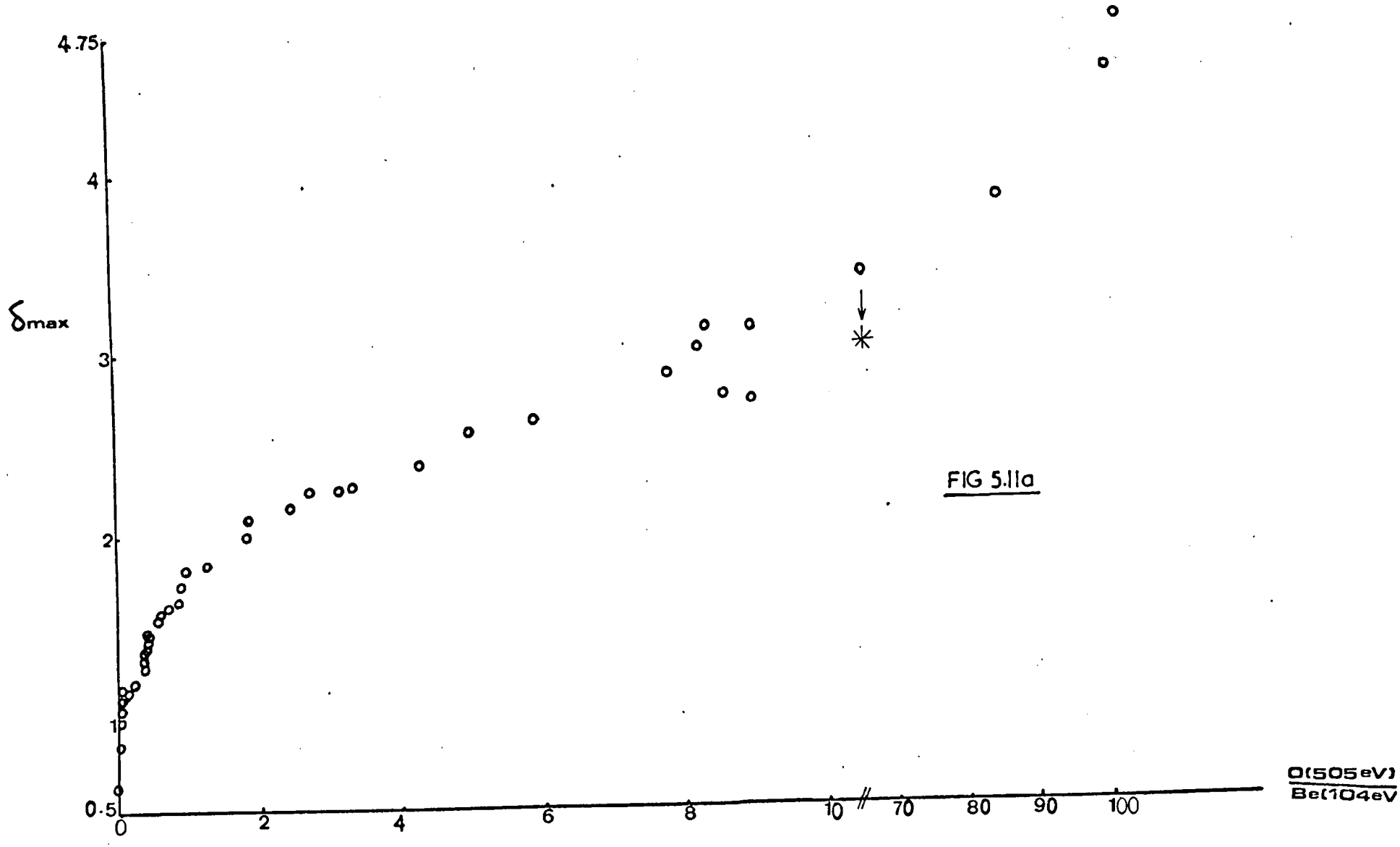

FIG 5.11a

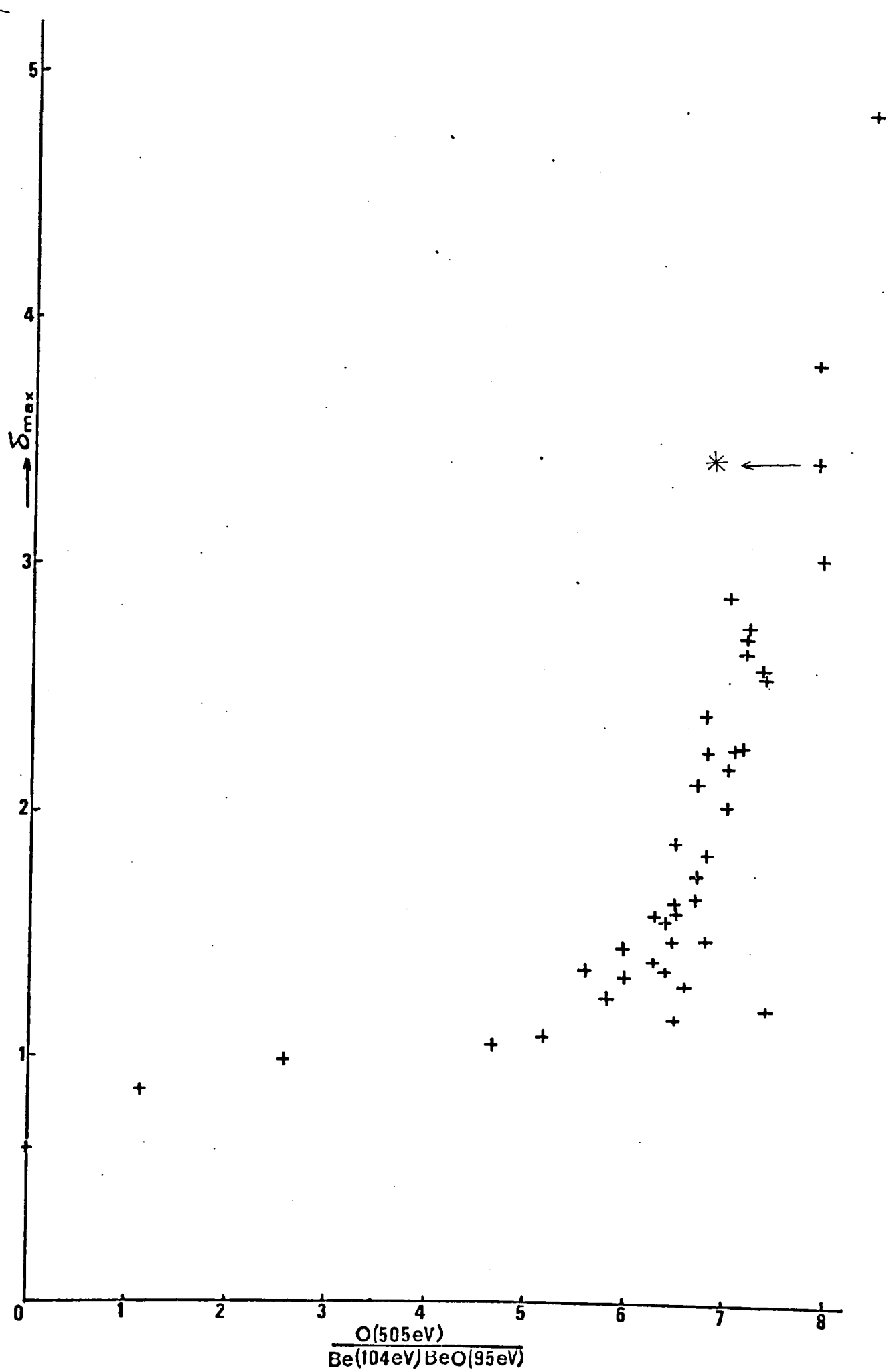

FIG. 5.11b

Table (5.1)

hours	E_{pc_1}(eV)	E_{pc_2}(eV)	E_{Pmax}(eV)	δ_{max}
0	-	-	200	0.65
21	-	-	210	0.98
33	142.3	297	210.3	1.05
82	105.1	389.8	216.5	1.18
186	68	482	201	1.36
427	43.3	696	216	1.64
472	40.2	739.4	219.6	1.82
	.	.	.	.
	.	.	.	.
981	21.6	-	229	3
1185	21.6	-	235	3.28
From this point the target was heated up for diffusing more oxygen into the surface.				
*2	18.6	-	247.5	3.6
*4	18.5	-	297	3.8
*6	18.5	-	303	4.4
*8	18.5	-	331	4.74

*2 = the target was heated up for two hours.

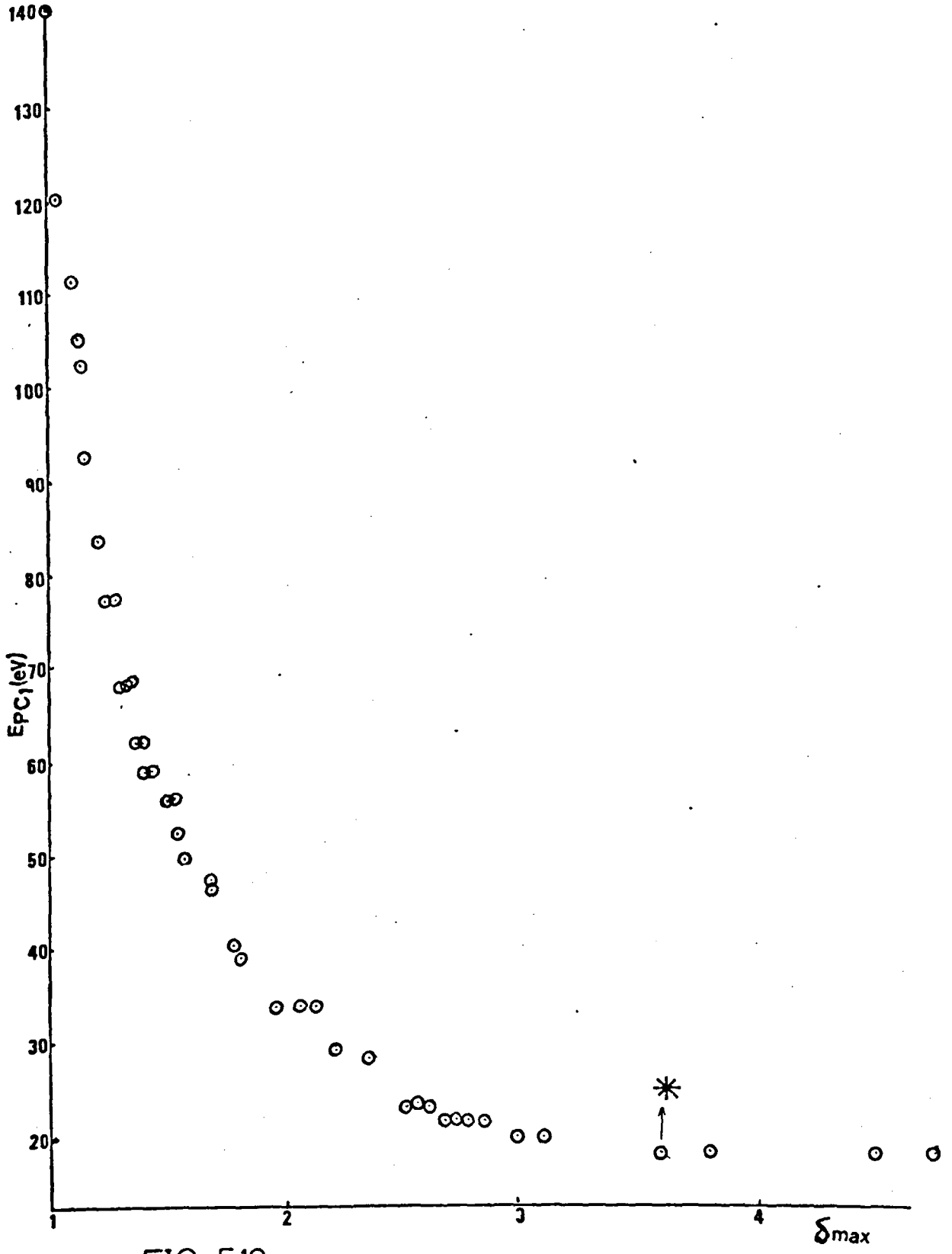

FIG. 5.12

we could get different values of R, which is proportional to escape depth by $R = (1 + r^2)\, x_\alpha$, (x_α, escape depth of secondaries). Figure (5.13) shows a plot of range of primaries as a function of δ_{max}. It is evident from this graph that the range increases quite slowly (from 34A°) initially, but when δ_{max} starts to increase rapidly at 2.7, the range or in other words escape depth of secondaries start to increase comparatively much faster (to 56A°).

5.4 Discussion of Results of Be → BeO

5.4.1 Auger Spectra

The Be atom has only four electrons, so the electron configuration is generally given as $1s^2\ 2s^2$. Therefore the possible Auger emission is core-valence-valence (KVV) transition. The binding energy of K-shell electron of Be (Fig. (5.14)) is about 111.4 eV (Bearden et al., 1967; Harmin et al., 1970; Höchst et al., 1977a). The width of the valence band is ∿ 11.0 - 12.0 eV (Sagawa, 1968; Nilsson et al., 1974; Höchst et al., 1977b). The energy diagram of Be is given in Fig. (5.14) in which the work function of Be is assumed as 5.1 eV (Dixon and Lott, 1969). From this data one may expect an Auger peak corresponds to a KVV transition at around 100 eV, but the observed peaks are at 104 eV, 84 eV and 65.5 eV (section 5.3.1). However the correct identification of the Auger peaks can be gained from the knowledge of the band structure, and one must consider the energy distribution of electrons within the ∿ 12 eV wide valence band of Be. The total density of states (DOS) which was calculated by Inoue et al. (1973) and also the partial density of states of the p electrons (P DOS) of Be which was determined from XPS measurement by Wiech (1968) are shown in Fig. (5.14b). From this data Höchst et al. (1977b) has determined the partial density of states of the s electrons (S DOS) of Be (Fig. (5.14a)), which is in agreement with

R has been calculated from $R=(E_P/E_R)^{1+1/n}/C$, where

$$C=2\pi(n-1)(NZ)\Gamma^2(1/n)a^2(a_H/a)^{2/n}(1+2\epsilon E_P)^2\left[(n-1)(1+\epsilon E_P)^{1+1/n}\right]^{-1}\times$$

$$\sin^2\left\{\frac{1}{n}\left[\frac{\pi}{2}-\tan^{-1}\frac{aE_1(1+2\epsilon E_P)}{4a_H\left[E_PE_R(1+\epsilon E_P)\right]^{1/2}}\right]\right\},$$

$$E_P=E_{Pmax},\quad n=1+2\exp(-f+2\times10^{-f}),$$

$$f=\log\left(\frac{\epsilon_i}{2}\right),\quad \epsilon_i=\frac{a}{b}$$

$$a=0.77a_HZ^{-1/6}$$

$$b=4a_H(E_R/E_P)(1+2\epsilon E_P)/(1+\epsilon E_P)$$

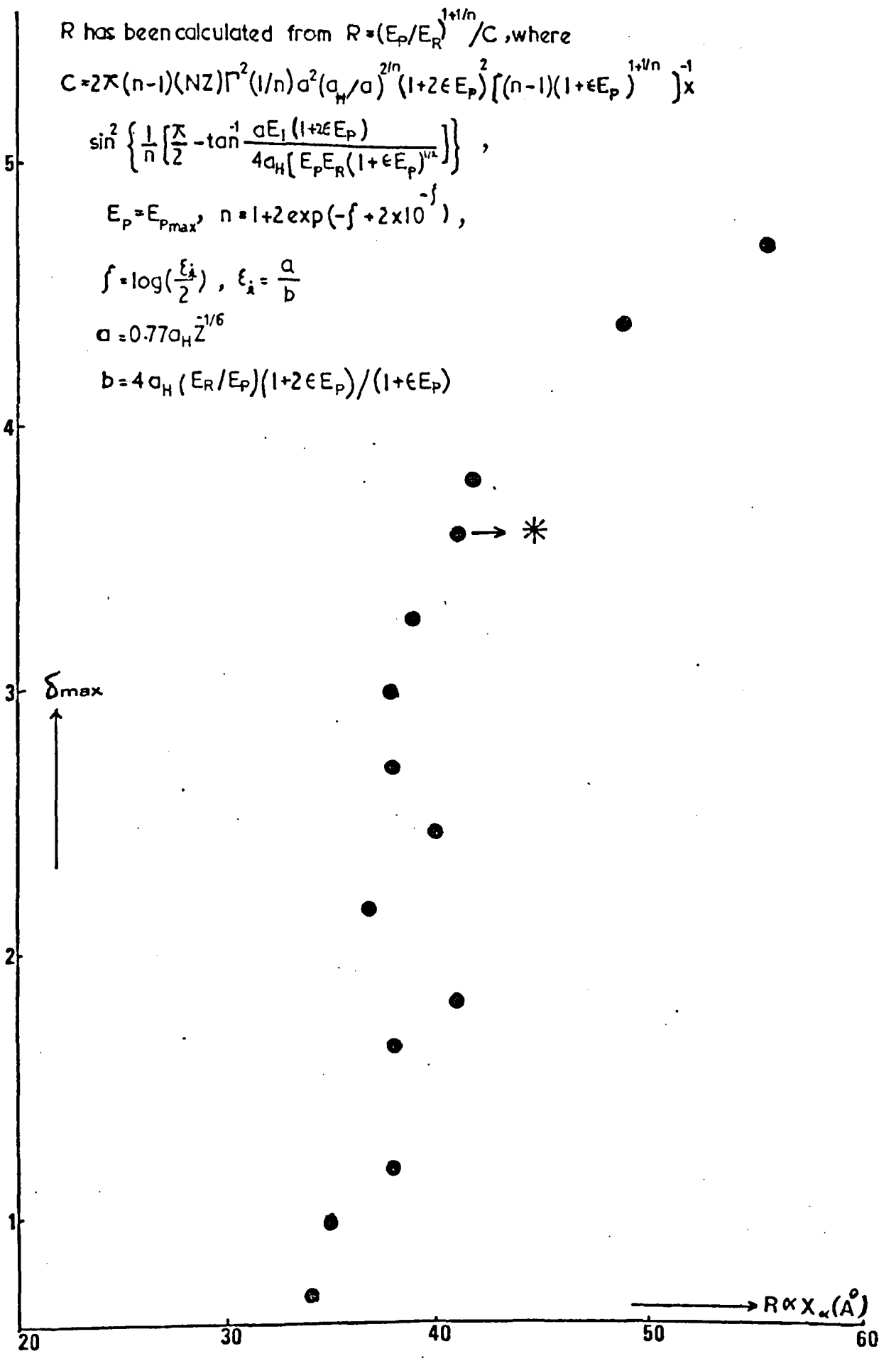

FIG.5.13

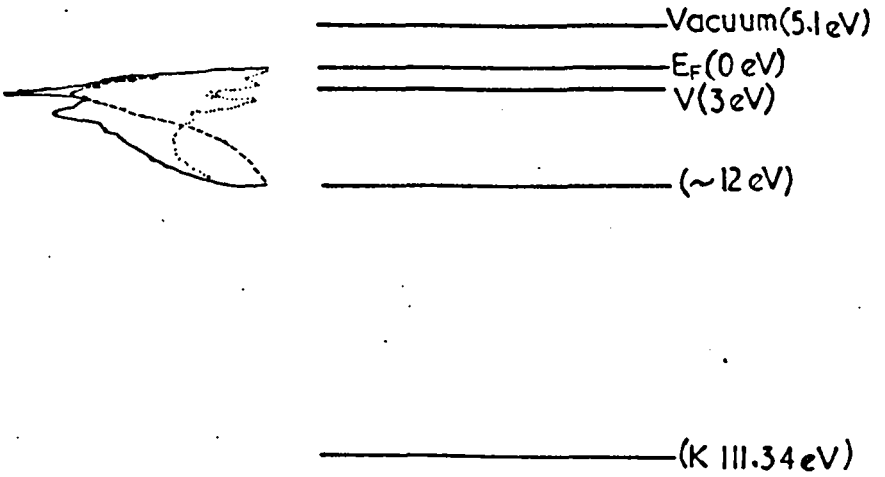

FIG. 5.14 Energy band diagram of Be : Full curve is the total density of states(DOS), (Inoue and Yamashita 1973), broken curve is the p partial DOS(Wiech 1963) and dotted curve is the s partial DOS which is the difference between the total DOS and the p partial DOS (Höscht et al 197.7b).

the theoretical calculation of Jenninson et al. (1980). Further Jenninson et al. mentioned that by integrating the two curves P DOS and S DOS one can get the electronic configuration of Be as $1s^2\ 2s^{0.68}\ 2p^{1.32}$. Therefore the main peak in the KVV emission has to involve pp transition. Both the partial density of states of p electrons and total DOS (Fig. (5.14)) shows a maximum at $\sim$ 3 eV, therefore, it is reasonable to assume that the electrons in the maximum take part in the Auger process, therefore, V $\simeq$3 eV. On the basis of this assumption the calculated value for the KVV transition peak is 105 eV. This is in good agreement with the observed peak at 104 eV.

The origin of other two peaks (84 eV and 65.5 eV) cannot be traced easily since their energy values are too low for any possible transition due to K-shell ionization. However, one reasonable explanation can be given from the possibility of plasma losses from the main Auger peak, Mularie & Rusch (1970) and Taylor (1969). In other words the Auger electrons originating from the KVV may have suffered energy losses in the excitation of plasmons. The measured value of a strong bulk plasmon loss in the energy distribution curve, for a clean Be surface was found to be 19 eV (table 5.2). The observed Auger peak at 84 eV is about 20 eV below the main Auger peak, indicating that the peak (84 eV) may well be a plasma loss from the main peak. The Auger peak at 65.5 eV then may be considered as a second loss from the main peak, since a strong second order plasma loss was also found in the energy loss spectrum. Presently there is no accepted explanation available for the peaks observed at 55.5 eV and 45.5 eV. However we believe that the peak at 45.5 eV corresponds to third order plasma loss of the electrons involved in the KVV transition, since we have also observed the third order of bulk plasmon loss in the energy loss spectrum.

Previously Auger studies on Be surfaces has been reported by

several workers (Musket et al., 1971; Suleman et al., 1971, 1973; Zehner et al., 1973; Maguire et al., 1974; Jenninson et al., 1980). This work is in agreement with Suleman et al. (1971, 1973) and Jenninson et al. (1980). However Musket et al. (1971), Maguire et al. (1974) and Zehner et al. (1973) have observed an additional peak around 92 eV. However, the explanation given for the origin of this peak is contradictory. Musket et al. (1971) have proposed an ss transition for this peak, but contamination by Si was mentioned by Zehner et al. (1973). In contrast to these two authors Maguire et al. (1974) have said that generally the Be KVV Auger spectrum consists of two peaks, which are due to the pp transition and the ss transition, and these peaks are well separated in the spectrum from the thermally cleaned polycrystalline Be surface, but are insufficiently separated in the spectrum from the surface which is cleaned by Argon-ion bombardment or prepared by evaporation. However Suleman et al. (1971, 1973) have suggested that the oxygen contamination was responsible for the additional peak observed by other workers. Further XPS and AES work of Madden and Houston (1977) on Li (which is nearly like Be) surfaces suggest the Li (KVV) Auger spectrum is mainly due to PP transition, and that the ss transition is negligibly small. But this suggestion was described as an accident by Madden and Zehner (1978) from their work on Be surface. However the recent calculation of Jenninson et al. (1980), who considering the screening effect, showed that the experimentally observed Be (KVV) spectrum consists of three components, which are due to pp, sp and ss transitions respectively, and the maximum of the Be (KVV) Auger line corresponds to the maximum of the pp component. This situation is clearly shown in Fig. (5.15). In conclusion the Be Auger spectrum consists only one peak due to KVV transition at 104 eV and the other peaks observed in the spectrum are due to the plasmon loss of the main

FIG 5.15 Jenninson et al (1980)

peak (104 eV).

In the Auger spectrum of oxidized Be, Auger peaks were found at 104, 95, 85, 77.5, 65 eV (104 eV is due to the remnant of elemental Be in the sample surface). These results are the same as those that Madden et al. (1979) obtained from BeO, with the exception that they could get another peak at $\sim$ 50 eV which they have interpreted as a ss transition.

In order to interpret the Auger spectrum of BeO, one can make some qualitative statement on the gross features of the bands in BeO considering the atomic levels of both Be ($1s^2$, $2s^2$) and O ($1s^2$, $2s^2$, $2P^4$). A valence band built up by the two 2s electrons of Be and four 2P electrons of O. As shown in Fig. (5.16) the valence band electrons involving in the O (KVV) and Be (KVV) transitions are the same. Therefore, in both type of spectra, the pp, sp and ss transition peaks should be separated by the same energy from one another. The O (KVV) transition peaks are observed at 505 eV, 485 eV and 470 eV. The peak corresponds to 505 eV is due to the pp transition. Generally from the energy order, and probability of transitions (485 more intense than 470), one can attribute the 485 eV peak to the sp transition and the 470 eV peak to the ss transition. This is in agreement with Madden's et al. (1979) explanation, so the energy separation of the pp transition from the sp transition, and the sp transition from the ss transition are 20 eV and 15 eV respectively, so we can expect the same separation in pp, sp and ss transition peaks in Be (KVV) spectra. However this spectra consists four peaks at 95, 85, 77.5 and 65 eV. Therefore, a possible selection for the pp transition is at 85 eV and the sp transition at 65 eV since 85 eV and 65 eV have the same energy difference as 505 eV and 485 eV. Therefore the 85 and 505 eV are due to pp transition, 65 eV and 485 eV are due to sp transition, 470 eV is due to ss transition (we couldn't get ss transition for Be because the

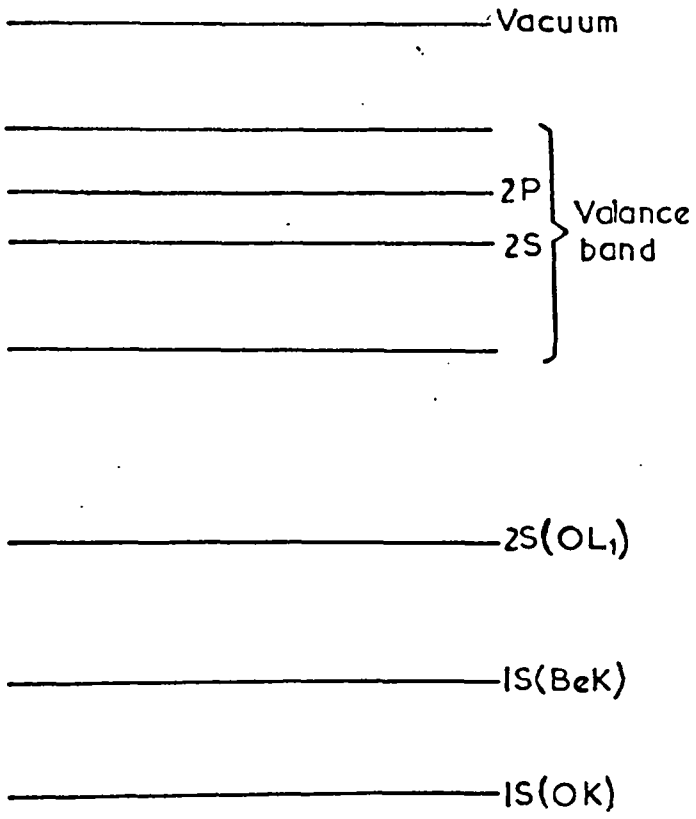

FIG. 5.16

resolution of the system was not enough). In these transitions both valence electrons that take part in the Auger decay coming from the same oxygen site. Peaks at 95 eV and 77.5 eV in the Be Auger spectrum are due to non-localized interatomic transitions (cross-transitions) with the valence electrons involved coming from different oxygen sites. The reason for the difference in energy in these features (localized-site spectra and non-localized transitions) is that; once the s-shell (for localized site oxygen) has filled the initial state hole in the k-shell then the binding energy of the p electron is increased because the coulomb repulsion of p electron has removed (the energy of p electrons increases with respect to the Fermi level) so it needs more energy to remove an electron from the p shell, but for non-localized transitions this coulombic force is negligible.

5.4.2 Energy Loss Spectra

The energy loss spectra of the 700 eV primary electrons for a clean Be surface is shown in Fig. (5.2) and the table (5.2) gives all the losses observed together with their identification. The calculated value of a bulk plasmon, using $\hbar w_p = \frac{ne^2}{m\varepsilon_0}$ (section 3.3.1.1), is 18.4 eV, Raether (1980), but the experimentally observed values are 19 eV (Watanabe, 1956), 18.5 $\pm$ 1 (Aiyama & Yada, 1974) and 19.5 eV (Höchst et al., 1977a). The Höchst et al. result for the bulk plasmon losses is shown in Fig. (5.17). In our work bulk plasmon losses up to the 9th order was detected, and the value of the 1st order is 19 eV. The comparison between our results and Höchst's et al. (1977a) is given in Table (5.2), with most of them are in very good agreement. Further, the surface plasmon loss energy of 13 eV is in reasonable agreement with the calculated value of 13.4 eV, by using the expression $\frac{\hbar w_p}{\sqrt{2}}$ ($\hbar w_p$, bulk plasmon energy). The values that Höchst et al. have reported as second to fourth harmonic of surface plasmons, are estimated

FIG·5·17 Hoscht et al (1977a)

Table (5.2)

Observed energy losses for clean Be (in eV)
with assignments

Our result		Hocsht et al[a] 1977	
Observed loss	assignment	loss peaks	assignment
6	I		
13	S	11.50	S
19	B and S + I	19.5	B
		30.70	2S
36	2B and 3S	38.69	2B
		50.90	3S
56	3B	58.20	3B
		70.40	4S
77	4B	77.50	4B
95	5B		
115	6B and ionization loss		
152	8B		
164	8B + S		
178	8B + I		

I = Ionization or Interband transition
B = Bulk plasmon loss
S = Surface plasmon loss

values and experimentally we were unable to detect them. The strong peak at 115 eV could correspond to an ionization loss of the k-shell electrons of Be; which is generally equal to the binding energy of the k-shell electrons in Be. This value is in good agreement with others values, which varies from 111 eV to 114.8 eV (Siegbahn et al., 1967; Zehner et al., 1973; Madden et al., 1979).

During the oxidation of Be surface the bulk plasmon loss energy increases gradually from 19 eV to 23 eV. Suleman (1971) has reported this shift from 19 to 25 eV for gradually oxidised Be. This difference between the bulk plasmon energies of BeO is probably due to the thickness of oxide layer or the difference in cleaning techniques, since Suleman obtained his clean surface by evaporation and in the present work the clean surface was obtained by the Argon bombardment technique. The value of the bulk plasmon for BeO has also been reported by Gründler et al. (1978) as 24.4 eV, by measuring the energy of the main peak of the loss function and by ascribing it as a volume plasmon, this value is in good agreement with the corresponding value of the free electron model, Roessler et al. (1969);

$$\hbar w_p = \hbar \sqrt{\frac{4\pi ne^2}{m}} = 24.5 \text{ eV}$$

(where n is the density of valance electrons, m is free electron mass and e is the electronic charge, the density of valence electrons in BeO was calculated by assuming the number of valence electron per BeO is six, and its value is $6 \times 7.32 \times 10^{22}$ electrons/cc) but Powell (1969) and Grundler et al. (1978) have demonstrated the influence of more or less strong interband transition on the energy position of the main maximum of $\mathrm{Im}(-\frac{1}{\varepsilon})$. It may be that interband transitions below and above $\hbar w_p$ cause this main maximum to be located accidentally near the corresponding free electron model. So, it is obvious that determination of

an exact value of the bulk plasmon loss for BeO is very difficult. The loss peak at 23 eV can also be interpreted as the ionisation loss from the L_1 shell of oxygen in BeO (section 6.4.2).

The energy loss spectrum of BeO also shows a strong peak at 119.5 eV which has shifted from 115 eV (Ionization loss of clean Be) during the oxidisation. This peak is the energy of k-shell of Be in BeO, and this energy shift on forming BeO has been reported by Lukirskii et al. (1964) (3.2 eV), Swanson et al. (1968) (6.3 eV) and Hayasi et al. (1969) (3.8 eV). All these authors used soft X-ray spectroscopy for their results, Harmin et al. (1970) used ESCAS and got the shift for the Be k-shell as 2.8 eV. Recently Madden and Zehner (1979) have done some experimental work on BeO by using AES, CLS and XPS techniques and in the energy loss spectrum for a clean Be surface, they have got the ionization loss energy at $\sim$ 114.8 eV and for oxidised Be, they have got it at $\sim$ 120 eV, therefore, the shifting and the energy of the k-shell of Be and BeO, in our results, are in good agreement with their results.

5.4.3 Secondary Electron Emission Yield

As described in the section (5.3.3) the δ_{max} and $E_{P_{max}}$ of a clean Be surface has been determined as 0.65 and 200 eV respectively. These values are in agreement with theoretical calculations and experimental results. The experimental results have determined the values of δ_{max} and $E_{P_{max}}$ of clean Be surface as 0.5 - 0.75 and 200 - 300 eV respectively (Kollath, 1956; Bruining, 1954). It must be remembered however that measurements made in this era were not able to be characterised by techniques such as AES and some doubt must always remain as to their precise surface state. Theoretically the values of these maximas have been calculated from the two equations (2.47) and (2.44) as:-

$$\delta_{max} = 0.12\ Z^{1/15}\ I^{4/5}\ (1 + 1.26r) = 0.61$$

$$E_{p_{max}} = 57.9\ Z^{1/15}\ I^{4/5}\ (1 + 5r^2)^{4/5} eV = 270\ eV$$

where r is the backscattering coefficient (0.08), I is the first ionisation loss (6 eV) and Z is the atomic number (4).

Two of the most important factors in secondary electron emission are the range of primary electrons and the escape depth of the secondary electrons. The range of the primary electrons has been calculated from the equation $R = \left(\frac{E_p}{E_R}\right)^{1+1/n}/C$, where C and n are defined in section (2.5.1). If in this formula $E_p = E_{p_{max}}$, then the value of $34A^o$ is obtained for the range of primaries of a clean Be surface.

Since the range and escape depth x_α are related by the equation $Am = \frac{R}{x_\alpha} = (1 + 5r^2)$, section (2.5.5), thus the escape depth x_α can be obtained as a function of range of E_{Pmax}. For clean Be $E_{Pmax} = 200$ eV gives an escape depth of $33A^o$. This value is in close agreement with the calculated value of x_α from the relation $x_\alpha = 2.67 \times A_0 I/\rho\ Z^{2/3} = 30.9A^o$ (section 2.5.2), and with the experimental value which is determined by Bronshteyn et al. (1968) as $30\ A^o$.

A progressively oxidised Be surface yield curve has its maximum energy at 331 eV and its maximum yield at 4.74. For comparing our results with theoretical and experimental results, the normalized yield curve ($\frac{\delta}{\delta_{max}}$ vs $\frac{E}{E_{max}}$) was plotted, which was in good agreement with the theoretical curve obtained by Kanaya et al. (1978), and the experimental curve by Bronshteyn et al. (1968) (Fig. (5.18)), but because of low primary energy (1 KeV) (instrumental limit) we could not get the complete curve of the normalized yield curve. In the sequence of yield curves of Be → BeO, in so far as there was not any significant elementary Be on the surface (from Auger spectra), the normalized

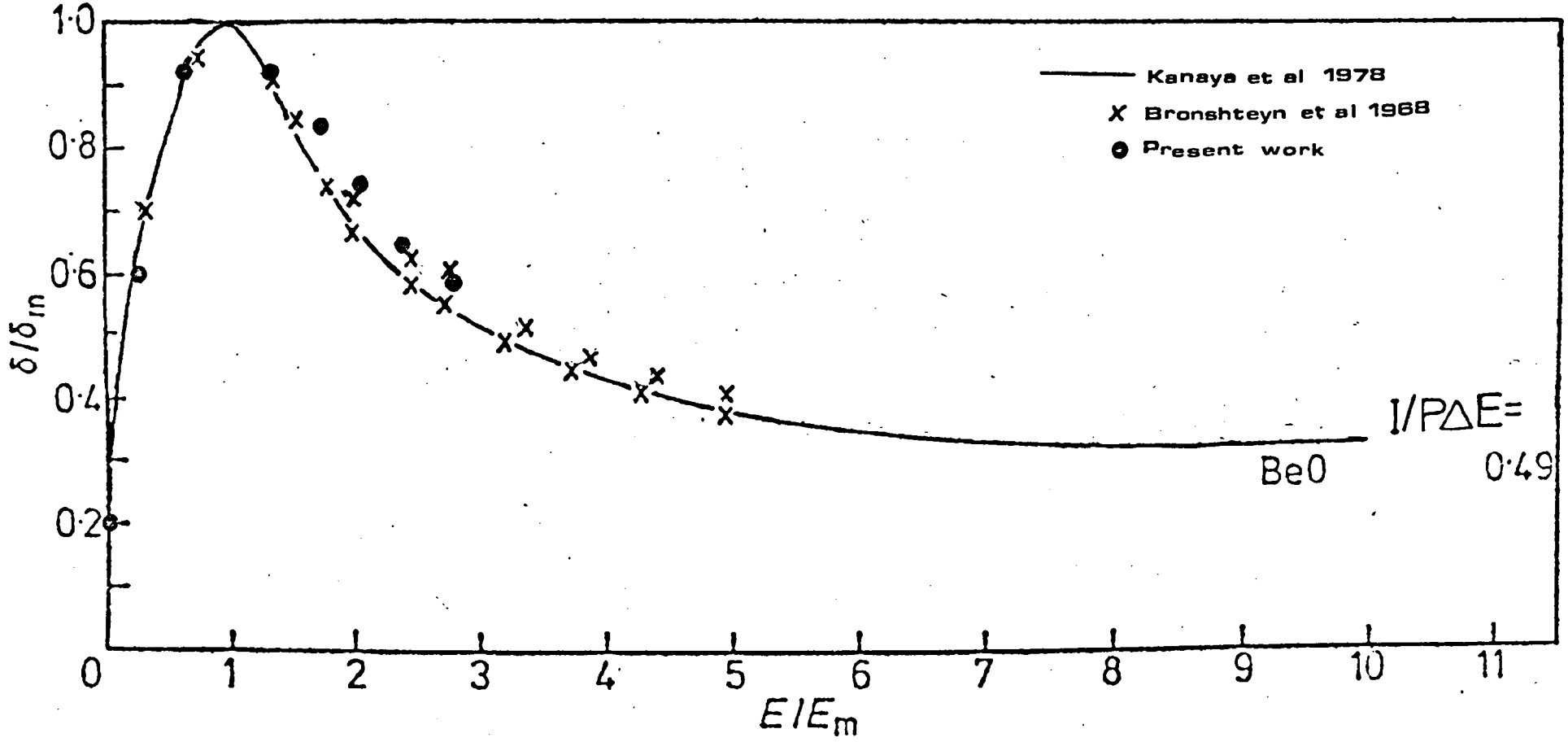

FIG 5·18 Theoretical and experimental comparison of normalized yield curve

yield curve was fitted quite well to the theoretical normalized curve for BeO, but when a peak of pure Be in Auger spectrum of the surface was distinguishable the normalized yield curve would not fit any more and it shifts to higher limit of $\frac{\delta}{\delta_{max}} - \frac{E}{E_{max}}$ curve. Since theoretically the value of $\frac{I}{P\Delta E}$ (section 2.5.5) for this normalized curve has been determined as 0.49, and from our result the first ionization loss, I = 7 eV and $\Delta E = 28.8\ (\rho\nu/A)^{\frac{1}{2}}$eV = 20 eV (section 2.5.2), we can calculate p (normalized ratio of one plasmon loss under consideration to the most probable plasmon loss ΔE) as 0.7. Therefore, by using the equation (2.32) $x_\alpha = \frac{370}{P}\ (\frac{I}{\Delta E})\ (\ln \frac{80\ I}{\Delta E})^{-1}$ the escape depth of 55.5 A^o is obtained which is also in agreement with the value 53 A^o which has been calculated from the range relation ($x_\alpha = \frac{R}{1 + 5r^2}$, range relation $R = (\frac{E_p}{E_R})^{1+1/n}/C$, where $E_p = E_{Pmax}$ = 331 eV and r is the backscattered coefficient for BeO which is 0.113). The escape depth of secondaries of BeO has been determined as 230 A^o by Bronshteyn et al. (1968), and this difference is probably because of thicker BeO layer on their sample.

It is evident that as the oxidation process takes place the value of escape depth of secondaries increases from ≃ 33 A^o to 53 A^o, range of primaries which is proportional to escape depth also increases from ≃ 34A^o to 56A^o, $E_{P_{max}}$ shifts progressively from 200 eV to 331 eV and δ_{max} changes from 0.65 to 4.74.

To get some ideas about the reason for the increase in δ_{max} (in other words the increase in secondary electrons), Figures (5.11a, b), (5.12) and (5.13) have been plotted to see the changes in δ_{max}, escape depth x_α and first crossover energy $E_{P_{c_1}}$ relative to the oxidisation process of the surface. In Fig. (5.12), $E_{P_{c_1}}$ (the first crossover energy for δ = 1) rapidly shifts to lower energies as yield increases. As pointed out by Dionne (1975) the first crossover to a first

approximation is proportional to η which is equal to ϕ (work function) for metals, and is equal to $E_g + \chi$ (E_g, the band gap and χ, electron affinity) for insulators and semiconductors, therefore, a decrease in the first crossover energy indicates a decrease in the work function of Be surface as the oxidation proceeds. A decrease of work function of Be during oxidation has also been reported by Green and Bauer (1978). One reason for the increase of secondaries during the oxidation could be the decrease in work function. Fig. (5.11b) is a graph of δ_{max} against a measure of the ratio of total oxygen on the surface to the total Be on the surface, i.e. the peak to peak height of oxygen 505 eV peak divided by the sum of the pk-pk height of the Be 104 eV peak plus the pk-pk height of the BeO 95 eV peak. The former is a measure of elemental Be (the KVV line) whilst the 95 eV peak is the same transition when a Be atom is combined with oxygen. If it is assumed that the ionisation probabilities are very much the same for the K levels in the two atoms then this sum is a measure of the total Be on the sample surface. This Figure (5.11b) shows a rapid increase in the ratio $\frac{O(505\ eV)}{Be(104\ eV) + BeO(95\ eV)}$ from 0 to $\sim$ 6.5 whilst the yield increases from 0.65 to 1.2, and then during the increase of δ_{max} from 1.2 to 4.74 the ratio stays nearly constant (between 6.5 to 8.5). The rapid increase of this ratio (O/(Be + BeO) at the early stage of oxidisation is probably because of the formation of the BeO on the surface (in other words, it is due to the conversion of the elementary Be to the oxide form on the surface), and when this ratio stays approximately constant while the δ_{max} increases, it seems that the oxygen is being consumed only to get a thicker BeO layer on the surface. As may be seen from Figure (5.11a), the rapid increase of δ_{max} (vs $\frac{O(505\ eV)}{Be(104\ eV)}$ at early stage of oxidation is also probably due to the conversion of Be to BeO on the surface. This figure also shows that δ_{max} stays

comparatively constant after the initial rapid increase and then when it reaches the value of 2.7, it starts to increase rapidly. At $\delta_{max} = 2.7$ in Fig. (5.13), the escape depth also starts to increase relatively rapidly to its higher values. At this point it appears that the oxide layer has reached a thickness sufficient to cause band bending (Simon and Williams, 1968; Kortov et al., 1975), which can be due to a reduction in the potential barrier height, especially by generation of a negative electron affinity (NEA), Martinelli (1970, 1974). NEA is a condition at the surface where the vacuum level is beneath the bulk conduction band minimum (as shown in Fig. (5.19)) provided the electron affinity χ is smaller than the band gap of the semi conductor, E_g. Therefore, electrons which are excited into the conduction band of the semi-conductor can still be emitted after they have become thermal electrons provided they can pass through a bent region. It is usually achieved by the absorption of Cs or CsO and O_2 to the atomically clean surface of a semiconductor in the U.H.V. ambient. There is a report by Kortov and Slesarev (1975), which indicated that band bending in BeO could reduce the potential barrier height (χ) by a factor of almost 2, and this could increase strongly the emission probability. Also it has been reported by Fitting et al. (1978) that the electron yield raises linearly as the surface barrier is lowered and they have approximated that the number of emitted electrons is proportional to escape depth, where the escape depth is a function of electron affinity, and energy loss parameter. For a certain value of energy loss parameter the escape depth increases while potential barrier height decreases. Therefore, an increasing of δ_{max} and the escape depth in Figs. (5.11a, b and 5.13) can indicate a decrease in potential barrier height caused by band bending.

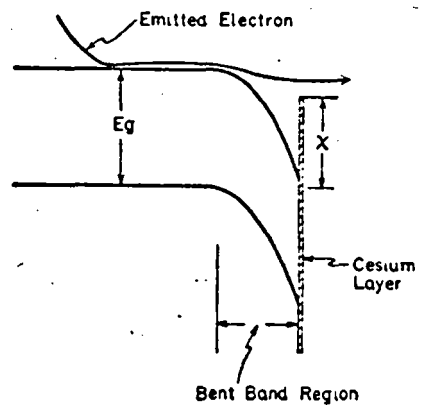

FIG. 5.19. *Schematic band diagram of a semiconductor with a negative effective electron affinity.*

5.5 Conclusion

In conclusion it may be stated that Auger spectroscopy is a valuable aid in examining the changes in secondary electron yield due to over layer formation of an oxide on such a material as Be. It may also be pointed out that to evaluate more accurately the secondary emission parameters it would be necessary for the Auger spectroscopy to be quantitative.

We will now move on to look at the results of a similar experiment performed on Mg → MgO. The MgO oxide is also a good emitter, so it is worthwhile to check all these properties on its surface.

CHAPTER 6

RESULTS AND DISCUSSIONS OF Mg → MgO

6.1 Introduction

As was mentioned in the previous chapter MgO is a very good emitter of secondaries and a maximum yield of nearly 21 has been obtained for a crystal cleaved in vacuum (Lye, 1955).

In this chapter the different secondary electron aspects (AES, CELS and SEE yield) of a thin film of magnesium is studied from an atomically clean state to the first stages of oxidation. In order to compare the properties of secondaries of Mg → MgO with those of Be → BeO, the same secondary electron yield parameters have been obtained. Thus, concurrently for each yield curve the corresponding Auger spectrum and characteristic energy loss spectrum have been taken over a series of stages of surface oxidation starting with the clean surface. The results of AES, CELS and SEE yield for Mg → MgO are presented at the beginning of this chapter followed in the sections by discussion and comparison with Be.

6.2 Preparation of clean Mg

Following the experiments on beryllium, and without opening the UHV system to the atmosphere, a magnesium thin film was prepared in the same UHV chamber. The clean magnesium thin film surface was prepared in the usual manner, by evaporation (or more correctly by sublimation) of magnesium from a tungsten wire basket, onto the polycrystalline Be substrate (the Be substrate was the same one as was used for getting the results of Be) in UHV. The magnesium was in the form of granules (purity 5N8), which was retained in a tungsten basket. The cleanliness of the magnesium surface was checked by taking Auger spectra immediately after each evaporation. Normally for the first few evaporations, some oxygen and carbon contaminations on the surface cannot be avoided. However, in our case, since most of the residual oxygen molecules had already been used by beryllium in its oxidation process and because of the continuous pumping (by the ion pump) over such a long period ($\sim$ 16 weeks), an oxygen-free surface of magnesium was obtained after only two evaporations. This surface remained oxygen free for several hours. During a period of nearly two weeks a whole sequence of Auger electron spectra, characteristic energy loss spectra and secondary electron yield were obtained. The surface was then heated in an attempt to diffuse more oxygen from the bulk. By plotting the Auger spectrum of this latter treated surface, it was demonstrated that there was no significant contaminants on the surface other than oxygen. This heating process was repeated several times again in an attempt to get maximum coverage of oxygen on the surface, however, a decrease of the oxygen signal in the Auger spectrum of the surface was observed after each heating process indicating that diffusion was into the bulk or that a restructuring of the surface was occurring.

A primary beam of 15 - 25 μA with an electron gun energy of 1.3 KeV was used and the commonly used modulation voltages were 2 V pk-pk for the Mg Auger spectra and 7.2 V pk-pk for the oxygen spectra.

6.3 Results of Mg → MgO

6.3.1 Auger spectra

A low energy Auger spectra of a clean Mg surface is shown in Fig. (6.1a), and the same range spectra of the Mg surface with increasing amounts of oxygen sorbed onto the Mg surfaces are shown in Figs. (6.1b - 6.1g). The main features of the clean Mg Auger spectrum are; a large peak at 45 eV, and two smaller peaks at 35 and 59 eV. The height of the main peak (45 eV) is some 35 times bigger than the 59 eV peak. The peak at 35 eV is seen to split to form an additional shoulder at 30 eV. During the oxidation of the Mg surface by residual oxygen gas over a considerable period of time, some changes were observed in the AES, as may be seen in Figs. (6.1a - 6.1g). The initial effect of oxidation is the rapid attenuation of the 45 eV peak, coincident with the growth of the 35 eV peak and the oxygen Auger peak at 505 eV. Also, a slight discontinuity develops at 26.8 eV and its intensity increases to a maximum intensity after 188 hours, and after which it starts to decrease with more oxidation, and at the end it is only a discontinuity. After 300 hours, the surface is fully oxidised, with the main peak at 45 eV disappearing almost completely and the peak at 35 eV becoming the largest peak in the spectrum (Fig. (6.1g)). The peak at 59 eV has also disappeared, and a new peak (shoulder type) has appeared at 49 eV. At this stage a large triplet oxygen Auger peak was found at 505, 485 and 470 eV. However the intensity of these oxygen Auger peaks (after heating the target) as shown in Fig. (6.1g)

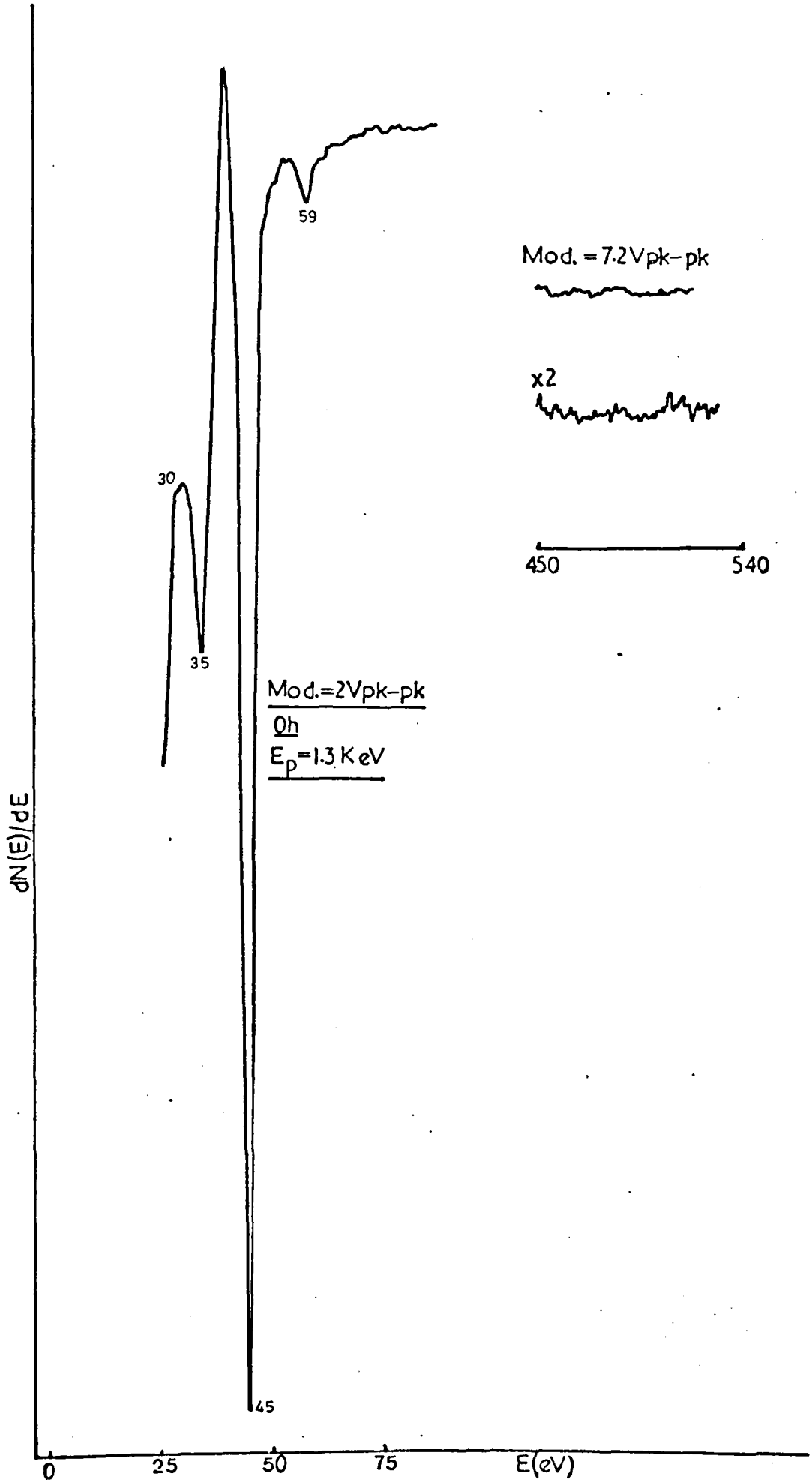

FIG. 6.1a Auger spectrum of clean Mg

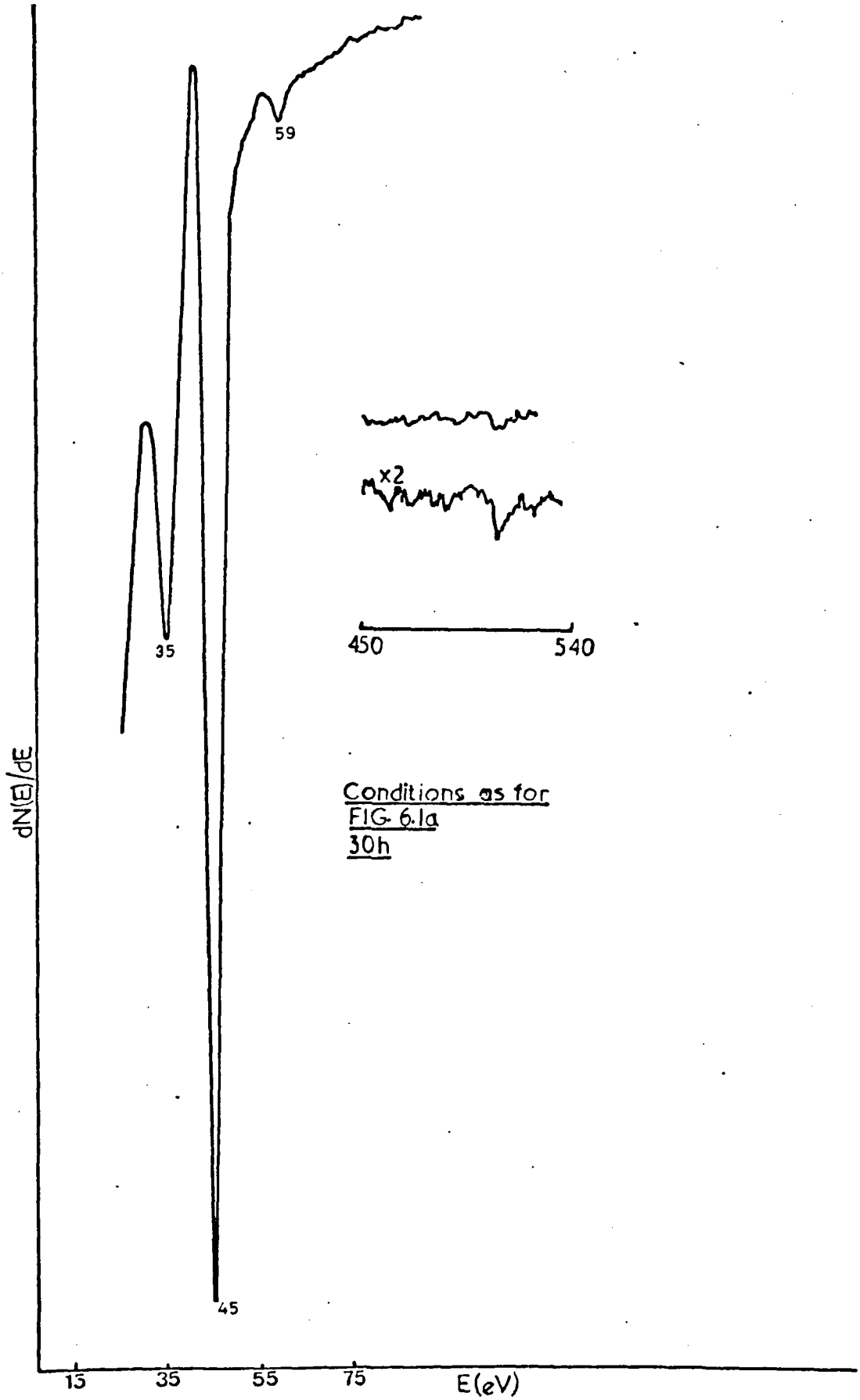
59
35
45
x2
450
540
Conditions as for
FIG. 6.1a
30h
dN(E)/dE
15
35
55
75
E(eV)

FIG. 6.1b

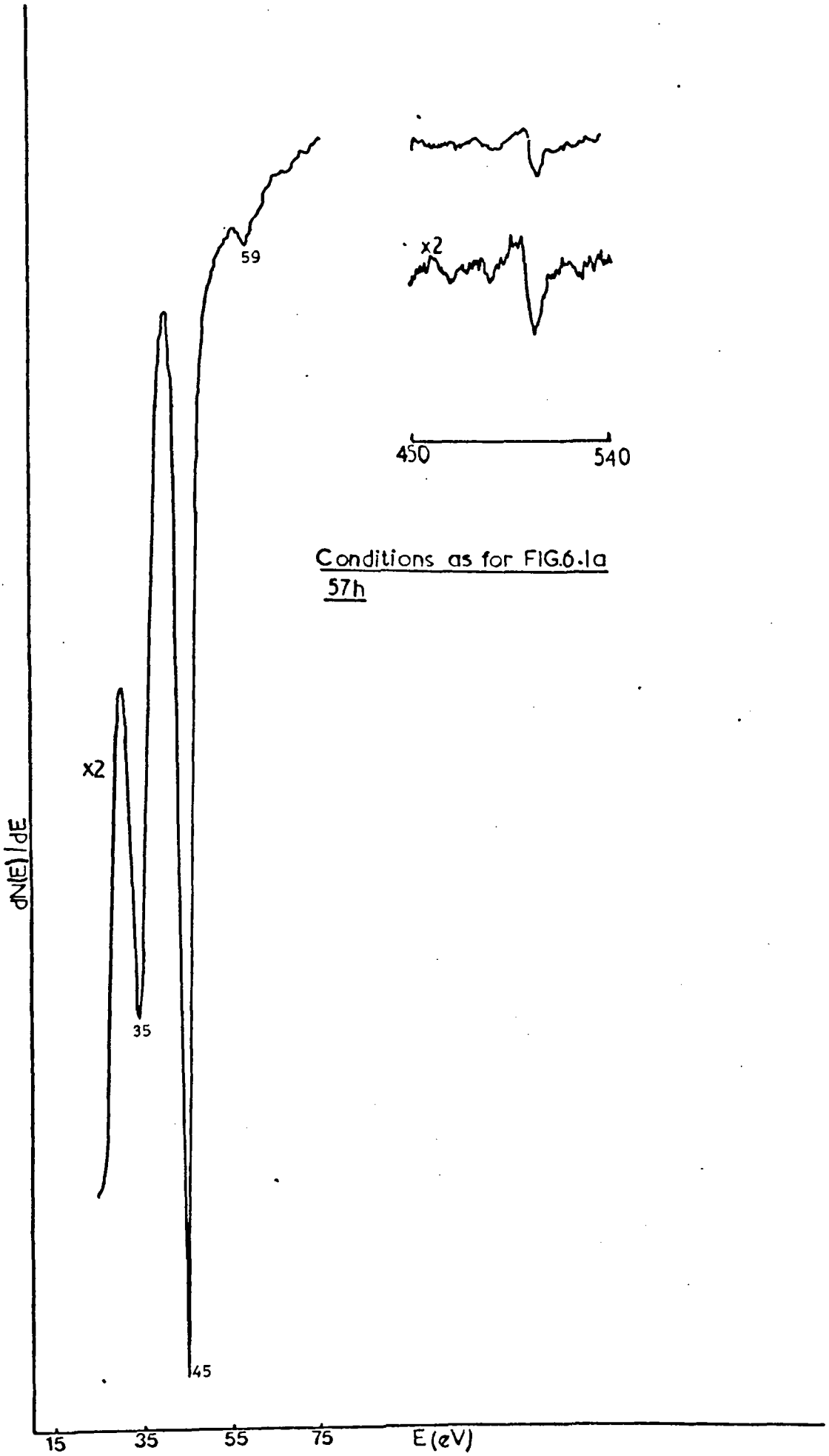
x2
59
450
540
Conditions as for FIG.6.1a
57h
x2
35
45
dN(E)/dE
15
35
55
75
E(eV)

FIG·6·1c

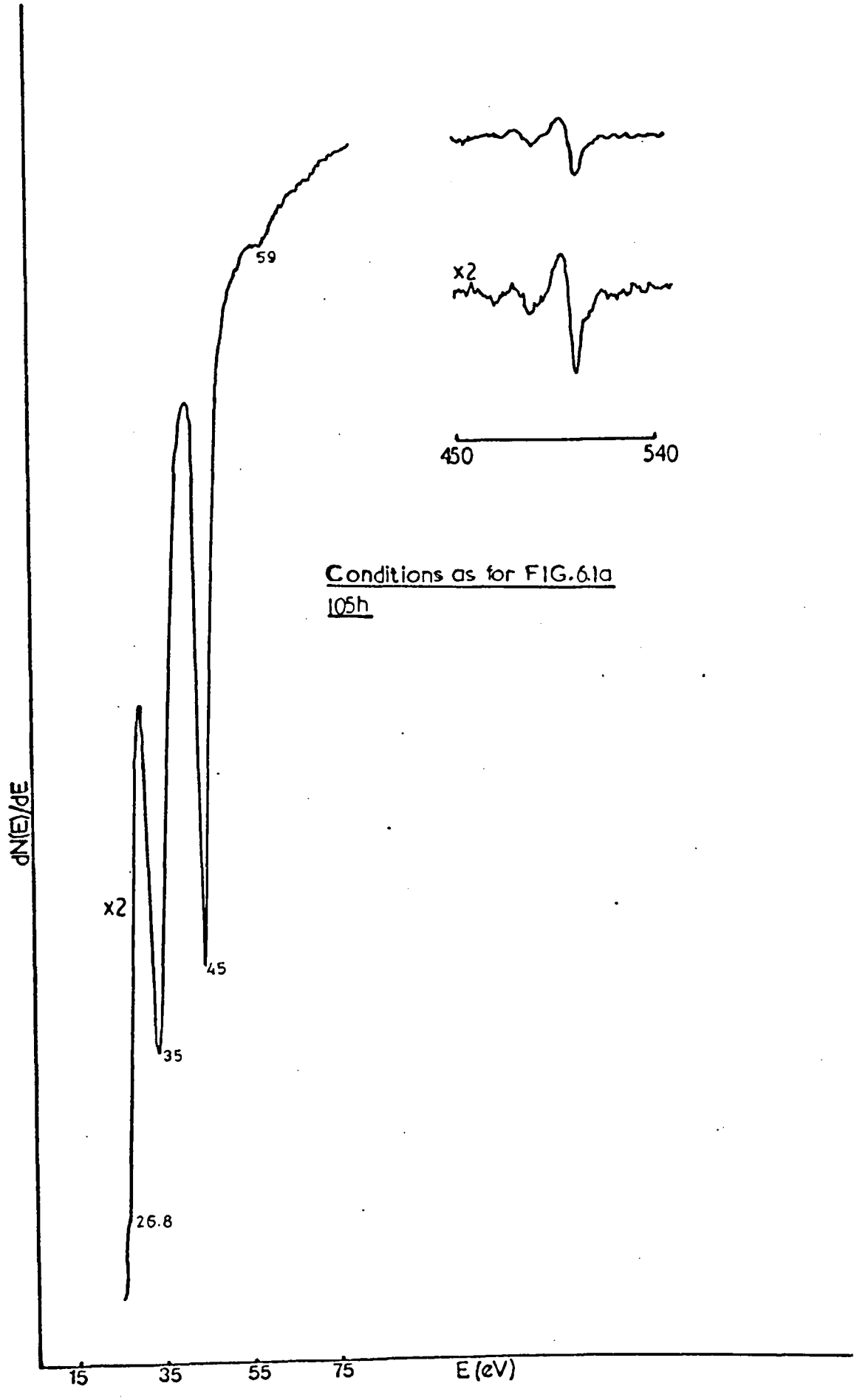
dN(E)/dE
x2
26.8
35
45
59
x2
450
540
Conditions as for FIG.6.1a
105h
15
35
55
75
E (eV)

FIG. 6.1d

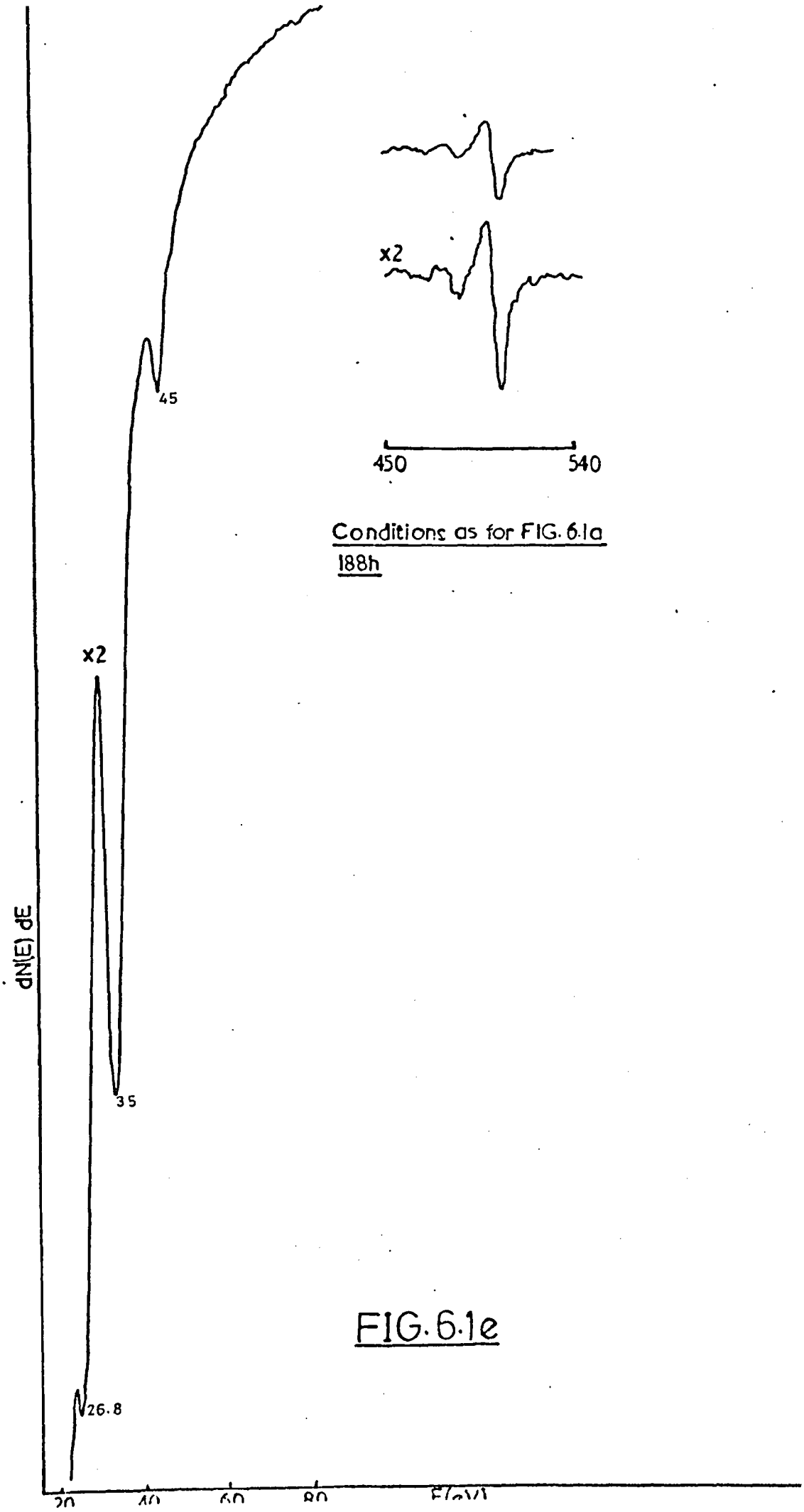

Conditions as for FIG. 6.1a
188h

FIG. 6.1e

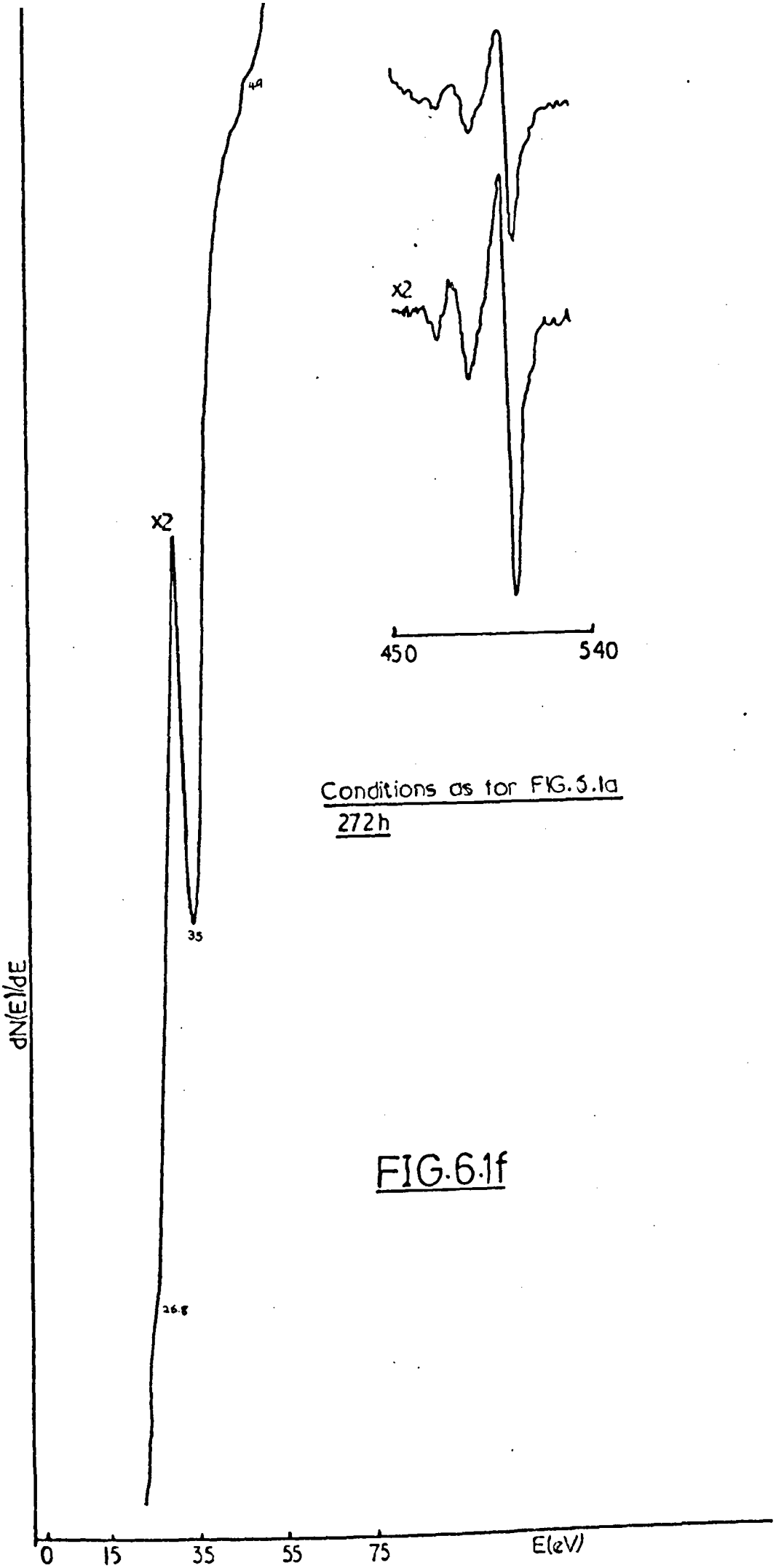

Conditions as for FIG. 6.1a
272 h

FIG. 6.1f

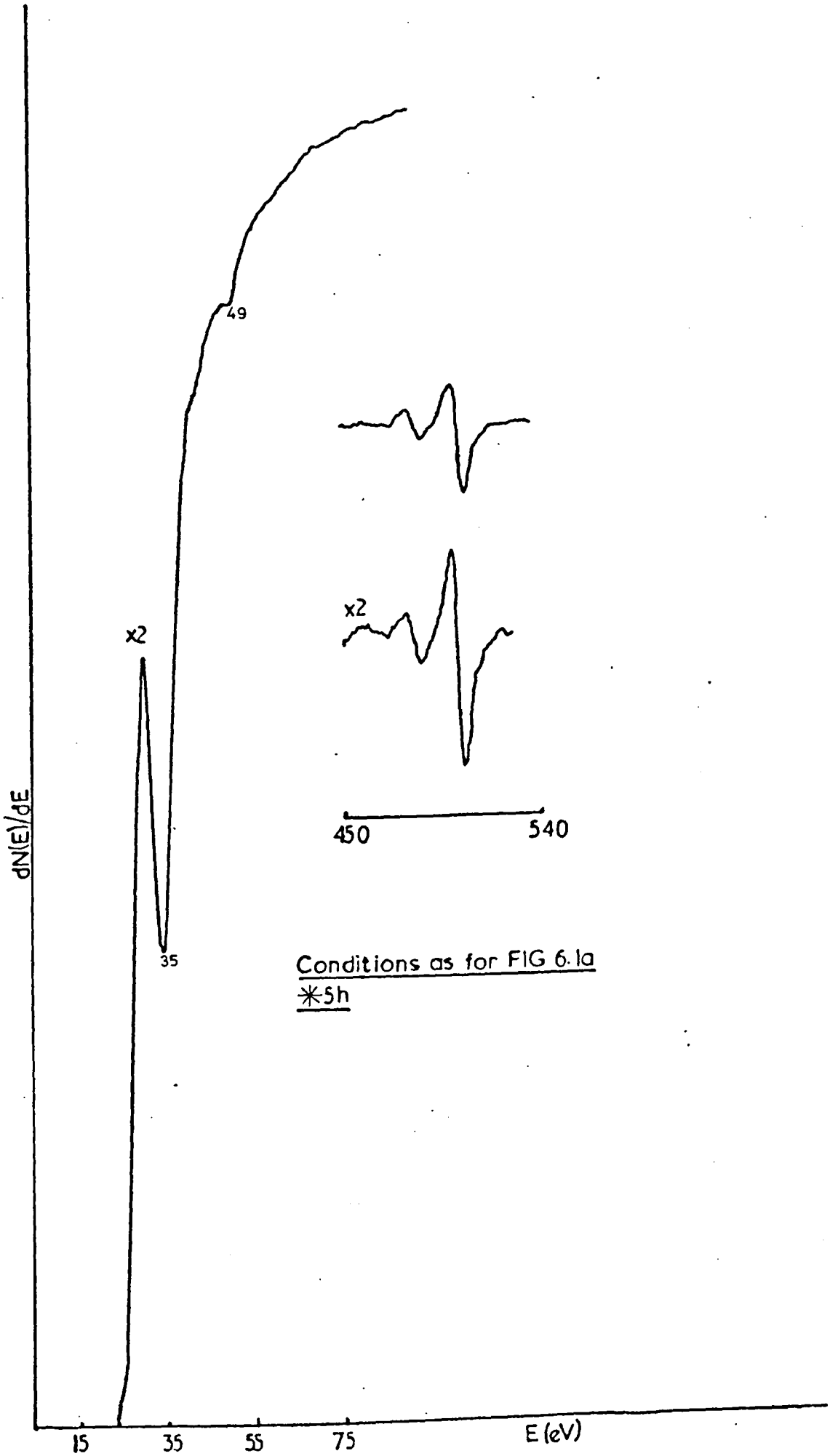

Conditions as for FIG 6.1a
*5h

FIG·6·1g

are less than the ones in Fig. (6.1f). The carbon level was in the noise level for the whole series, although not shown.

6.3.2 Characteristic Energy Loss Spectra

The corresponding energy loss spectra of clean and oxidised Mg surfaces for a primary electron energy of 700 eV, are shown in Figs. (6.2) and (6.3) respectively. For the clean Mg surface the energy loss peaks appeared at 4, 7, 10.5, 14.5, 18, 21, 25, 31, 42, 52, 64 and 75 eV, but for an oxide covered Mg surface (oxygen pk-pk of 4 cm on Auger signal) the peaks appeared at 4, 11, 16 (shoulder type), 22, 42, 58.5 and 75 eV. Figs. (6.4) and (6.5) shows the effect of primary electron energy variation on the energy losses of magnesium [Fig. (6.4) was taken with a modulation voltage of 2 V pk-pk and (6.5) is the magnified spectra of (6.4), obtained by using the modulation voltage of 7.2 V pk-pk]. As the primary electron energy rises, the 7 eV loss becomes weaker, while the losses at 14.5, 32, 42, 52, 64 and 75 eV intensify.

The changes in the features of the loss peaks during the oxidation over 28 days are given in the Figs. (6.6) and (6.7), with energy ranges of 0-95 eV and 30-95 eV respectively. The only difference between these two figures is that Fig. (6.7) is the amplified version (by increasing the modulation voltage) of Fig. (6.6). The primary energy of 700 eV has been used for taking these spectra. As shown in the figures, the peaks at 4 eV and 75 eV in clean magnesium loss spectrum have intensified while the intensity of the peak at 42 eV decreased, during the surface oxidation. The peaks at 7, 18, 25 and 64 eV have disappeared, but the peak at 31 eV has shifted and then disappeared. Finally, the other changes which have been observed during the oxidation are that; the intensity of the peaks at 10.5 and 14.5 eV have decreased and they have shifted to 11 and 16 eV

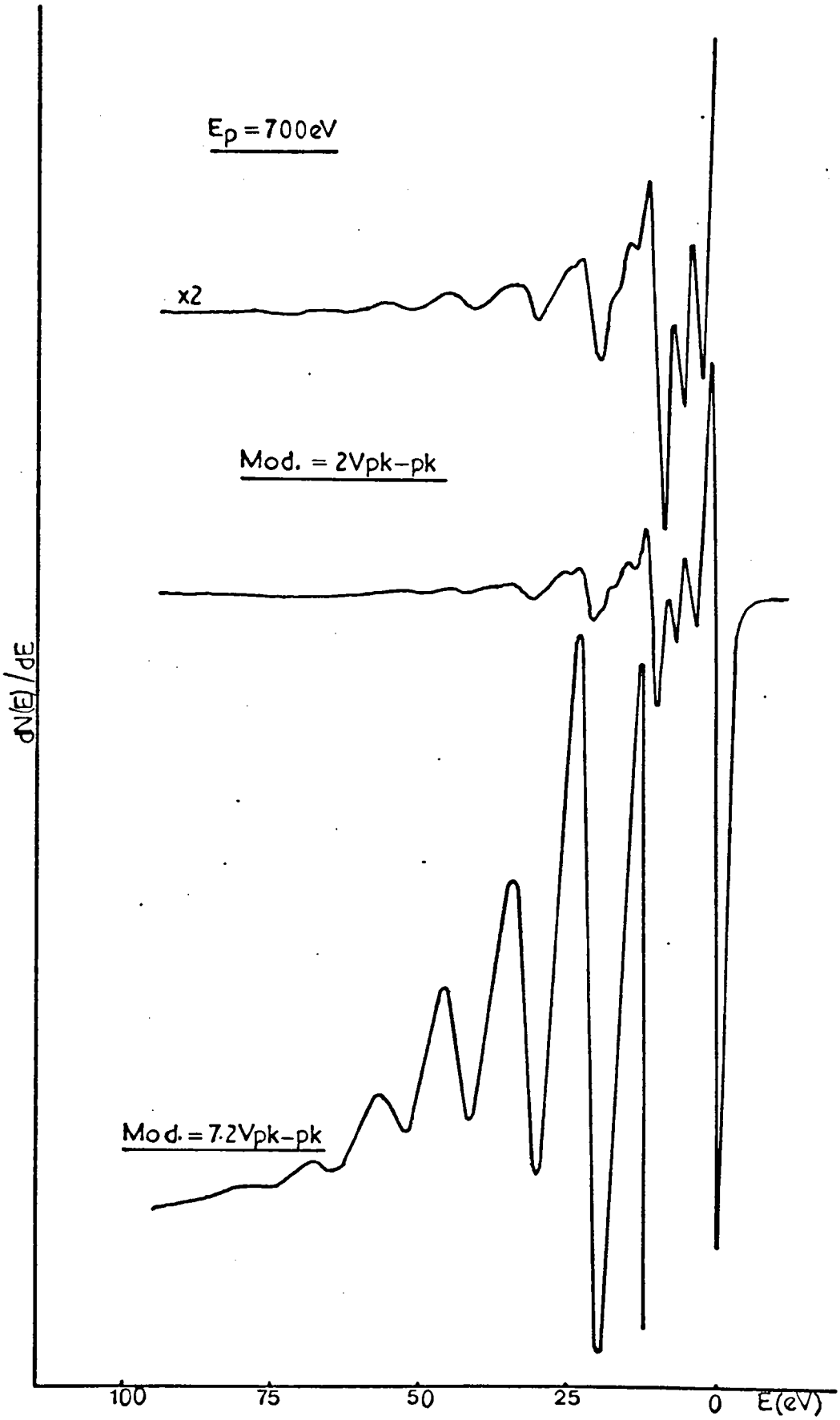

FIG. 62 Energy loss spectra of clean Mg

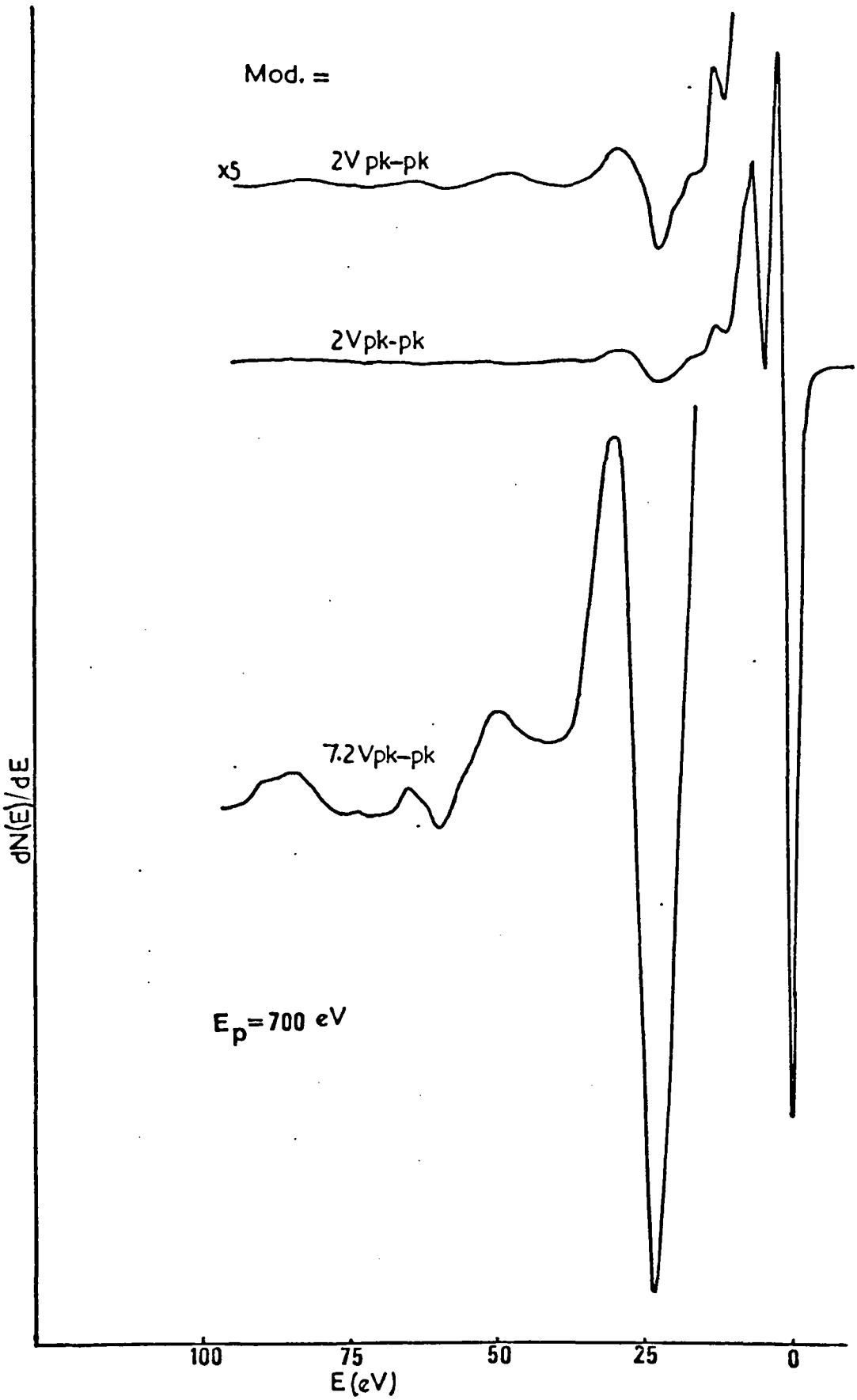

FIG.6.3 Energy loss spectra of an oxidised Mg surface

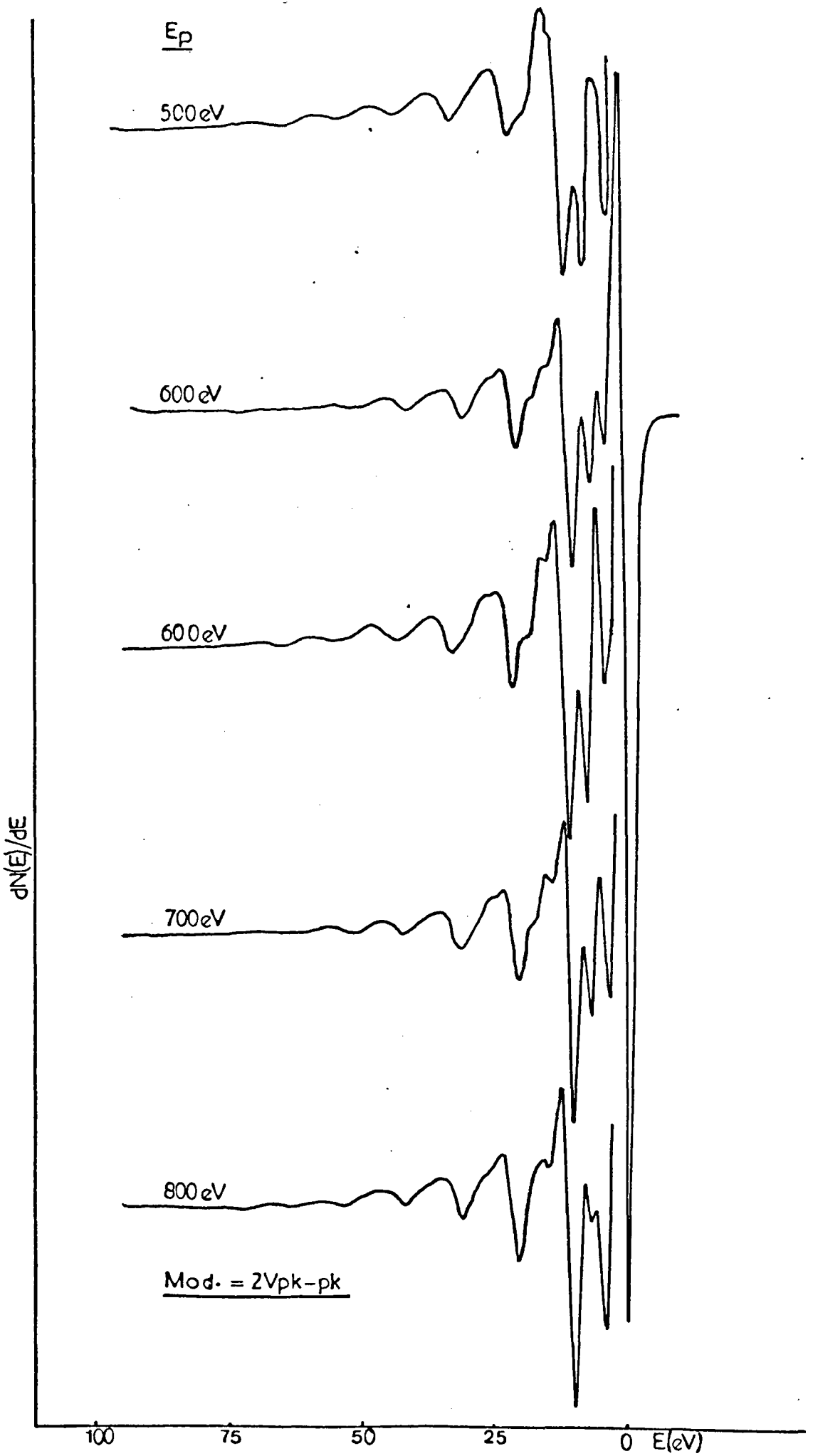

FIG. 6.4 Energy loss spectra of Mg surface with different primary electron energy

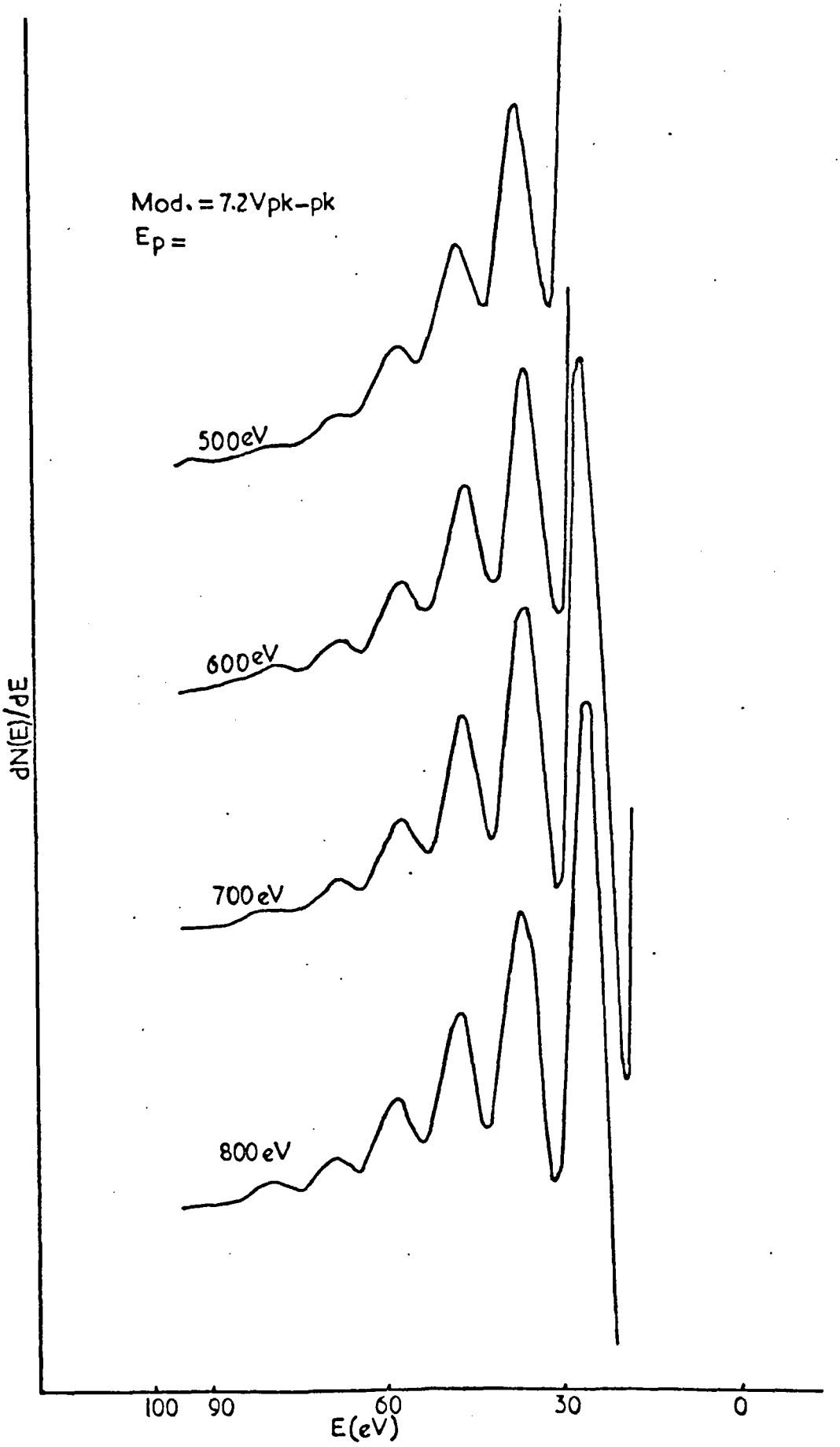

FIG 6.5 Energy loss spectra of Mg surface with different primary electron energy

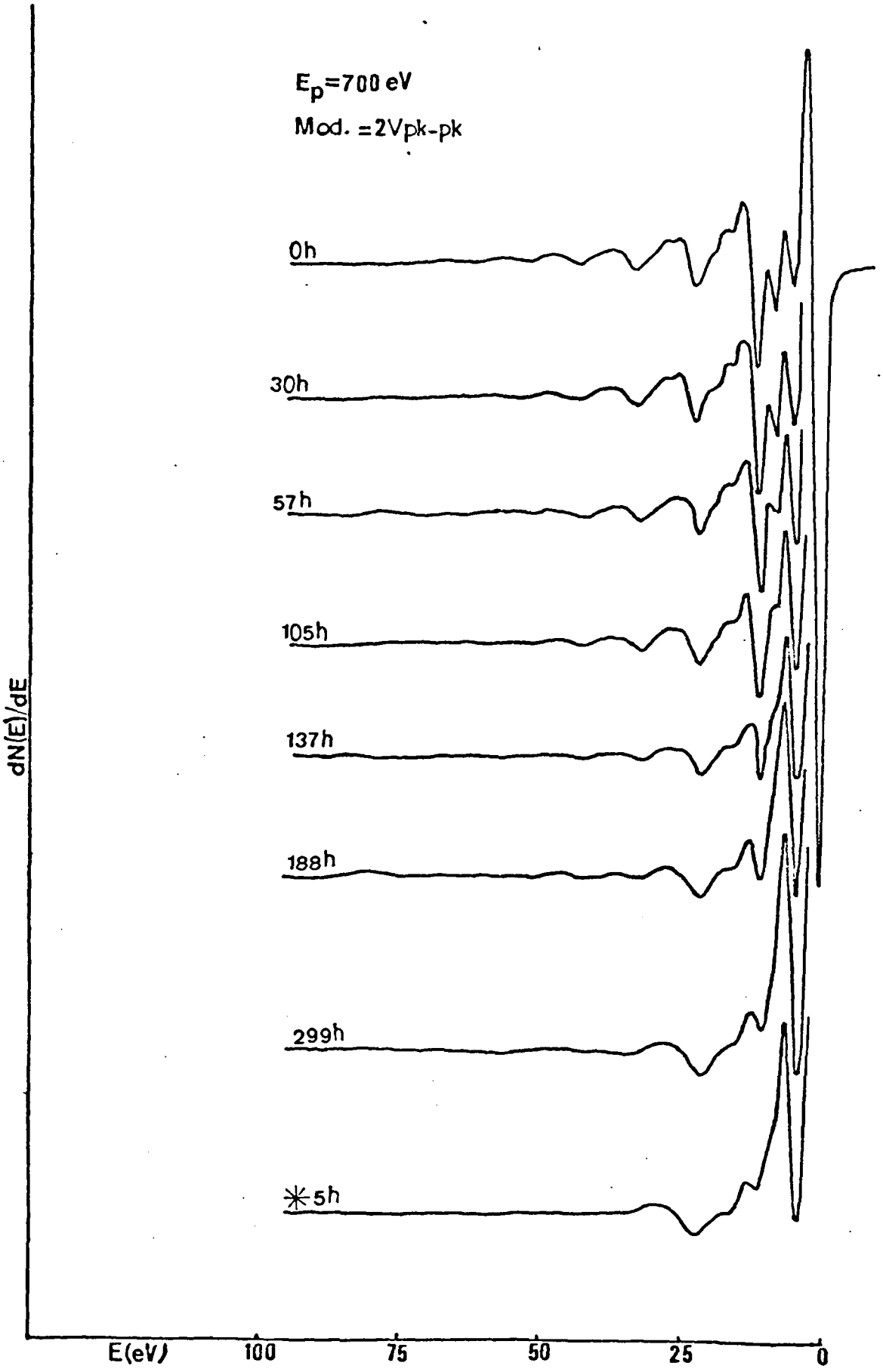

FIG.66 Oxidation effects on the energy losses of Mg

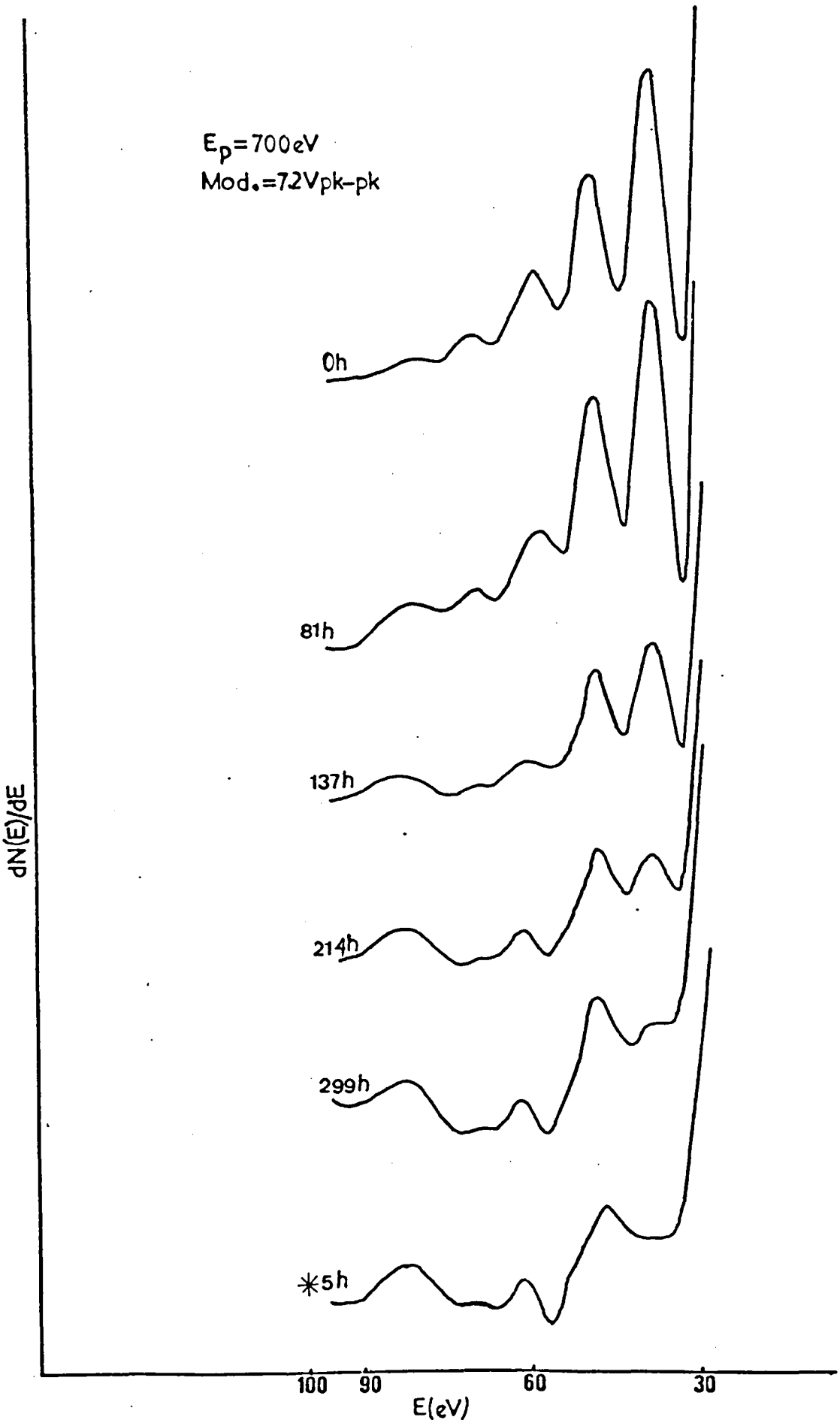

FIG 6.7 Oxidation effects on the energy losses of Mg

respectively, and the peaks at 21 and 52 have also shifted to 22 eV and 58.5 eV respectively, without any significant changes in their intensities. To show the changes in the amplitude of the energy loss peaks during the oxidisation, a behaviour of the intensity of a typical loss peak (31 eV, the third order of bulk plasmon loss, section 6.4.2) as a function of oxygen coverage (as given by Auger peak to peak heights) is given in Fig. (6.8). For further information about changes of loss peaks during the oxidisation, the corresponding Auger spectrum of each of them is given in Appendix C.

6.3.3 Secondary Electron Emission Yield (SEE yield)

For the SEE yield measurements of magnesium, the system was operated the same condition as for beryllium SEE yield measurements.

The secondary electron yield curve of a clean magnesium surface is shown in Fig. (6.9). This yield curve shows a relatively flat maximum centered at a primary energy E_{Pmax} of 312 eV (δ_{max}, the maximum yield, is 0.89 at this E_{Pmax} of 312 eV) and it decreases to 0.7 at E_p = 1 KeV).

A sequence of yield curves is shown in Fig. (6.10). These curves represent the maximum change due to slow oxidation from residual oxygen in the UHV system over a considerable period of time (28 days) (the corresponding AES spectra of these yield curves are shown in Appendix C). From this sequence it may be seen that the δ_{max} has increased from 0.89 to 2.73 as the E_{Pmax} shifts from 312 eV to 353 eV. The full rate of change in δ_{max} as a function of oxygen coverage given by the ratio of the peak to peak height of the oxygen 505 eV peak to the peak to peak height of the magnesium 45 eV peak in the Auger spectrum, is shown in Fig. (6.11). As may be seen after the initial rapid rise, the yield increases comparatively slowly to about 1.85, however, further measurements are impossible since the peak to peak height of Auger spectrum of

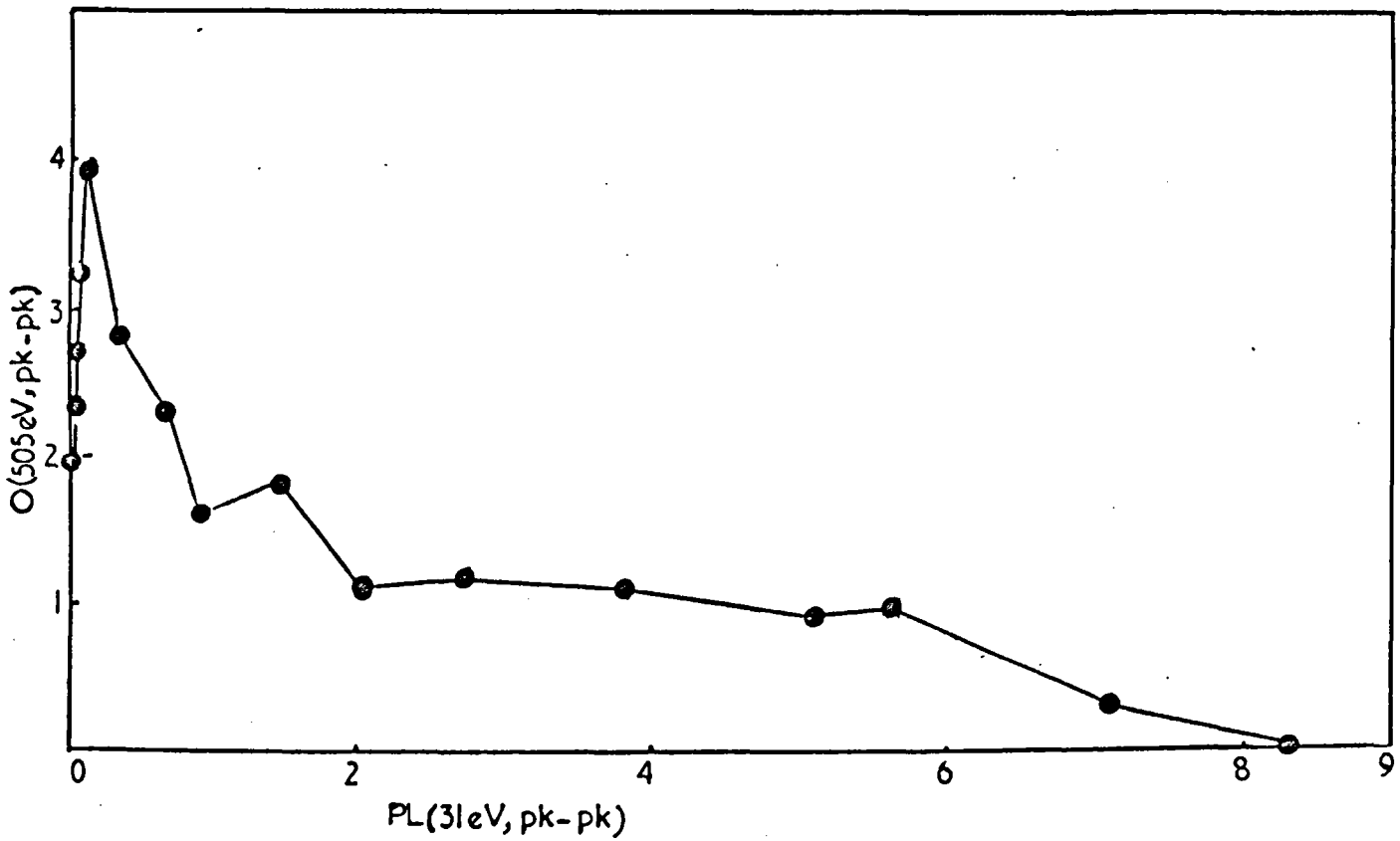

FIG.6.8 The behaviour of a typical plasmon loss peak(31eV) as a function of oxygen coverage(as given by Auger peak peak height)

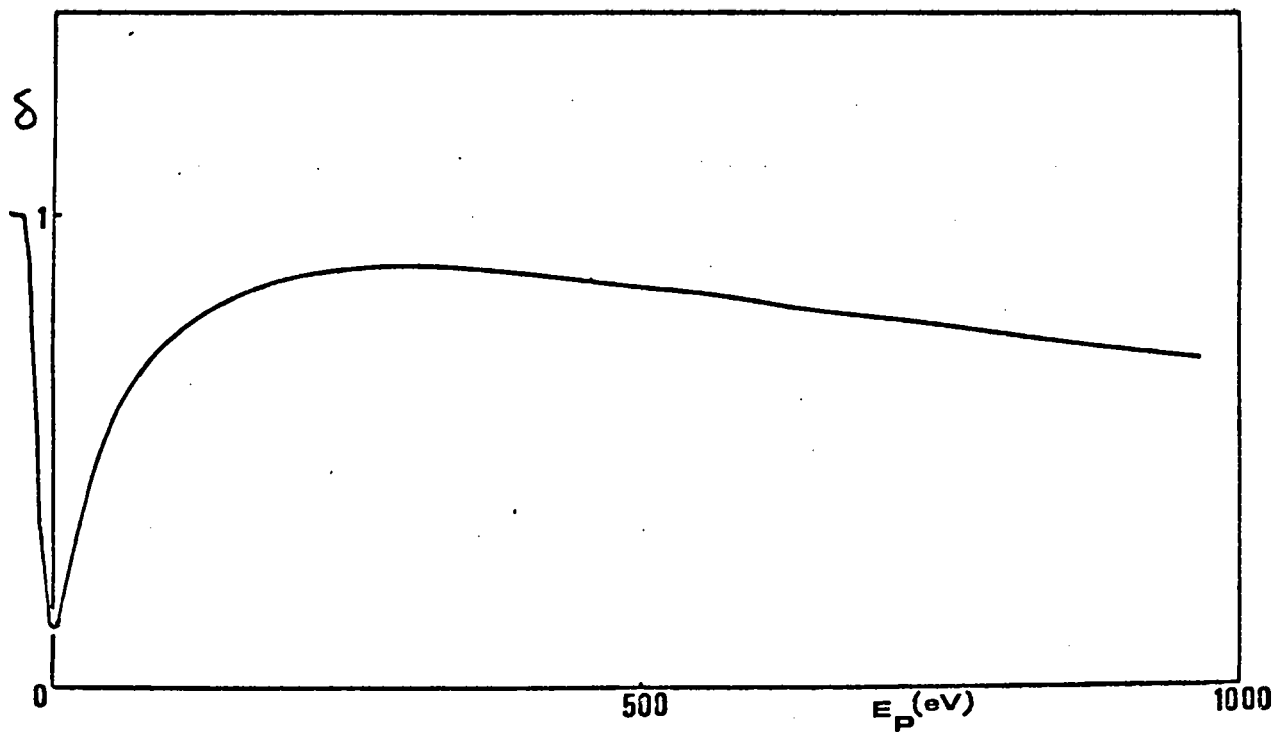

FIG.6.9 Yield curve of clean Mg

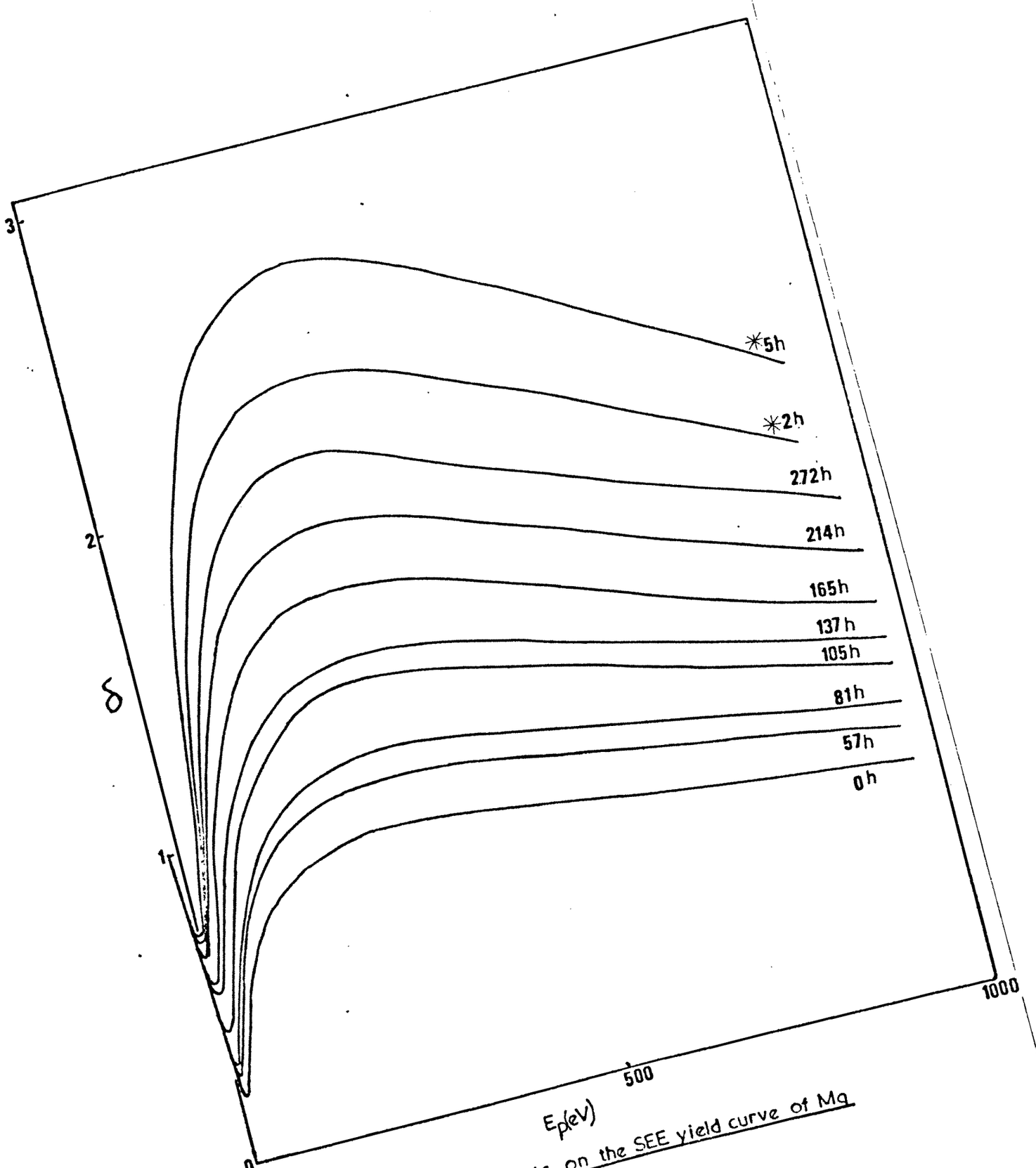

FIG 6.10 Oxidation effects on the SEE yield curve of Mg

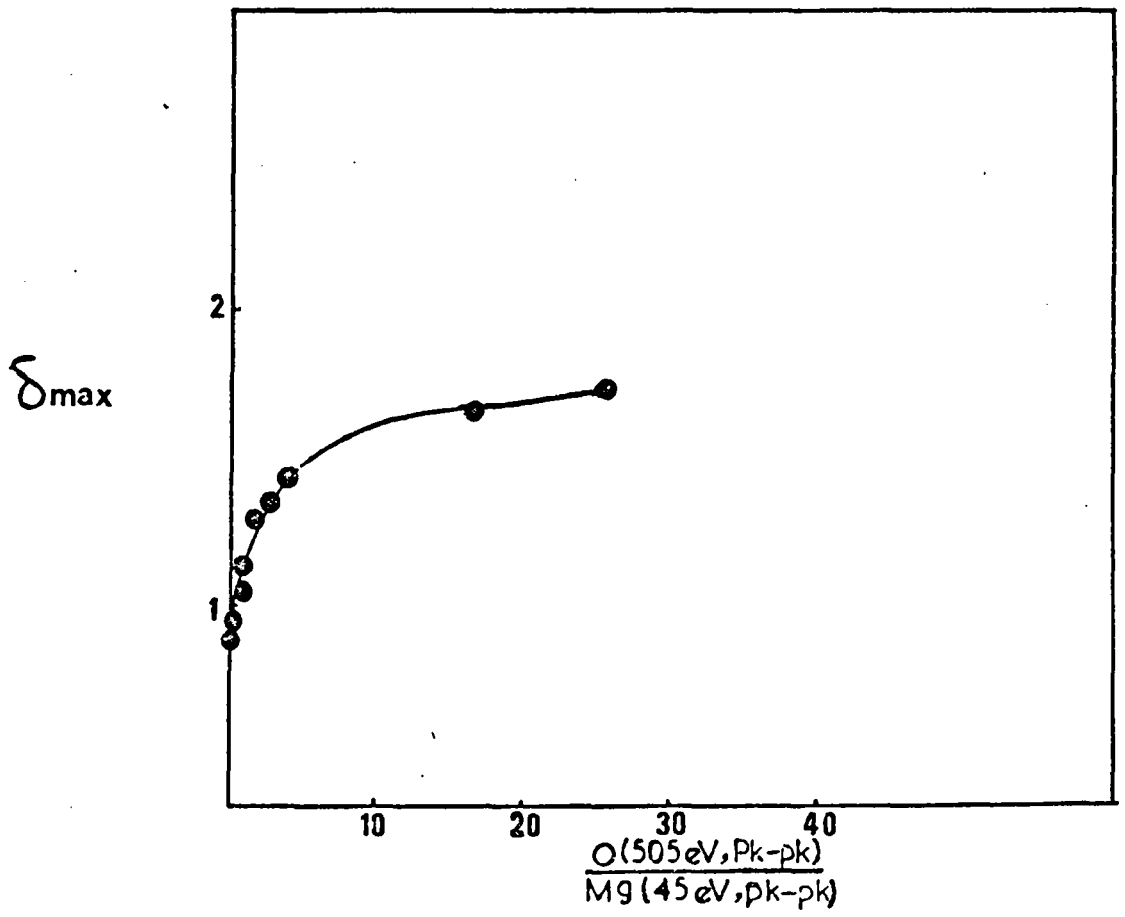

FIG·6·11

Mg (45 eV) vanishes. Therefore an attempt has been made to plot δ_{max} vs the ratio of peak to peak height of oxygen (505 eV) to the total peak to peak height of Mg (in both forms viz:- pure Mg (45 eV) and oxide MgO (35 eV)). This plot is shown in Fig. (6.12). This figure shows the initial rapid rise of the δ_{max} and then δ_{max} begins to increase comparatively slowly to about δ_{max} = 2 (where the target has been heated up), and at this point the ratio starts to decrease while the δ_{max} continues to increase. δ_{max} has also been plotted Vs the peak to peak height of Auger signal of oxygen (505 eV), which is shown in Fig. (6.13). The changes in this plot is more or less the same as Fig. (6.12). As may be seen from Fig. (6.13), after heating the target, the peak to peak height of oxygen has reduced whilst the δ_{max} has increased. This is probably because of diffusion of more oxygen through the top surface layer with a consequent reduction of amount of oxygen on the surface. In other words, it means that the number of MgO layers may have increased, although the amount of surface oxygen, as revealed by Auger signal, has reduced, i.e. the total oxygen whether in form of MgO or otherwise contributing to the yield may well have increased whilst the proportion on the surface decreased.

Other yield curve parameters like E_{Pmax} , E_{Pc1} and E_{Pc2} are given in the table (6.1). The first crossover energy, E_{Pc1} is plotted versus δ_{max} (Fig. (6.14)), it has a rapid decrease until the δ_{max} reaches to 2, then it decreases comparatively slowly.

The data in table (6.1) may be used to calculate the range of primaries and the escape depth of secondaries, just like the beryllium case (section 5.3.3). Fig. (6.15) shows a plot of range of primaries as a function of δ_{max}. It is evident from the graph that the range (which is proportional to escape depth) stays mostly constant initially, but when δ_{max} starts to increase rapidly at 2, the range also starts

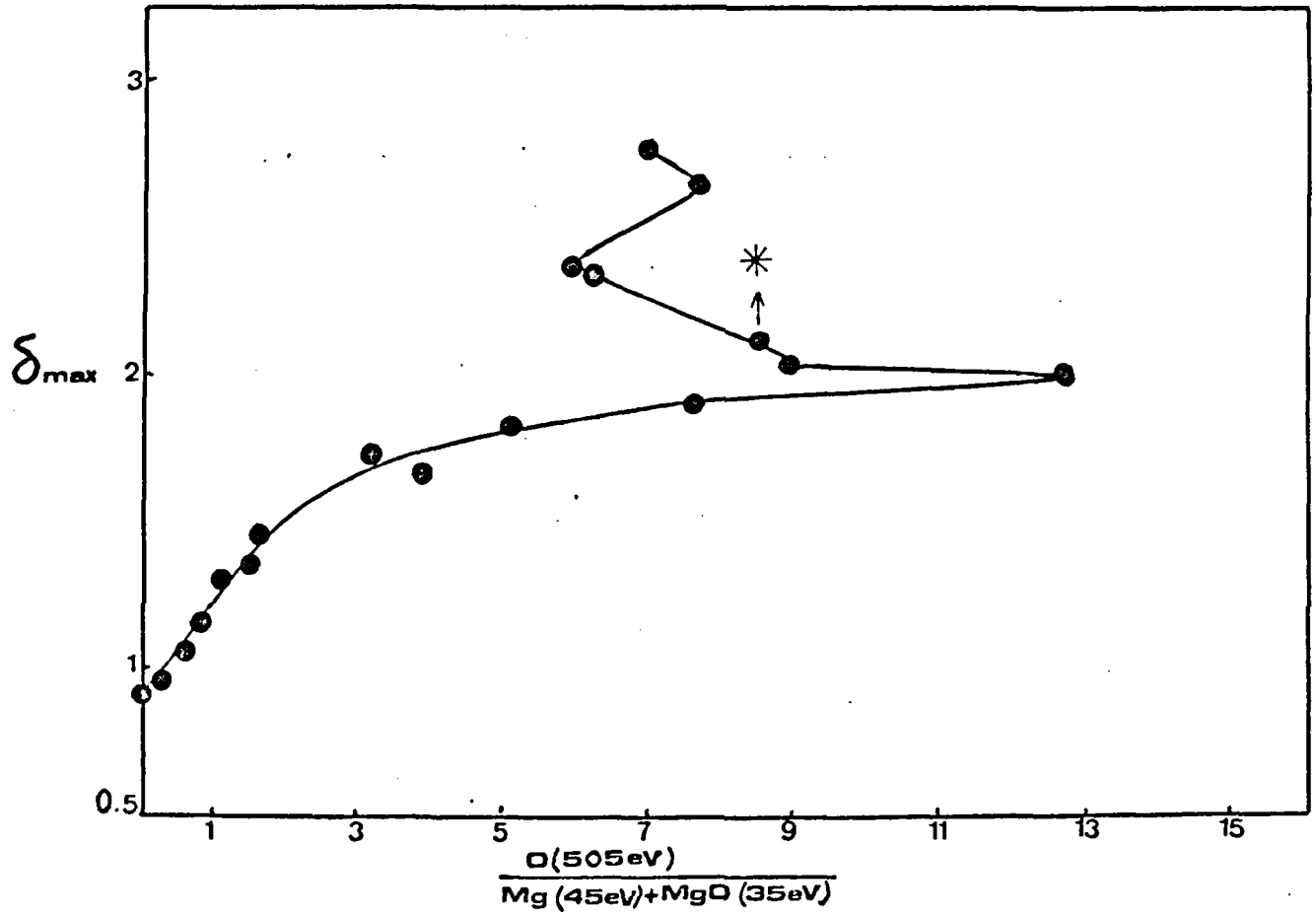

FIG.6.12

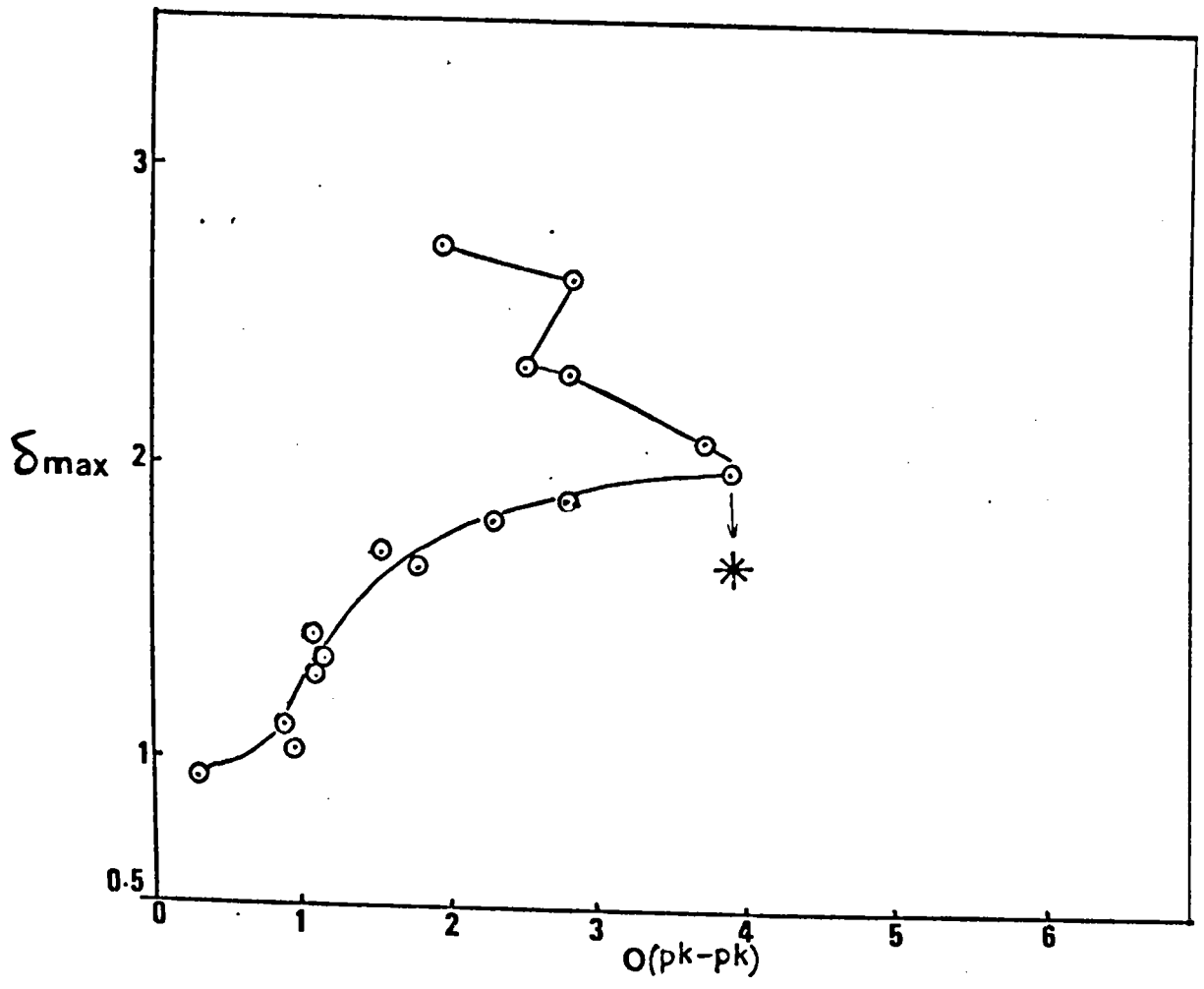

FIG. 6.13

Table (6.1)

hours	$E_{p_{c1}}$ (eV)	$E_{p_{c2}}$ (eV)	$E_{p_{max}}$ (eV)	δ_{max}
0	-	-	312	0.89
30	-	-	315	0.93
57	198	501	325	1.04
81	148.5	649.7	315	1.14
105	117.5	977.6	325	1.26
113	95.9	-	315	1.35
137	83.5	-	315	1.44
165	64.9	-	315	1.64
188	58.8	-	315	1.72
214	55.68	-	315	1.85
238	49.5	-	315	1.88
272	49.5	-	315	2
299	43.5	-	319	2.1
At this point the target was heated up (for diffusing more oxygen into the surface)				
*2	43.3	-	328	2.3
*3	40.2	-	340	2.36
*4	37.1	-	343	2.65
*5	34	-	353	2.73

*2 = the target was heated up for two hours.

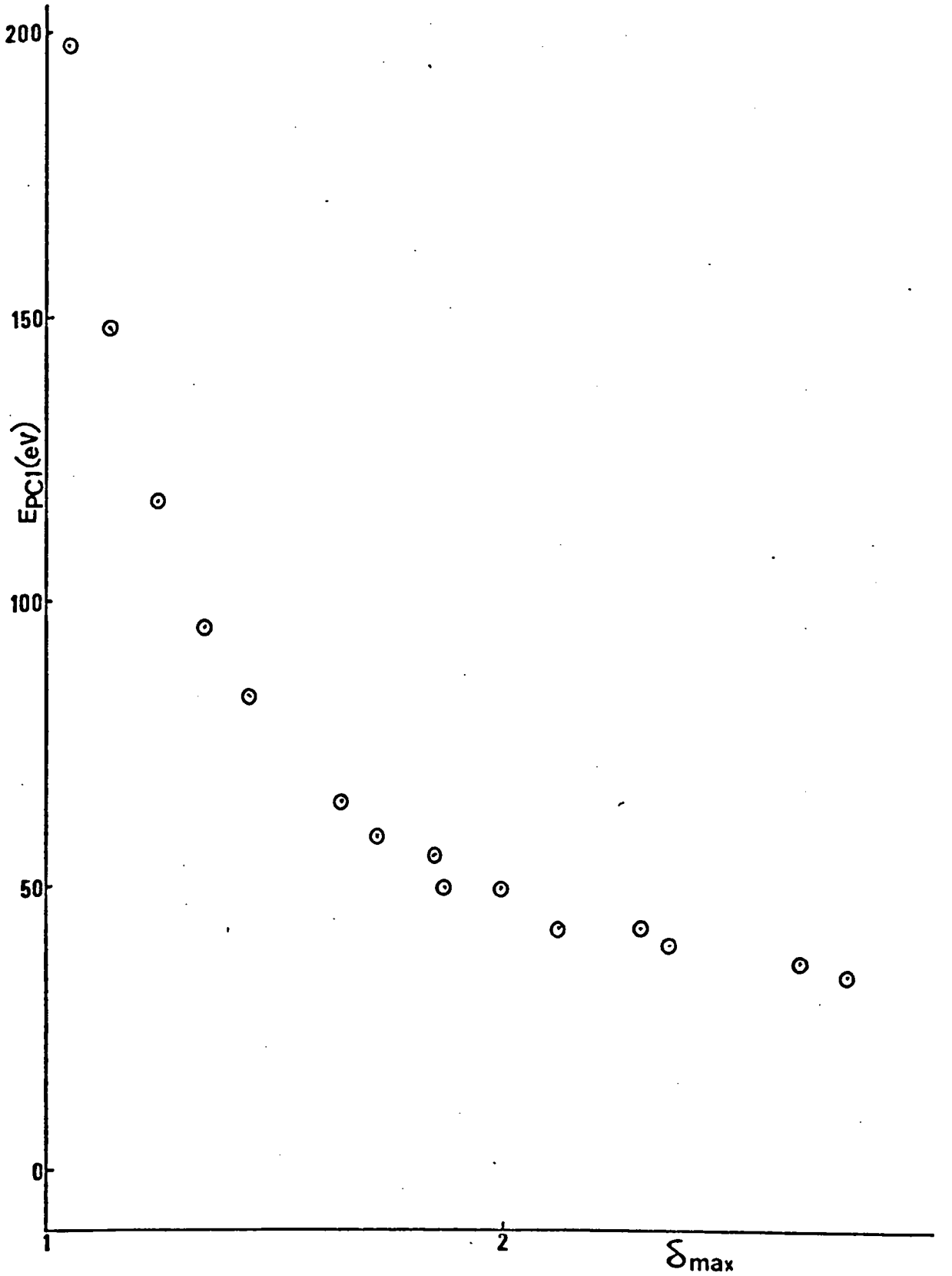

FIG. 6.14

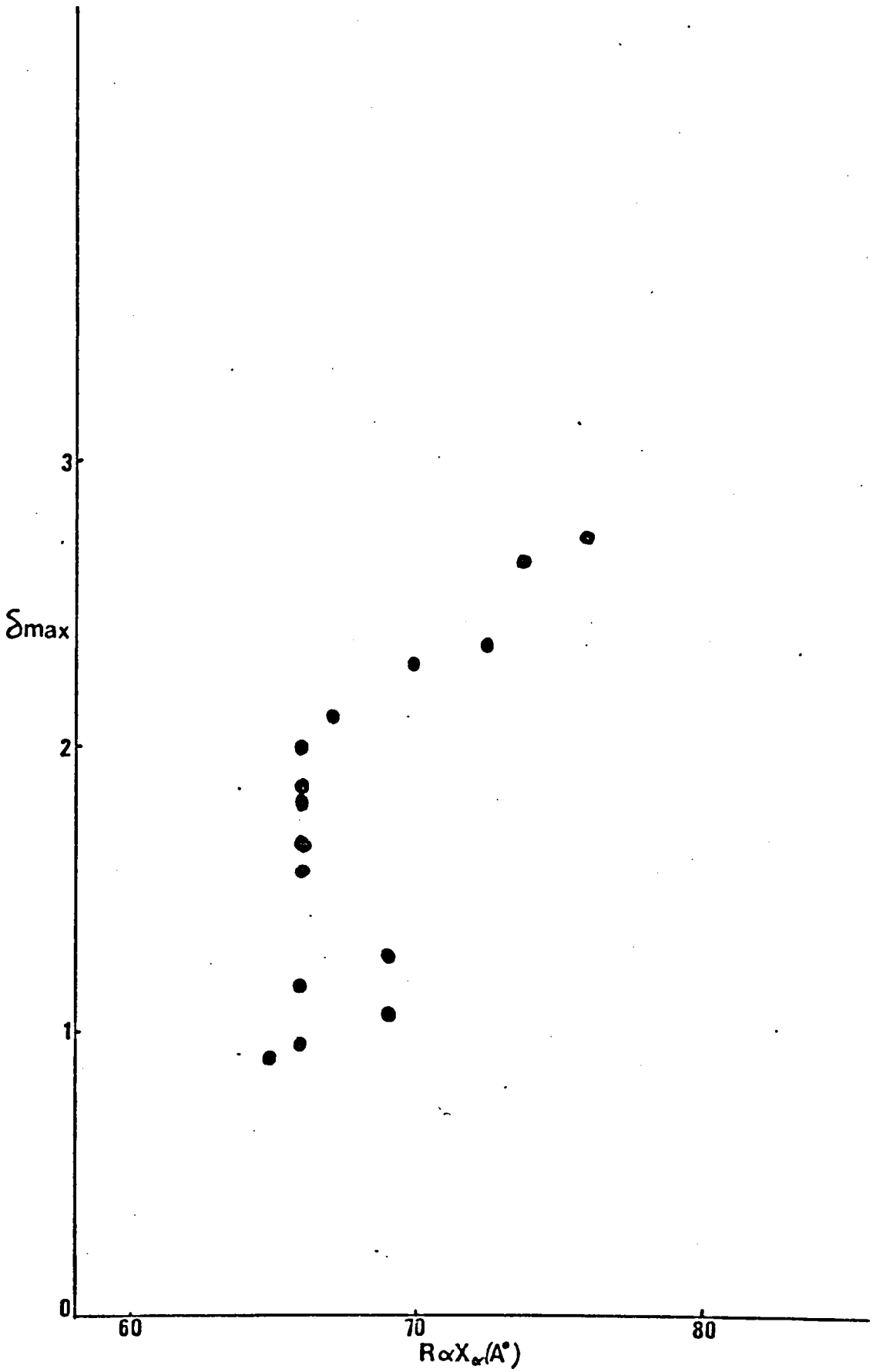

FIG.6.15

to increase comparatively faster. This plot may be compared with the corresponding plot for Be → BeO target (Fig. (5.13)).

The behaviour of two other important properties of the surface during the oxidation process are the plasmon loss (PL) and the ionisation loss (I). It was only nearing the end of the present work that we realized the possible importance of the change in the first ionisation loss (I) and plasmon loss (PL) for different δ_{max} during the oxidation from the work of Kanaya et al. (1978) and One and Kanaya (1979). Therefore, the experimental work was carried out with a greater concentration on these phenomena for the magnesium sample. However, the theory of these authors concerned the change in energy of the PL and I, whilst in the present work the energy of PL and I were constant during the oxidation, however, a considerable change in the amplitude of these parameters was observed. Figs. (6.16) $\left[\delta_{max} \text{ vs } \frac{\text{I(4eV, pk-pk height)}}{\text{Elastic peak (pk-pk height)}}\right]$ and (6.17) $\left[\delta_{max} \text{ vs } \frac{\text{PL(10 eV, pk-pk height)}}{\text{Elastic peak (pk-pk height)}}\right]$ show the change of the amplitude of the ionisation loss peak and the plasmon loss peak respectively, during the oxidation. From these figures, it may be seen that PL amplitude is decreasing and I is increasing during the increase of δ_{max}. However, after the heating process the changes are by no means as regular as before and they have a kind of zig zag shape. This is probably because of a change of surface structure after or during the heating process. Fig. (6.18) shows the change of δ_{max} versus the ratio of the amplitudes of (I/PL) and it may be noted that the shape of this curve viz δ_{max} versus I/PL shows a distinct similarity to the section of the curve in Fig. (6.11) and the lower part of Figures (6.12) and (6.13) before the heating process. It must be noted however that $(\frac{I}{PL})$ in the work of Kanaya et al. is the ratio of the two energies involved and the authors do not specifically discuss changes in amplitudes.

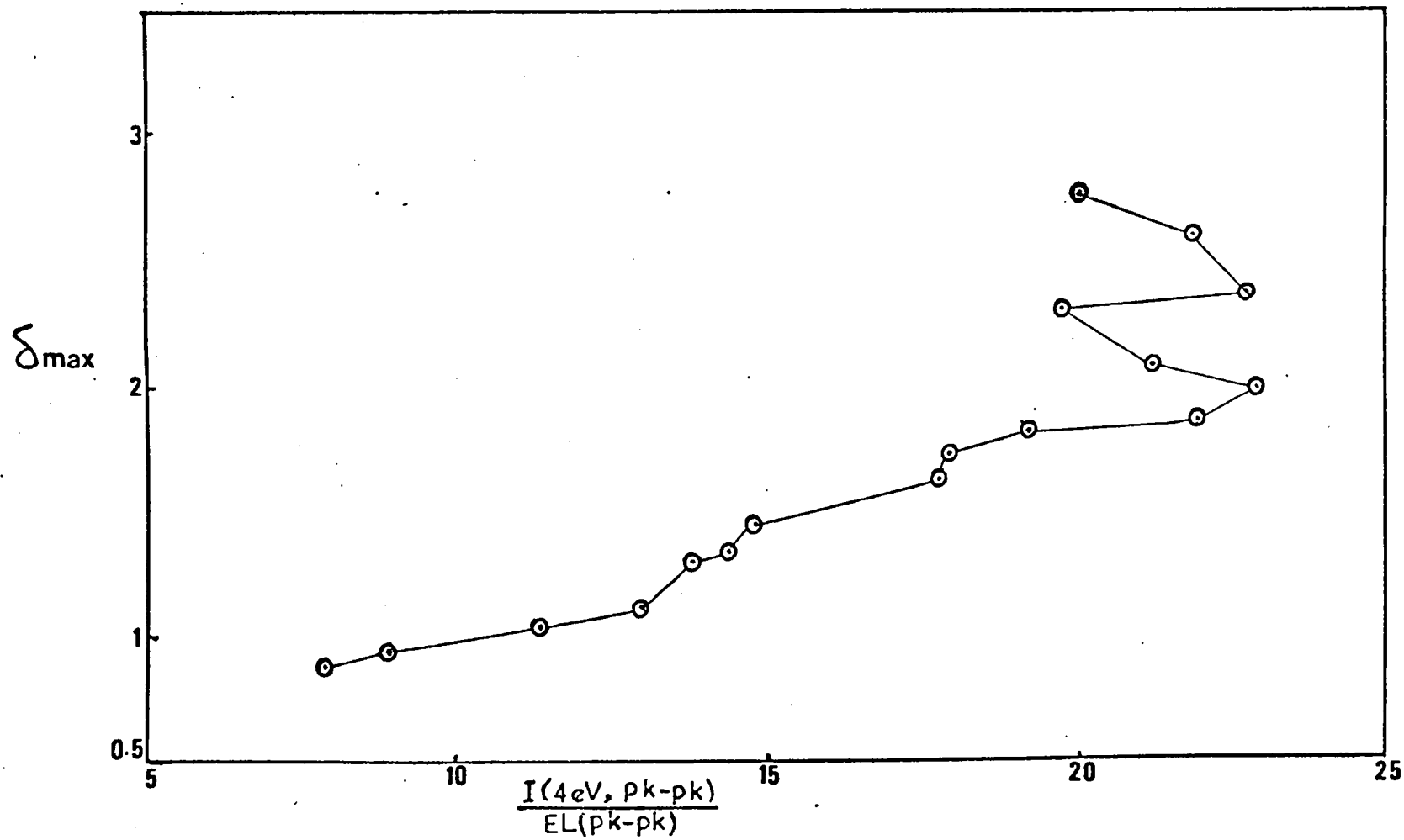

FIG. 6.16

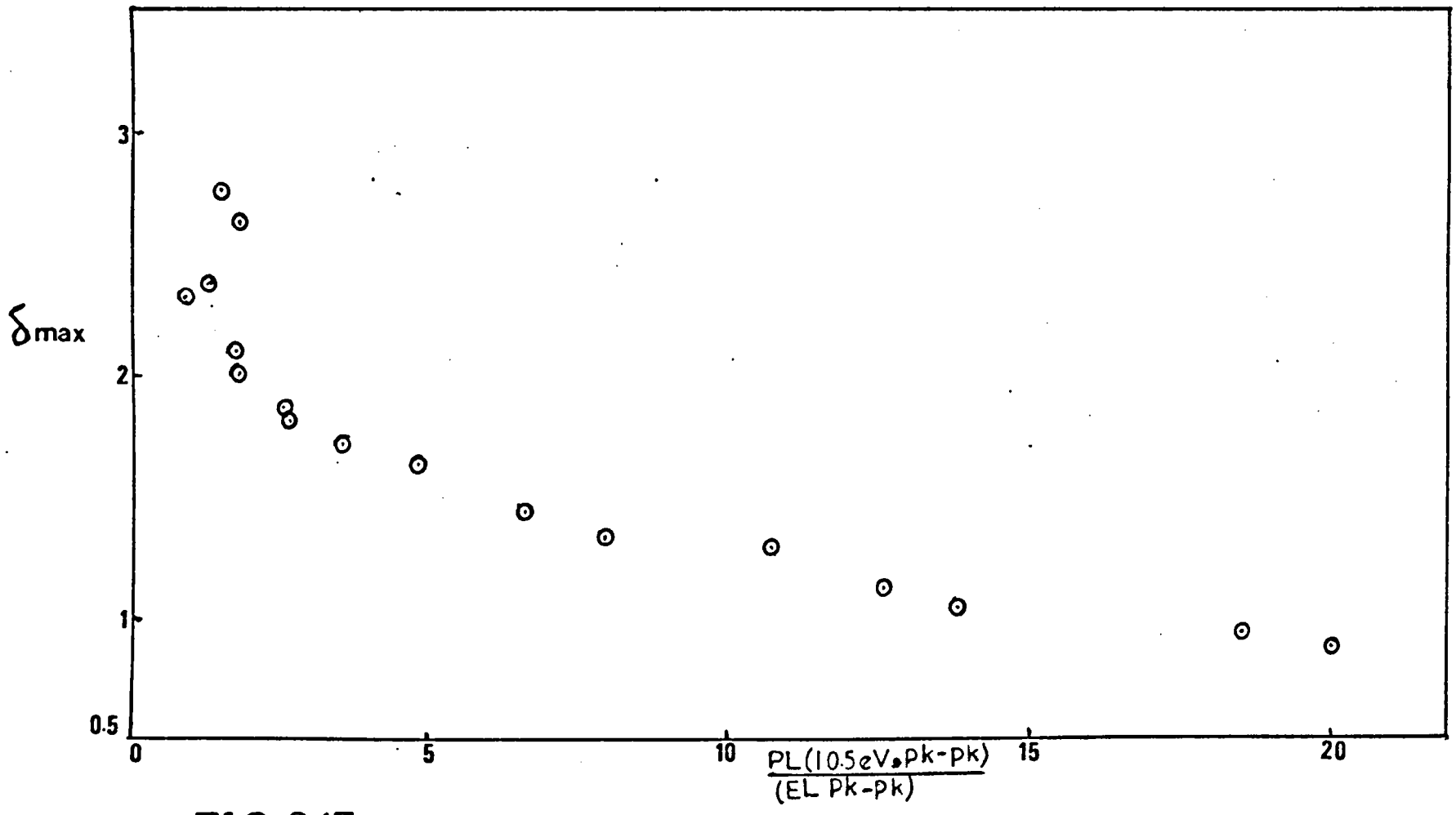

FIG·6.17

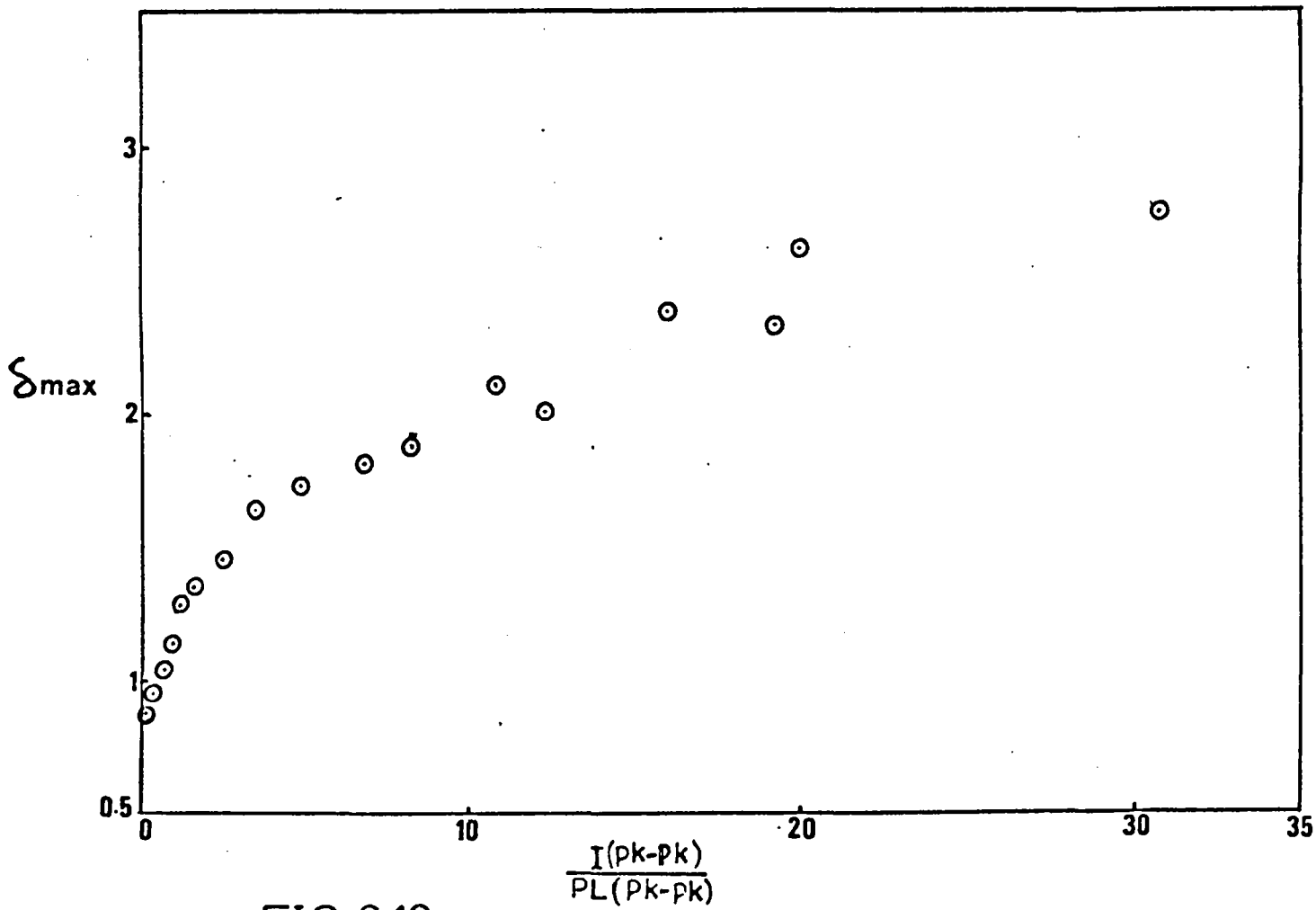

FIG. 6.18

6.4 Discussion of results of Mg → MgO

6.4.1 Auger Spectra

The magnesium atom has 12 electrons, so the electron configuration is generally given as $1s^2(K)\ 2s^2(L_1)\ 2P^6(L_{2,3})\ 3s^2(V)$. Therefore the possible Auger emissions are KLL, KLV, LLL, LLV and LVV. KLL and KLV transitions are the high energy Auger > 1000 eV and the LLL, LLV and LVV transitions are the low energy Auger of clean magnesium. An attempt was made to observe the high energy Auger spectrum of Mg. However the poor sensitivity of the instrument in this energy region prevented a thorough investigation of this region. This was largely caused by not being able to supply the electron gun with higher appropriate voltage without interelectrode breakdown. Therefore, an investigation was carried out only on the low energy Auger spectra of magnesium. The low energy AES of magnesium has been thoroughly investigated by the number of workers including Jenkins and Chung (1972), Suleman and Pattinson (1973), Salmeron et al. (1974, 1975) and Baro and Tagle (1978).

The binding energy of K, L_1 and $L_{2,3}$ shells of Mg (as given by photoemission) are 1303.0 - 1303.6 eV, 88.5 - 89 eV and 49.4 - 49.9 respectively (Wagner and Biloen, 1973; Tejeda et al., 1973; Ley et al., 1975; Fuggle et al., 1975; Halder et al., 1975, 1976; Fuggle, 1977 and Attekum and Trooster, 1979). The result of the last authors are shown in Fig. (6.19). The width of the valence band is 6.9 eV. The energy diagram of Mg is given in Fig. (6.20) in which the work function of magnesium is assumed as 3.3 eV (Gessell and Arakawa, 1972). To get the correct identification of the Auger peaks, one must use knowledge of the band structure and the energy distribution of electrons within the $\sim$ 6.9 eV wide valence band of Mg. The total density of states

FIG.6.19 (a) Photoemission spectrum of the 2*s* and 2*p* core levels and valence band of Mg metal after removal of the Auger lines and x-ray satellites. The solid line is the calculated spectrum (b) After the removal of the plasmon-loss lines Attekum and Trooster (1979)

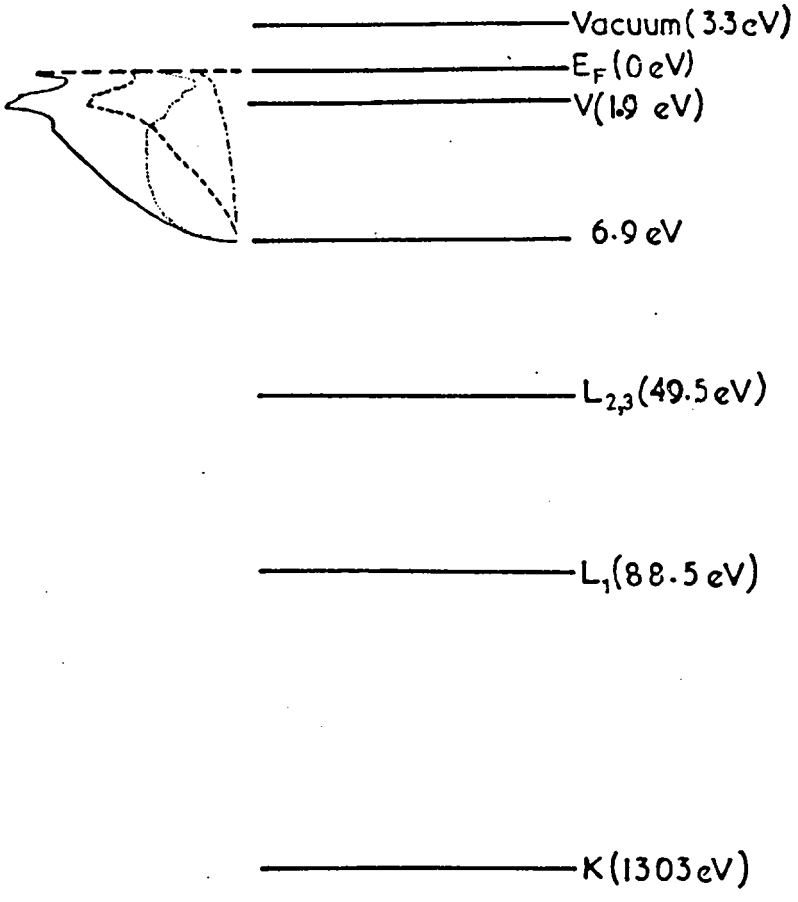

FIG.6.20 Energy band diagram of Mg; density of states is given by Gupta and Freeman (1976), full curve, total DOS; dotted curve, s partial DOS; broken curve, p partial DOS; chain curve, d partial DOS.

(DOS) and p, s and d partial density of states have been obtained by Gupta and Freeman (1976) which are also shown in Fig. (6.20). The total density of states shows a maximum at ∿ 1.9 eV, therefore it is reasonable to assume that the electrons in the maximum take part in the Auger process, therefore V ≃ 1.9. On the basis of this assumption the calculated value for the $L_{2,3}VV$ is 45.8 eV. This is in good agreement with the observed peak at 45 eV.

As mentioned in section (6.3.1) except for the peak at 45 eV, three more peaks are observed in the low energy part of the Auger spectrum of clean Mg at 30, 35 and 59 eV. Since the $L_1\ L_{2,3}\ V$ Auger transition energy has reported by Ley et al. (1975) as 32.1, and the energy of 30 eV peak is close to this value, therefore, this peak is interpreted as $L_1\ L_{2,3}\ V$ transition. The reasonable explanation for 35 eV peak can be given from the possibility of plasma losses from the main Auger peak. Such a possibility is quite likely since a strong bulk plasmon loss peak was observed at 10.5 eV (table 6.2) in the energy loss spectrum of a clean magnesium surface. Therefore for a bulk plasmon of 10.5 eV a loss peak in the Auger spectrum should occur at about 34.5 eV. Thus the observed peak at 35 eV agrees reasonably well with the expected value. The peak at 59 eV is unlikely to be a plasmon gain because the difference between its position and the main Auger peak (45 eV) is 15 eV which is higher than the bulk plasmon loss energy (10.5 eV). The other possibility is that this peak has produced by the double ionization mechanism (Salmeron et al., 1974). Moreover, the line shape and width of the 59 eV peak appear to be the same as that from the 45 eV. This fact further supports the double ionisation mechanism because the remaining two levels involved in the Auger transition are the same for both single and double ionization peak.

As mentioned in section (6.3.1), Auger peaks of the progressively

oxidised Mg appeared at 26.8, 35 and 49 eV, however the peaks at 26.8 and 49 eV were very weak. The effects of oxidation on the low energy Auger spectrum of Mg have been considered by a number of authors (Zinke, 1957; Dufour et al., 1972; Suleman and Pattinson, 1973; Janssen et al., 1974, 1975; Salmeron et al., 1975; Bermudez and Ritz, 1979). All these three peaks are also observed by all these authors, however, Bermudez and Ritz (1979) and Janssen et al. (1974, 1975) have obtained a lot more peaks for the low energy Auger spectrum of MgO, because of better resolution.

In order to interpret the oxidised Mg spectrum, it is essential to know the energy values of the different levels including the valence band in MgO as opposed to clean Mg. The XPS spectrum of the MgO outermost levels is shown in Fig. (6.21) (Kowalczyk et al., 1977). The energy of these peaks are determined with respect to the top edge of the valence band. Since the band gap in MgO is $\sim$ 9 eV and Fermi level is located approximately midway in the gap, the energy values of the levels with respect to Fermi level would be 6 eV (Mg, 3s), 8.5 eV (O, 2p), 22.5 eV (O, 2s), 51.5 eV (Mg, 2p) and 89.5 eV (Mg, 2s) (Fig. (6.22)). These values are in good agreement with the work of Halder et al. (1975, 1976) and Fuggle (1977). The $L_{2,3}$ level of Mg has been reported to shift 1 - 4 eV (Fuggle, 1977; Salmeron, 1975) while it was oxidised. From this data the Mg ($L_{2,3}$) O ($L_{2,3}$) O ($L_{2,3}$) is $\sim$ 34.5 eV which is in good agreement with an observed value of 35 eV, and it shows a 10 eV shift in $L_{2,3}$ VV (45 eV) of clean magnesium. The properties of the peak at 26.8 eV is just the same as the peak at 27 eV which is reported by Salmeron et al. (1975), and Janssen et al. (1974). In the case of Janssen it is reported as an Auger cross transition type Mg ($L_{2,3}$) O (L_1) Mg (V). The peak at 51 eV is also assigned by Jansset et al. as a double ionization of the main peak

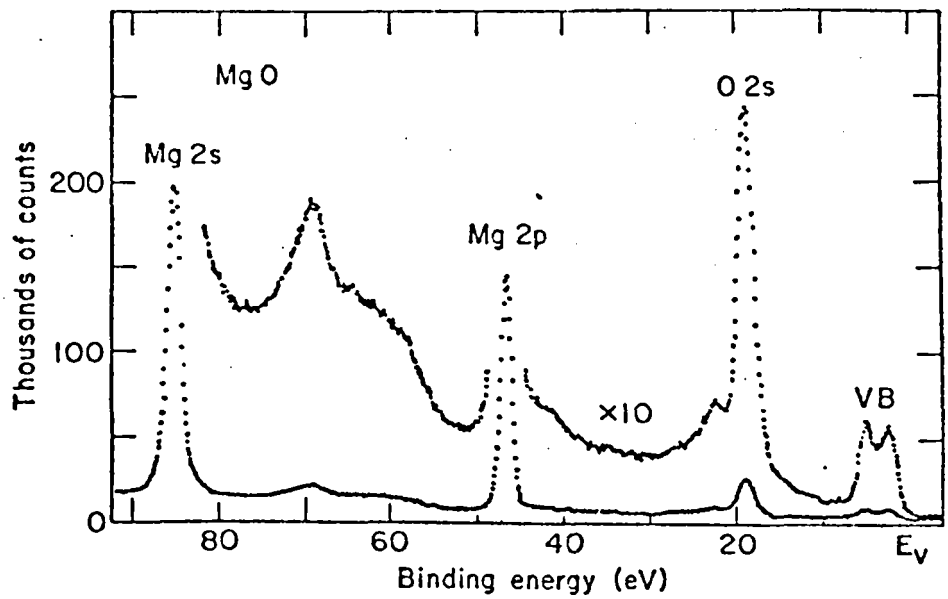

FIG.6.21 XPS spectrum of the outermost levels in MgO. (Kowalczyk et al 1977)

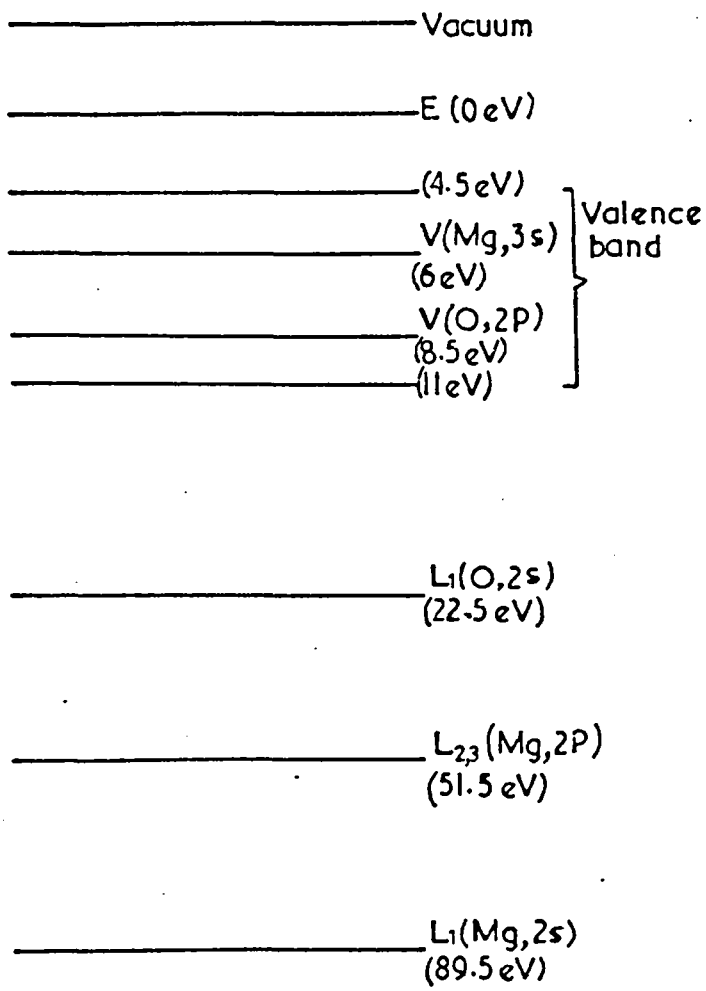
Vacuum
E (0 eV)
(4.5 eV)
V(Mg,3s)
(6 eV)
V(O,2P)
(8.5 eV)
(11 eV)
Valence band
L1(O,2s)
(22.5 eV)
L2,3(Mg,2P)
(51.5 eV)
L1(Mg,2s)
(89.5 eV)

FIG.6.22

(M_g ($L_{2,3}$) O ($L_{2,3}$) O ($L_{2,3}$) or $L_{2,3}$ VV in magnesium oxide.

In contrast to the above assignments Bermudez and Ritz (1979) have calculated and identified the 35 eV peak as a cross transition involving 3 atoms where one oxygen atom is combined with the Mg atom and emission occurs from a second oxygen atom. This transition is assigned as $M_gL_1OL_,OL'_1$ (' means that L_1 and L'_1 are the L_1 levels of two different neighbour ions) and the 27 eV and 49 eV peaks are assigned as $M_gL_1OL_1OL_1$ and $M_gL_1OL_1OL_{2,3}$ respectively. To calculate the Auger electron kinetic energies E_{xyz}, they used the relation which is used by Citrin et al. (1976). It has mentioned by Bermudez et al. that the transitions involving deep core levels should be weaker than those involving valence electrons and as a result the peaks assigned as $M_gL_1OL_1OL_1$ (27 eV) and $M_gL_1O_{L_1}OL'_1$ (35 eV) were the weakest in their spectrum. Since the strongest peak in our results for MgO is 35 eV, the present results are not in agreement with theirs and the interpretation as Salmeron et al. (1975) and Janssen et al. (1974) is preferred.

6.4.2 Energy Loss Spectra

The plasmon energies of magnesium are well known (Jenkins and Chung, 1972; Powell and Swan, 1959; Janssen et al., 1974) and other workers' results are in reasonable agreement with those presented in table (6.2). The table gives all the losses observed in the present work Fig. (6.2) with their identification.

Figures (6.4) and (6.5) indicate that the loss at 7 eV is highly surface sensitive, because by increasing the primary energies the intensity of 7 eV decreases. The same effect has been shown by Simons and Scheibner (1972) and used to identify the surface plasmons and the bulk plasmons in energy loss spectrum of clean Al. The other effect of the increase of primary energy is the rise of a loss peak at 14.5 eV

Table (6.2)

Energy Losses for Clean Mg

Present work (eV)	Assignment	Janssen et al. (1974) (eV)	Assignment
4	I	-	-
7	S	8	S
10.5	B and S + I	11	B
14.5	2S and B + I	16	2S
18.5	S + B	-	-
21	2B and 3S	22	2B
25	2B + I and 3S + I	-	-
31	3B	33	3B
42	4B	44	4B
52	5B and I (Ionization of $MgL_{2,3}$	55	5B
64	6B	68	6B
75	7B	-	-

which is probably because of a contribution to the peak from a combination loss of a bulk plasmon (10.5 eV) plus the loss at 4 eV. The fact that the loss of 18.5 eV stays reasonably constant as E_p is varied is good evidence for the assignment of a combination loss of surface plus bulk plasmon.

The calculated value of a bulk plasmon, using $\hbar w_p = \frac{ne^2}{m\varepsilon_0}$ (section 3.3.1.1) is 10.9 eV (Raether, 1980) and the experimentally observed values are 10.35 $\pm$ 0.1 (Chen, 1976), 10.3 $\pm$ 0.1 (Aiyama and Yada, 1974) and 10.7 (Attekum and Trooster, 1979). In our work, bulk plasmon losses up to the 7th order was detected, and the value of the 1st order is 10.5 eV. Further, the surface plasmon loss energy of 7 eV is in agreement with the calculated value of 7 eV, by using the expression $\frac{\hbar w_p}{\sqrt{2}}$. The peak at 52 eV could correspond to an ionization loss of the $L_{2,3}$ shell electrons of Mg. This value is in reasonable agreement with the value of $L_{2,3}$ shell (49 - 53 eV) which has been obtained by other methods (Fuggle, 1977; and Attekum and Trooster, 1979).

For MgO as may be seen from energy loss spectrum Fig. (6.3) loss peaks have been observed at 4, 11, 16, 22, 42, 58.5 and 75 eV. The interpretation of the 4 eV loss peak is that this peak results from a shifted surface plasmon loss in magnesium, due to a dielectric over layer of MgO. Using a dielectric constant of $\varepsilon_0 = 3.65$ (Chen, 1976) for MgO in the equation ($\hbar w_s = \frac{\hbar w_p}{1+\varepsilon_0}$) derived by Stern and Ferrell (1960), the calculated value of the shifted surface plasmon loss is 4.8 eV (assuming infinite dielectric thickness) which is in reasonable agreement with the observed value. The peak at 11 eV is probably the 1st bulk plasmon loss. The weak loss at 16 eV in MgO was more difficult to identify, however it has been assigned as the first surface plasmon loss by Janssen *et al.* (1974). The strong peak at 22 is reported (Roessler and Walker, 1967; Jull, 1956) to be a bulk plasma

resonance in the valence band of MgO. However it is too strong to be a bulk plasmon. Therefore, it was thought that the contribution to this loss must come from the L_1 ionization loss in oxygen at 22.5 eV (Bearden and Burr, 1967). In previous chapter the peak at 23 eV in BeO loss spectrum has been interpreted as a shifted bulk plasmon, but it may well be the same peak as 22 eV loss peak in MgO which is interpreted here as the ionization loss from the L_1 shell of oxygen. The weak loss peak at 58.5 eV in the oxidised magnesium loss spectrum is probably due to the $L_{2,3}$ ionization loss in Mg. This peak in clean magnesium was reported at 52 eV. In other words oxidation has caused 6.5 eV shift in $L_{2,3}$ level of magnesium atom. There are not enough evidence to identify the peaks at 42 eV and 75 eV.

6.4.3 Secondary Electron Emission Yield

To get some general idea about the SEE yield of Mg and Be, during the oxidation, it is helpful to compare the results of these two samples. For this purpose, the same procedure which was used for the discussion of SEE yield of Be results will be repeated for Mg as well. However, at the beginning of this section, the results are compared with the previous works on SEE yield of Mg → MgO.

As it is mentioned in section (6.3.3), the δ_{max} and E_{pmax} of a clean magnesium surface has been determined as 0.89 and 312 eV respectively. These values are in agreement with theoretical calculations and experimental results. Previous experimental results have determined the values of δ_{max} and E_{pmax} of clean Mg surfaces as 0.8 - 0.95 and 300 eV respectively (Kolath, 1956; Bruining and De Boer, 1938; Bruining, 1954). Theoretically the values of these maximas have been calculated from the same equations which were used for Be, sections (2.6 and 5.4.3).

$$\delta_{max} = 0.12Z^{1/15} I^{4/5} (1 + 1.26r) = 0.84$$

$$E_{pmax} = 57.9Z^{1/15} I^{4/5} (1 + 5r^2)^{4/5} eV = 370 \text{ eV}$$

where r = 0.2, I = 7 eV and Z = 12.

The two important factors, range of primaries, R, and escape depth of secondaries, x_α, [where $R = (E_p/E_R)^{1+1/n}/C$, section 2.5.1 and $x_\alpha = R/(1 + r^2)$, section 2.5.2] have been obtained as a function of E_{pmax}. For clean Mg E_{pmax} = 312 eV gives the range and escape depth of 65A° and 55A° respectively. The value for escape depth (55A°) is in close agreement with the calculated value of 50A° from the relation (2.32) section (2.5.2).

The surface obtained in the present work with the highest yield had its maximum energy at 353 eV with a maximum yield at 2.73. This represents the surface with the thickest layer of MgO. To compare these results to the other theoretical and experimental works on MgO, the normalized yield curve (δ/δ_{max} vs E/E_{pmax}) was plotted (Fig. (6.23)). As it is shown in the figure, this curve is in good agreement with the theoretical curve obtained by Kanaya et al. (1978) and the experimental curve by Dekker (1958). However, (just like the BeO normalized yield curve) the complete normalized yield curve of MgO could not be obtained, because of the instrumental limit on the primary energy (1 KeV). In the sequence of yield curves of Mg → MgO, in so far as there was not any significant elementary Mg on the surface (as indicated from the Auger spectra) the normalized yield curve was able to be fitted quite well to the theoretical normalized curve for MgO, however when a peak of Mg (45 eV, $L_{2,3}$ VV) in Auger spectrum of the surface was distinguishable, the normalized yield curve would not fit any more and in a similar matter to the BeO, $\delta/\delta_{max} - E/E_{pmax}$ curve, it also shifts to the higher limit of $\delta/\delta_{max} - E/E_{pmax}$ curve. To determine the escape depth, x_α,

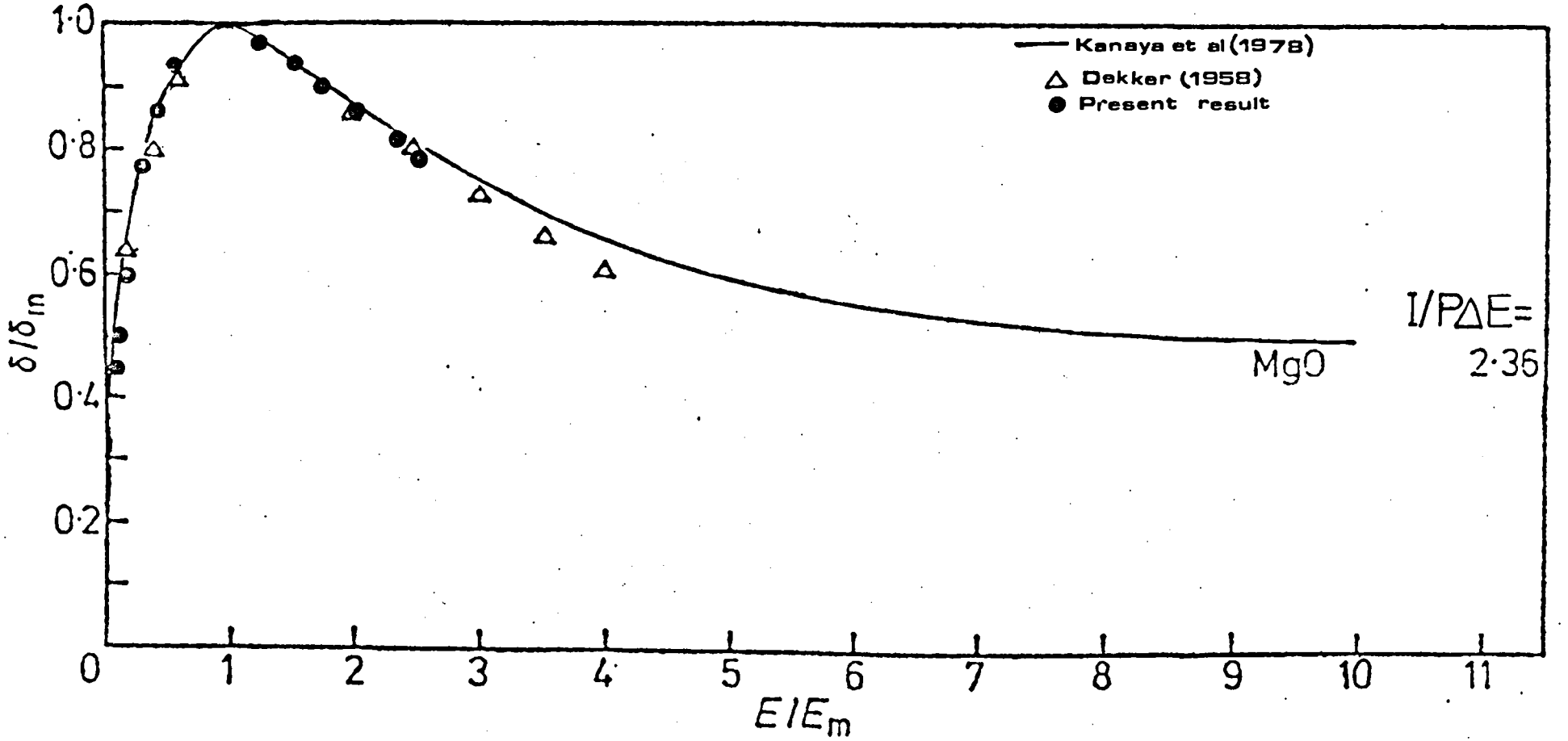

FIG·6·23 Theoretical and experimental comparison of normalized yield curve

of the secondaries in MgO, by using the $\delta/\delta_{max} - E/E_{pmax}$ curve, the same technique as BeO was tried. The calculated value of $\frac{I}{P\Delta E}$ (2.5.5) for MgO normalized curve is 2.36 (where I = 4 eV and ΔE = 10.5 eV). Thus a value of P can be calculated as 0.16. By using the equation (2.32), x_α is obtained as 274A°. However, the value of 71A° has been obtained for the escape depth from the range relation. Unfortunately, the reason for this difference is not evident. However, it is certain that, when the oxidation process takes place the value of the escape depth of secondaries increases, and by using the range relation it increases from ≃ 55A° to 71A°, as $E_{p_{max}}$ shifts progressively from 312 eV to 353 eV and δ_{max} changes from 0.89 to 2.73.

It should also be mentioned that the maximum yield (2.73) in our work is much lower than that, which has been reported by others. Goldstein and Dresner (1978) have obtained values of 10 - 15 and Borisov et al. (1976) could even obtain values of 24 - 32 for the maximum secondary emission yield, δ_{max} of forms of MgO. The probable reasons for the difference between our results and others for δ_{max} lies in the special methods of preparation used by the above authors who were attempting to maximise an effect namely the yield rather than study the first stages of oxidation, for example, Goldstein and Dresner (1978) obtained a thick film of MgO (δ_{max} = 10 - 15) by heating an Al - 1% Mg alloy in oxygen, whilst Borisov and Lepshinskaya (1976) reported that a high secondary emission efficiency of MgO is obtainable by producing its films with an special ordered structure. They obtained high yield surfaces (δ_{max} = 24 - 32) of MgO by preparing the films on a molybdenum (100) single crystal. In addition in the case of the present work there was a lack of oxygen in the vacuum system to build any thick layer of MgO due to most of the residual oxygen molecules having already been consumed in the formation of BeO for the previous experiments.

Therefore, there was not enough oxygen in the vacuum to give very thick MgO film. This assumption is probably true because, as shown in the Auger spectra of MgO (Appendix C and Fig. (6.1)), after heating the target, the oxygen on the surface has even reduced because of the diffusion of some oxygen into the surface and there was then not enough residual oxygen in the vacuum to replace the diffused oxygen on the surface. It may be noted that at this stage there was considerable reluctance to open the system either to admit more oxygen because of the contamination problems.

To compare and contrast the results of Mg to Be, and to get some general ideas about the reasons for the increase in δ_{max} during the first stages of the oxidation process, Figures (6.11-6.15) have been plotted to see the changes in δ_{max}, escape depth x_α and first crossover energy $E_{p_{c1}}$ clearly. As may be seen from a comparison of the Figures (6.14) (δ_{max} vs $E_{p_{c1}}$), (6.15) (δ_{max} vs $R\alpha x_\alpha$) and (6.11) $\left[\delta_{max} \text{ vs the ratio } \frac{O(505\ eV)}{Mg(45\ eV)}\right]$ of the magnesium sample to Figures (5.12) (δ_{max} vs $E_{p_{c1}}$), (5.13) (δ_{max} vs $R\alpha x_\alpha$) and initial part of (5.11a) $\left[\delta_{max} \text{ vs the ratio } \frac{O(505\ eV)}{Be(104\ eV)}\right]$ of the beryllium sample, respectively, the similarity of these figures are evident. Fig. (6.14) shows the reduction of $E_{p_{c1}}$, which is proportional to the change in work function of the surface (Dionne, 1975) on oxidation, therefore, probably one of the reasons for the increase of secondaries during the oxidation could be the decrease in work function. Fig. (6.12) is a graph of δ_{max} against a measure of the ratio of total oxygen on the surface to the total Mg on the surface, i.e. the peak-peak height of oxygen 505 eV peak divided by the sum of the pk-pk height of the Mg 45 eV peak plus the Pk-Pk height of the MgO 35 eV peak. The former is a measure of elemental Mg (the $L_{2,3}$ VV line) whilst the 35 eV peak is the same transition when a Mg atom is combined with oxygen. If it is assumed that the

ionisation probabilities are very much the same for the K level in oxygen atom and the $L_{2,3}$ level in magnesium atom, then this sum is a measure of the total Mg on the sample surface. As may be seen from this Fig. (6.12), δ_{max} has started to increase rapidly from its initial value of 2. Reference to Fig. (6.15) at this value of δ_{max} shows that the escape depth has also started to increase comparatively rapidly. So by a similar argument to that used in case of Be → BeO we may arrive at the result that the increase in the secondary electrons of Mg → MgO at $\delta_{max} = 2$ is also consistent with a decrease of potential barrier height at this point caused by band bending. Most probably, this band bending has been caused only by an increase in the MgO thickness not an increase in alone oxygen, since as shown in Figures (6.12) and (6.13) [δ_{max} vs oxygen coverage (pk-pk height of 505 eV peak)] δ_{max} is increasing all the time although the oxygen coverage on the surface has decreased after heating the target at $\delta_{max} = 2$.

6.5 Conclusion

Results for AES, CELS and SEE yield of magnesium both for a clean surface and whilst it was in the initial stages of oxidation is presented in this chapter. An interpretation of most of the observed peaks in CELS and AES has been presented. The tentative explanation of the effect of oxidation on SEE yield has been attempted. However, there is still considerable uncertainty about the latter results.

CHAPTER 7

CONCLUSIONS AND SUGGESTIONS FOR FUTURE WORK

In this final chapter an overall picture of the work is presented together with suggestions for future work.

Chapter two and three consists of some theoretical aspects of SEE yield, AES and CELS and in particular the highly relevant work of the school of Kanaya et al. (1978) and Ono and Kanaya (1979) on SEE. Some of the theoretical aspects of the latter work have been used for analyzing the present results. However, at the present there are still too many uncertainties which remain regarding such parameters as escape depth, the backscattering factor, the ionization cross section, the Auger transition probabilities, and the surface roughness factor which obscure a meaningful use of theoretical ionization cross-section.

The three grid retarding field analyser (RFA) which was originally constructed by Suleman (1971) has been described in the fourth chapter. The measured resolution of the device is $\sim$ 0.2%. With respect to the experimental apparatus, some modifications have been made in order to improve its overall performance. For example, originally the evaporation filaments were inside the main chamber, thus the evaporation process could easily contaminate the analyser assembly. Further, facilities for cleaning the Be foil surface, electron bombardment and heating process were not efficient enough, so it was decided to incorporate facilities for cleaning the target by the ion sputtering technique. Since it was impractical to connect the ion gun to the main chamber, a special sample manipulator was constructed and connected to the main chamber. The main feature of this manipulator was that a

relatively large translational motion could be obtained in addition to the rotary motion. This made it possible to take the sample into the other section for evaporation or ion sputtering purposes and then bring it back into the main chamber for analysis. Further, since the beam spot size is very important in obtaining a good resolution, a fluorescent screen was made and this was connected beside the target to measure the beam size.

The instrument can be operated to yield an output which is proportional to N(E) or $\frac{dN(E)}{dE}$, where N(E) is the secondary electron emission spectrum. AES and CELS were obtained by modulating the collector current in $\frac{dN(E)}{dE}$ mode, whereas SEE yield was obtained by modulating the target current in the N(E) mode. An electronic circuit has been developed to measure automatically secondary electron yield with increased sensitivity, speed and accuracy. The main feature of the present method is that the yield can be obtained in conjunction with AES and CELS simply by operating the external detection system in the Auger and CELS or yield mode. In the case of yield data, the present work was only concerned on parameters like $E_{p_{max}}$, δ_{max}, $E_{p_{c1}}$ and $E_{p_{c2}}$. However some structure is discernable at the low energy part. It may be pointed out that this part is of considerable current interest especially in connection with the study of single crystals, where some of the phenomena may be correlated with surface resonances (surface band structure) (McRae et al., 1977). If this part of yield curve was detected in the differential mode, or passed through a data analysis system incorporating a digital technique and in particular a digital filter (McRae et al., 1978), then better resolution and more information concerning the band structure could be obtained.

The AES, CELS and SEE yield of Be and Mg both in a clean condition and whilst they were slowly oxidising has been obtained and discussed in

the fifth and sixth chapters. The result of Auger spectra of clean Mg and Be suggest that the peaks can be related to the peaks in the theoretical density of states of the valence band of these elements. In addition some fine structure peaks in the Auger spectra are believed to originate from plasmon energy loss and double ionisation mechanisms. The changes in the Auger spectra which take place as a result of oxidation can in the main be explained in terms of chemical shifts in the inner energy levels and the changes in the density of states of valence band. Some Auger peaks in the Auger spectra of oxidised surfaces are however also believed to be due to cross-transitions between the energy levels of the oxygen and metal atoms. In CEL spectra of clean and oxidised Be and Mg, some peaks are identified due to the bulk and surface plasmons and some due to ionization losses in the inner shells. The energy of these ionization loss peaks also determines the energy of the inner core shells. During the oxidization the shift in the energy of ionization losses (or in other words the shift in inner core shells) was observed for both surfaces (Mg and Be).

In SEE yield curve the changes of yield parameters such as δ_{max}, E_{Pmax}, E_{Pcl} and x_{α} were nearly the same for both materials (Mg and Be) during the oxidation and a try has been made to compare the present results with the recent theoretical work of Kanaya et al. (1978) and Ono and Kanaya (1979). Their work presents an interesting development towards solution of the secondary electron yield of metals, semi-conductor compounds and insulators by applying free electron scattering theory to the absorption of secondary electrons generated within a solid target, also they have presented a reasonably satisfactory explanation of the high yield of insulators in terms of integral multiples of plasmons and the ionization loss in effect combining the free electron scattering theory with the plasmon theory. They have

also mentioned that the high yield (1.5 - 20) of insulators are due to the escape depth (x_α) of secondaries and they have calculated the escape depth as a function of ionization loss and plasmon losses. Since the escape depth of secondaries is proportional to the range of primaries, therefore the high yield can be related to the increase of range (R). From the present results, by using the change of $E_{p_{max}}$ during the oxidation, the range of primaries ($R \alpha x_\alpha$) is calculated for both materials (Mg and Be). For Mg the range has increased from 65 to 76A^o and the escape depth from 55A^o to 71A^o and for Be the range have increased from 34A^o to 56A^o and the escape depth from 33A^o to 53A^o. The normalized yield curves (δ/δ_{max} vs E/E_{max}) are also plotted for MgO and BeO, they are in very good agreement with their theoretical normalized yield curves. From the normalized yield curves the value of p (the normalized ratio of the plasmon loss under consideration to the most probable plasmon loss) for MgO and BeO have been obtained, and by using the relation which was obtained by these authors, the escape depths have been calculated. For BeO the value of 55.5A^o was obtained which is in good agreement with a value of 53^o which has been calculated from the range relation; however for MgO the value of 274A^o has been obtained which is considerably higher than the value of 71A^o calculated from the range relation. The reasons for this discrepancy are not evident. Further work is needed on this point possibly with considerably thicker MgO layer.

The increase of escape depth (for Mg from 55 to 71A^o and for Be from 33 to 53A^o) and the change of first crossover energy have been used to interpret the reasons for the increase of secondary electrons ($\alpha\delta_{max}$) during oxidation. The decrease of the first crossover energy, after the appearance of the oxygen peak in the Auger spectrum has been interpreted as a reduction in the work function of the surface by

oxidation. At one stage of oxidisation the secondary electrons ($\alpha\delta_{max}$) suddenly started to increase comparatively fast and at that point the value of the escape depth has also started to increase fast. It was reported by Fitting et al. (1978) that the escape depth is a function of electron affinity and energy loss parameter, where for a certain value of energy loss parameter the escape depth increases while potential barrier height decreases. Thus, an increase of δ_{max} and the escape depth has been interpreted as a reduction of potential barrier height at that point by band bending. It is also believed that during the oxidation, the increase of the thickness of oxides (MgO or BeO) on the surface has caused the band bending, not oxygen on its own.

In the present results, a value of δ_{max} of 2.73 was obtained for magnesium oxide, however, this value does not represent a maximum value and is much lower than the values measured by others. This is because in the present work only a very thin layer at most of MgO (or BeO) is obtained during oxidation. In future work some control of the thickness of the films is desirable. Also, there is evidence that MgO prepared on the special single crystals like Mo(100) (Borisov and Lepeshinskaya, 1976) to give an ordered MgO surface or prepare it from an Al - 1% Mg alloy (Goldstein and Dresner, 1978) has considerable influence on the maximum yield obtainable. A study of the yield parameters during the oxidation of such surfaces, employing Auger analysis for the determination of the surface composition at different stage of oxidation, could be most valuable for comparing with the present results, especially in connection with effect of structure of the maximum yield. Also it would be interesting if the same measurements could be carried out on the surfaces of alloys like Be-Li or MgLi or MgBe. The effect of oxygen on the alloys containing both Mg and Li have been studied by Borisov and Lepeshinskaya (1976). They have observed that the

composite oxide (MgLi) O [this component is not a simple mechanical mixture of two oxides] is responsible for the high efficiency of the emitter on the base of alloy AgAlMgLi. However, no clear theoretical reason for this phenomena is obvious. The only suggestion is that the existence of Li leads to a favourable condition for the excitation of electrons and the existence of Mg on the surface produces a good condition for the emission of these electrons. Apart from these effects of Mg and Li, generally, alkali metals like Cs, Li or Caesium oxide plays an important role on the surfaces of semi-conductors, since a very thin layer of caesium, littium or caesium oxides would reduce the electron affinity to the much lower values. For instance, the electron affinity of GaAs after coating it with caesium will reduce from 4 to 0.5 (Fischer, 1966). Therefore, it would be a good idea to work on the effect of Cs, Li or CsO on MgO or BeO to check if they have the same effect on these two oxides as in the case of semi-conductors. Further, since the change of work function has an important role in the change of efficiency of secondary electron emission, it would be useful to facilitate the instrument to measure the change of work function during the oxidation and so observe the relation between work function and δ_{max}.

In conclusion, it seems that, for the secondary-emission yield, one of the most important factors is apparently the change in the height of the potential barrier, which can result from the presence of various atoms on the surface.

APPENDIX a

CALCULATING OF THE SENSING RESISTOR VALUE

When the current flow through the sensing resistor (Fig. a.1) the noise across it is given by;

$$(\Delta e)^2 = 4KTR_s\Delta f + 2eIR_s^2\,\Delta f$$

where $(\Delta e)^2$ = mean square value (r.m.s. value) noise across the resistor

$4KTR_s\Delta f$ = thermal noise

$2eIR_s^2\Delta f$ = shot noise

K = Boltzmann's Constant

= 1.380×10^{-23} JK^{-1}

e = 1.6×10^{-19} Coul

T = $300^{o}K$ (at room tem.)

Δf = frequency bandwidth of the measurement circuit (Hz)

R_s = resistor value in Ω

When $\frac{2eIR^2\Delta f}{4KTR\Delta f} > 1$ then shot noise is greater than thermal noise

i.e. $\frac{eIR}{2KT} > 1 \rightarrow IR > \frac{2KT}{e} \sim 0.05$ eV

$\sim$ 50 mV at room temp.

By using the data sheet of ZN424 and choosing 4.8 KHz for the frequency the value for $e_n^2 = 3 \times 10^{-17}$ V^2/Hz is obtainable. Then

$$R_s >> \frac{3 \times 10^{-17}\ V^2/Hz}{4 \times 1.38 \times 10^{-23}(JK^{-1}) \times 300^{o}K}$$

i.e. $R_s >> 1.8$ KΩ

If the value of $R_s >> 1.8$ KΩ , then $e_n^2\,\Delta f$ can be omitted from the

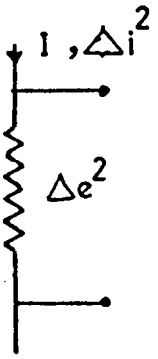

FIG. a1

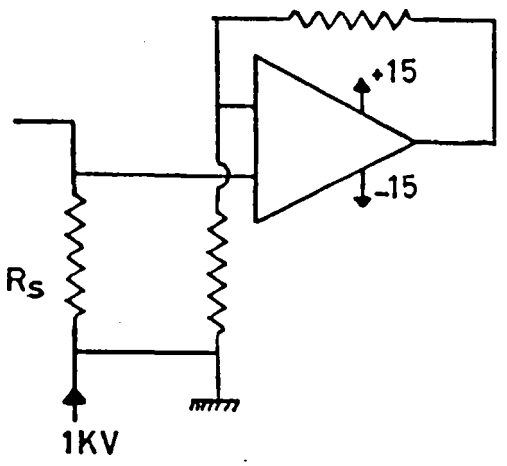

FIG. a2

denominator of equation (a.1), therefore,

$$\frac{2eIR^2_s + i^2_n R^2_s}{4KTR} > 1$$

$$\text{i.e. } R_s > \frac{4KT}{2eI + i^2_n}$$

For $I = 1\ \mu A$ and $i^2_n = 6 \times 10^{-25}$ amps/Hz (from the data sheet)

$$R_s > \frac{4 \times 1.38 \times 10^{-23} \times 300}{2 \times 1.6 \times 10^{-19} \times 10^{-6} + 6 \times 10^{-25}}\ \Omega$$

$$R_s > 18\ K\Omega$$

Therefore, $R_s = 33\ K\Omega$ was chosen because of the specification of the instrument.

$$\text{i.e. } R > \frac{0.05}{I}\ \Omega \quad \text{at room temp.}$$

Therefore for $I = 1\ \mu A$ need $R > 0.05 \times 10^{-6} = 50\ K\Omega$

therefore, say $R_s = 100\ K\Omega$

then $IR_s = 100\ mV$

Now we try to calculate the R_s by considering the amplifier noise, from Fig. (a.2)

$$(\Delta n)^2 = 4KTR\Delta f + e^2_n \Delta f + 2eIR^2\Delta f + i^2_n R^2 \Delta f$$

$4KTR_s\Delta f$ = thermal noise of R_s resistor

$e^2_n \Delta f$ = thermal noise of amplifier

$2eIR^2_s\Delta f$ = current noise (shot noise) resistor R_s

$i^2_n R^2_s \Delta f$ = shot noise of amplifier

$\overline{e^2_n}$ = the mean square noise voltage of amp.

$\overline{i^2_n}$ = the mean square noise current of amp.

Then shot noise dominates when

$$\frac{2eIR_s^2\Delta f + i_n^2 R_s^2 \Delta f}{4KTR_s\Delta f + e_n^2\Delta f} > 1 \qquad \text{(a.1)}$$

In denominator if $4KTR\Delta f >> e_n^2\Delta f$

i.e. $R_s >> \frac{e_n^2}{4KT}$

The Noise Figure (NF) is:-

$$NF = 10 \log \frac{\text{total noise}}{\text{beam shot noise}}$$

$$= 10 \log \frac{2eI + i_n^2}{2eI}$$

$$= 10 \log (1 + \frac{i_n^2}{2eI})$$

$$= 10 \log (2.87)$$

$$= 4.5 \text{ dB}$$

APPENDICES b and c

Sequences of changes in the Auger Electron Spectra of Be and Mg due to oxidation are shown in Appendices b and c, respectively. For all the Auger spectra a primary energy of 1.3 KeV was used. The amplitude of the oxygen Auger peak at various stages of oxidation is also shown along with the spectra of Be and Mg.

APPENDIX b

Sequence of changes in the AES of beryllium due to oxidation.

Ep = 1.3 KeV.

Modulation voltage = 7.2 V pk-pk

* = from this point the target has been started to heat up.

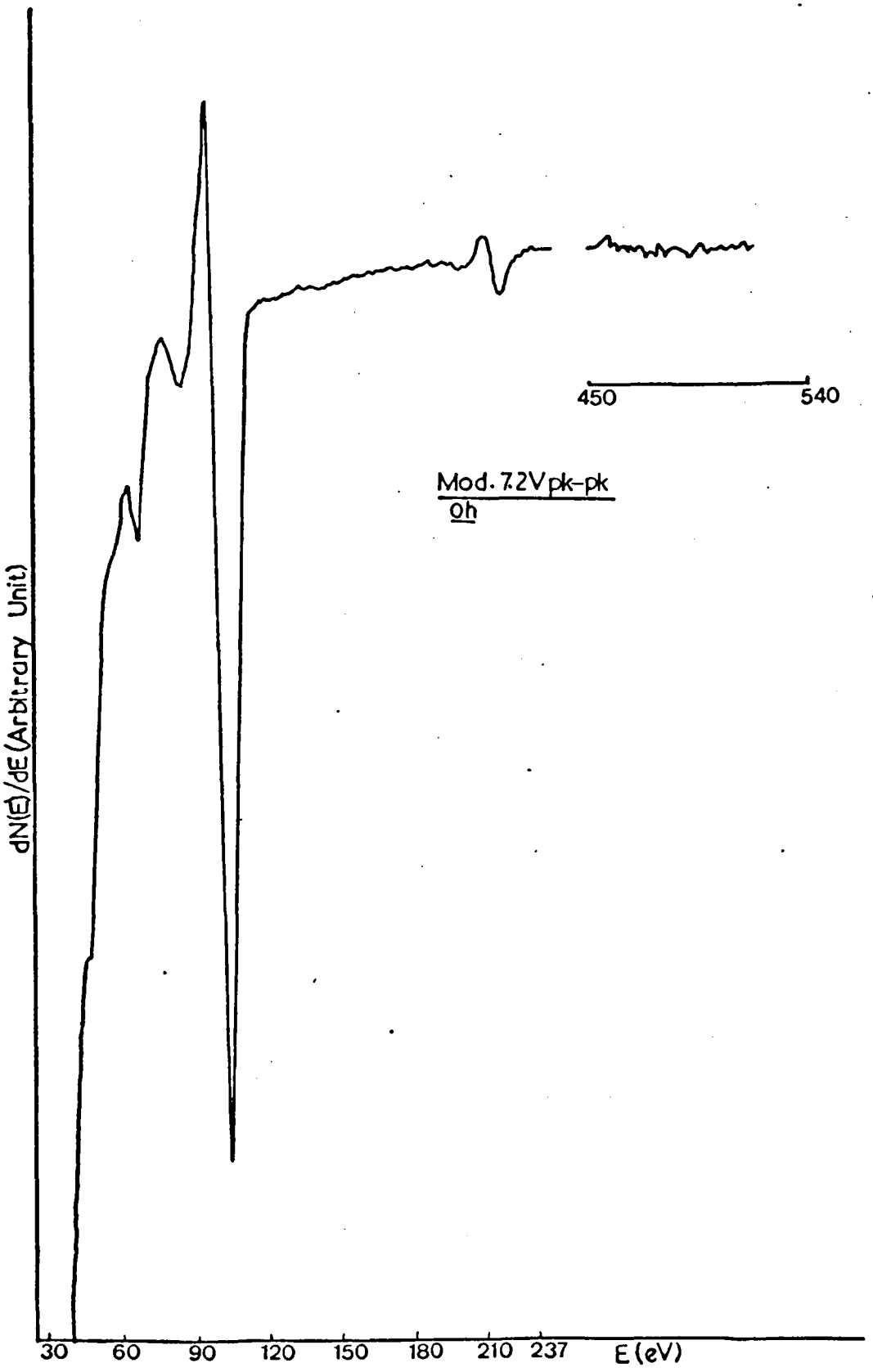
dN(E)/dE (Arbitrary Unit)
450
540
Mod. 7.2V pk-pk
0h
30
60
90
120
150
180
210
237
E (eV)

FIG. b1

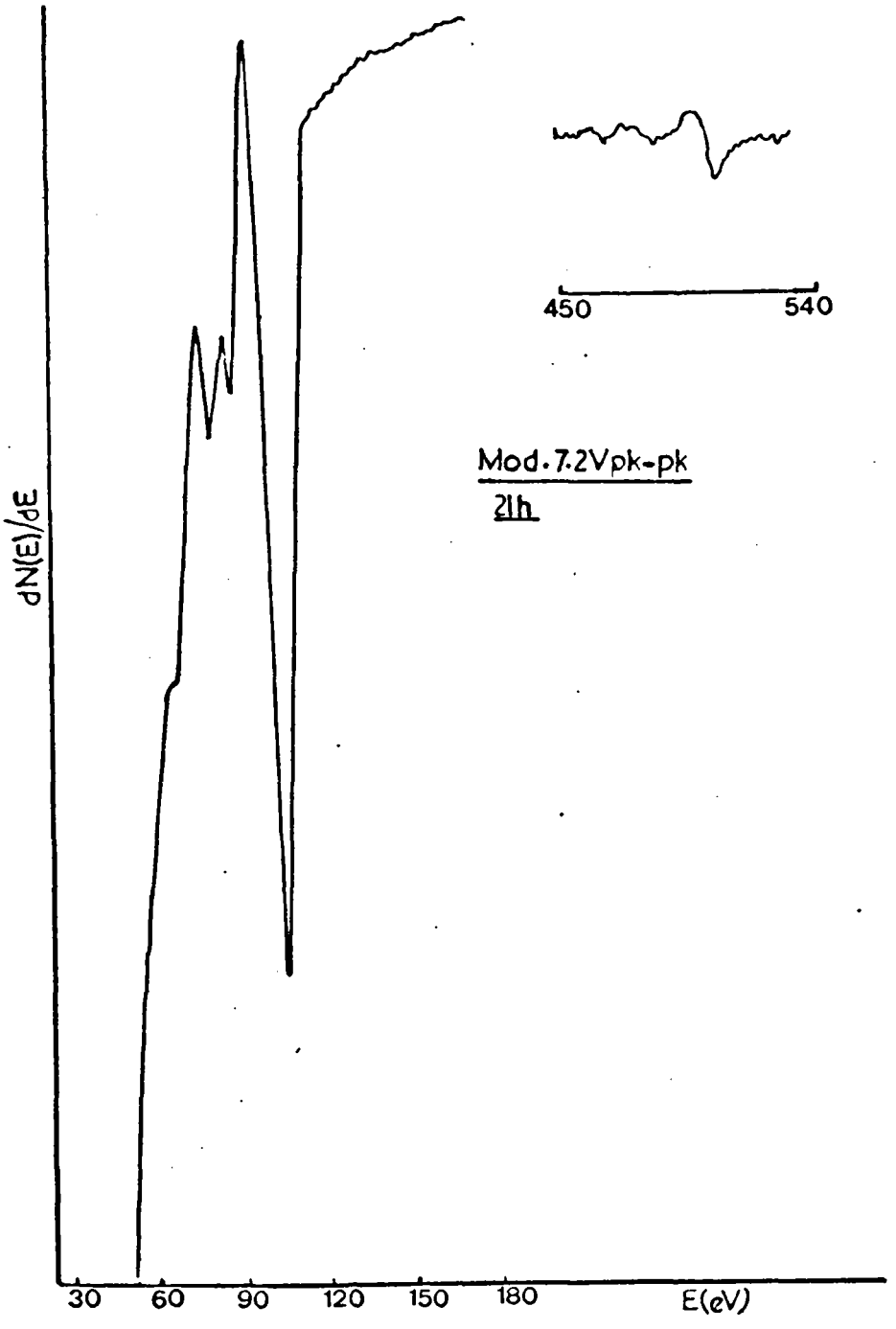

FIG. b2

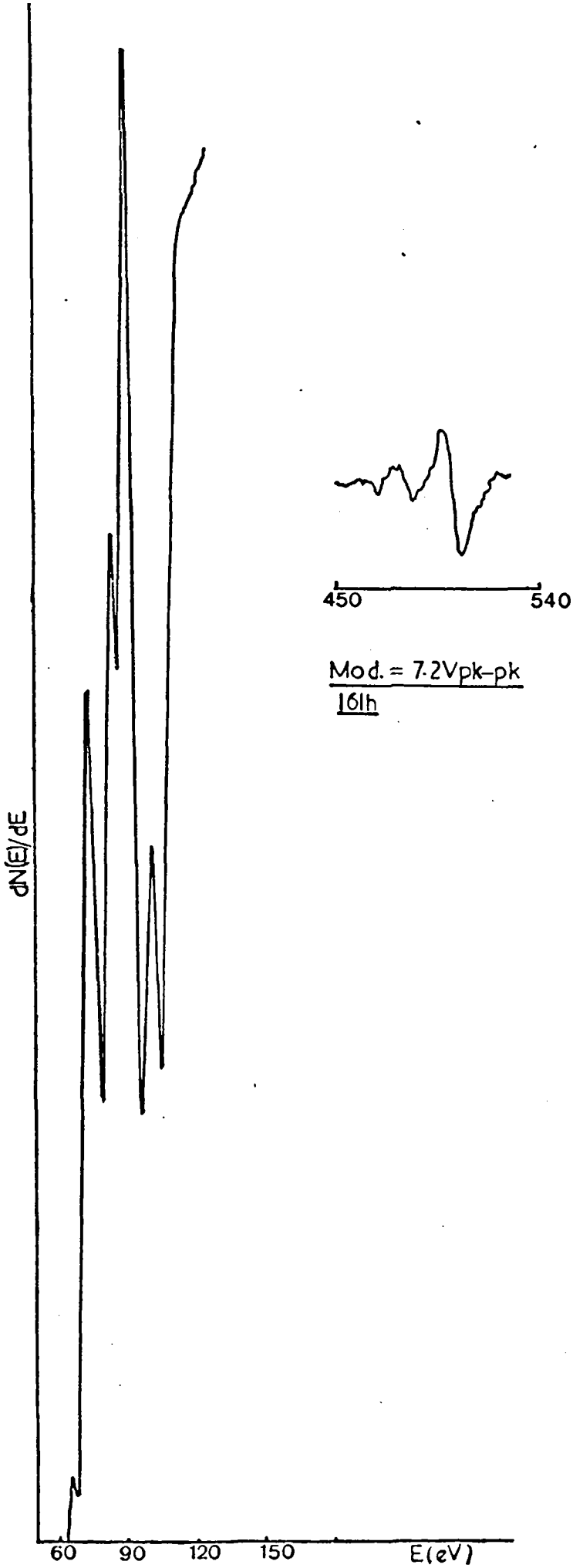

FIG b3

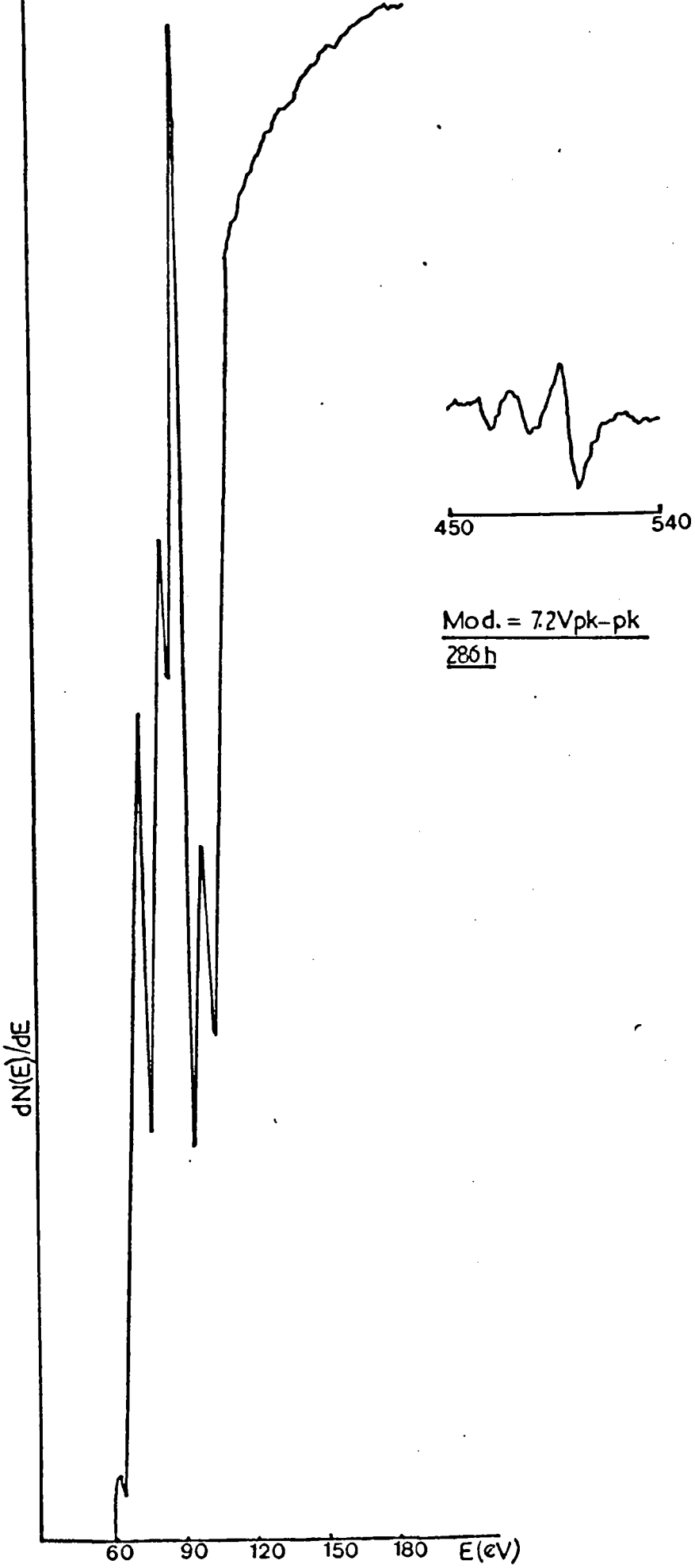

FIG. b4

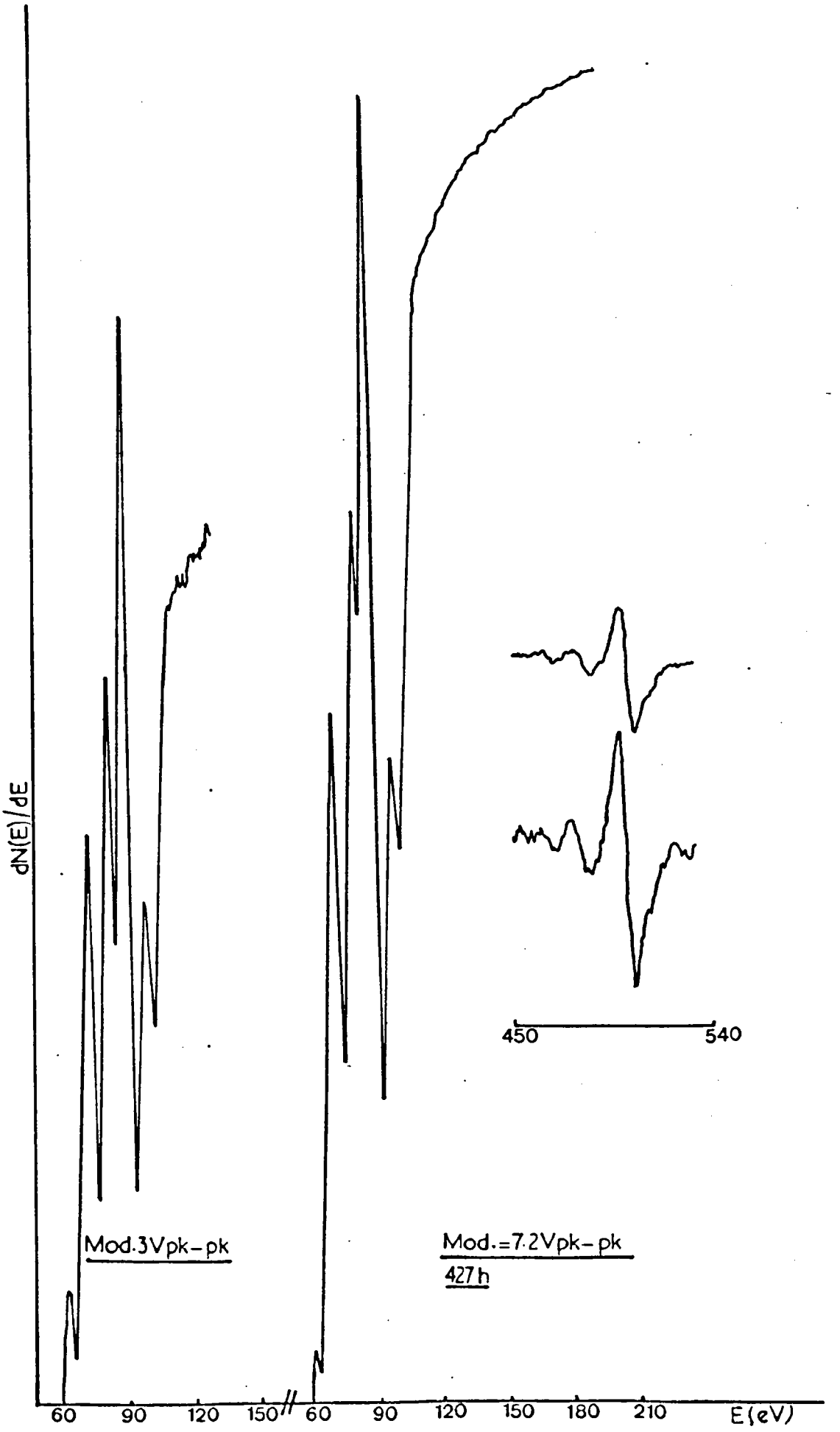
dN(E)/dE
Mod.3Vpk-pk
Mod.=7.2Vpk-pk
427h
450
540
60
90
120
150
60
90
120
150
180
210
E(eV)

FIG. b5

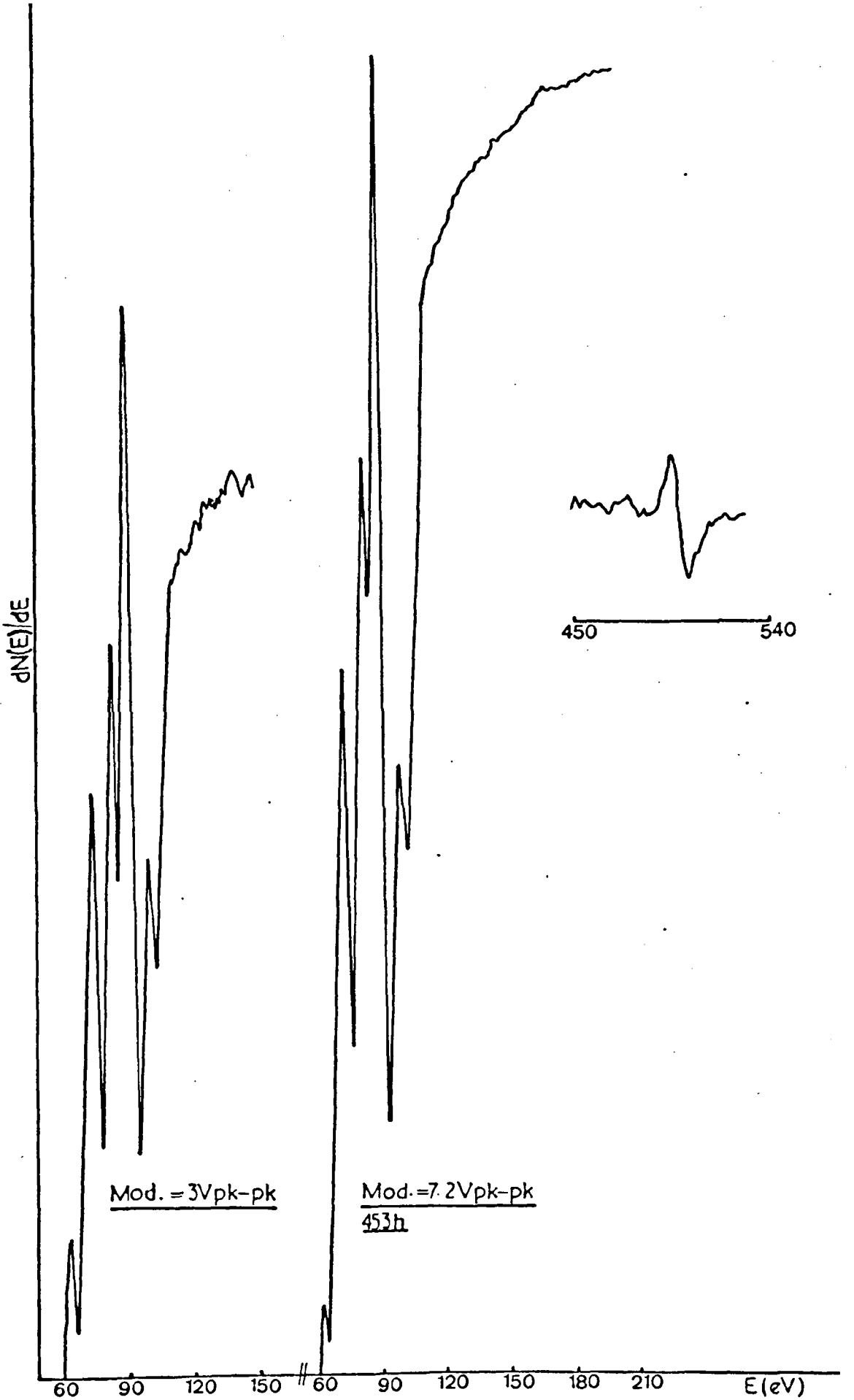
dN(E)/dE
450
540
Mod. = 3Vpk-pk
Mod. = 7.2Vpk-pk
453h
60
90
120
150
60
90
120
150
180
210
E(eV)

FIG. b6

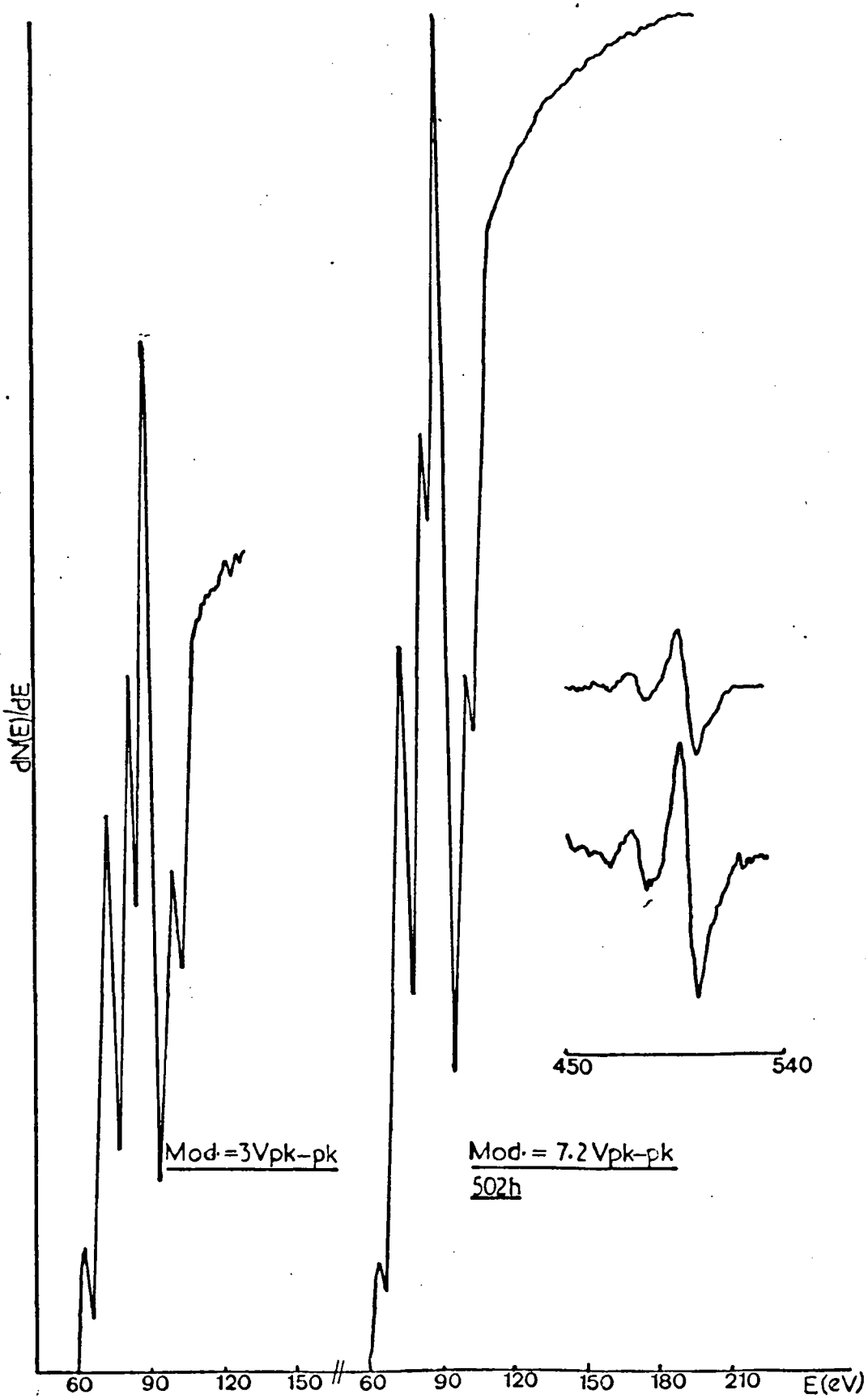
dN(E)/dE
Mod. = 3Vpk-pk
Mod. = 7.2Vpk-pk
502h
450
540
60
90
120
150
60
90
120
150
180
210
E(eV)

FIG. b7.

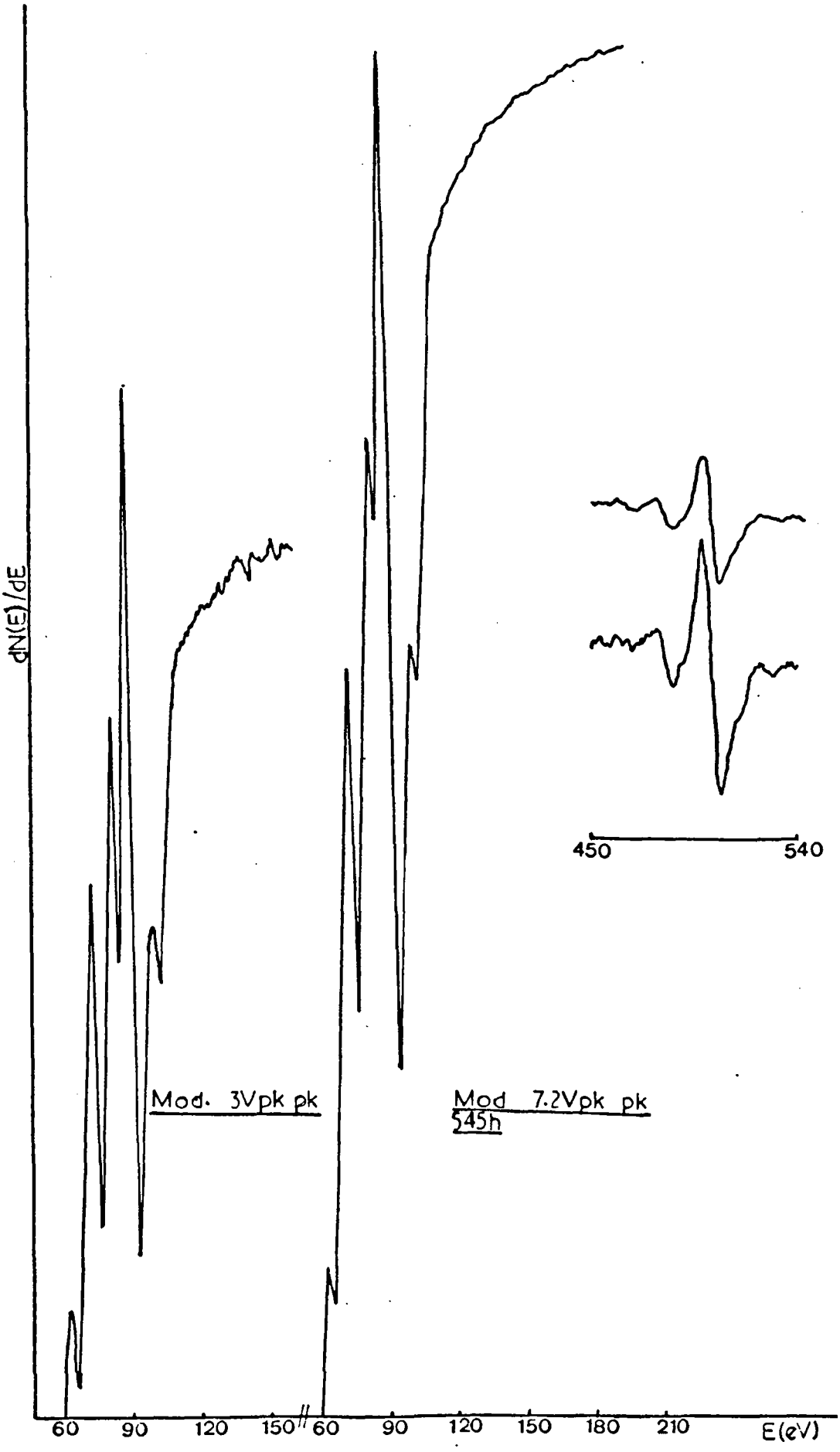
dN(E)/dE
Mod. 3Vpk pk
Mod 7.2Vpk pk
545h
450
540
60
90
120
150
60
90
120
150
180
210
E(eV)

FIG. b8

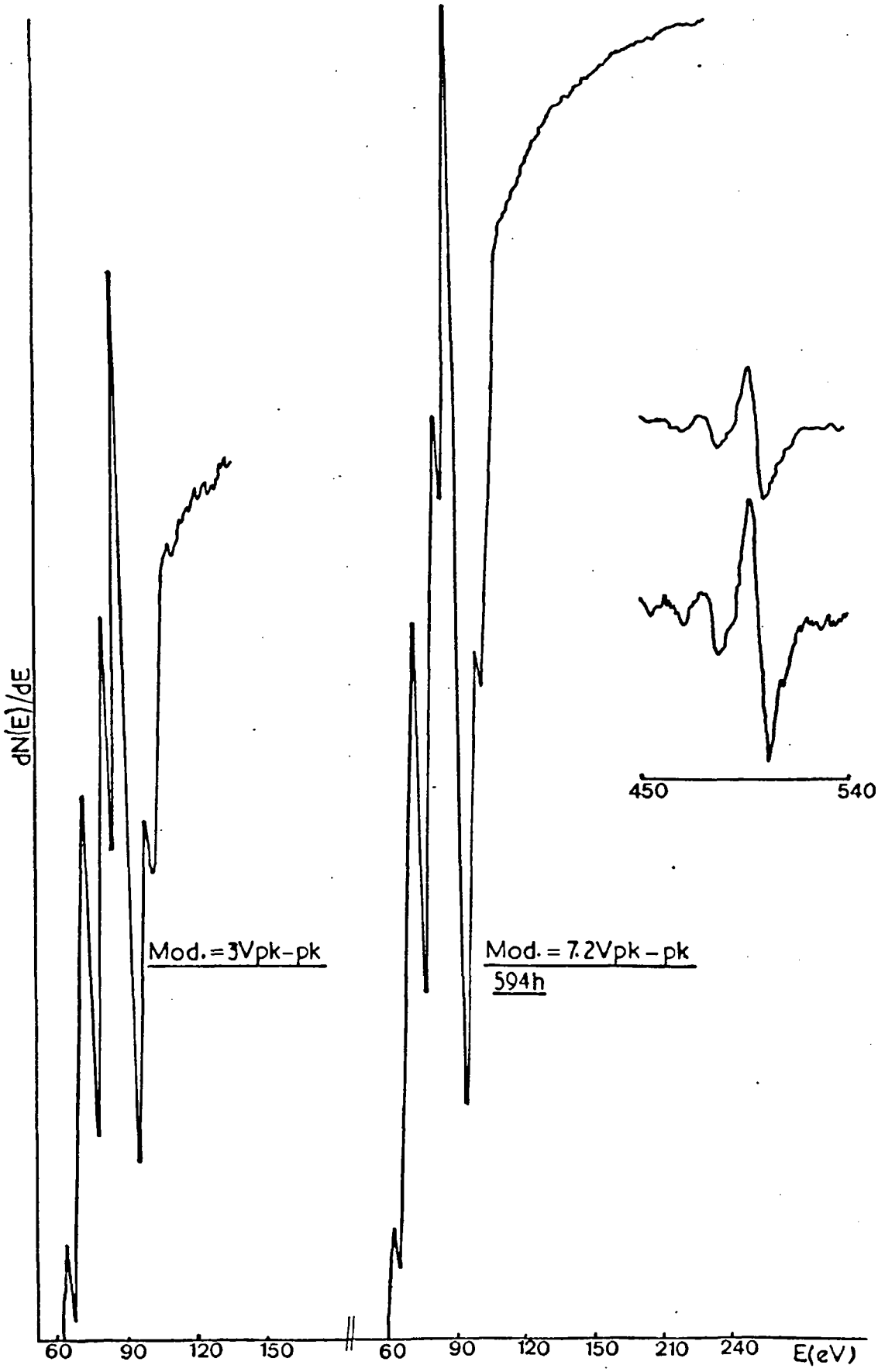
dN(E)/dE
Mod. = 3Vpk-pk
Mod. = 7.2Vpk-pk
594h
450
540
60
90
120
150
60
90
120
150
210
240
E(eV)

FIG. b9

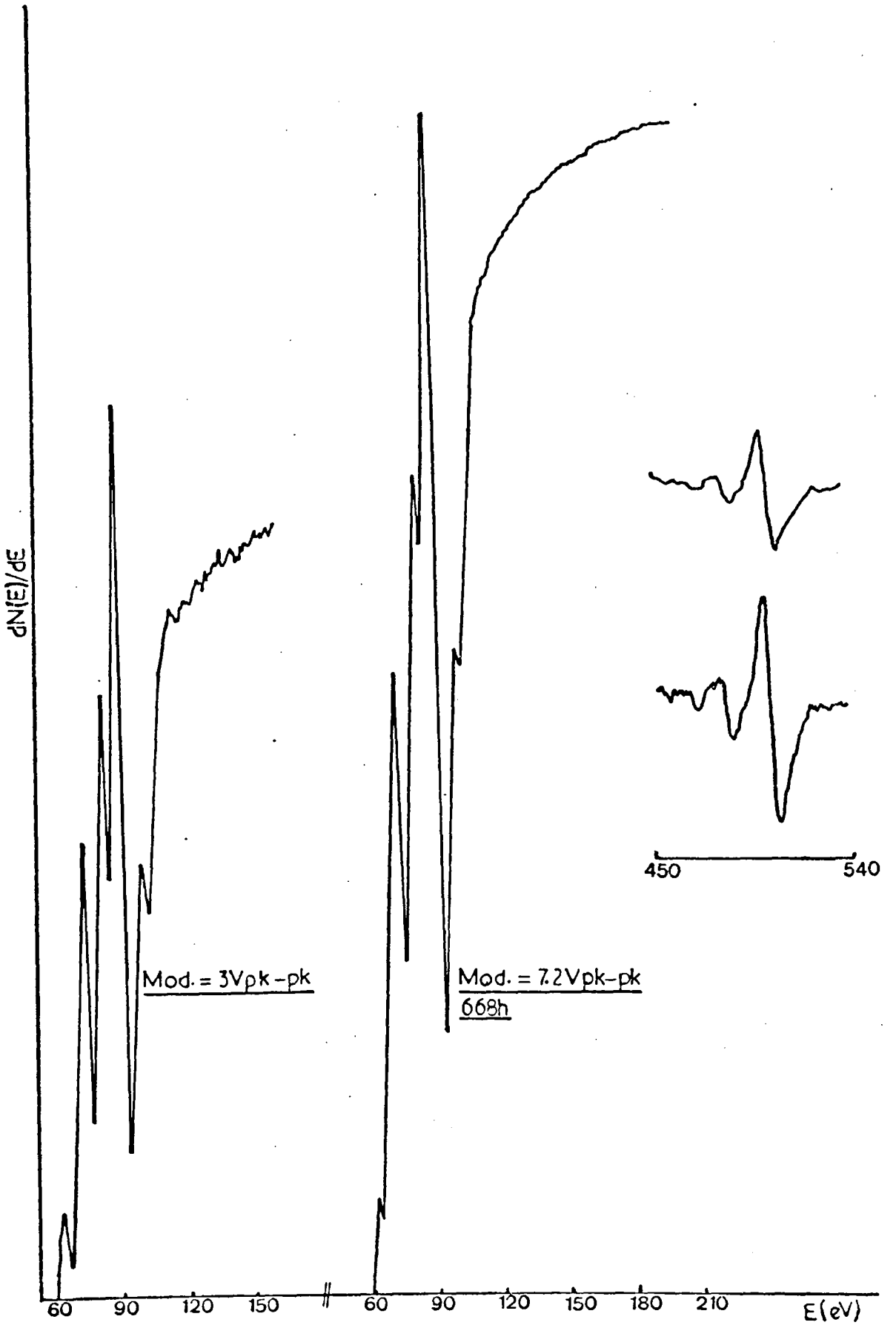
dN(E)/dE
Mod. = 3Vpk-pk
Mod. = 7.2Vpk-pk
668h
450
540
60
90
120
150
60
90
120
150
180
210
E(eV)

FIG. b10

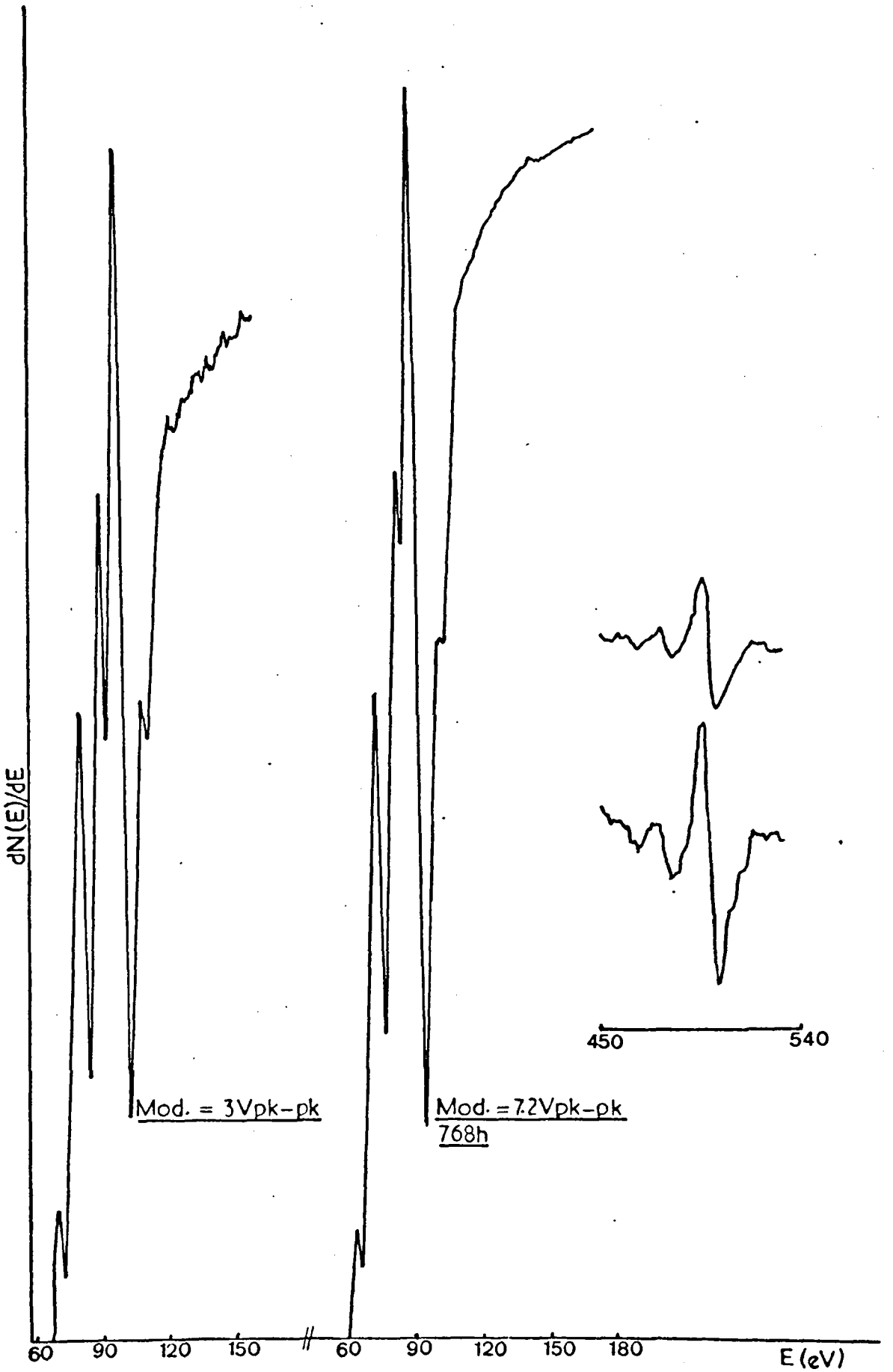
dN(E)/dE
Mod. = 3Vpk-pk
Mod. = 7.2Vpk-pk
768h
450
540
60
90
120
150
60
90
120
150
180
E (eV)

FIG. b11

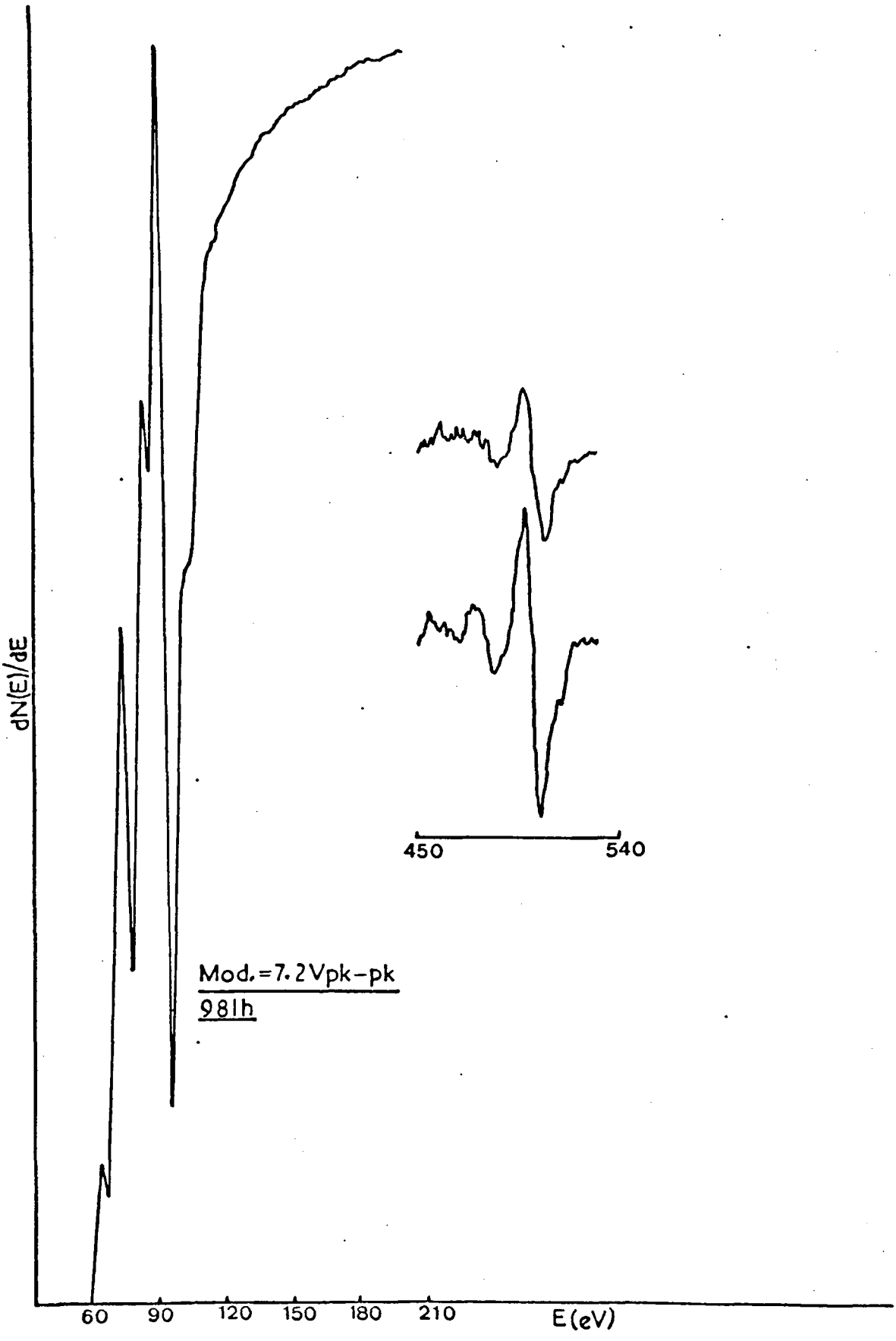

FIG. b12

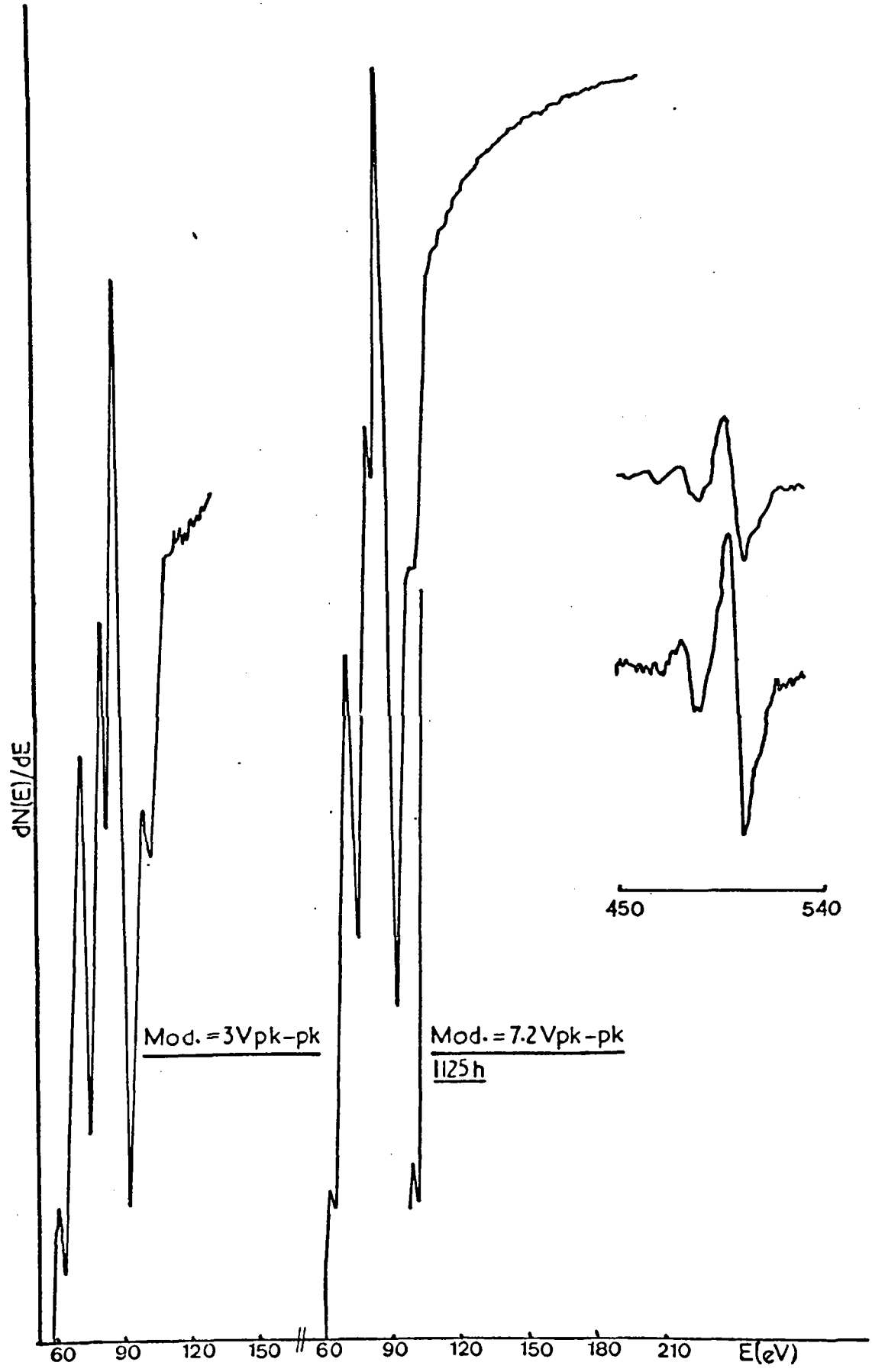
dN(E)/dE
Mod. = 3Vpk-pk
Mod. = 7.2Vpk-pk
1125h
450
540
60
90
120
150
60
90
120
150
180
210
E(eV)

FIG. b13

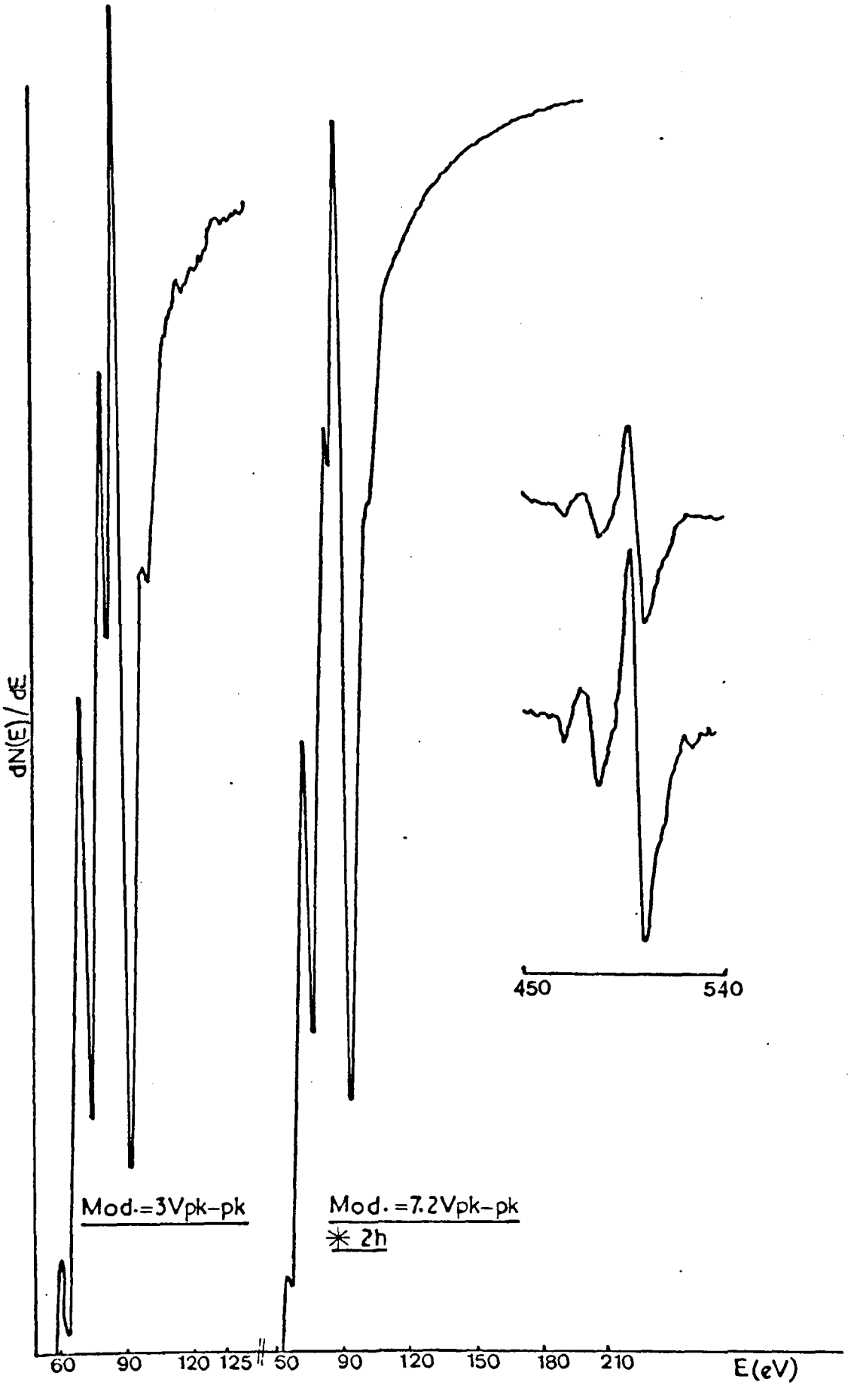
dN(E)/dE
Mod.=3Vpk-pk
Mod. =7.2Vpk-pk
* 2h
450
540
60
90
120
125
50
90
120
150
180
210
E(eV)

FIG. b14

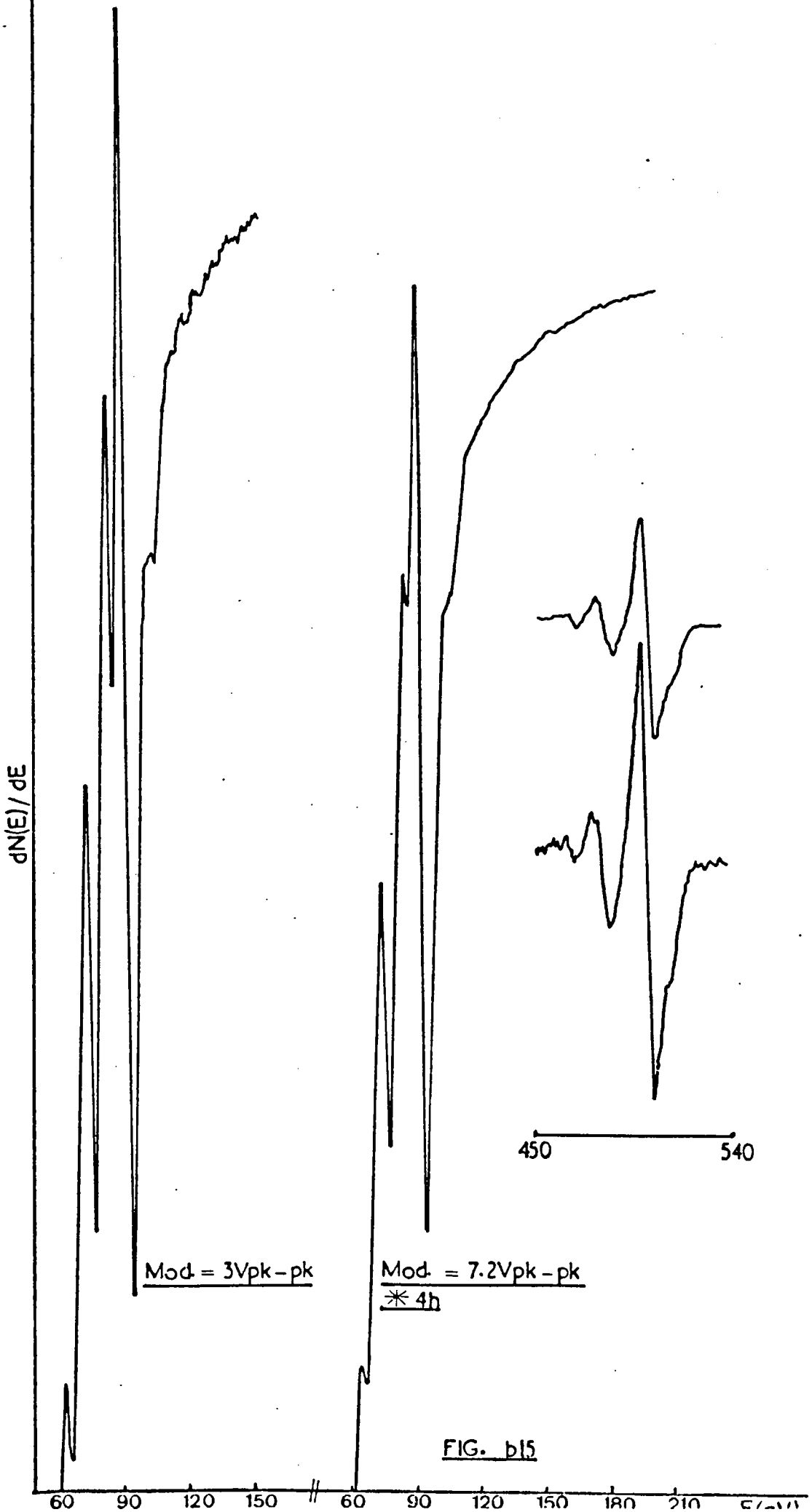
dN(E)/dE
450
540
Mod. = 3Vpk-pk
Mod. = 7.2Vpk-pk
* 4h
60
90
120
150
60
90
120
150
180
210
E(eV)

FIG. b15

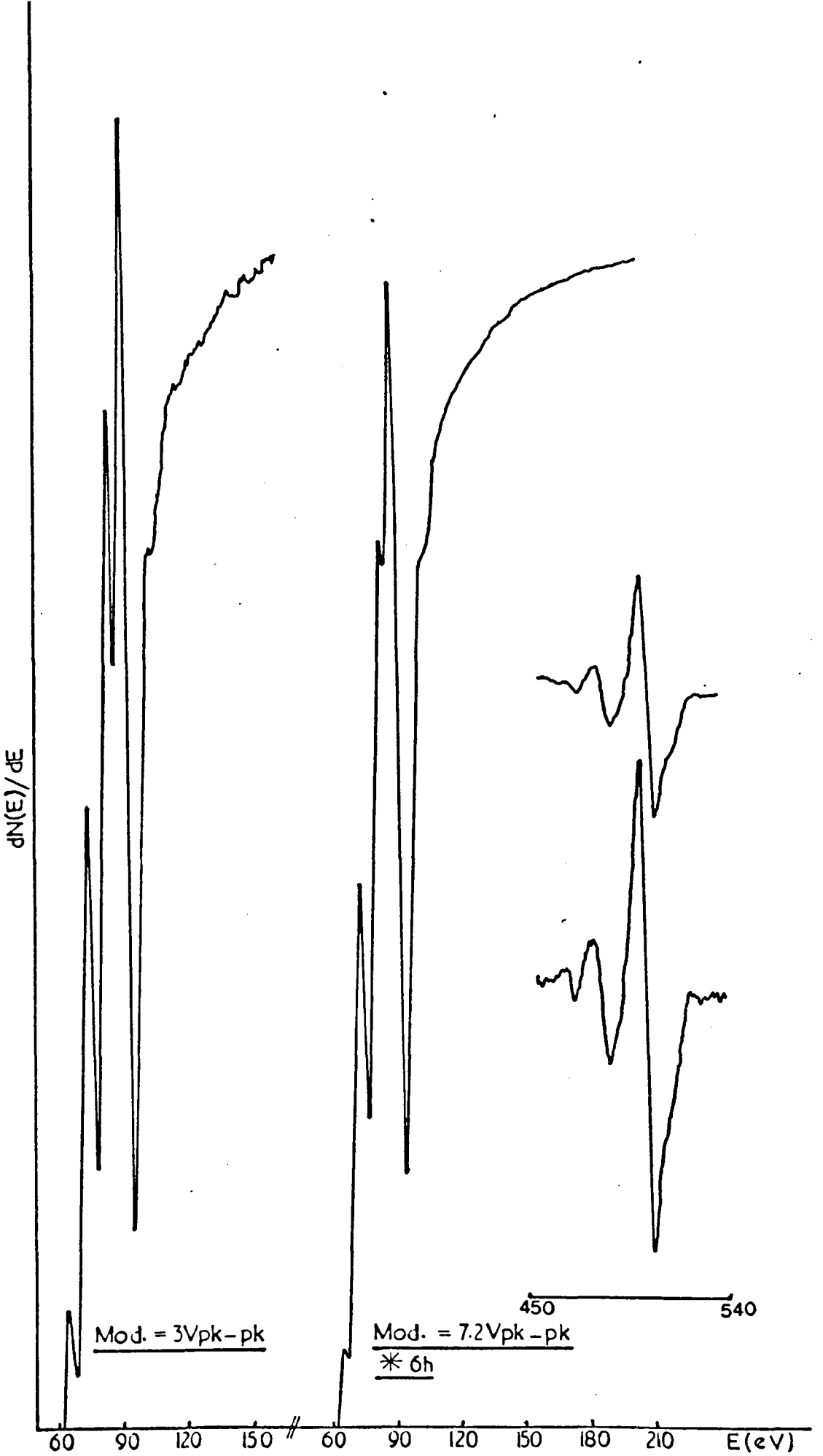
dN(E)/dE
Mod. = 3Vpk-pk
Mod. = 7.2Vpk-pk
* 6h
450
540
60
90
120
150
60
90
120
150
180
210
E(eV)

FIG. b16

APPENDIX c

Sequence of changes in the AES of magnesium due to oxidation.

Ep = 1.3 KeV

Modulation voltages of 7.2 V pk-pk and 2 V pk-pk were used to detect oxygen and magnesium Auger Spectra respectively.

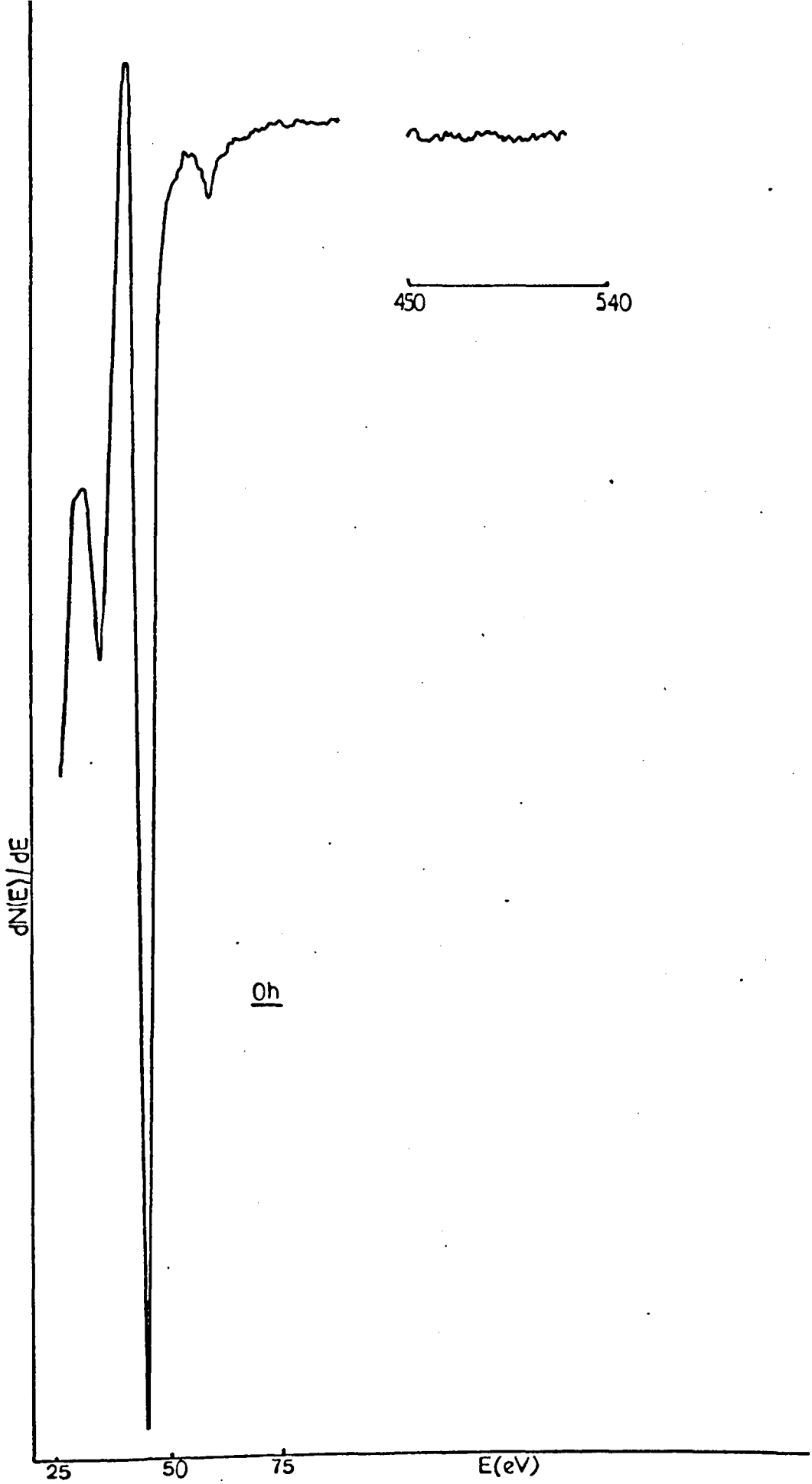

FIG. c1

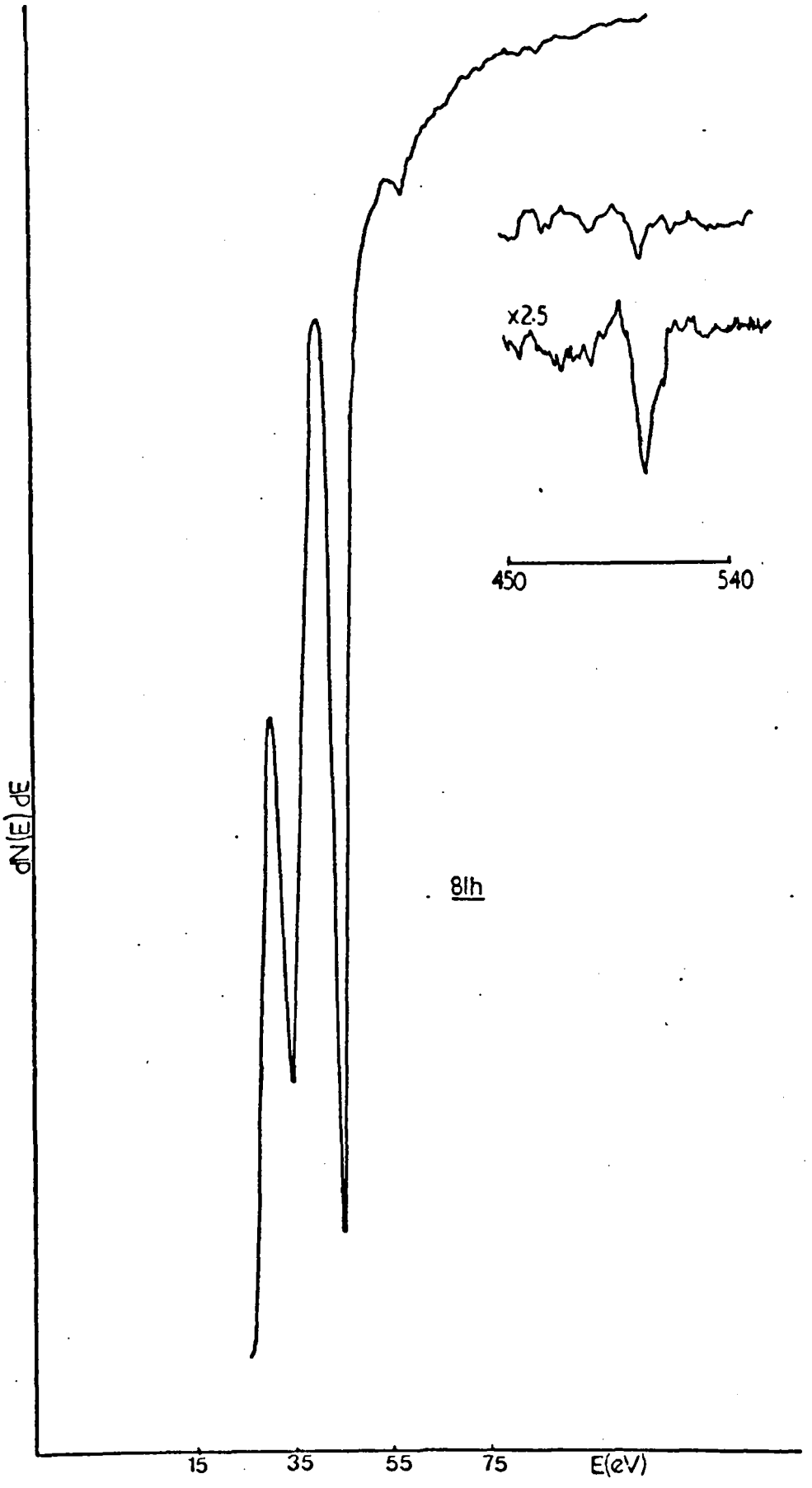

FIG. c2

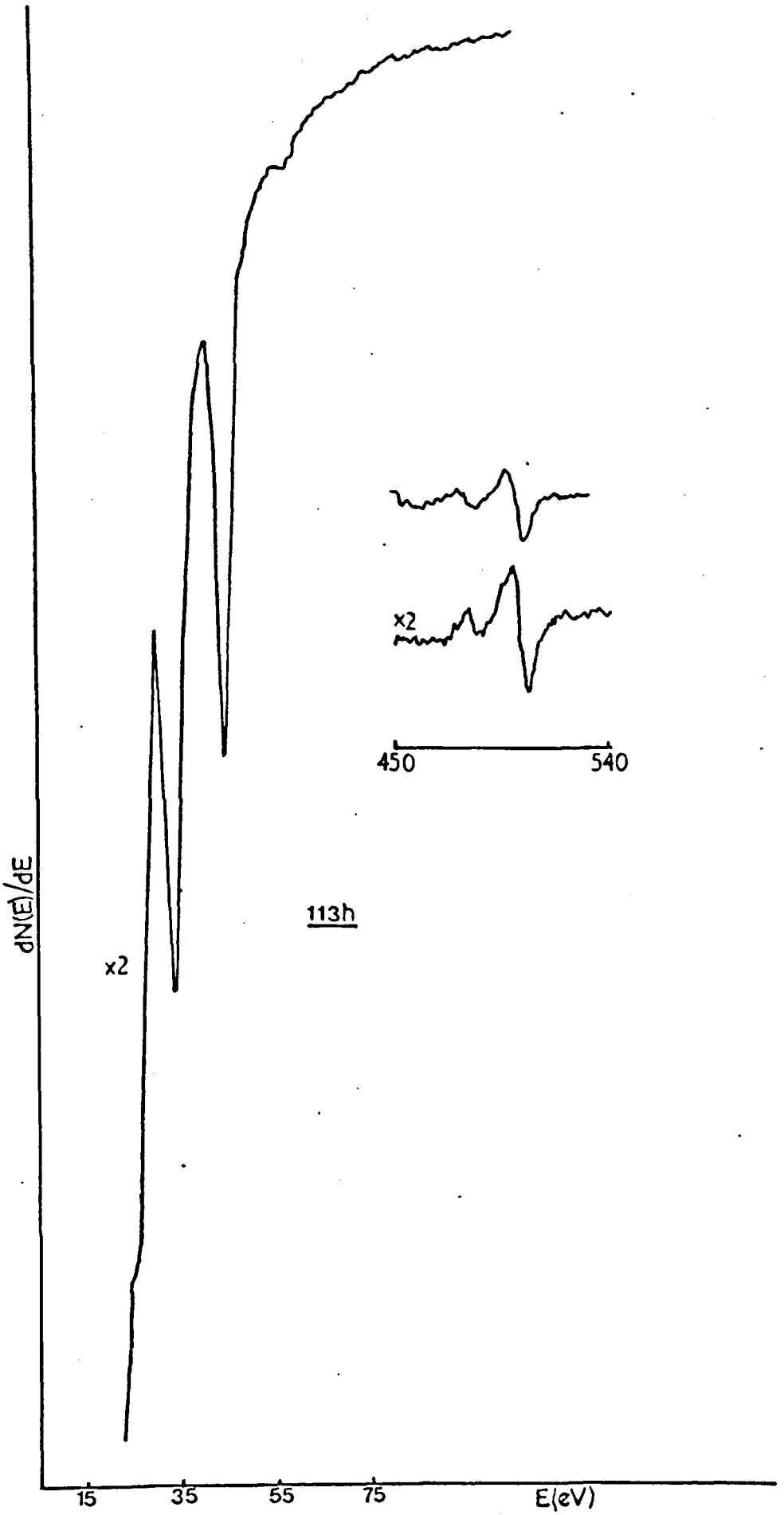

FIG. c3

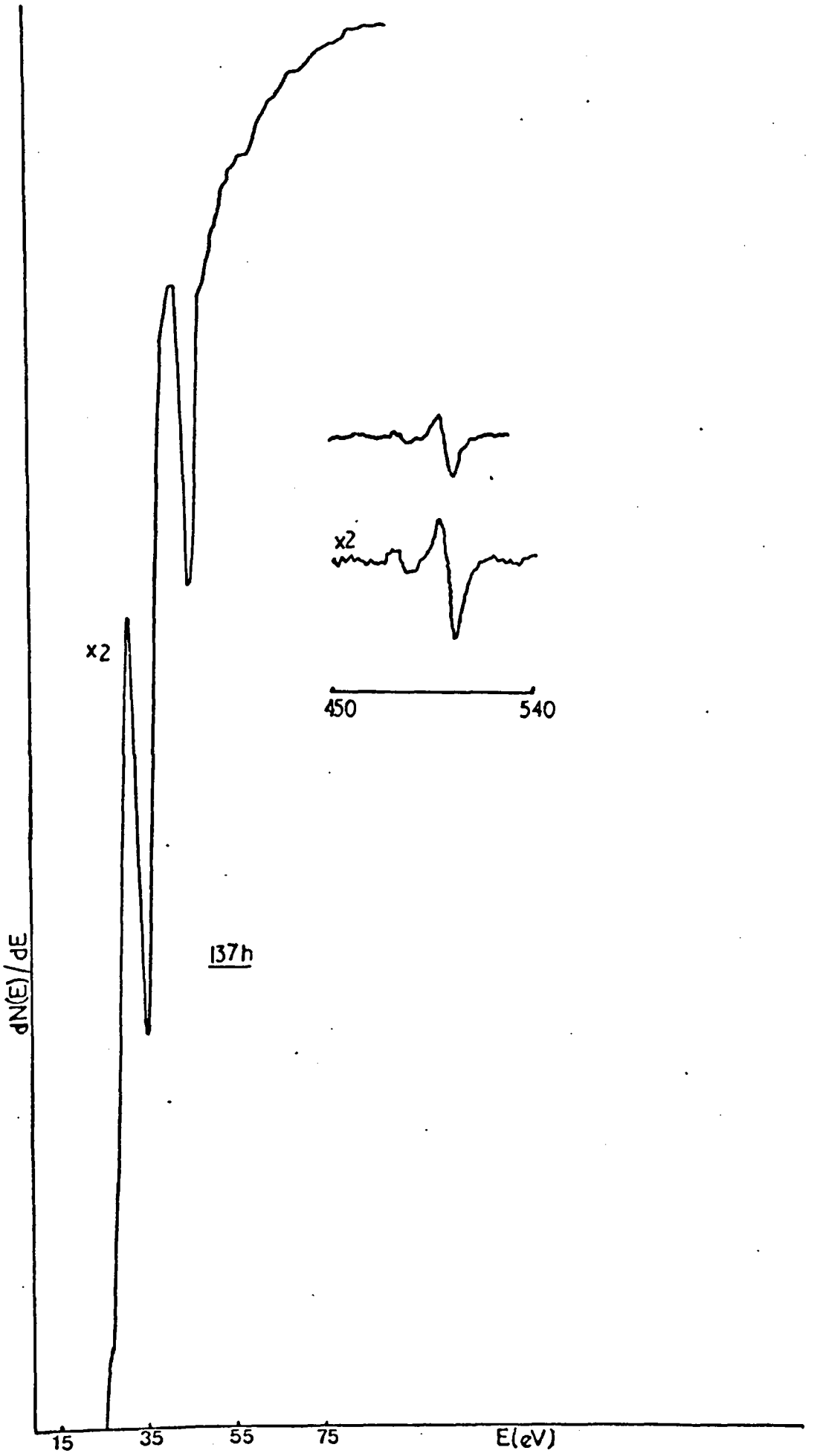

FIG. c4

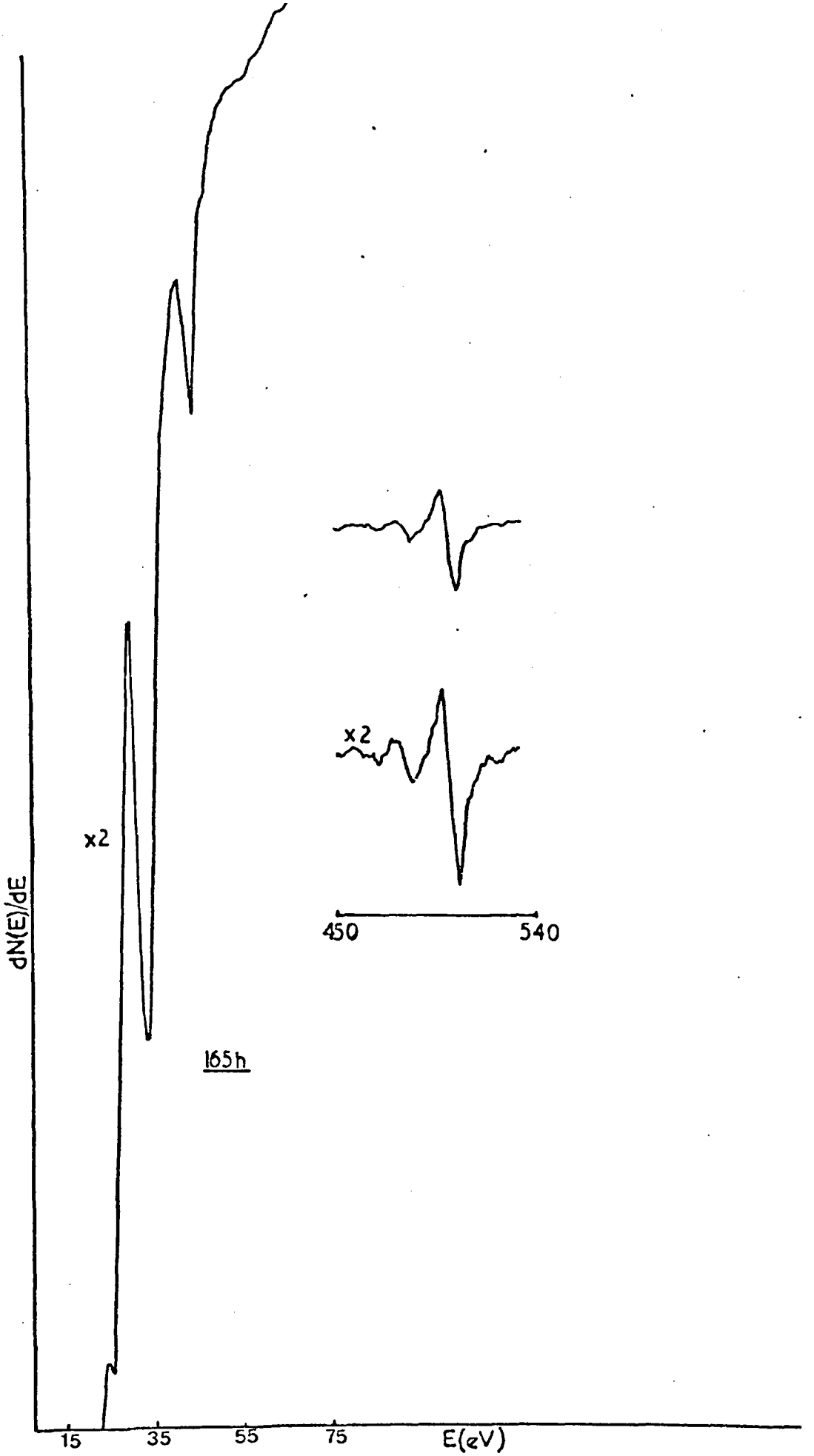

FIG. c5

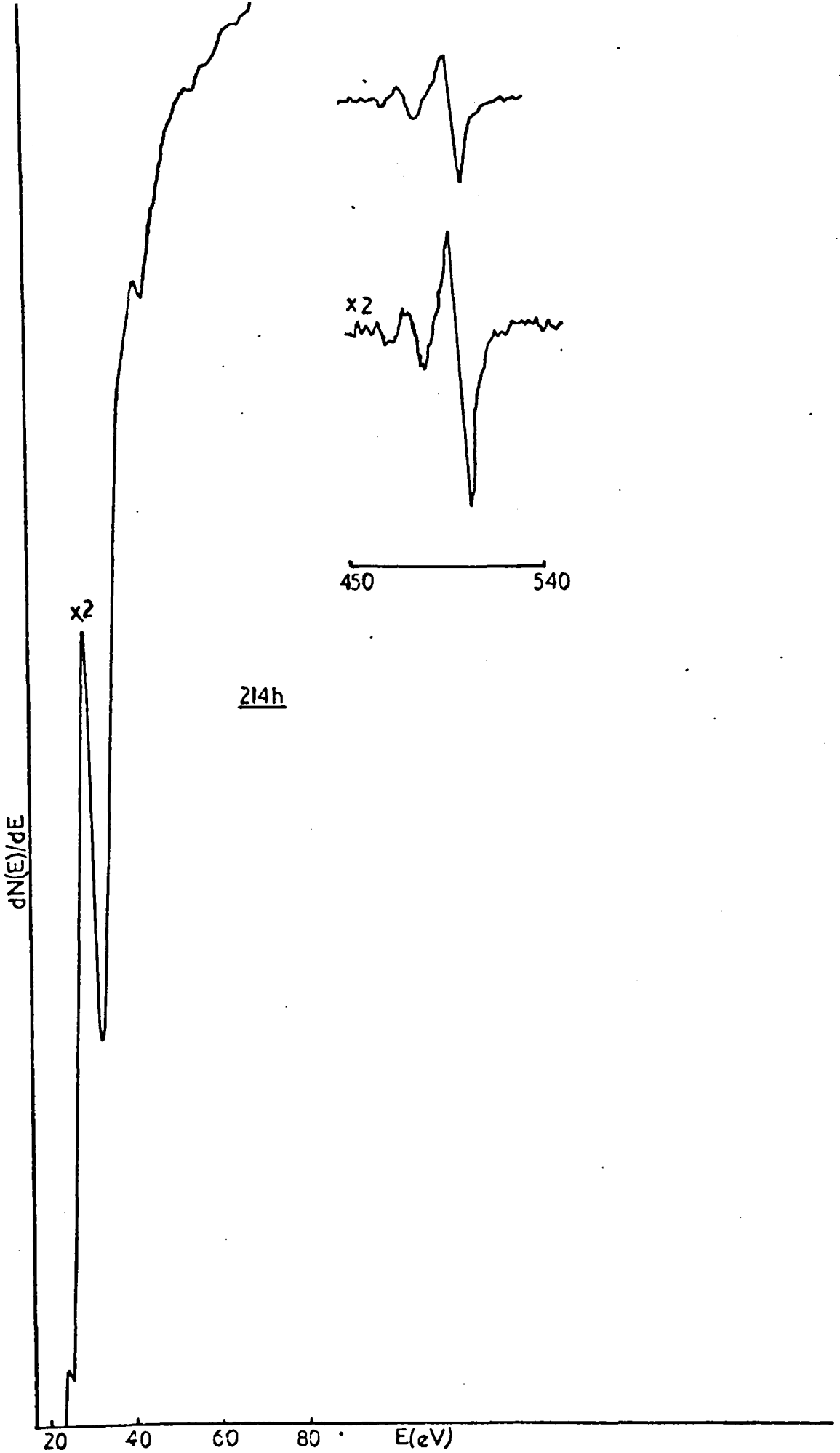

FIG. c6

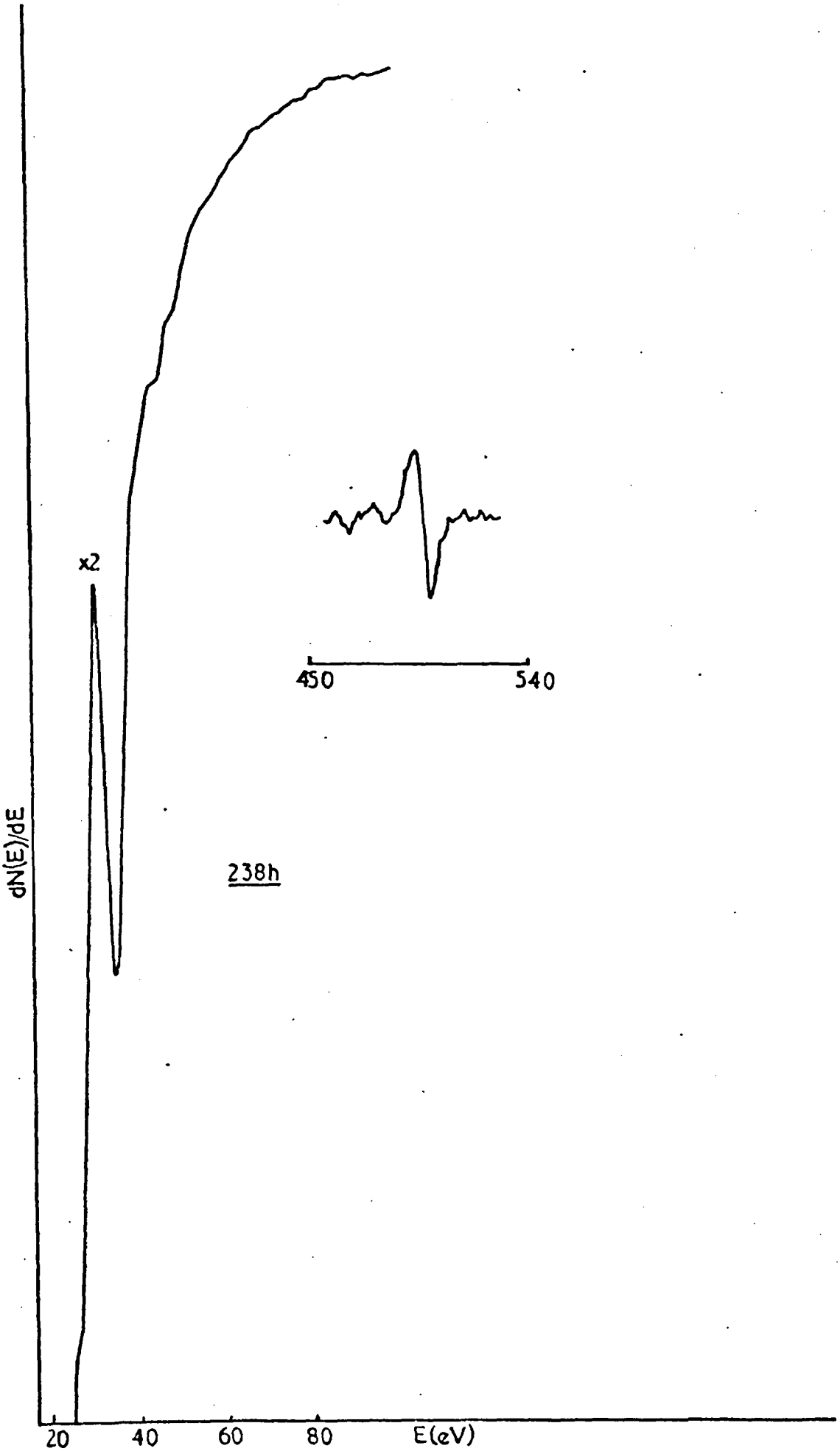

FIG. c7

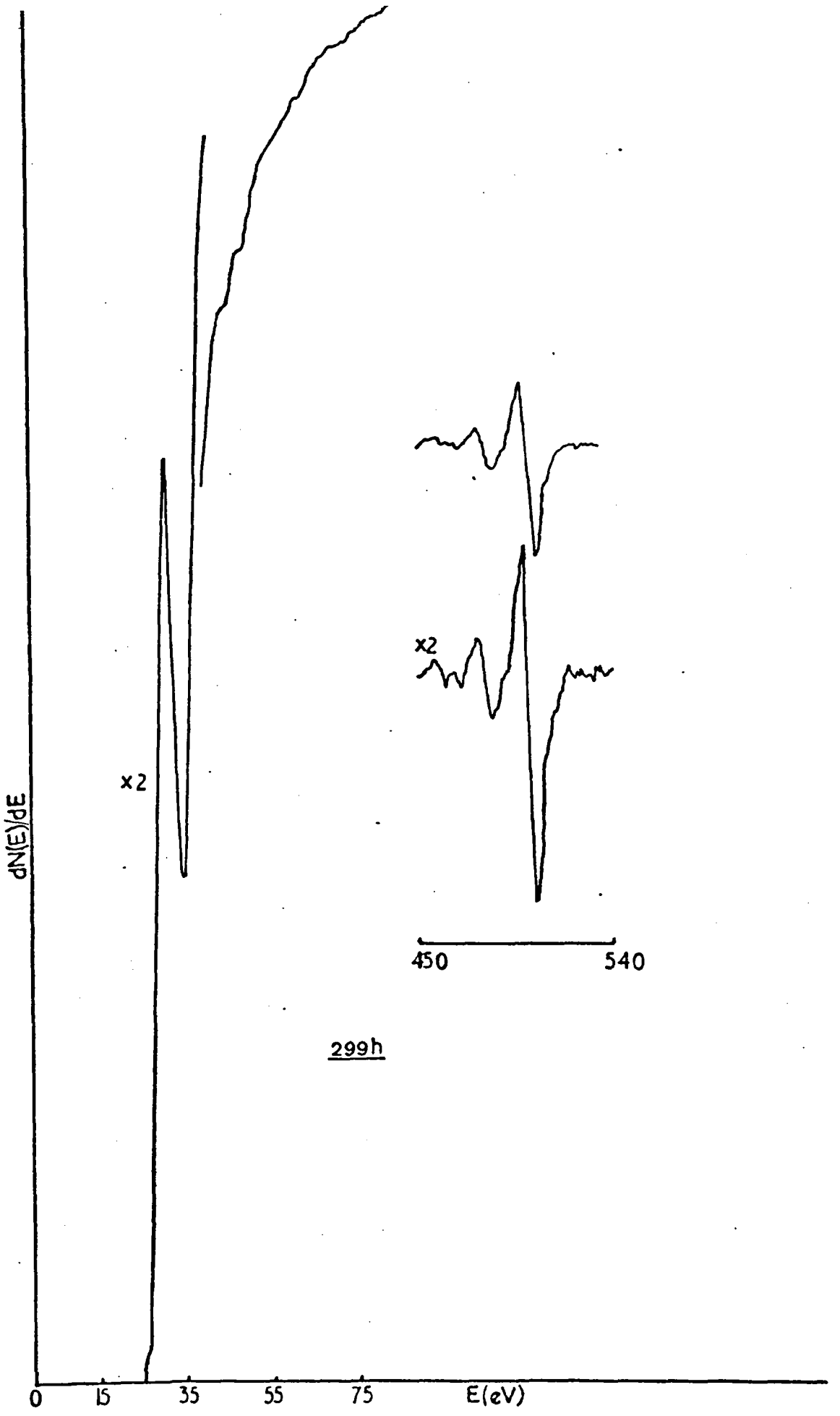

FIG. c8.

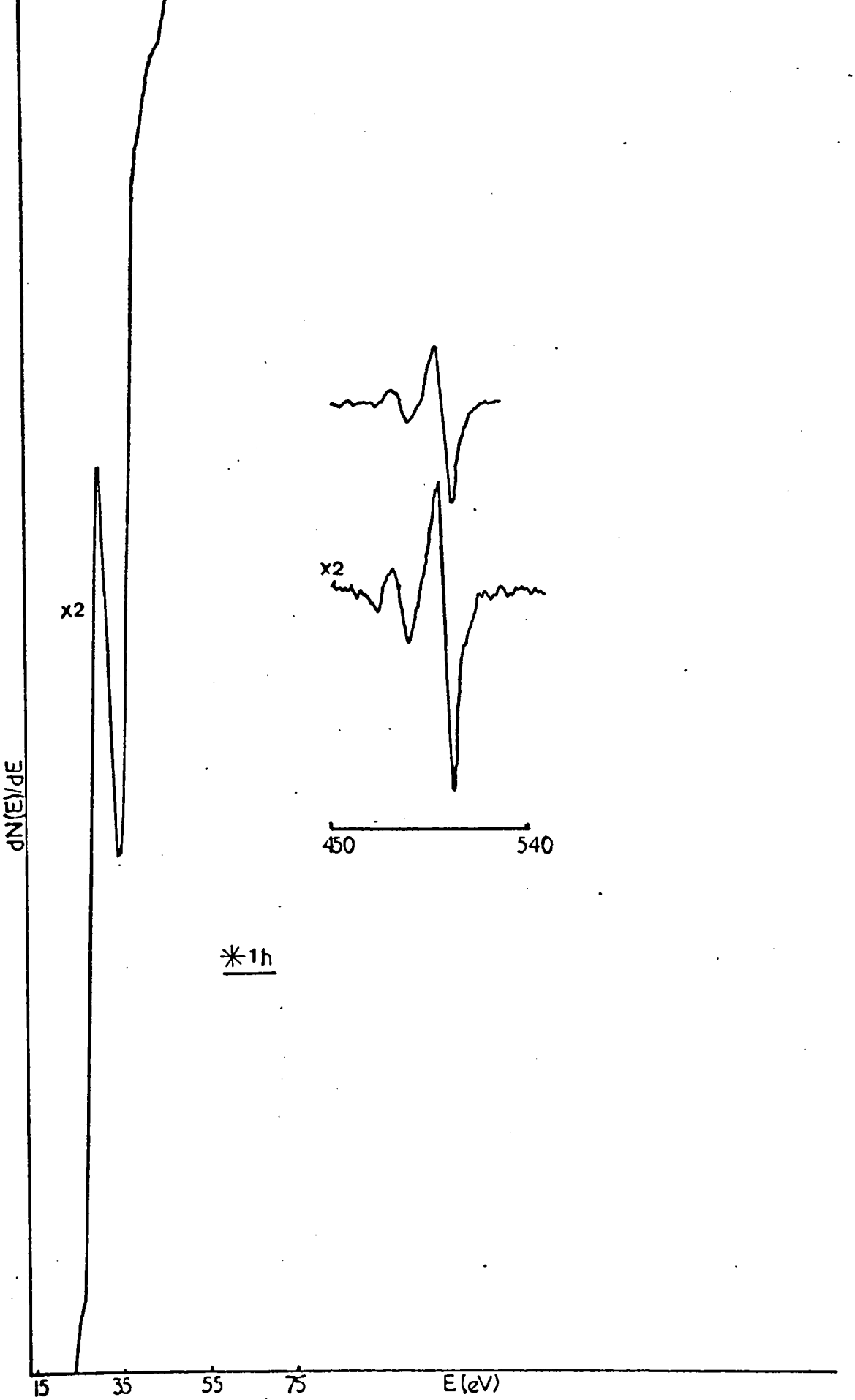

FIG.c9

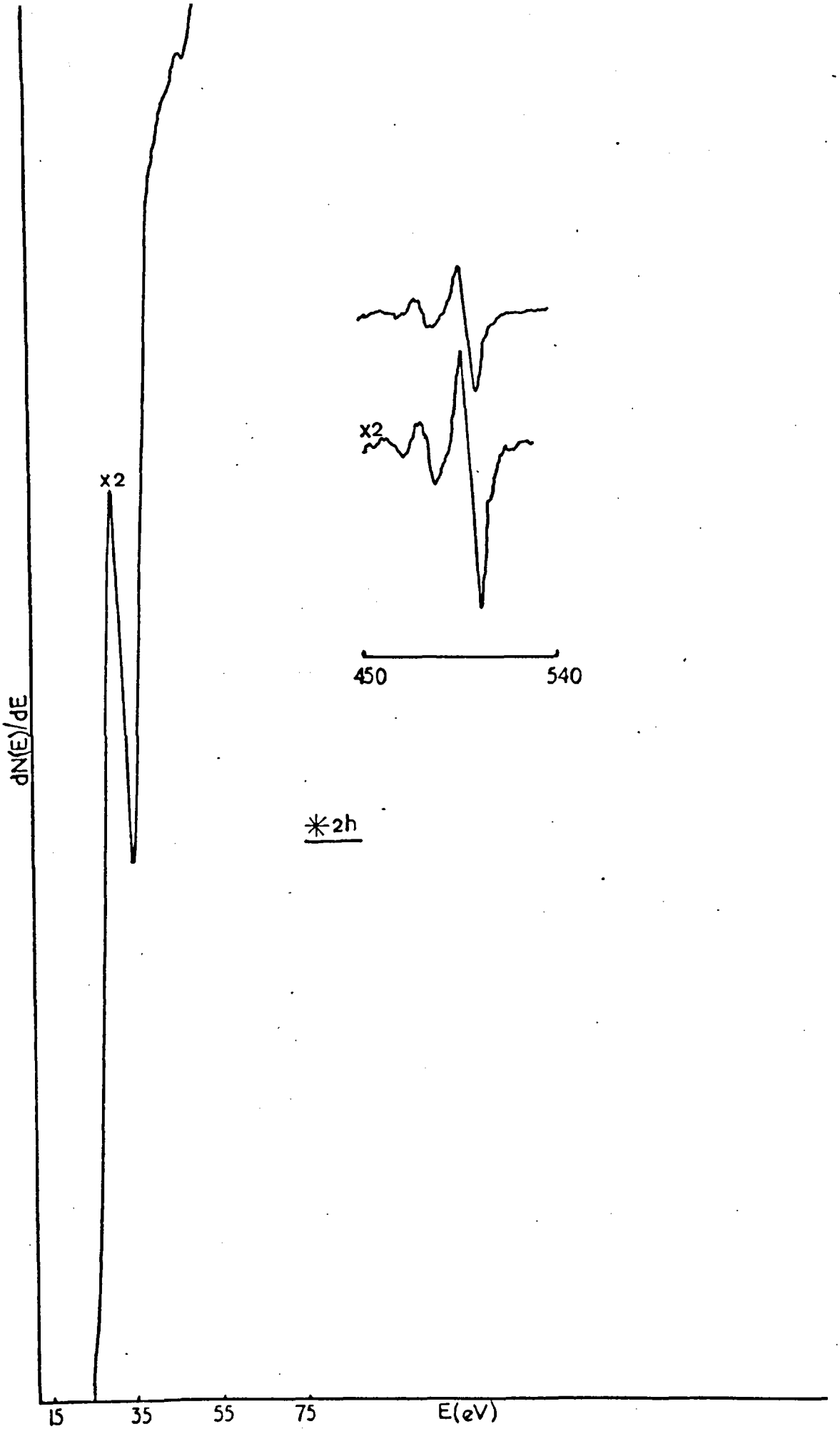

FIG. c10

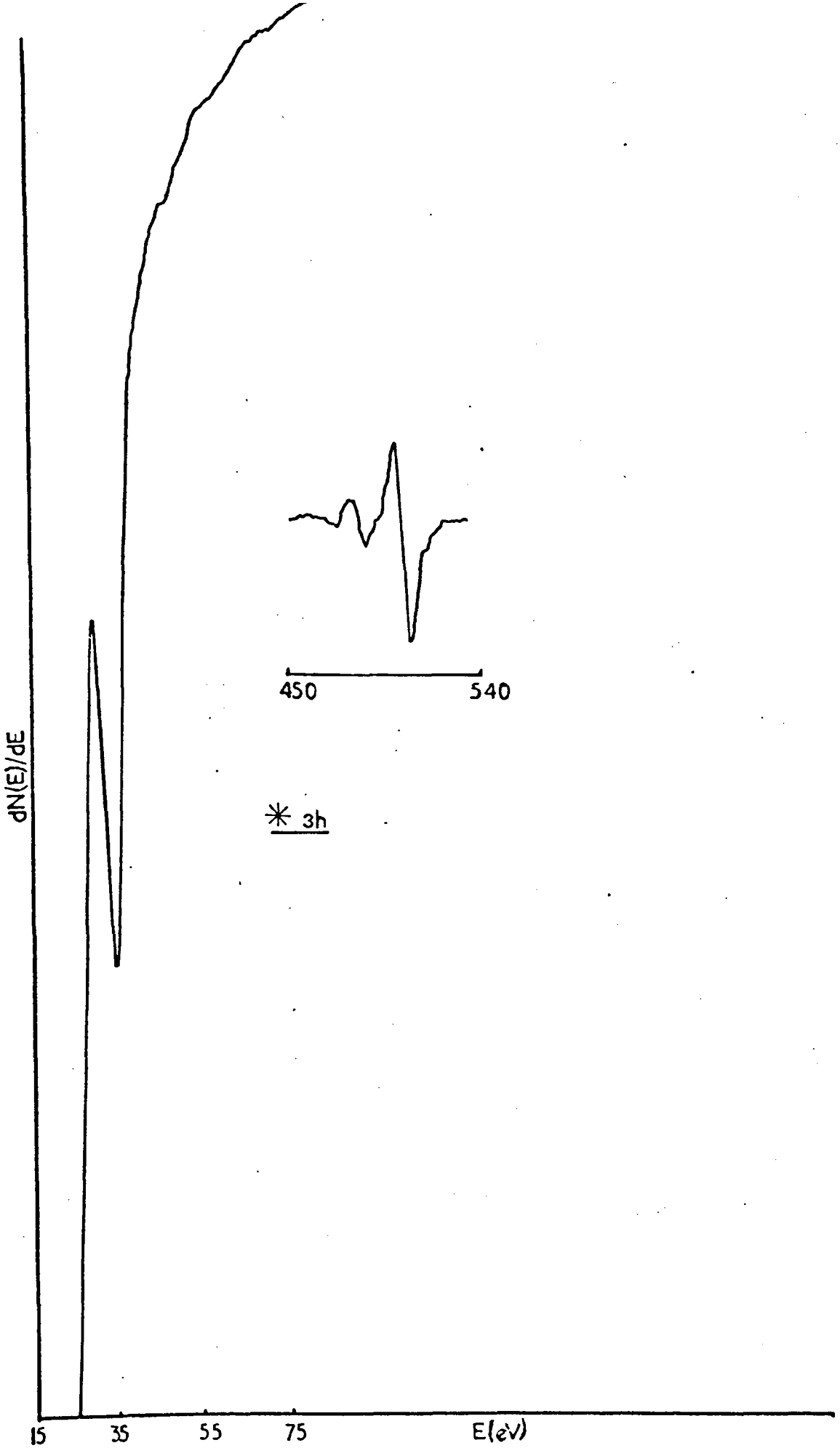

FIG. c11

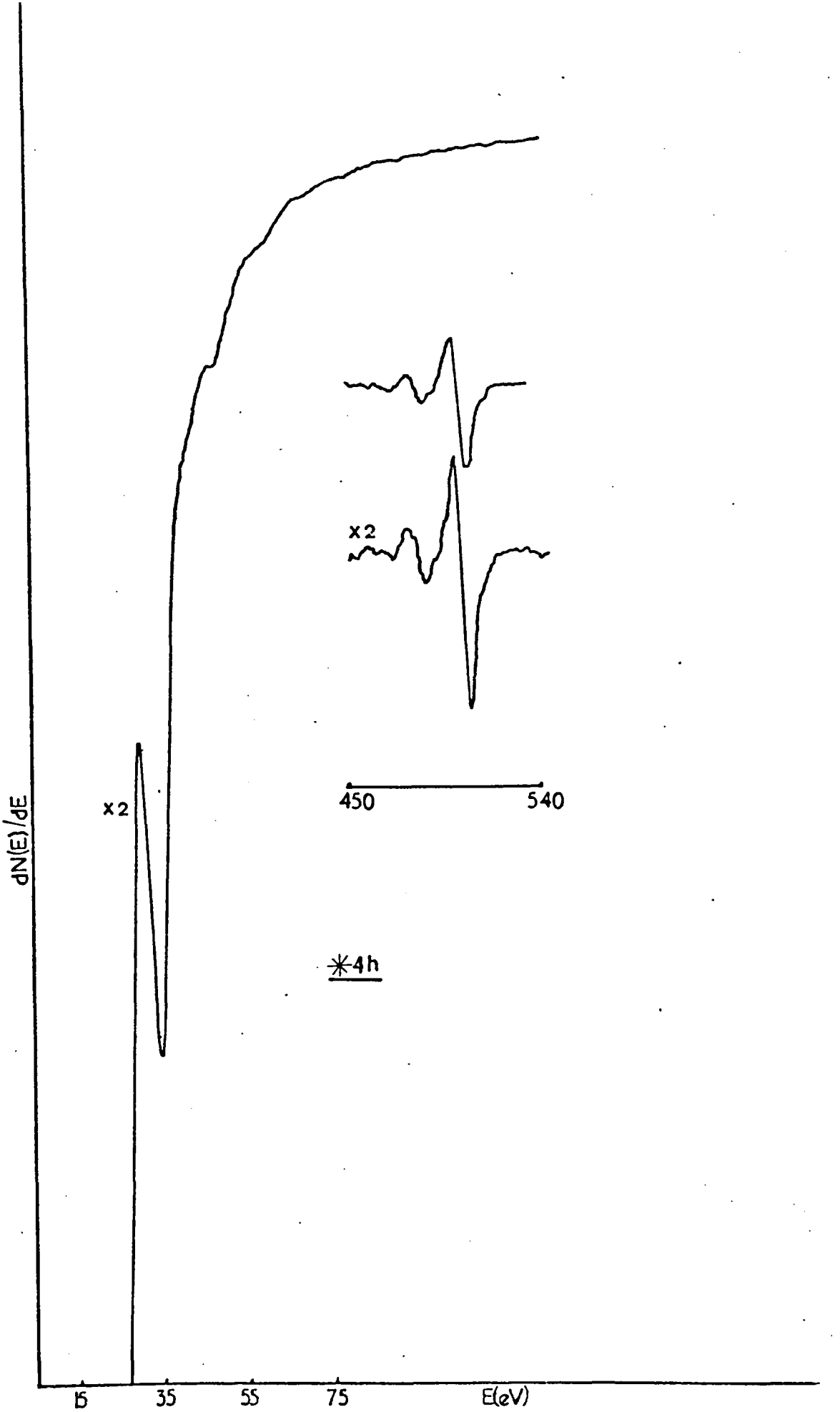

FIG. c12

REFERENCES

Aiyama, T. and Yada, K. J. Phys. Soc. Jn., 36 (6), 1554 (1974).

Alekseev, V. A., Borsov, V.L. Sov. Phys. Solid State, 4, 191 (1962).

Archard, G. D. J. Appl. Phys., 32, 1505 (1961).

Ardenne, M. von. Tabellen der Elektronenphysile, Ionenphysile and Ubermikroskopie (Berlin: Springer-Verlag) (1956).

Ardenne, M. von. Tabellen Zur Angewandten Physik (Berlin: Springer-Verlag) pp. 97-104 (1962).

Asaad, W. N. Nucl. Phys., 5/65, 494 (1966).

Attekum, P. M. Th. M. van and Trooster, J. M. Phys. Rev. B., 20 (6), 2335 (1979).

Auger, P. J. Phys. Radium 6, 205 (1925).

Austin, L. and Starke, H. Ann. Phys., 9, 271 (1902).

Baro, A. M. and Tagle, J. A. J. Phys. F: Metal Phys., 8 (3), 563, (1978).

Baroody, E. M. Phys. Rev., 78, 780 (1950).

Baroody, E. M. Phys. Rev., 89, 910 (1953).

Baroody, E. M. Phys. Rev., 101, 1679 (1956).

Barrie, A. J. Elect. Spect., 7, 75 (1975).

Barrie, A., Drummond, I. W. and Herd, Q. C. Surf. & Interface Anal., 1, 36 (1979).

Bauer, E. Vacuum, 22, 539 (1972).

Bauer, E. and Poppa, H. Thin Solid Films, 12, 167 (1972).

Beaglehole, D. Proc. Phys. Soc., 85, 1007 (1965).

Bearden, J. A. and Burr, A. F. Rev. Mod. Phys., 39, 125 (1967).

Berger, M. J. and Seltzer, S. M. Tables of Energy Losses and Ranges of Electrons and Positrons, NASA SP-3012 (1964).

Bergstrom, I. and Hill, R. D. Ark Fys., 8, 21 (1954).

Bergstrom, I. and Nordling, C. In: Alpha-, Beta- and Gamma-Ray Spectroscopy, vol. 2 (K. Siegbahn, ed.), North Holland, Amsterdam (1965).

Bermudez, V. M. and Ritz, V. H. Surf. Sci., 82, L601 (1979).

Bindi, R., Lanteri, H. and Rostaing, P. Phys. Abst. Classification No. 79, 20H, Part of the "These d'Etat" of R. Bindi, Nice (1978).

Bishop, H. E. and Riviere, J. C. J. Appl. Phys., 40, 1740 (1969).

Bishop, H. E. and Riviere, J. C. Appl. Phys. Lett., 16, 21 (1970).

Blauth, E. Z. Phys., 147, 228 (1957).

Bohm, D. and Pines, D. Phys. Rev., 85, 338 (1952).

Bohm, D. and Pines, D. Phys. Rev., 92, 609 (1953).

Borisov, V. L. and Lepeshinskaya, V. N. Bulletin Academy of Sci. of USSR Physical series, 40, 83 (1976).

Bouwman, R. et al. Vacuum, 23 (5), 169 (1972).

Bronshteyn, I. M., Brozdnichenko, A. N. and Klimin, A. N. Radio Engineering and Electronic Phys., 13 (8), 1289 (1968).

Bruining, H. Die Sekundar-Elektronen-Emission fester Korper, (Berlin: Springer) p. 60 (1942).

Bruining, H. "Physics and Applications of Secondary Electron Emission", McGraw-Hill, New York (1954).

Bruining, H. and De Boer, J. H. Physica Haag, 5, 17 (1938).

Bruining, H. and De Boer, J. H. Physica, 10, 17 (1938).

Burhop, E. H. S. The Auger Effect and Other Radiationless Transitions, Cambridge Univ. Press, London (1952).

Canfield, L. R., Haas, G. and Hunter, W. R. J. Phys. (Paris), 25, 124 (1964).

Carlson, T. A. "Photoelectron and Auger Spectroscopy" (Plenum Press, New York (1975).

Chang, C. C. In: "Characterization of Solid Surfaces" (Eds. P. F. Kane and G. B. Larrabee), (Plenum, New York) Chapt. 20 (1974).

Chattarji, D. "The Theory of Auger Transitions" (Academic Press, London, New York, San Francisco) (1976).

Chen, C. H. J. Phys. C.: Solid State Phys., 9, L321 (1976).

Chung, M. F. and Jenkins, L. H. Surf. Sci., 22, 479 (1970).

Citrin, P. H., Rowe, J. E. and Christman, S. B. Phys. Rev., B14, 2642 (1976).

Clausing, R. E. and Easton, D. S. Surf. Sci., 36, 377 (1973).

Cosslett, V. E. and Thomas, R. N. Br. J. Appl. Phys., 15, 1283 (1964).

Daniels, J. Z. Phys., 227, 234 (1969).

Daniels, J., Festenberg, C. V., Raether, H. and Zeppenfeld, K. In: "Springer Tracts in Modern Physics", 54, 77 (1970).

Dawson, P. H. J. Appl. Phys., 37, 3644 (1966).

Dekker, A. J. Solid State Phys., 6, 251 (1958).

Dekker, A. J. and Van Der Ziel, A. Phys. Rev., 86, 755 (1952).

Dekker, A. J. and Van Der Ziel, A. Phys. Rev., 92, 34 (1953).

Dionne, G. F. J. Appl. Phys., 44, 5361 (1973).

Dionne, G. F. J. Appl. Phys., 46, 3347 (1975).

Dixon, R. D. and Lott, L. A. J. Appl. Phys., 40, 4938 (1969).

Dufour, G., Guennou, H. and Bonnelle, C. Surf. Sci., 32, 731 (1972).

Economu, E. N. and Ngai, K. L. Adv. Chem. Phys., 27, 265 (1974).

Ertl, G. and Küpper, J. In: "Monographs in Modern Chemistry", vol. 4, Ed. H. F. Ebel (1974).

Estrup, P. J. and McRae, E. G. Surf. Sci., 25, 1 (1971).

Ferrell, R. A. Phys. Rev., 101, 554 (1956).

Ferrell, R. A. Phys. Rev., 107, 450 (1957).

Ferrell, R. A. Phys. Rev., 111, 1214 (1958).

Fiermans, L. and Vennik, J. J. Surf. Sci., 38, 257 (1973).

Fischer, T. E. Phys. Rev., 147, 601 (1966).

Fitting, H. J., Glaefeke, H. and Wild, W. Surf. Sci., 75, 267 (1978).

Florio, J. V. and Robertson, W. D. Surf. Sci., 18, 398 (1969).

Franks, J. and Chandler, A. M. Vacuum, 24, 489 (1974).

Fröhlich, H. Ann. Physik., 13, 229 (1932).

Froitzheim. In: "Electron Spectroscopy for Surface Analysis", Ed. H. Ibach, Springer-Verlag, Berlin, Heidelberg, New York) (1977).

Fuggle, J. C., Watson, L. M., Fabian, D. J. and Affrossman, S. J. Phys., F5, 375 (1975).

Gallon, T. and Matthews, J. A. D. Phys. Stat. Sol., 41, 343 (1970).

Gallon, T. E., Higginbotham, I. G. and Prutton, M. J. Phys. E. S_2, 2, 284 (1969).

Ganachaud, J. P. and Cailler, M. Surf. Sci., 83, 498 (1979).

Ganachaud, J. P. and Cailler, M. Surf. Sci., 83, 519 (1979).

Gerlach, R. L. and Du Charme, A. R. Surf. Sci., 29, 317 (1972).

Gerlach, R. L., Houston, J. E. and Park, R. L. Appl. Phys. Lett., 16, 179 (1970).

Gesell, T. F. and Arakawa, E. T. Surf. Sci., 33, 419 (1972).

Glendenin, L. E. Nucleonics, 2, 12 (1948).

Gobrecht, H. and Speer, F. Z. Phys., 135, 603 (1953).

Goldstein, B. and Dresner, J. Surf. Sci., 71, 15 (1978).

Green, A. K. and Bauer, E. Surf. Sci., 74, 676 (1978).

Gründler, R., Breuer, K. and Tews, W. Phys. Stat. Sol. (b), 86, 329 (1978).

Gupta, R. P. and Freeman, A. J. Phys. Rev. Lett., 36, 1194 (1976).

Haas, T. W. and Grant, J. T. Appl. Phys. Lett., 16, 172 (1970).

Haas, T. W., Grant, J. T. and Dooley, G. J. J. Appl. Phys., 43, 1853 (1972).

Hachenberg, O. and Brauer, W. Advances in Electronics and Electron Physics (Ed. Marton, L.), vol. 11, Academic Press, New York (1959).

Hafner, H., Simpson, J. A. and Kuyatt, E. C. Rev. Sci. Instru., 39, 33 (1968).

Halder, N. C., Alonso, J. and Swartz, W. E. Naturforsch Z., 30a, 490 (1975).

Halder, N. C., Alonso, J. and Swartz, W. E. Naturforsch Z., Phys. Rev., B13, 2428 (1976).

Harmin, K. et al., Physica Scripta, 1, 277 (1970).

Harris, L. A. J. Appl. Phys., 39, 1419 (1968).

Harris, L. A. J. Appl. Phys., 39, 1428 (1968).

Harris, L. A. J. Appl. Phys., 39, 4862 (1968).

Hawkins, D. T. "Auger Electron Spectroscopy - A bibliography: 1925-1975", Plenum Press, New York (1977).

Hayasi, T. et al. Sci. Rep. Tohoku Univ. Ser. 1, 52, 1 (1969).

Henrich, V. E. Rev. Sci. Instru., 44 (4), 456 (1973).

Höchst, H., Steiner, P. and Hüfner, S. Phys. Lett., 60A (1), 69 (1977a).

Höchst, H., Steiner, P., and Hüfner, S. J. Phys. F. : Metal Phys., 7 (11), L309 (1977b).

Holliday, J. E. and Sternglass, E. J. J. Appl. Phys., 30, 1428 (1959).

Ibach, H. "Electron Spectroscopy for Surface Analysis", (Springer-Verlag, Berlin, Heidelberg, New York) (1977).

Inoue, S. T. and Yamashita, J. J. Phys. Soc. JPN, 35 (3), 677 (1973).

Jahrreiss, H. and Opell, W. J. Vacuum Sci. Technol., 9, 173 (1972).

Janssen, A. P., Schoonmaker, R. C., Mathew, J. A. D. and Chambers, A. Solid State Commun., 14, 1263 (1974).

Janssen, A. P., Schoonmaker, R. C. and Chambers, A. Surf. Sci., 47, 41 (1975).

Jenkins, L. H. and Chung, M. F. Surf. Sci., 33, 159 (1972).

Jenninson, D. R., Madden, H. H. and Zehner, D. M. Phys. Rev. B., 21 (2), 430 (1980).

Johnson, J. B. and McKay, K. G. Phys. Rev., 93, 668 (1954).

Jonker, J. L. H. Philips Res. Rept., 6, 372 (1951).

Jonker, J. L. H. Philips Res. Repts., 7, 1 (1952).

Jonker, J. L. H. Philips Res. Repts., 9, 391 (1954).

Jonker, J. L. H. Philips Res. Repts., 12, 249 (1957).

Jull, G. W. Proc. Phys. Soc., B69, 1237 (1956).

Kanaya, K., Hojou, K., Koga, K. and Toki, K. Jn. J. Appl. Phys., 12, 1297 (1973).

Kanaya, K. and Kawakatsu, H. J. Phys. D. : Appl. Phys., 5, 1727 (1972).

Kanaya, K. and Ono, S. J. Phys. D. : Appl. Phys., 9, 161 (1976).

Kanaya, K. and Ono, S. J. Phys. D. : Appl. Phys., 11, 1495 (1978).

Kanaya, K., Ono, S. and Ishigaki, F. J. Phys. D. : Appl. Phys., 11, 2425 (1978).

Kanter, H. Phys. Rev., 121, 677 (1961).

Kanter, H. Phys. Rev., 121, 681 (1961).

Katz, L. and Penfold, A. S. Rev. Mod. Phys., 24, 28 (1952).

King, R. J. Vacuum, 22, 493 (1972).

Kirby, R. E. and Lichman, D. Surf. Sci., 41, 447 (1974).

Kliever, K. and Fuchs, R. Adva. Chem. Phys., 27, 356 (1974).

Knapp, G. S. and Fradin, F. Y. In: "Electron and Positron Spectroscopies in Materials Science and Engineering", (Ed. O. Buch, J. K. Tien and H. L. Marcus, Academic Press), (1979).

Knoll, M. Z. Tech. Phys., 16, 467 (1935).

Kollath, R. Handb. Phys., 21, 232 (Berlin: Springer Verlag) (1956).

Kortov, V. S. and Slesarev, A. I. Sov. Phys. Solid State, 17, 591 (1975).

Kowalczyk, S. P., Pollak, R. A., McFeeley, F. R., Ley, L. and Shirley, D.A. Phys. Rev., B8, 2387 (1973).

Kowalczyk, S. P., Pollak, R. A., McFeeley, F. R., Ley, L. and Shirley, D.A. Phys. Rev., B9, 381 (1974).

Kowalczyk, S. P., McFeeley, F. R., Ley, L., Gritsyna, V. T. and Shirley, D. A. Solid State Commun., 23, 161 (1977).

Lander, J. J. Phys. Rev., 91, 1382 (1953).

Lane, R. O. and Zaffarano, D. I. Phys. Rev., 94, 960 (1954).

Laponsky, A. B. and Whetten, N. R. Phys. Rev., 120 (3), 80 (1960).

Larkins, F. P. In: "Atomic Inner Shell Processes VI", (Ed. B. Craseman) Academic Press, New York (1975).

Leder, L. B. and Simpson, J. A. Rev. Sci. Instru., 29, 571 (1958).

Lee, P. A. Phys. Rev., B13, 5261 (1976).

Lenard, P. Quantitatives Über Kathodenstrahlen aller Geschwindigkeiten (Heidelberg: Karl Winters Universitätsbuchh) (1918).

Lay, L., McFeeley, F. R., Kowalczyk, S. P., Jenkins, J. G. and Shirley, D. A. Phys. Rev., B11, 600 (1975).

Linford, P. A. Surf. Contam. Genesis, Detect. Control., 2, 587 (1979).

Lukirskii, A. P. and Brytov, I. A. Soviet Phys. Solid State, 6 (1), 33 (1964).

Lye, R. G. Phys. Rev., 99, 1647 (1955).

Lye, R. G. and Dekker, A. J. Phys. Rev., 102, 977 (1957).

Lytle, F. W., Sayers, D. E. and Stern, E. A. Phys. Rev., B11, 4825 (1975).

Madden, H. H. and Houston, J. E. Solid State Commun., 21, 1081 (1977).

Madden, H. H. and Zehner, D. M. Bull. Am. Phys. Soc., 23, 335 (1978).

Madden, H. H. and Zehner, D. M. Energy Research Abstract, 4 (21), Abstract No. 51947 (1979).

Madey, T. E. and Yates, J. T. Jr. J. vac. sci. Technol., 8, 525 (1971).

Madey, T. E. and Yates, J. T. Jr. Surf. Sci., 63, 203 (1977).

Maguire, H. G. and Augustus, P. D. Phil. Mag., 30, 95 (1974).

Marshak, R. E. Rev. Mod. Phys., 19, 185 (1947).

Marshall, J. E. Phys. Rev., 88, 416 (1952).

Martinelli, R. U. Appl. Phys. Lett., 17 (8), 313 (1970).

Martinelli, R. U. J. Appl. Phys., 45 (7), 3203 (1974).

Martinelli, R. U. and Ettenberg, M. J. Appl. Phys., 45 (9), 3896 (1974).

Marton, L., Leder, L. B. and Mendlowitz, H. Adv. Electron. Electron Phys., 6, 183 (1954).

Mathieu, H. J. and Landolt, D. Surf. Sci., 53, 228 (1975).

Matthew, J. A. D. Surf. Sci., 40, 451 (1973).

McRae, E. C., Lanwehr, J. M. and Caldwell, C. W. Phys. Rev. Lett., 38, 1422 (1977).

McRae, E. G., Aberdam, D., Baudoing, R. and Gauthier, Y. Surf. Sci., 78, 518 (1978).

McRae, E. G. Rev. Mod. Phys., 51, 541 (1979).

Mermin, D. Phys. Rev., B1, 2362 (1970).

Meyer, F. and Vrakking, J. J. Surf. Sci., 38, 275 (1973).

Meyer, U. D., Berbele, A. S. and Lassettre, E. W. J. Chem. Phys., 43, 805 (1965).

Möllenstedt, G. and Lenz, F. Adv. Electronics, 18, 251 (1963).

Mularie, W. M. and Rusch, T. W. Surf. Sci., 19, 469 (1970).

Müller, H. O. Z. Phys., 104, 475 (1937).

Müller, E. W. "Modern Diffraction and Imaging Techniques in Materials Science", (Ed.: S. Armelinckx et al.), Amsterdam: North Holland, p. 701 (1970).

Müller, K. In: "Springer Tracts in Modern Physics", 77, 97 (1975).

Murata, Y. and Ohtani, S. J. Vac. Sci. Tech., 9, 789 (1972).

Musket, R. G. and Ferrante, J. J. Vac. Sci. Tech., 7, 14 (1970).

Musket, R. G. and Fortner, R. J. Phys. Rev. Lett., 26, 80 (1971).

Neave, J. H., Foxon, C. T. and Joyce, B. A. Surf. Sci., 29, 411 (1972).

Needham, P. B., Driscoll, T. J. and Rao, N. G. Appl. Phys. Lett., 21, 502 (1972).

Nilsson, P. O., Arbman, G. and Gustafsson, T. J. Phys. F. : Metal Phys., 4, 1937 (1974).

Oatley, C. W., Nixon, W. C. and Pease, R. F. W. Adv. Electronics, 21, 181 (1965).

Ono, S. and Kanaya, K. J. Phys. D. : Appl. Phys., 12, 619 (1979).

Palmberg, P. W. J. Appl. Phys., 38, 2137 (1967).

Palmberg, P. W. Appl. Phys. Lett., 13, 183 (1968).

Palmberg, P. W. Surf. Sci., 25, 598 (1971).

Palmberg, P. W. and Rhodin, T. N. J. Appl. Phys., 39, 2425 (1968).

Palmberg, P. W., Bohn, G. K. and Tracy, J. C. Appl. Phys. Lett., 15, 254 (1969).

Park, R. L. Surf. Sci., 48, 80 (1975).

Park, R. L., Houston, J. E. and Shreiner, D. G. Rev. Sci. Instru., 41, 1810 (1970).

Parratt, L. G. Rev. Sci. Instru., 30, 297 (1959).

Perdereau, M. Surf. Sci., 24, 239 (1972).

Petzel, B. Thesis Dresden (1958).

Pillon, J. and Ganachaud, J. P. Proc. 7th Int. Vac. Congr. Vienna, P473 (1977).

Pines, D. In: "Solid State Phys." (Eds. F. Satz and D. Turnbull), Academic Press, New York, vol. 1, P873 (1955).

Pines, D. "Elementary Excitations in Solids", (Ed. W. A. Benjamin), New York, Amsterdam (1963).

Powell, C. J. J. Opt. Soc. Amer., 59, 738 (1969).

Powell, C. J., Stein, R. J., Needham, P. B. and Driscoll, T. J. Phys. Rev., B16 (4), 1370 (1977).

Powell, C. J. and Swan, J. B. Phys. Rev., 115, 869 (1959).

Powell, C. J. and Swan, J. B. Phys. Rev., 116, 81 (1960).

Powell, C. J. and Swan, J. B. Phys. Rev., 118, 640 (1960).

Prutton, M. Metall. Rev., 5, 57 (1971).

Purcell, E. M. Phys. Rev., 54, 818 (1938).

Quinto, D. T. and Robertson, W. D. Surf. Sci., 27, 645 (1971).

Raether, H. In: "Springer Tracts in Modern Physics", 38, 84 (1965).

Raether, H. Surf. Sci., 8, 233 (1967).

Raether, H. Phys. Thin films, 7, 145 (1977).

Raether, H. "Springer Tracts in Modern Phys.", 88, 1 (1980).

Rauth, A. M. and Simpson, J. A. Radiat. Res., 22, 643 (1964).

Ritchie, R. H. Phys. Rev., 106, 874 (1957).

Ritchie, R. H. Surf. Sci., 34, 1 (1973).

Robins, R. L. and Swan, J. B. Proc. Phys. Soc. (London), 76, 857 (1960).

Roessler, D. M. and Walker, W. C. Phys. Rev., 159, 733 (1967).

Roessler, D. M., Walker, W. C. and Loh, E. J. Phys. Chem. Solids, 30, 157 (1969).

Rowe, J. E., Ibach, H. and Froitzheim, H. Surf. Sci., 52 (2), 281 (1975).

Roy, D. and Carette, J. D. "Topics in Current Physics", (Ed. H. Ibach), Springer, New York, vol. 4, p. 13 (1977).

Roy, D. and Carette, J. D. Can. J. Phys., 49, 2138 (1971).

Rudberg, E. Phys. Rev., 50, 138 (1936).

Rudberg, E. and Slater, J. C. Phys. Rev., 129 (4), 1550 (1964).

Sagawa, T. In: "Soft x-ray Band Spectra and the Electronic Structure of Metals and Materials", (Ed. D. J. Fabian), Academic Press, London, p. 29 (1968).

Salmeron, M., Baro, A. M. and Rojo, J. M. Surf. Sci., 41, 11 (1974).

Salmeron, M., Baro, A. M. and Rojo, J. M. Surf. Sci., 53, 689 (1975).

Salow, H. Z. Tech. Physik, 21, 8 (1940).

Sar-el, H. Z. Rev. Sci. Instru., 38, 1210 (1967).

Scheibner, E. J. and Tharp, L. N. Surf. Sci., 8, 247 (1967).

Seah, M. P. Surf. Interface Analysis, 1 (3), 86 (1979).

Seiler, H. Z. Angew. Phys., 22, 249 (1967).

Sevier, K. D. "Low Energy Electron Spectroscopy", Wiley, Interscience, New York (1972).

Shimuzu, R. J. Appl. Phys., 45, 2107 (1974).

Shimuzu, R. and Murata, K. J. Appl. Phys., 42, 387 (1971).

Shirley, D. A. Chem. Phys. Lett., 16, 220 (1972).

Shirley, D. A. Phys. Rev., A7, 1520 (1973).

Sickafus, E. N. J. Vac. Sci. Technol., 11 (1), 299 (1974).

Siegbahn, K. et al. "ESCA Atomic, Molecular and Solid State Structure Studies by Means of Electron Spectroscopy", Almquist & Wiksells, Uppsala (1967).

Siegbahn, K. et al. "ESCA Applied to Free Molecules", North Holland, Amsterdam (1969).

Simons, G. W. and Scheibner, E. J. J. Appl. Phys., 43, 693 (1972).

Simons, R. E. and Williams, B. F. IEEE Trans. Nucl. Sci., A15, 167 (1968).

Smith, D. P. Surf. Sci., 25, 171 (1971).

Smith, T. Surf. Sci., 27, 45 (1971).

Smith, D. L. and Huchital, D. A. J. Appl. Phys., 43, 2624 (1972).

Stein, D. F. J. Vac. Sci. Technol., 12 (1), 268 (1975).

Steinrisser, F. and Sickafus, N. Phys. Rev. Lett., 27, 992 (1971).

Stern, E. A. and Ferrell, R. A. Phys. Rev., 20, 130 (1960).

Stern, E. A., Sayers, D. E. and Lytle, F. W. Phys. Rev., B11, 4836 (1975).

Stohr, J., Danley, D. and Perferri, P. Phys. Rev., B18, 4132 (1978).

Suleman, M. Ph.D. Thesis, Phys. Dept., Keele University (1971).

Suleman, M. and Pattinson, E. B. J. Phys. F., 1, L24 (1971).

Suleman, M. and Pattinson, E. B. J. Phys. F., 3, 497 (1973).

Suleman, M. and Pattinson, E. B. Surf. Sci., 35, 75 (1973).

Suleman, M. and Pattinson, E. B. J. Phys. D. : Appl. Phys., 13, 693 (1980).

Swanson, N. and Codling, K. J. Opt. Soc. Am., 58, 1192 (1968).

Tate, J. T. Phys. Rev., 17, 394 (1921).

Taylor, N. J. Surf. Sci., 15, 169 (1969).

Taylor, N. J. Rev. Sci. Instru., 40, 792 (1969).

Tejeda, T., Cardona, M., Schevchik, N. J., Langer, D. W. and Schonherr, E. Phys. Status Solidi (b), 58, 189 (1973).

Tharp, L. N. and Scheibner, E. J. J. Appl. Phys., 38, 4355 (1967).

Thomas, S. and Pattinson, E. B. J. Phys. D. : Appl. Phys., 3, 1469 (1970).

Thomson, J. and Callick, E. B. "Electron Physics and Technology", The English Universities Press Ltd. (1959).

Tracy, J. C. NATO Summer School, on "Electron Emission Spectroscopy", Gent, Belgium (1972).

Tracy, J. C. Surf. Sci., 38, 265 (1973).

Van der Ziel, A. Phys. Rev., 92, 35 (1953).

Viel et al. Surf.Sci., 54, 635 (1976).

Vrakking, J. J. and Meyer, F. Surf.Sci., 33, 271 (1972).

Wagner, C. D. and Biloen, P. Surf.Sci., 35, 82 (1973).

Watanabe, H. J. Phys. Soc. Jpn., 11 (2), 112 (1956).

Watanabe, H. J. Phys. Soc. Jpn., 16, 912 (1962).

Weber, R. E. and Peria, W. T. J. Appl. Phys., 38, 4355 (1967).

Wehenkel, C. J. Phys. (Paris), 36, 199 (1975).

Wells, O. C. "Scanning Electron Microscopy", (McGraw-Hill, New York), Chapt. 3 (1974).

Whiddington, R. Proc. Roy. Soc., A86, 360 (1912).

Wiech, G. "Soft Gamma Ray Band Spectra and the Electronic Structure of Metals and Materials", (Ed. D. Y. Fabian), New York: Academic Press, p. 59 (1968).

Wolff, P. A. Phys. Rev., 95, 56 (1954).

Wooldrige, D. E. Phys. Rev., 56, 562 (1939).

Wright, B. Ph.D. Thesis, Phys. Dept., Keele University (1974).

Young, J. R. J. Appl. Phys., 27, 1 (1956).

Young, J. R. Phys. Rev., 103, 292 (1956).

Zehner, D. M., Burbulesco, N. and Jenkins, L. H. Surf. Sci., 34, 385 (1973).

Zeitler, E. Quantit. Electron Microsc., 14, 36 (1965).

Zinke, O. H. Phys. Rev., 106, 1163 (1957).